Simultaneous Detection of *Salmonella Typhimurium* and *Bacillus Anthracis* Spores Using Remote Phage-Based Magnetoelastic Microbiosensors

by

Shichu Huang

A dissertation submitted to the Graduate Faculty of
Auburn University
in partial fulfillment of the
requirements for the Degree of
Doctor of Philosophy

Auburn, Alabama
May 14, 2010

Keywords: *S. typhimurium*, *B. anthracis* spores, phage, magnetoelastic, biosensor, Simultaneous

Approved by

Bryan A. Chin, Chair, Professor of Materials Engineering
Zhong-Yang Cheng, Associate Professor of Materials Engineering
Dong-Joo Kim, Associate Professor of Materials Engineering
JongWook Hong, Associate Professor of Materials Engineering
Valery A. Petrenko, Professor of Pathobiology

Abstract

This dissertation discusses the results of a study to develop a free standing, magnetoelastic (ME) biosensor for the detection of *S. typhimurium* and *B. anthracis* spores. This affinity-based biosensor is composed of ME resonator platforms immobilized with filamentous phage as the bio-recognition element. Two different phages, E2 phage, genetically engineered to bind with *S. typhimurium*, and JRB7 phage, genetically engineered to bind with *B. anthracis* spores, were used to form the biosensors. A time-varying magnetic field is used to oscillate the magnetoelastic resonator at its characteristic resonance frequency. Upon contact with a target pathogen, the specific phage binds the pathogen to the biosensor, increasing the mass of the sensor. This mass change causes a corresponding decrease in the resonance frequency.

The effect of annealing and sputtering a gold layer onto the surface was studied, and annealing between 200-250 °C found to greatly improve both the corrosion resistance and the Q factor of the signal spectrum. The effect of different salt and phage concentrations on the binding affinity of ME biosensors was also investigated and 420 mM NaCl at a phage concentration of 5×10^{11} vir/ml found to produce the optimal distribution of coated phages onto the sensor surface, consequently promoting better binding of spores to the biosensor's surface. When sensors immobilized with JRB7

phage under this optimum condition were exposed to *B. anthracis* spores in different concentrations (5×10^1 - 5×10^8 cfu/ml) in a flowing system, the binding sensitivity of the ME biosensor was 226 Hz/decade. The multi-sensors detection system was exposed to different conditions of analyte including: *S. typhimurium* / *B. anthracis* spores (5×10^1-5×10^8 cfu/ml) in water, *S. typhimurium* (5×10^1-5×10^8 cfu/ml) in a mixture of *E. coli* O157:H7 (5×10^7 cfu/ml) and *B. anthracis* spores (5×10^1-5×10^8 cfu/ml) in a mixture of *B. cereus* (5×10^7 cfu/ml), separately. The sensitivity of both measurement biosensors (length ≈ 2 mm) was about 170-280 Hz/decade, with an average binding valence of about 3 and a dissociation constant K_d of about 250 cfu/ml under different testing analytes.

Acknowledgments

The author is deeply indebted to her advisor, Dr. Bryan A. Chin, for his wisdom, training, guidance, patience and encouragement throughout this research and the completion of this dissertation. The author is also very grateful to all her committee members, Dr. Zhongyang Cheng, Dr.Valery A. Petrenko, Dr. Dong-Joo Kim, and Dr. Jong Wook Hong, for their academic guidance and many helpful discussions. The author would like to thank the collaboration and support of her group members: Dr. Hong Yang, Dr. Jing Hu, Dr. Ramji S. Lakshmanan, Dr. Suiqiong Li, Dr. Fei Xie, Dr. Rajesh Guntupalli, Dr. Jiehui Wan, Shin Horikawa, Michael L. Johnson, Kanchana Weerakoon, Wen Shen, John Shu, Junping Teng, Yating Chai, Lilin Fu and Kewei Zhang. The author would also like to recognize the following individuals and groups for their valuable assistance in the conduct of this investigation: Dr. James M. Barbaree, I-Hsuan Chen, L.C. Mathison, Roy Howard, Alison Mitchell and Charles Ellis. The author is grateful to her friends: Zhimin Li, Huihua Shu, Feng Qian, Dongna Shen, and Lydia Wood for their encouragement. Finally special thanks go to the author's friends in China for their love, understanding and support. This work is dedicated to the author's best parents and friends, Xiuyu Wang and Yilian Huang.

Table of Contents

List of Tables

List of Figures

CHAPTER 1

INTRODUCTION

1. The need

Every year, over 76 million Americans suffer from food-borne illnesses, resulting in an estimated 325,000 hospitalizations and 5,000 deaths [1] costing $9.3 to 12.9 billion in direct medical expenses [2]. Food-borne illness is primarily caused by four types of pathogens: bacteria, fungi, parasites and viruses, all of which are commonly found in the natural environment. Bacterial pathogens alone account for more than 50% of food-borne illnesses.

The large number of food-borne illnesses can be attributed to changing human demographics, lifestyle choices, food consumption trends, mass transportation of foods and microbial adaptation [3, 4]. The nation's aging population also contributes to this problem: as human beings grow older their immune system weakens and hence a further increase in food-borne illness is anticipated. Another factor is the new interest in international cuisines, which has resulted in the import of exotic foods from many countries. These foods are grown, harvested and often processed in foreign countries and must be shipped longer distances to reach the final consumer. Since the health standards of foreign countries are often significantly different from those in the United

States, food importation becomes an additional possible contamination source. Greater transportation distances and the storage of food for longer periods of time also allow small amounts of bacteria and other pathogens to multiply and potentially reach an infective dose. The Food and Drug Administration (FDA) and Centers for Disease Control (CDC) have concluded that food-borne illness is one of the most serious, yet avoidable, health problems facing our nation.

In recent years bioterrorism has become another serious concern and is now classed as a serious threat to the United States' population. In 1984, the largest deliberate food poisoning incident in the United States to date was perpetrated in Oregon [5]. Two members of the Rajneesh religious cult grew *Salmonella typhimurium* and spread this bacterial pathogen over the food in local restaurant salad bars. This attack resulted in 751 people becoming sickened by the *Salmonella* contaminated food, achieving the cult's objective of reducing the number of voters and thus enabling them to influence the outcome of a local election in their favor.

Most of the pathogens that are considered bioterrorism agents may be obtained naturally from the environment, including serious threats such as *Salmonella typhimurium* and *Bacillus anthracis,* or anthrax spores. However, their ability to cause illness and death can be greatly increased when they are genetically modified. Of these agents, *Anthrax* has a particularly high potential for adverse public health impact since it is difficult to detect/cure and can be disseminated on a large scale relatively easily. *Salmonella* has also been identified as a bioterrorism agent. It is a common bacterial

pathogen that can be easily cultured, stored and distributed amongst an unsuspecting public. Both these agents can be deadly; for instance once contracted, thirty percent of those infected with *B. anthracis* (anthrax) will die. The incubation time associated with exposure to *S. typhimurium* bacteria and *B. anthracis* spores may range from hours to weeks, depending upon the pathogen and the conditions of exposure. During this incubation time, the infected individual functions normally and may travel large distances from the source of exposure. A single infected individual may spread the infection amongst many. This both increases the impact of this terror tactic and makes it difficult to pinpoint the initial source and point of exposure.

1.1. Identification of the problem

1.1.1. *Salmonella* outbreaks

Bacteria are responsible for over 90% of the confirmed food-borne human illness cases and deaths reported to the Centers for Disease Control and Prevention (CDC). Of the food-borne bacterial pathogens, *Salmonella* causes the most illnesses worldwide [6].

In 1985, a large U.S. outbreak of salmonellosis that occurred in Chicago was attributed to *S. typhimurium* in pasteurized milk from a single dairy plant [7]. In 2008 several *Salmonella* outbreaks occurred in the U.S. The most serious of these occurred in mid-April, when the *Salmonella St. Paul* outbreak involving contaminated tomatoes became one of the largest *Salmonella* outbreaks in recent history, sickening at least 869 people and resulting in the hospitalization of 257 individuals. Based on the CDC's

estimated ratio of non-reported salmonellosis cases to reported cases (38.6:1), around 52,826 illnesses resulted from the *Salmonella St. Paul* outbreak. For the nation's entire population, the CDC estimates that there are 173 cases of *Salmonella* illness per million people each year [8]. In the United States, human illness due to *Salmonella* infection is most commonly caused by the *S. typhimurium*, *S. enteritidis*, or *S. heidelberg* serotypes [9].

Salmonella and other food-borne pathogens can be spread easily throughout the food chain. Oat cereal [3, 10], tomatoes [11], eggs [12], milk [13], vegetables and fruits (e.g. raw tomatoes), water [12], green onions, jalapeño peppers, red plum, peanut butter [14] and cilantro [15], all foods that are eaten daily, have recently been found to be contaminated with *Salmonella*. Although it appears that more outbreaks are being linked to vegetable and fruit products, this has not been proven because of the difficulty that scientists and inspectors often experience in locating the source of the pathogen contamination. Food-borne contamination is difficult to monitor because produce may be cleaned at the harvesting site, transported to a warehouse and then repackaged several times before it reaches retail outlets, leaving a lengthy trail that covers many states and often more than one country. In order to reduce the incidence of food-borne illness there is therefore an urgent need to develop a device capable of the rapid, in-field detection of bacterial pathogens. This device needs to be both inexpensive and easy to use so that it can readily be adopted by every link in the food chain, up to and including the final home consumer.

1.1.2. *Bacillus anthracis* (anthrax) attacks

Research on anthrax as a biological weapon began more than 80 years ago [16]. In the early 1970s, most countries agreed to sign the Biological Weapons Convention (BWC) and terminate their offensive bioweapons programs. However, a few countries continued their biological weapons research and development, including Iraq, which admitted producing and weaponizing *B. anthracis* to the United Nations Special Commission in 1995 [17], and the former Soviet Union, which is also known for its offensive bioweapons program, including the production of *B. anthracis* [18].

Every year, there are about 2000 cutaneous anthrax cases (the most common naturally occurring form) reported worldwide [19]. The largest outbreak in recent years occurred in Zimbabwe, where more than 10,000 people were infected in an epidemic between 1979 and 1985 [20]. In 1979, in the Soviet city of Sverdlovsk, inhalational anthrax occurred because of an unintentional release of *B. anthracis* spores from a biological weapons factory. During the 20th century, 18 occupational exposure cases to *B. anthracis* happened in the United States. However, in a terrorism incident in 2001 several media offices and two U.S. senators received letters containing anthrax spores [21], resulting in 22 cases, including 11 inhalational cases and 11 cutaneous cases. These exposure led to 5 deaths and widespread national panic. Since a bioterrorist attack is especially difficult to predict, detect, and prevent, it is one of the most feared terrorism scenarios [22]. The possibility of biological warfare attacks has thus been the source of increasing concern in the U.S. [23].

Anthrax may be spread in many ways, but aerosol-delivery is the most common method of release for large-scale dissemination. *B. anthracis* released this way is usually both invisible and odorless, and is capable of traveling many kilometers before dissipating [24, 25]. Based on data from the World Health Organization, distributing 50 kg of *B. anthracis* over a population of 5 million people is predicted to result in over 250,000 illnesses and 100,000 deaths [24].

1.2. Current methods of detecting outbreaks

The surveillance system traditionally used to collect food-borne disease outbreak data has been overwhelmed by the emergence of mega-farms, distribution centers, and transporters. To address these issues, an automated bioterrorism surveillance system, Real-time Outbreak Disease Surveillance (RODS), was implemented by the University of Pittsburgh in 1999. RODS collects data from multiple sources (e.g. clinics, laboratories, and drug sales) and uses this data to identify a bioterrorism event. Within a year, this system had been modified by RODS lab member Michael Wagner and his coworkers to collect data from 20,000 national retail locations, and was being supported by a $300 million grant to equip all 50 states with biosurveillance systems [26].

In addition to surveillance systems that monitor for information indicating that an outbreak has occurred, the prevention of food-borne illness and bioterrorism depends on the availability of rapid, simple, effective, and portable detection devices capable of identifying and distinguishing various pathogens and biological agents that may be

present in our daily food, clinical medicine, or natural environment. Today, intensive research is being conducted to develop new techniques for the early detection of the causes of food-borne illness. Traditional methods of identifying the pathogens responsible for food-borne illness are very time-consuming and typically require the services of highly trained personnel in laboratories equipped with expensive equipment, taking several days to yield results [27]. There is, therefore, a real need for the development of portable, rapid, specific, sensitive biosensors to enable the real-time, on-site detection of food-borne pathogens.

2. The biosensor solution

The deliberate contamination of our food supply has become a serious concern, with *B. anthracis* and *S. typhimurium* being two of the pathogens of particular interest. There is an increasing need to develop rapid and cost-effective methods to monitor these pathogens. Consequently, this dissertation project focused on the construction of a novel biosensor composed of a magnetoelastic sensor platform and a bio-recognition element of a landscape phage.

2.1. Bio-recognition element

The bio-recognition element is responsible for the specificity, sensitivity, selectivity and thermal stability of a biosensor. The use of a landscape phage as the bio-recognition element is promising for biosensor applications because it is both

environmentally robust and specific to target analytes. In this dissertation, two genetically engineered landscape phages were used as the bio-recognition elements for the detection of *S. typhimurium* and *B. anthracis* spores, respectively. Extensive studies [28-32] have successfully developed landscape phages by modifying filamentous bacteriophages. A filamentous bacteriophage is a type of phage that has a thread-like appearance. The inside of the filamentous phage contains ss-DNA as its genetic material, while the outside surface is covered by peptides. The construction of a landscape phage involves the use of recombinant DNA techniques to insert a small section of foreign randomized DNA into a filamentous phage. The engineered landscape phage therefore displayed 4000 copies of the inserted peptides on its surface and can then be selected through phage display techniques against its target. A detailed discussion of landscape phages is provided in Chapter 2.

2.2. Sensor platform

The sensor platform is an integral part of any biosensor. It is responsible for transforming information about the specific interaction between the analyte and the recognition element into a measurable signal that can then be interpreted by the associated software.

In this dissertation, a magnetoelastic material is used as the sensor platform because it can be operated wirelessly and remotely and is low cost and easy to fabricate. Magnetoelastic materials are amorphous ferromagnetic alloys that change dimensions in

the presence of a magnetic field and can be made to oscillate at their characteristic resonance frequency when an AC magnetic field is applied. The landscape phages are immobilized on the sensor platform surface to form a magnetoelastic biosensor. As the target bacterium/spores are captured by the specific landscape phages immobilized on the sensor platform's surface, the additional attached mass decreases the resonance frequency of the sensor. Based on this change of frequency, the number of bacterial cells/spores that have attached to the sensor can be calculated and hence their binding affinity to phage estimated. The detailed working principle of the magnetoelastic sensor platform is discussed and reviewed in Chapters 2 and 3.

2.3. Advantages offered by magnetoelastic biosensors

Magnetoelastic biosensors have the potential to help us in many ways, including: 1) maintaining the safety of our food chain by providing a low cost way to monitor food quality as it progresses from the farm through industrial processing and the distribution system to the final consumer; 2) avoiding food-borne illness by providing a simple and portable system for on-site monitoring; and 3) making possible the early and rapid detection of potential bio-terrorism agents.

3. The objectives of this research

The main objective of this research is to investigate whether it is possible to simultaneously detect two different biological pathogens, one a bacteria and the other a spore, using the same type of magnetoelastic sensor platform. The usefulness of multiple magnetoelastic biosensors will be proven by the determination of sensitivity, pathogen-specificity and detection limits in aqueous environments.

This research can be broadly divided into five parts:

1) Design and fabricate the magnetoelastic (ME) biosensors. Improve their performance (surface environmental stability and the *Q*-factor of their frequency spectrum) through optimization of the ME platform surface conditions via Au layer coating and annealing.

2) Improve the binding sensitivity of the magnetoelastic biosensors by optimizing the bio-recognition element (bacteriophage).

3) Investigate the use of multiple biosensors for the simultaneous detection of *B. anthracis* and *S. typhimurium*.

4) Characterize the performance of the multiple sensor detection system in a flowing liquid environment by quantifying its sensitivity, specificity, detection limit and dynamic range.

5) Apply the magnetoelastic biosensor to the detection of bacterium/spores in real food-products (in this case, apple juice).

4. References

[1] P. S. Mead, L. Slutsker, V. Dietz, L. F. McCaig, J. S. Bresee, C. Sharpiro, P. M. Griffin, and R. V. Tauxe, "Food-related illness and death in the United States," *Emerging Infectious Diseases,* vol. 5, pp. 607-625, 1999.

[2] http://www.foodborneillness.com/, "About Foodborne Illness," 2005.

[3] S. F. Altekruse, M. L. Cohen, and D. L. Swerdlow, "Emerging Foodborne Diseases," *Emerging Infectious Diseases,* vol. 3, pp. 503-510, 1997.

[4] L. Slutsker, S. F. Altekruse, and D. L. Swerdlow, "Foodborne Diseases: Emerging Pathogens and Trends," *Infectious Disease Clinics of North America,,* vol. 12, pp. 199-216, 1998.

[5] T. J. Török, R. V. Tauxe, R. P. Wise, J. R. Livengood, R. Sokolow, S. Mauvais, K. A. Birkness, M. R. Skeels, J. M. Horan, and L. R. Foster, "A large community outbreak of salmonellosis caused by intentional contamination of restaurant salad bars," *JAMA,* vol. 278, pp. 389-395, 1997.

[6] E. C. Todd, "Costs of acute bacterial foodborne disease in Canada and the United States.," *International Journal of Food Microbiology,* vol. 9, pp. 313-326, 1989.

[7] C. A. Ryan, M. K. Nickels, N. T. Hargrett-Bean, M. E. Potter, T. Endo, L. Mayer, C. W. Langkop, C.Gibson, R. C. McDonald, and R. T. Kenney, "Massive outbreak of antimicrobial-resistant salmonellosis traced to pasteurized milk," *JAMA,* vol. 258, pp. 3269–3274, 1987.

[8] A. C. Voetsch, T. J. Van Gilder, F. J. Angulo, M. M. Farley, S. Shallow, R. Marcus, P. R. Cieslak, V. C. Deneen, and R. V. Tauxe, "FoodNet Estimate of the Burden of Illness Caused by Nontyphoidal Salmonella Infections in the United States," *Clinical Infectious Diseases,* vol. 38, pp. S127-S134, 2004.

[9] R. Berkow, *The Merck Manual of Diagnosis and Therapy 1992*, 16th ed.: Merck Publishing Group, 1992.

[10] CDC, "The Management of Acute Diarrhea in Children: Oral Rehydration, Maintenance, and Nutritional Therapy," *MMWR Weekly,* vol. 41(RR-16):1, 1992.

[11] CDC, "Preliminary FoodNet data on the incidence of infection with pathogens transmitted commonly through food---10 sites, United States, 2004," *MMWR* vol. 54, pp. 352-356, 2005.

[12] CDC, "Summary of Notifiable Diseases --- United States, 2006," in *MMWR Weekly*. vol. 55, 2008, pp. 1-94.

[13] CDC, "Multistate Outbreak of Salmonella Serotype Typhimurium Infections Associated with Drinking Unpasteurized Milk --- Illinois, Indiana, Ohio, and Tennessee, 2002--2003. ," in *NMWR Weekly*. vol. 52 (56), 2003, pp. 613-615.

[14] CDC, "Multistate Outbreak of Salmonella Serotype Tennessee Infections Associated with Peanut Butter --- United States, 2006--2007 " *MMWR Weekly,* vol. 56, pp. 521-524, 2007.

[15] "CDC broadens its investigation of salmonella outbreak," in *USA Today*, 2008-06-30.

[16] G. Christopher, T. Cieslak, J. Pavlin, and E. Eitzen, "Biological warfare: a historical perspective," *JAMA,* vol. 278, pp. 412-417, 1997.

[17] R. A. Zilinskas, "Iraq's biological weapons," *JAMA,* vol. 278 pp. 418-424, 1997.

[18] K. Alibek and S. Handelman, *Biohazard: The Chilling True Story of the Largest Covert Biological Weapons Program in the World*. New York, NY: Random House, 1999.

[19] P. Brachman and A. Friedlander, "Anthrax," in *Vaccines*, Philadelphia, PA, 1999, pp. 629-637.

[20] K. Myenye, S. Siziya, and D. Peterson, "Factors associated with human anthrax outbreak in the Chikupo and Ngandu villages of Murewa district in Mashonaland East Province, Zimbabwe," *Cent Afr. J Med. ,* vol. 42, pp. 312-315, 1996.

[21] "Investigation of bioterrorism-related anthrax: Connecticut, 2001," in *MMWR Morb Mortal Wkly Rep.* vol. 50, 2001, pp. 1077-1079.

[22] A. Carter, J. Deutsch, and P. Zelicow, "Catastrophic terrorism," *Foreign Aff. ,* vol. 77, pp. 80-95, 1998.

[23] A. R. McClain, "Rationale behind the events of September 11," *Newsweek,* vol. 18, pp. 10-22, 2001.

[24] "Health Aspects of Chemical and Biological Weapons," Geneva, Switzerland: World Health Organization 1970.

[25] J. Simon, "Biological terrorism: preparing to meet the threat," *JAMA,* vol. 278, pp. 428-430, 1997.

[26] M. Wagner, A. Moore, and R. Aryel, *Handbook of Biosurveillance*. San Diego: Academic Press, 2006.

[27] E. de Boer and R. R. Beumer, "Methodology for detection and typing of foodborne microorganisms," *International Journal of Food Microbiology,* vol. 50, pp. 119-130, 1999.

[28] V. A. Petrenko and G. P.Smith, "Phages from landscape libraries as substitute antibodies," *Protein Engineering,* vol. 13, pp. 589-592, 2000.

[29] V. A. Petrenko and G. P. Smith, "Vectors and Modes of Display," in *Phage Display in Biotechnology and Drug Discovery*, S. S. Sidhu, Ed. Bo Raton, FL, USA: CRC Press, Taylor & Francis Group, 2005, p. 714.

[30] V. A. Petrenko, G. P. Smith, X. Gong, and T. Quinn, "A library of organic landscapes on filamentous phage," *Protein Engineering,* vol. 9, pp. 797-801, 1996.

[31] V. A. Petrenko and I. B. Sorokulova, "Detection of biological threats. A Challenge for directed molecular evolution," *Journal of Microbiological Methods,* vol. 58, pp. 147-168, 2004.

[32] V. A. Petrenko and V. J. Vodyanoy, "Phage display for detection of biological threat agents," *Journal of Microbiological Methods,* vol. 53, pp. 253-262, 2003.

CHAPTER 2

LITERATURE REVIEW

1. Current Detection Methods

1.1. Enzyme-linked Immunosorbent Assay (ELISA)

ELISA (Enzyme-Linked Immunosorbent Assay), which may also be referred to as EIA (Enzyme Immunoassay), is a biochemical technique that is primarily used to quantify the presence of an antibody, hormone or an antigen in a sample [1]. ELISA has many applications. In the medical and plant pathology fields, for example, it is used to determine the concentrations of serum antibody (e.g. in tests for HIV [2] or West Nile Virus [3]) and the toxicity of certain classes of drugs [4]. In the food industry it is used as a rapid quality control test to identify the presence of food allergens such as milk, peanuts, walnuts, almonds, and eggs [5].

ELISA is based on the reaction between a substrate-specific enzyme and an appropriate antibody (specific to that antigen) to produce a visible signal. Older ELISAs utilized a chromogenic or color generation substrate to produce a visible signal, but newer ELISA assays employ a fluorogenic substrate, where the amount of fluorescence can be accurately quantified by a spectrophotometer, hence providing much higher sensitivity.

There are three types of ELISA: 1) “direct” or sandwich ELISA, which uses an immobilized antibody to detect the presence of a particular antigen in a sample; 2) indirect ELISA, which uses an antigen to look for a specific antibody in a sample; and 3) competitive ELISA, where the competitive binding abilities of two antibodies are determined by comparing the binding signals to their immobilized antigen.

Generally, indirect ELISA is used for determining the serum antibody concentrations. This method, shown in Figure 2-1, involves five-steps: 1) *Antigen immobilization* - a sample solution of a known antigen is added to a plate well and incubated for 1hour; 2) *Blocking* – the plate is washed with a buffer solution (PBS/tween) to remove any unbound antigens and a blocking buffer (e.g. Bovine Serum Albumin/casein) is added to the well. After incubation for another hour, the plate is again washed with a buffer (PBS/tween). This step blocks the non-specific absorption of other proteins onto the plate; 3) *Primary antibody immobilization* - primary antibodies specific to the antigens are added to the well and incubated for 1 hour, followed by washing to remove all unbound antibodies; 4) *Secondary antibody immobilization* - secondary antibodies that will bind with the primary antibody are added to the well and incubated for 1 hour. These antibodies are then conjugated to the enzyme to form an antibody-enzyme complex, which is then removed by washing with buffer solution (PBS/tween); 5) *Substrate reaction* - the specific substrate is reacted with the antibody-enzyme complex and incubated for color development. This final signal can be viewed/quantified using a spectrophotometer or spectrofluorometer.

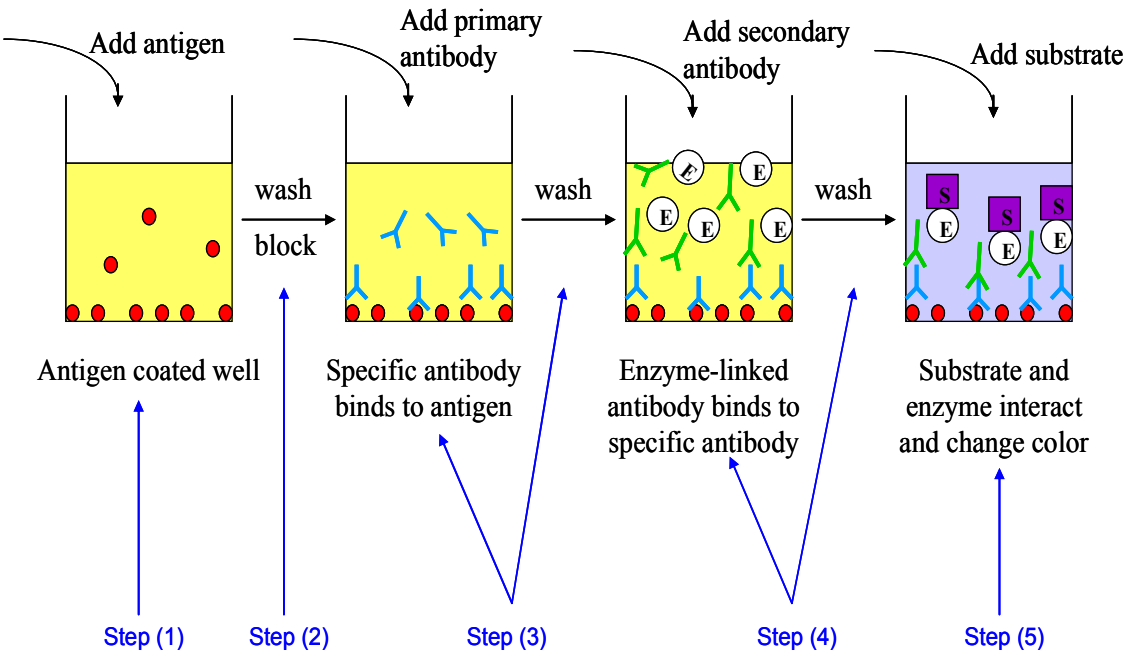

Figure 2- 1. Schematic of ELISA procedure for indirect ELISA.

In most cases, this final signal is quantified by measuring the optical density (OD) with a microplate reader. A standard curve is plotted as the concentration of standard antigen versus the corresponding mean OD value, and the sample concentration can then be interpolated from the standard curve. However, indirect ELISA suffers from two major disadvantages: 1) since the antigen immobilization on the well is non-specific, any protein in the sample will bind to the plate and produce a noisy signal; and 2) during the antigen immobilization, the analyte in the serum must compete with other serum proteins, thus decreasing the antigen protein binding levels.

In order to overcome these problems, the sandwich or direct ELISA was developed and used to detect sample antigens of biological warfare agents [6]. The procedure is shown in Figure 2-2 and is generally similar to that used for the indirect ELISA. The following steps are used in the sandwich ELISA method: 1) coat a known quantity of antibody to the plate well; 2) wash the plate with buffer solution (PBS/tween) and immobilize the blocking agent to block any non-specific binding sites on the well; 3) add the antigen solution to the plate to bind with the antibody, followed by washing with the buffer solution. After washing, the non-antibody binding antigens are washed free of the plate; 4) add primary antibodies to bind specifically to the antigen; 5) add the enzyme-linked secondary antibody (conjugate) to bind with the primary antibody. Wash the well again to remove the unbound antibody-enzyme conjugates; 6) add a chemical that will react with the enzyme on the secondary antibody to convert the enzyme into a fluorescent, electrochemical or color signal. The antigen can be quantified by measuring the absorbance, fluorescence or electrochemical signal (i.e. current). Compared to other ELISA methods, the sandwich ELISA has higher binding affinity because even for impure samples the antibodies still bind selectively with any antigens that may be present. Moreover, by using the primary antibody, the chance that any other proteins in the sample will adsorb non-specifically to the plate well decreases when the quantity of immobilized antigens increases. Generally, using a polyclonal antibody for ELISA will increase the number of possible detection objects, while a monoclonal antibody will improve specificity and lower background noise.

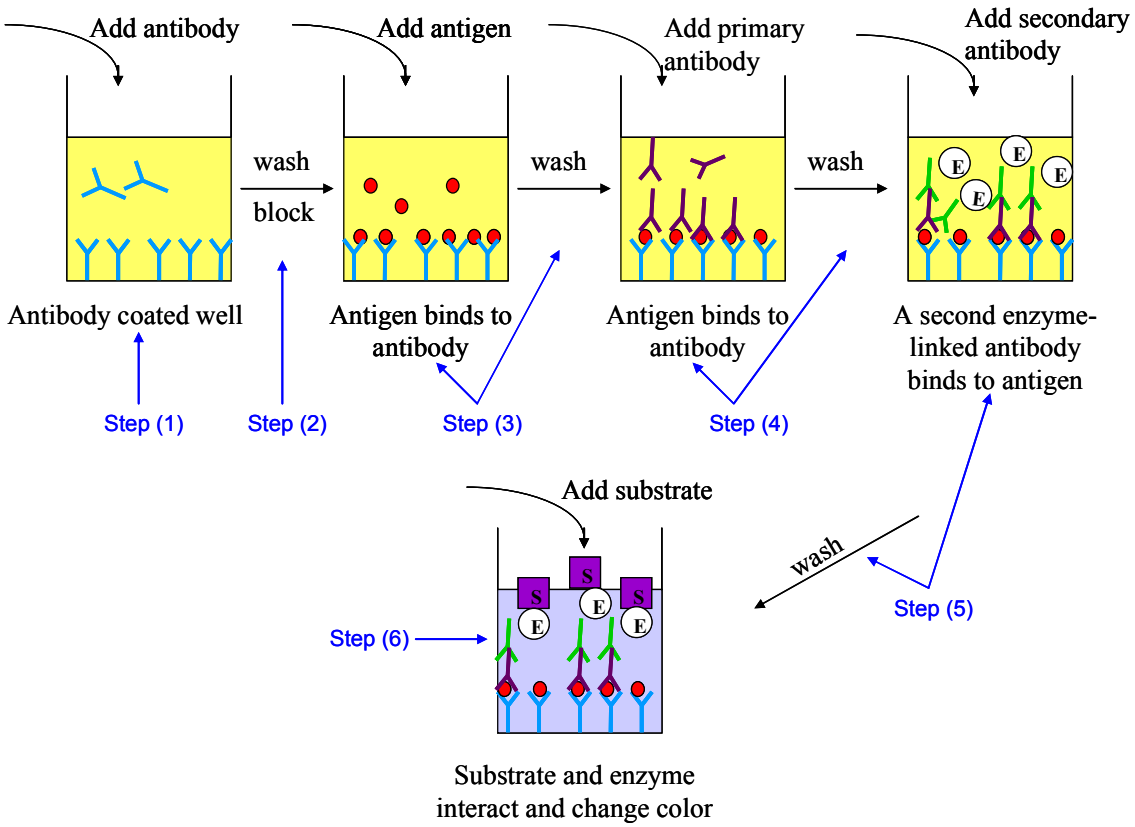

Figure 2- 2. Schematic of ELISA procedure for sandwich ELISA.

A third type of ELISA uses competitive binding and is therefore referred to as "competitive" ELISA. This method is somewhat different from the previous two. First, the unlabeled antibody is incubated in its antigen to form an antibody-antigen complex that is added to an antigen coated well and the unbound antibody washed away. The secondary antibody (specific to the primary antibody) which has been conjugated with the enzyme is then applied to the well, and a substrate added to react with the remaining enzymes to convert the bound antibody to a detectable signal (i.e. a chromogenic or fluorescent signal). This approach was dubbed "competitive" because

when the complexes are formed, the more antigens there are in the sample, the fewer antibodies will be able to bind to the antigen in the well, so the higher the original antigen concentration, the weaker the final signal.

Generally, an ELISA test uses at least one antibody. Sometimes only a single antibody is needed because it can directly conjugate with the enzyme to produce a detectable color change. However, if this antibody is not capable of direct conjugation, a secondary antibody is required that will both react with the primary antibody and conjugate with the enzyme. In most cases, even if the primary antibody can conjugate, a secondary antibody may still be used because it avoids the expensive process of creating specific enzyme-linked antibodies for every antigen of interest, making ELISA both less expensive and more convenient to use and thus greatly broadening the range of potential applications. ELISA is a serological test and is now one of the most commonly used immunological assays for detecting a particular antigen or antibody. It is also the first screening test and the most commonly used way of diagnosing HIV.

Unfortunately, there are some major disadvantages that make ELISA less than ideal for field applications. In Germany, indirect ELISAs have been used to detect *S. typhimurium* in blood serum and meat juice [7-10]. The results showed that the *Salmonella* ELISAs often lacked specificity, although they did have high sensitivity. ELISA is less economical and requires the use of sophisticated equipment and high maintenance fees. It is also very labor intensive and requires highly trained staff and special software to evaluate the results. As well as *S. typhimurium* detection, ELISA is

capable of detecting the germination of *B. anthracis* spores by looking at the antibody-spore complex [11, 12]. However, the procedures required for spore ELISA are complex, lengthy and need trained personnel to perform the test.

1.2. Polymerase chain reaction (PCR)

1.2.1. PCR principles and procedures

Polymerase chain reaction (PCR) is a vital tool that is used to amplify specific regions of a DNA strand (i.e. a single gene, a part of a gene, or a non-coding sequence). It derives its name from its core component, DNA polymerase, which is used to amplify a piece of DNA by enzymatic replication. Generally PCR methods consist of 20-40 cycles of replication. For example, the DNA polymerase enzyme first duplicates the original piece of DNA target and this is then split into two pieces. After separating, each piece will in turn replicating, resulting in four pieces of the original DNA target. This is the second replication cycle. This is repeated in a third cycle, and so on. This replication is exponentially amplified and is therefore called a “chain reaction”.

After each replication cycle, a high temperature (>90°C) is required to separate the two DNA strands in the DNA double helix. Consequently, the DNA polymerase must also be capable of withstanding high temperatures (>90°C). The discovery of Tag polymerase [13, 14] fulfilled this requirement, making the PCR reaction both easier and more rapid.

In order to set up a PCR process, several components and reagents are required [15]. These include: 1) a DNA template that contains the specific regions of DNA to be amplified. Although RNA could also be used as a target, DNA is more stable and easier to isolate; 2) a DNA polymerase (i.e. tag polymerase or another DNA polymerase with an optimum temperature of 70°C) that can duplicate the DNA target by enzymatic replication; 3) a buffer solution that provides the DNA polymerase with an optimum chemical environment to maintain good stability and activity; 4) two primers to complement the DNA strands at the 5' and 3' ends of the DNA target region; 5) Deoxymucleoside triphosphates (dNTPs) to block the DNA polymerases from synthesizing a new DNA strand; and 6) divalent cations (i.e. Mg^{2+} or Mn^{2+}) and a monovalent cation (i.e. K^{+}).

In PCR, a small amount of the DNA target is added in the test tube to the six components listed above. Each replication cycle of this mixture is composed of three steps (shown in Figure 2-3) that are mainly controlled by the temperature: 1) *Denaturation* - heat the reaction to a temperature of 94-96°C and hold for 1-9 minutes. This inactivates the DNase molecules in the target and causes the DNA template to denature into two single DNA strands. If the denaturation is not complete, the utilization of the template in the first replication cycle will be inefficient, resulting in a poor PCR product; 2) *Annealing* - lower the temperature to 50-65°C (3-5°C lower than the melting temperature of the primers) and incubate for 20-40 seconds, allowing the two primers to anneal their complementary DNA sequences. Only when both sequences of

primer and DNA match can the DNA-DNA hydrogen bonds be formed; and 3) *Extension* – raise the temperature to 72°C for one to several minutes, which allows the Tag polymerase to attach to each priming site (where the annealed primers are) and synthesize a new DNA strand. Since the temperature for this step is related to the optimum activity temperature required for the DNA polymerase, it will vary depending on the type of DNA polymerase used. The strands (including the synthesized and original strand) in this first amplification cycle will provide the template strands for the second cycle. Each cycle includes denaturation, annealing and extension steps. The amount of DNA target will double after the extension step in each cycle, resulting in exponential amplification of the DNA target. Since each cycle requires only a few minutes, more than a billion molecules of DNA can be produced in one hour. After the last PCR cycle, the temperature is kept at 70-74°C for 5-15 minutes to ensure that all the single strand DNA present is fully extended. Finally, the temperature is decreased and maintained at 4-15°C for short-term storage of the reaction products. Following amplification, the final PCR products are analyzed to confirm that the DNA fragment has the original defined length. Agarose gel electrophoresis is used to determine the length of the DNA fragments through comparison with a DNA ladder, which is made up of molecular weight markers containing DNA fragments of known size.

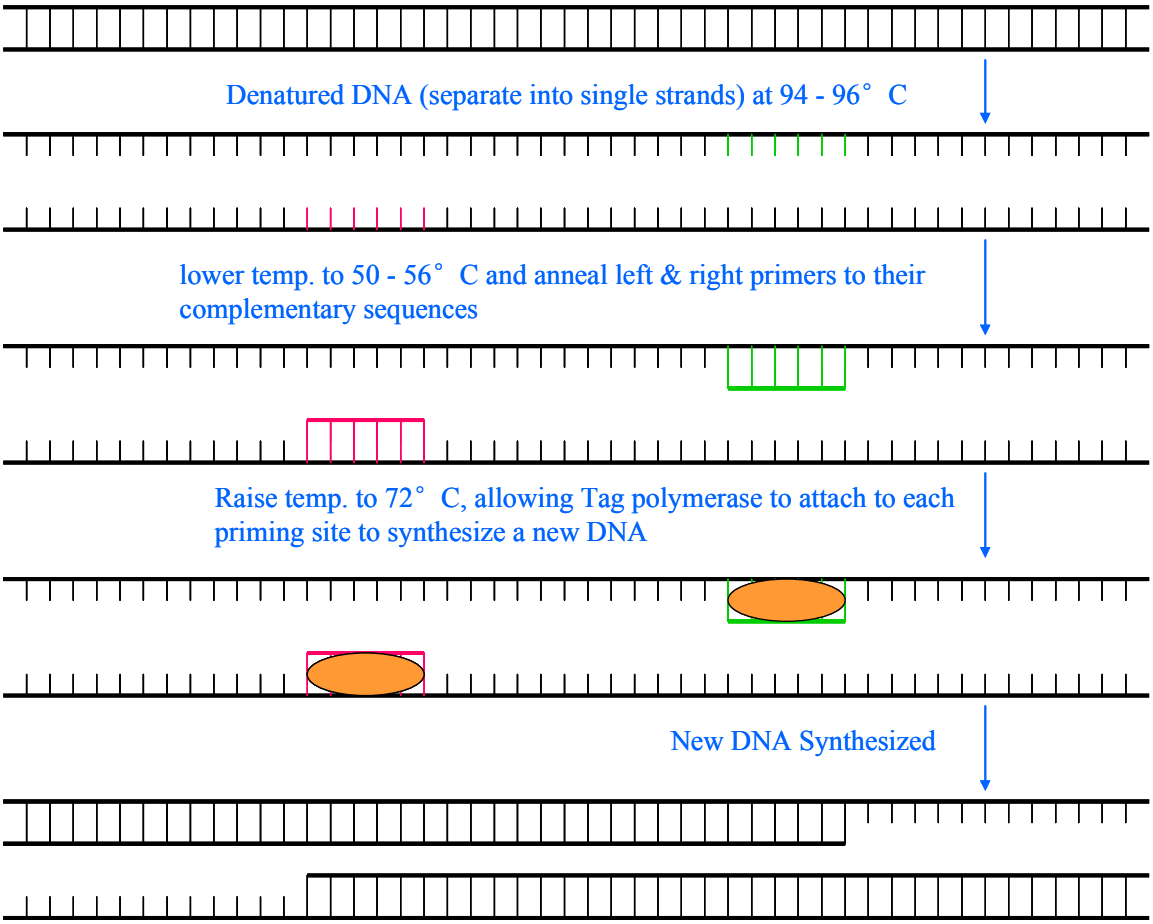

Figure 2- 3. Schematic diagram of PCR first replication cycle.

1.2.2. PCR applications

PCR has become one of the most common techniques and is widely used in such fields as molecular biology, clinical microbiology, forensic science, food safety, and many other applications [16]. In molecular biology, for example, the PCR technique can be used to selectively amplify a specific region of DNA and isolate the desired DNA fragments from genomic DNA. A large amount of specific DNA can be replicated without the need for large quantities of starting genomic DNA, making PCR particularly

useful for DNA cloning procedures and Southern blotting [16]. Additionally, PCR allows rapid screening of bacterial colonies for correct DNA vector constructs [17]. In clinical microbiology, PCR is used to diagnose microbial infections in epidemiological research. In forensic science, PCR is invaluable because even tiny amounts of DNA obtained from a droplet of blood or a single hair are now enough for amplification and analysis. PCR can also be used for genetic fingerprinting to identify a person or organism. In food safety, PCR is used to detect bacterial pathogens in water [18], milk, chicken fecal samples [19], and ground beef [20] and has been used to detect *B. anthracis* [21-23] in a variety of mediums.

Overall, PCR offers advantages such as high sensitivity, low detection limit and rapid replication. It is also very robust, and is capable of amplifying specific sequences from a few DNA molecules. However, several disadvantages do limit its use: 1) a number of techniques and procedures are required to optimize the PCR conditions and even a minor contamination of sample DNA can yield spurious results; 2) the selection of a suitable primer is also a challenge due to the need for some prior knowledge of the target DNA sequence; and 3) trained personnel, along with extremely clean and controlled environments, are required.

2. Biosensor Methods

The use of biosensors has increased dramatically in recent years. As defined in the Oxford English Dictionary, *a sensor is a device that detects or measures a physical property and records, indicates or otherwise responds to it* and a biosensor does this by applying biological agents in the detection process. There are two main parts to a biosensor: its transducer and its bio-receptor. Figure 2-4 shows a schematic representation of a biosensor that uses a bio-sensing element as its bio-receptor, along with a transducer system and the associated electronics or signal processors that display the results in a user-friendly way [24].

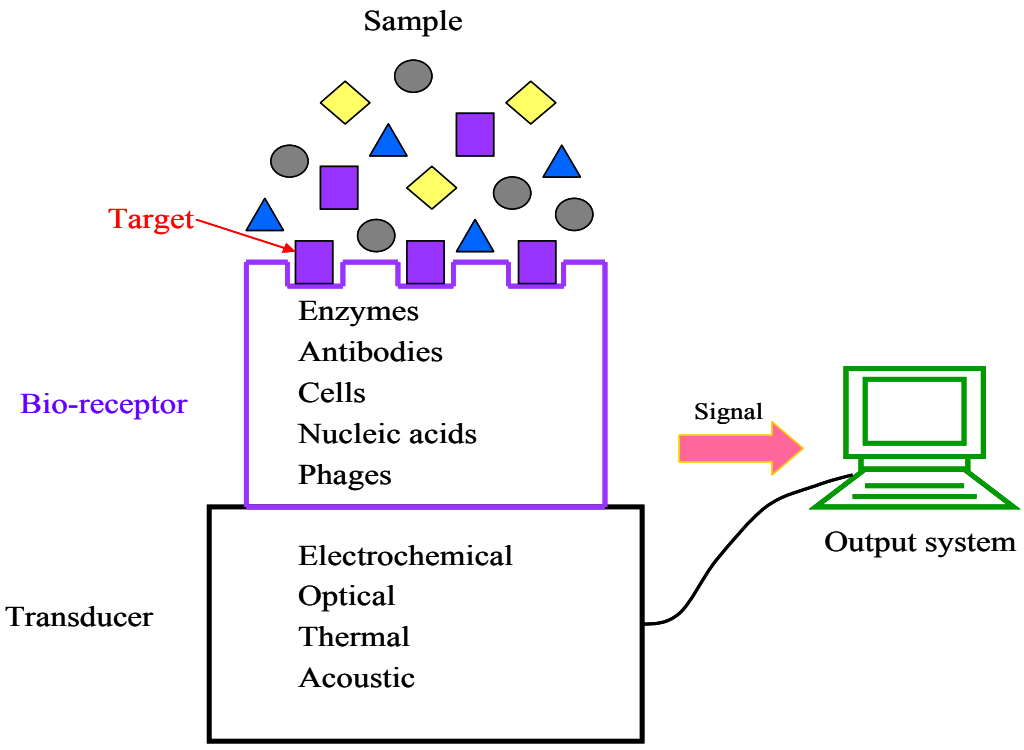

Figure 2- 4. Schematic configuration of a biosensor.

When a specific biological reaction occurs between the bio-sensing element and the interested target antigens it causes a physical and/or chemical change on the bio-interface. The transducer is responsible for converting this change into a measurable signal. This signal will then be sent to the output system to be amplified, processed and displayed [25].

Sensors can be divided into three types, namely physical, chemical, and biological. As their name suggests, physical sensors measure physical quantities such as length, weight, temperature, and pressure, while chemical sensors respond quantitatively to a particulate analyte in a selective way through a chemical reaction. Biosensors incorporate a biological sensing element, which is connected to the transducer.

Biosensors are now being used in many fields, for example industrial process monitoring, environmental monitoring, food-borne pathogens detection and medical care. The most popular medical application of biosensors is to monitor glucose levels in diabetic patients. One particularly desirable goal for medical biosensors is to create a type of implantable biosensor capable of continuously monitoring a metabolite; an implantable glucose biosensor would allow patients to continuously measure their glucose level in real time and adjust their medication accordingly. Biosensors also offer many advantages in detecting chemicals and food-borne pathogens compared to the conventional methods mentioned previously (Chapter **2** Sections **1.1.** & **1.2.**). They are not only highly target specific and sensitive, but also respond rapidly, making them ideal for real-time detection. Some are even reusable and portable for on-the-spot analysis.

2.1. Bio-recognition Elements

Bio-recognition elements, generally referred to as bio-receptors, include enzymes, tissues, antibodies and phages. Among these, antibodies and bacteriophages are the most commonly used biological components.

2.1.1. Antibodies

Antibodies, or immunoglobulins (Ig) [26], are produced by B cells, a type of white blood cell. These immune - system related proteins are present in the blood or other bodily fluids of vertebrates [26]. Since antibodies are capable of identifying and neutralizing foreign objects, they have become widely used diagnostic tools to detect bacteria and viruses.

Two large “heavy” chains and two small “light” chains form a basic antibody structural unit, which takes the “Y” shaped structure shown in Fig. 2-5. Disulfide bonds connect these two chains [27]. Each “heavy” chain consists of a constant region and a variable region. Based upon the types of “heavy” chain, antibodies can be classified into several different isotypes. In mammals, there are five different antibody isotypes (IgA, IgD, IgE, IgG and IgM) which are responsible for directing the appropriate immune response to the corresponding foreign objects they encounter [28]. For each antibody, only one type of “light” chain will be present, which also consists of constant and variable domains. At the tip of each antibody there is a small region, known as the hyper-variable region, that makes the tip structures of antibodies slightly different from

each other, enabling a huge diversity of antibodies capable of binding with an equally diverse range of targets, known as antigens [29]. The antigen has a unique part called an epitope that binds with an antibody, therefore the binding between antigen and antibody is highly specific. The tip of the antibody "Y" structure (Figure 2-5) is referred to as the "Fab" region and contains one constant and variable domain from both the "heavy" and "light" chains [30]. The base of the "Y" is called the "Fc" region, which contains two or three constant domains from two "heavy" chains [29].

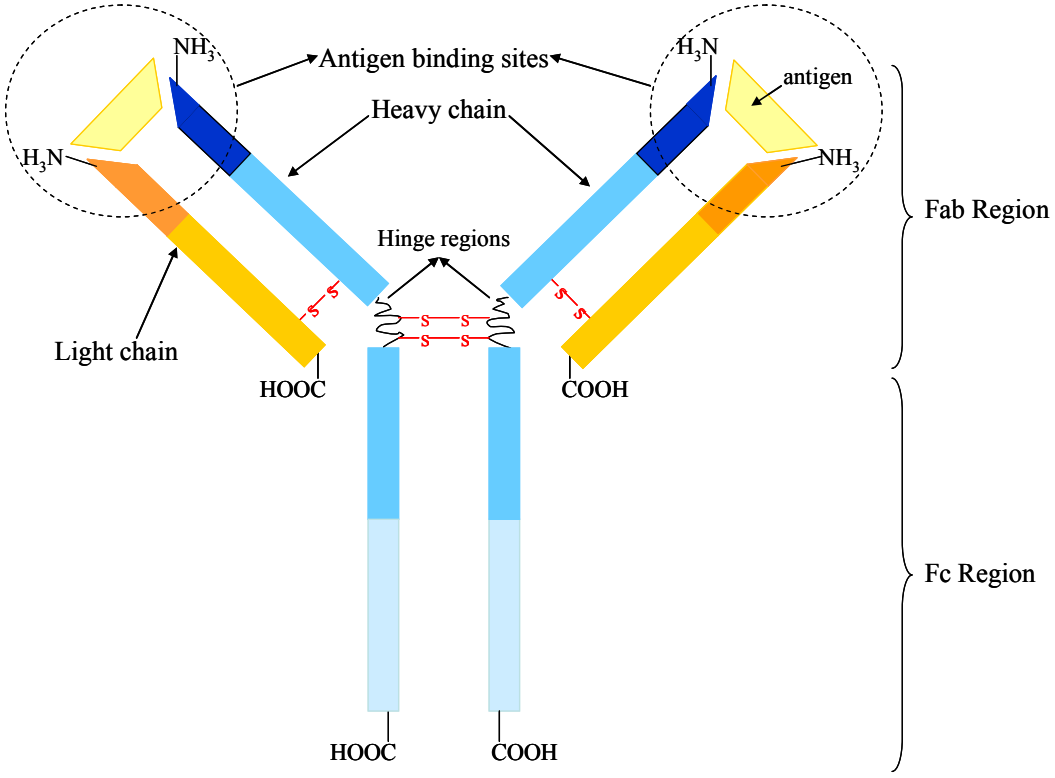

Figure 2- 5. The structure of an antibody.

In the immune system, antibodies can bind to pathogens to protect cells from being damaged. Polyclonal and monoclonal antibodies (mAb or moAb) are two kinds of antibodies widely generated for different research applications. Polyclonal antibodies are derived from many different B cell lines within the blood. They are a mixture of Ig molecules specific to an antigen, each recognizing a different epitope. They are produced by injecting the antigen into a mammal (i.e. goat, horse, rabbit or mouse), after which the antibodies are isolated from the blood/serum. Monoclonal antibodies are derived from a single cell line and are identical and secreted against a specific antigen. This characteristic allows them to inherit the original antibody's excellent performance. To produce monoclonal antibodies, antibody-secreting lymphocytes are fused with a cancer cell line after isolating from animals, and then grown in a culture.

Both polyclonal and monoclonal antibodies need to be purified by protein A/G or antigen-affinity chromatography [31]. Compared with polyclonal antibodies, monoclonal antibodies provide higher purity with less background. They also give higher homogeneity for more reproducible experimental results and higher specificity for efficient binding with the antigen.

Antibodies can be produced against almost any component, from small drug molecules to intact cells, and have become a key affinity ligand for both medical and research applications [32]. Medically, antibodies are used for disease diagnosis [33, 34], including determining the cause of liver damage in patients [35]. They are also used for disease therapy and prenatal therapy. For example, monoclonal antibodies offer useful

treatments for diseases such as multiple sclerosis [36], psoriasis [37] and many forms of cancer (i.e. non-Hodgkin's lymphoma [38], head and neck cancer and breast cancer [39]). In research, antibodies are used in a purified form to identify and locate proteins. For example, antibodies are used in flow cytometry to distinguish cell types based on the proteins they express [40] and also in immunoprecipitation to separate proteins from other molecules by binding to them [41]. In microscopy and electrophoresis, antibodies are used to examine protein expression and locate them for western blot analyses and immunohistochemistry [42, 43]. ELISA techniques [44, 45] make possible the quantification of proteins using antibodies. Since antibodies can bind with foreign substances, they are also required for many immunological assays, including immunochromatographic lateral flow assays [46], time-resolved fluorescence (TRF) assays [47], and immunomagnetic separation-electrochemiluminescence (IMS-ECL) assays [48, 49].

Currently, antibodies are being applied as a bio-recognition layer on sensors for the specific capture of analytes [32]. Antibody-based sensors offer several advantages: there is no need for extensive sample clean-up and they require only limited hands-on time, while at the same time offering high-throughput screening, real-time analysis, label-free detection and the possibility of quantification [32]. There are several different types of antibody-based biosensors in use, namely surface plasmon resonance (SPR) sensors, quartz crystal microbalances (QCR) and cantilevers. They have become well-established techniques for the detection of the pathogens *E. coli* [50], *Salmonella*

cells [51, 52], *B. cereus* and *L. monocytogenes* [53, 54]. Overall, antibody-based sensors are quite effective, adaptable for many applications and hold great promise in the field of research.

However, antibodies are generally quite fragile. When exposed to unfavorable environments, they tend to lose sensitivity and their other binding characteristics deteriorate. The quality of antibodies can also vary depending on the animal used to produce them and other production variables. Polyclonal antibodies are cheap but lack specificity, purity and are limited in the amount of serum that can be obtained from each immunized animal. While monoclonal antibodies have single epitope specificity (i.e. are highly selective) and can thus potentially provide unlimited amounts of identical antibodies, they are relatively expensive to produce, inherently unstable, and are very sensitive to harsh environments. In most biosensor applications, in order to use antibodies affinity purification and stabilization are required, which dramatically increases their cost. All of these limitations have limited the application of antibodies.

2.1.2. Bacteriophages

2.1.2.1. Fundamentals of Bacteriophages

Bacteriophages, or phages, are viruses that infect only bacteria but are much smaller in size (20-200 nm). Modern phage research began in 1915, when Frederick Twort, a British bacteriologist, discovered “a small agent that infected and killed bacteria.” Later in 1917, French-Canadian microbiologist Félix d'Hérelle dubbed this

agent a “bacteriophage” or “bacteria-eater.”

Each bacteriophage contains an outer protein hull (or lipoprotein coat, or capsid) and an enclosed nucleic acid genome. The enclosed genome can be ssRNA (single stranded RNA), dsRNA (double stranded RNA), ssDNA or dsDNA. These RNA/DNA strands have a circular or linear arrangement which is 5-500 kilo base pairs long.

Phages are absolute parasites, found ubiquitously wherever their bacterial hosts live, for example in soil, sewage, animals [55], deep sea vents, water and the food we consume [56]. Consequently, phages are estimated to be the most widely distributed and diverse entities (ranging from 10^{30}-10^{32} in total population) on the earth [57]. Each phage infects a specific group of bacteria, a subset of one species [56], although in some cases several related species can be infected by the same phage. Phages play a key role in regulating the microbial balance in every ecosystem [56]. They are highly specific and reproduce rapidly in appropriate hosts. Also, phages are very robust and retain their ability to infect for decades, even when there are no appropriate hosts available.

The general infection process for bacteriophages is: 1) *adsorption* – the phage binds to a specific receptor (i.e. a surface molecule or capsule) on the surface of its target host; 2) *penetration* - the genome of the phage passes into the host cell; 3) *synthesis of protein and nucleic acid* – once the normal synthesis of protein and nucleic acid of the bacteria host has been inactivated, the helper proteins that help assemble new copies of the phage are produced; 4) *morphogenesis* – new phages are constructed with the assistance of the helper proteins; and 5) *cell lysis* - phages are released into the host cell

via lysis, by extrusion, or, in a few cases, by budding.

2.1.2.2. Bacteriophage classification

Based on their life cycle, phages can be classified as either virulent or temperate. Virulent phages multiply only by the lytic cycle, where the phage first attaches to the host cell and injects its own genome to take over much of the host metabolism, after which new phages are liberated after the host cell lyses. Temperate phages, in contrast, have modes of replication that do not destroy the host bacteria.

The classification of bacteriophages is difficult but practical for phage research. The International Committee on Taxonomy of Viruses (ICTV) classifies bacteriophages based on their morphology and the type of nucleic acid they enclose. Recently, Ackermann studied 5000 bacteriophages by electron microscopy, making this the largest category of viruses examined by microscopy methods so far [56]. Table 2-1 provides an overview of bacteriophage classification. These phages take one of four different shapes: tailed, polyhedral (with cubic symmetry), filamentous (with helical symmetry), and pleomorphic (without obvious symmetry). Most of these classified phages contain dsDNA, while only a small group contains ssDNA, ssRNA or dsRNA. The dsDNA tailed phages are the major phages (95% of all those reported) on the planet [57] and also the oldest viruses [58]. Tailless phages only include about 190 known viruses and account for less than 4% of the currently recognized bacterial viruses. They are classified into 10 families [59].

Table 2- 1 Classification of bacteriophages

Shape	**Family**	**Morphology**	**Nucleic acid**
Tailed	*Myoviridae*	Non-enveloped, contractile tail	Linear dsDNA
	Siphoviridae	Non-enveloped, long non-contractile tail	
	Podoviridae	Non-enveloped, short noncontractile tail	
Polyhedral	*Microviridae*	Non-enveloped, isometric	Circular ssDNA
	Tectiviridae	Non-enveloped, isometric	Linear dsDNA
	Corticoviridae	Non-enveloped, isometric	Circular dsDNA
	Leviviridae	Non-enveloped, isometric	Linear ssRNA
	Cystoviridae	Enveloped, spherical	Segmented dsRNA
Filamentous	*Lipothrixviridae*	Enveloped, rod-shaped	Linear dsDNA
	Inoviridae	Non-enveloped, filamentous	Circular ssDNA
	Rudiviridae	Non-enveloped, rod-shaped	Linear dsDNA
Pleomorphic	*Fuselloviridae*	Non-enveloped, lemon-shaped	Circular dsDNA
	Plasmaviridae	Enveloped, pleomorphic	Circular dsDNA
	Guttaviridae	Droplet-shaped	Circular dsDNA

2.1.2.3. Applications of bacteriophages

Bacteriophages have been discovered to have many applications. They have been successfully used for treating bacterial infections in the medical field due to their antibacterial activity, while environmentally bacteriophages haves been used in hydrological tracing in river systems and as a dye marker due to their low adsorption when passing through ground-water and ease of detection at low concentrations [60]. Phages also have many uses in food production. In 2006, the United States Food and Drug Administration (FDA) approved the use of a bacteriophage to kill the *Listeria monocytogenes* bacteria on cheese [61]. Fluorescently labeled phages can serve as a recognition element for the detection of *S. typhimurium* and *E. coli* [62, 63].

Antibodies were the first proteins to be displayed on the surface of a phage [64]. This was achieved by fusing the coding sequence of the antibody variable regions to the amino terminus of the phage minor protein coat pIII. This type of phage-antibody combination is particularly useful for biological detection and has been demonstrated to have higher performance than monoclonal antibodies when used in several different assay formats, including surface plasmon resonance (SPR), flow cytometry, ELISA, and hand-held immunochromatographic assays [65, 66].

Recently, the landscape phage technique has been developed [67, 68]. This technique bypasses one of the most troublesome steps in phage-antibody technology, which requires the reengineering of selected antibody genes in order to express them at a high level [67]. These phage bio-probes have begun to be used as a biological

recognition molecule for acoustic wave devices such as thickness shear mode quartz sensors [69] and magnetoelastic sensors [70-72] for the real-time detection of a range of pathogens or the adsorption of biochemical macromolecules [73].

2.1.2.4. Phage display

Phages play an important role in molecular biology. For example, they are commonly used as a vector to infect the standard recombinant DNA host (bacterium *E. coli*) in recombinant DNA research. The method of using a phage as a vector to connect proteins to display genetic information, so-called "phage-display", has many applications, including: 1) the determination of the interaction partners of a protein, diagnosis and therapeutic targeting [74]; 2) the search for protein-DNA interactions [75]; 3) efforts to identify new ligands (i.e. enzyme inhibitors) to target proteins [76-78]; and 4) the selection of antibodies and peptides [79-81]. Tens of billions of heterogeneous phage clones can be collected together to create a "phage display library". Each clone displays multiple copies of a specified peptide on the virion surface [68, 82, 83], and a phage display library can be used to select high specificity phages to an immobilized molecule and then multiply these phage clones for further study.

2.1.2.5. Filamentous phage fd

The filamentous phage Ff class, which includes M13, f1, and fd phages, has been the subject of extensive research for phage display applications [83, 84]. Filamentous phage fd is a phage shaped like a rod filament, as shown in Figure 2-6. Each phage

filament is generally about 7 nm wide and 800-900 nm long. The outer coat is a tube like structure composed of a major protein coat pVIII, which has a single-stranded DNA buried inside. At the tip ends of the phage particle, there are several copies of four minor proteins, pIII, pVI, pVII, and pIX [85, 86]. The major protein coat occupies 98% of the phage's mass and is present in 2700 or more copies per phage.

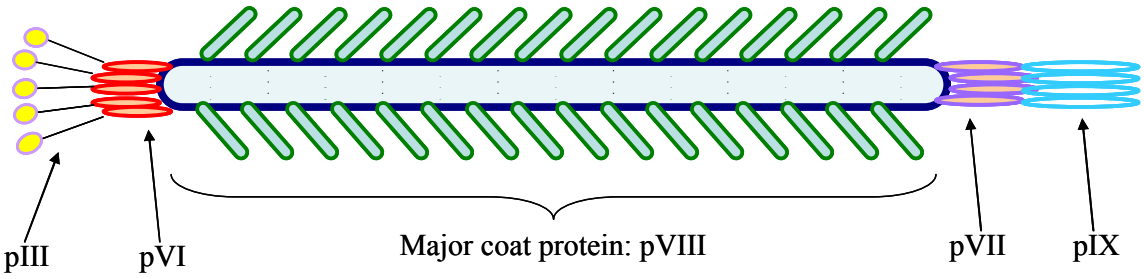

Figure 2- 6. Schematic showing filamentous phage structure. pIII, pVI, pVIII, pVII, pIX represent phage proteins. Exogenous peptides are usually displayed on protein pIII and pVIII.

In this dissertation, two types of phage clones are used, namely JRB7 and E2. Unlike common phage filaments, JRB7 and E2 have both been modified by using phage filaments as the framework and then fusing eight foreign random amino acids to the N-terminus of every copy of the major protein coat pVIII. Studies have shown that the replacement of three or four amino acids at the N-terminus of the protein pVIII with 12-19 foreign amino acids in a filamentous phage will not disturb the general architecture

of the virions [87]. Since the array of thousands of copies of these guest peptides appear in a repeating pattern, a dramatic change in the phage surface architecture occurs, resulting in the number of major protein coat subunits increasing to 4000. The major protein coat now comprises up to 50% of the phage surface [67, 68]. This modified phage is called a "landscape phage" and a mixture of a large number of such landscape phages is named a "landscape phage library," encompassing billions of phage clones with different surface structures and biophysical properties [88].

Landscape phages are now being investigated as a possible alternative to antibodies for detection probes, as they are more stable, reproducible, and inexpensive to produce [68, 89]. They are extraordinarily robust in harsh environments, and can be heated up to 80 ºC [83], as well as being resistant to organic solvents (e.g., acetonitrile), acid, alkali, and other chemicals [90]. Purified phages can be stored indefinitely at moderate temperatures without loss of infectivity and probe-binding activity. More importantly, phages have a high affinity to target antigens. This is because phages have an extremely high surface density (300-400 m^2/g) and up to 50% of the surface can be subtended by peptides to form the "active receptors" sites. This high density of binding sites exceeds that of the best-known absorbents and catalysts. The thousands of phage filaments also provide far more opportunities for binding.

2.2. Transducers

The transducer is the most important part of a sensor because it is responsible for detecting the analyte. There are four main types of transducers, namely electrochemical transducers, optical transducers, thermal sensors, and acoustic devices. Figure 2-7 lists these, along with some sensor examples of each type. In this dissertation, we will focus on using magnetoelastic material as the transducer, which can be considered to be a novel type of acoustic wave device.

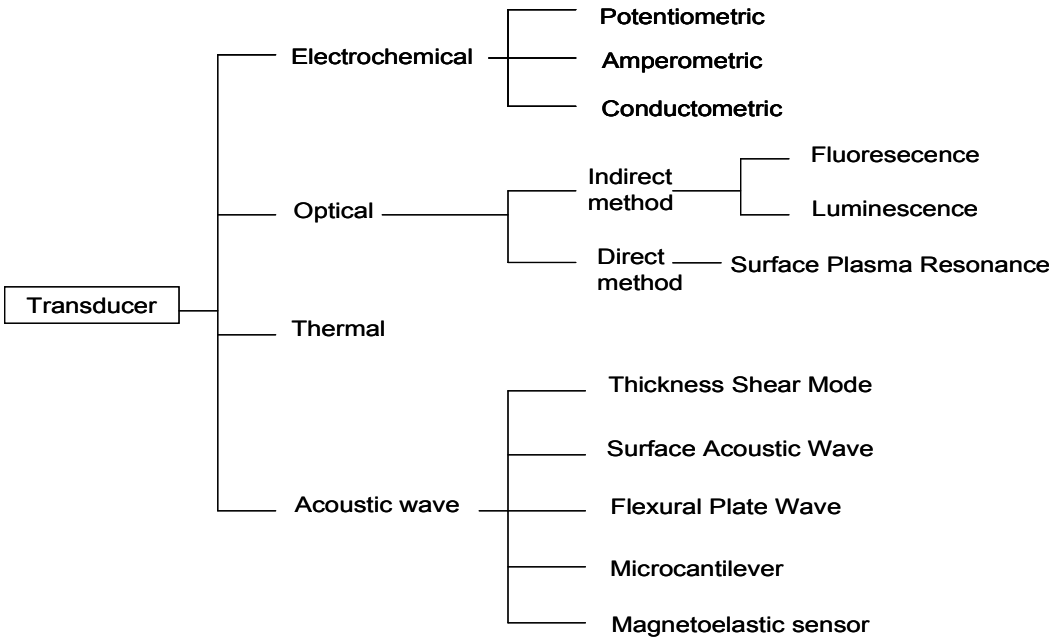

Figure 2- 7. Classification of sensor transducer types.

2.2.1. Electrochemical biosensors

Electrochemical biosensors are the most commonly used class of biosensors [91]. Their working principle depends on a bio-interaction occurring where an electrochemical species (e.g. electrons) are generated or consumed to produce an electrochemical signal which can be measured by an electrochemical detector. Based on the type of electrical signal, electrochemical sensors can be classed [91, 92] as either *potentiometric*, where the potential difference between an indicator and a reference electrode is measured, *amperometric*, where the current produced by an electrochemical oxidation or an electroactive species reduction under a constant potential is measured, or *conductometric/impedimetric*, where the alternating conductance between a pair of metal electrodes is measured [93, 94].

When the biological components interact, the conductance or capacitance of the medium will increase with decreasing impedance, so by measuring this change a conductometric biosensor is able to detect the concentration and physiological state of food-borne pathogens [95].

In potentiometric biosensors, the transducer can be either an ion-selective electrode (ISE) or an immunoelectrode. For ISE, when the target ions bind to the selective membrane at the indicator electrode, this results in a detectable difference in the potential between the indicator and reference electrode that is proportional to the logarithm of ion activity [91]. For the immunoelectrode, enzymes or antibodies are usually immobilized on the electrode surface and when target antigens in the sample

interact with enzymes or antibodies, there is a detected potential shift. This method is useful in biosensing [92, 96].

An amperometric biosensor measures the current generated by a chemical/biological reaction rather than measuring the potential change. By using an enzyme to catalyze electrooxidation or electroreduction, almost all microorganisms can be sensed by amperometric biosensors. An amperometric system has a linear relationship with the analyte concentration, which makes it particularly convenient and suitable for bacterial detection [96], such as *Staphylococcus aureus* [97, 98], *Salmonella* [99], and *E. coli* O157:H7 [100, 101].

Some advantages of electrochemical sensors include their high sensitivity, small size, low cost, versatility, rapid measurement time, and capability of stand-alone operation [102]. However, amperometric sensors suffer from poor selectivity, which is controlled using the redox potential of the electroactive species in the sample solution.

2.2.2. Optical biosensors

The working principle of optical biosensors is based on the modulation of optical properties that occurs when the bio-recognition element interacts with the target analytes on the interface. These optical properties include UV absorption, bio- and chemi-luminescence, reflectance, and fluorescence [103-107]. Applications of optical sensors include the measurement of pH, oxygen, carbon dioxide, and ions. Moreover, they are very attractive for the label-free and quick detection of bacteria [108].

Depending on the type of interaction that produces the output signal, optical devices are classified as either *indirect* or *direct*. Methods that utilize the fluorescence or bio-luminescence that results from antigen-probe interactions are defined as indirect methods, while those based on a direct change in the light properties due to the analyte-probe interactions are defined as direct methods. The total internal reflection of light incident at the interface, which depends on the refractive index, is an example of a direct optical method.

Some biospecies emit light with a lower wavelength when exposed to ultraviolet light, which is known as fluorescence [96]. Fluorescence biosensing is a type of optical biosensing method by frequency change, which includes direct sensing, indirect sensing, and fluorescence energy transfer (FET). Fluorescence spectroscopy is widely used for analytical chemistry, and offers a sensitive technique for low concentration analyte detection.

Some living microorganisms emit light when a biochemical reaction takes place, which is known as bioluminescence, and this is important for real-time monitoring. Luminescence biosensors have very high specificity but suffer from poor sensitivity when the concentration of target analyte becomes low [109]. Biosensors that monitor the color change in response to toxins produced by microbial pathogens in the presence of testing analytes are known as colorimetric biosensors. For example, a colorimetric whole cell bioassay [110] can be used for the detection of environmental pollutants.

Optical transducers incorporate optic fibers, which allows for greater flexibility and miniaturization. Surface plasmon resonance (SPR), where the surface plasmons are excited by light, is a very attractive optical biosensor transducer for many applications. The operational principles of an SPR biosensor are shown in Figure 2-8. It consists of two types of material with two different refractive indices: metal (gold) and glass. On the metal (gold) surface, incident light energy excites electrons to oscillate resonantly forming surface plasmons. SPR is excited along the metal surface at a specific incident angle (θ), at which the intensity of the reflected light reduces to minimum. Since this surface wave is on the boundary of the surface, the oscillation becomes sensitive to the environment of the metal surface. Any change on the metal surface such as an antibody-antigen interaction results in a change in the SPR angle (θ). Therefore, SPR biosensors can be used to detect food-borne pathogens by measuring this shift [111]. The advantages of SPR biosensors are that they are simple, real-time, and label-free. However, they are relatively expensive and it is hard to measure the target species when the concentration is very low. Also the signal of SPR biosensor is vulnerable to interference from the environment [96, 112].

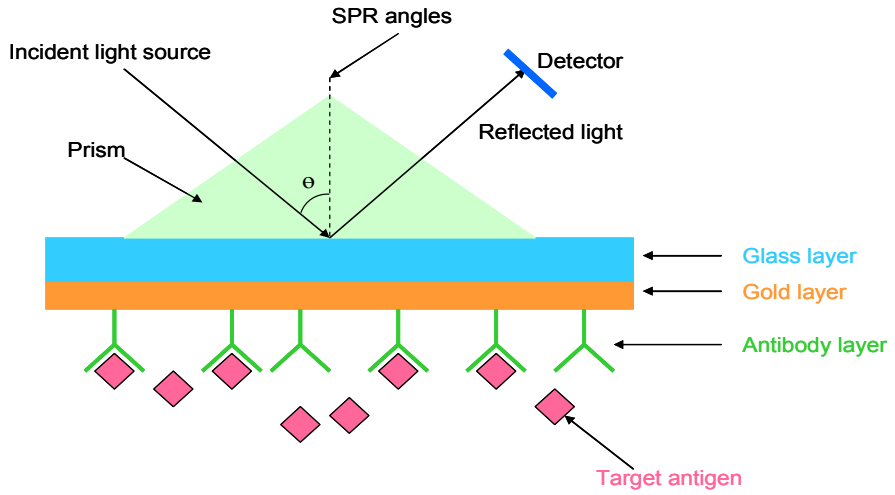

Figure 2- 8. Operational principles of an SPR biosensor.

2.2.3. Thermal biosensors

Thermal transducers involve the production or absorption of heat. They measure the concentration of an analytes based on the amount of heat adsorbed by a thermistor. Thermal sensors can either be used to measure the change in temperature of a substance directly during the course of a reaction or to measure the enthalpy of change in an enzymatic reaction.

2.3. Acoustic wave sensors

Recently, a great deal of attention has been devoted to efforts to develop simple and inexpensive microsensors. Among these, the acoustic wave (AW) sensor is a common device that has been used for many chemical and biological applications. Examples include sensors to monitor pressure, vapor, humidity, temperature, and film characterization. AW devices are very sensitive to small changes in many different

physical parameters [113]. They have been commercially available for more than 60 years because they offer real-time and fast detection, and are sensitive, simple to use, intrinsically reliable, and cost-effective [113]. Some can also be used wirelessly.

2.3.1. Operating principles and performance criteria

AW devices typically generate a mechanical or acoustic wave that propagates either through the bulk material or on its surface. The velocity and/or amplitude of this wave will change if the propagation path or its characteristics change in any way. Consequently, any variation that is observed in the properties of the acoustic wave, i.e. its velocity and/or amplitude, can be linked to corresponding changes in the material's physical characteristics, thus allowing them to be monitored in real-time by the AW sensor.

AW sensors usually use a piezoelectric material as the platform. When an oscillating electrical field is applied to the piezoelectric platform, a mechanical wave is generated. This phenomenon is known as the “converse piezoelectric effect.” The “direct piezoelectric effect” is the reciprocal of this and refers the application of strain to the material which results in the creation of an electrical change. The direct piezoelectric effect was discovered by brothers Pierre and Paul-Jacques Curie in 1880 and is defined as piezoelectricity [114]. Most AW piezoelectric sensors utilize the principle of converse piezoelectricity. When the acoustic wave produced propagates through or on the surface of the substrate, the velocity or amplitude of the wave will

change if the characteristics of the propagation path change. The frequency or phase characteristic of the sensor is measured to monitor such changes, which can then be correlated to the corresponding physical quantity.

An AW sensor can also be used as a mass sensor; when an AW device is used as a resonator, the resonance frequency of the AW device will change when there is a mass load on the device surface. Based on this principle, different biosensors can be developed by immobilizing a bio-molecular recognition layer (i.e. antibody, bacteriophage) on the AW sensor surface. When the target pathogen and the biomolecular recognition layer undergo a chemical reaction or sorptive interaction (i.e. adsorption / absorption) on the sensor's surface, the surface mass changes. This mass change can be detected by measuring the resulting shift in the characteristic resonance frequency of the sensor. Therefore, the majority of analytical applications of AW sensors are based on changes in mass loading.

There are extensive reviews and comparisons of different AW sensors in the literature [113, 115-117] based on their thermal stability, array capability, and so on. Mass sensitivity and the precision in determining the resonant frequency are the two main parameters used to characterize the performance of these sensors. Their theoretical treatment goes back to 1885, when Rayleigh suggested a link between surface mass loading and resonant frequency change [118], arguing that the resonance in a mechanical system occurs at frequencies where the peak kinetic energy U_k exactly balances the peak potential energy U_p. This general relationship between mass-loading Δm and frequency

shift Δf_m can be expressed by equation (2-1):

$$S_m = -\frac{df}{dm} \qquad (2\text{-}1)$$

where S_m is the mass sensitivity, m is the absolute mass of load, and f is the resonance frequency under mass load (m). The mass sensitivity S_m is widely used to compare sensors in terms of their ability to detect a small mass such as a single spore / bacteria cell [117, 119]. Since the mass sensitivity is related to the resonance frequency, the precision to which the resonance frequency can be determined is another parameter that affects the overall performance of an AW sensor. Precision is described by the quality merit factor (Q factor), which represents the spectrum quality. A higher Q value enables a more accurate determination of the resonance frequency. The Q-factor is given by equation (2-2).

$$Q = \frac{f_0}{\Delta w} \qquad (2\text{-}2)$$

where f_0 is the resonance frequency and Δw is defined as the peak width where the amplitude falls to half of its maximum value.

2.3.2. Different types of AW devices

An acoustic wave can propagate in an elastic medium, causing the device to vibrate. The direction of vibration can be either parallel or perpendicular to the propagation direction. The types of elastic wave that may propagate in a solid are

shown in Figure 2-9 [113], and these depend on the properties and the boundary conditions of the solid [120]. There are four AW devices that are most commonly utilized and investigated for sensing applications, namely the thickness shear mode (TSM) resonator, the surface acoustic wave (SAW) device, the flexural plate wave (FPW) device [113], and the microcantilever (MC) [121, 122]. As depicted in Figure 2-9 (a) and (b), bulk waves exist in a medium without any boundaries, such as a TSM resonator. When a single plane boundary exists, the wave will propagate along that boundary, for example in a SAW device (Figure 2-9 (c)). If two boundaries exist, the wave will propagate within the thin plate, as in an FPW device (Figure 2-9 (d)).

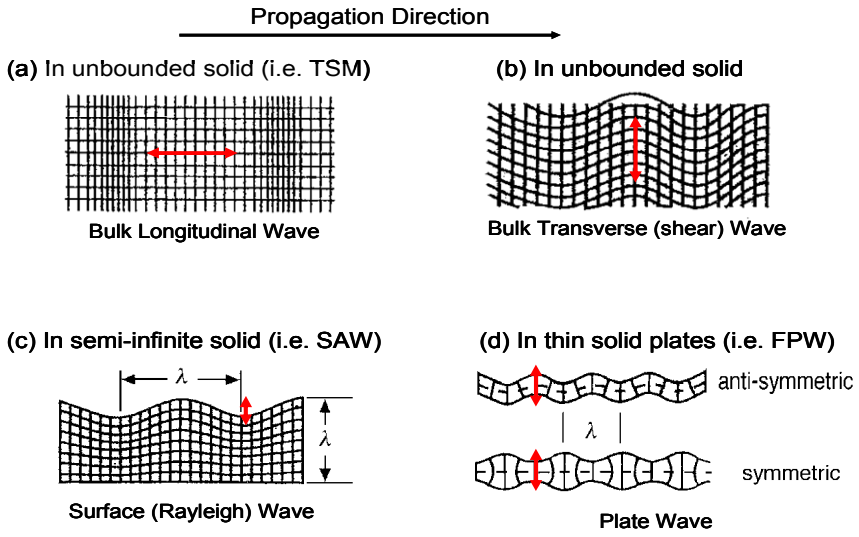

Figure 2- 9. Types of elastic wave propagation. (a) & (b) in an unbounded solid, (c) in a semi-infinite solid with a single boundary, and (d) in a thin solid plate with two boundaries. Vertical and horizontal displacements are exaggerated for clarity. The red (non-dimensional) arrow represents the vibration direction.

2.3.2.1. Quartz crystal microbalances

The familiar quartz crystal microbalance (QCM), also commonly referred to as a TSM resonator, is one of the most widely used acoustic wave sensor platforms in both research studies and commercial applications for biological threat detection. It typically consists of a thin AT-cut quartz disk with circular electrodes patterned on both sides [113]. When applying a voltage between these two electrodes, the crystal will undergo shear deformation due to the piezoelectric effect and will be electrically excited in a number of resonant thickness-shear modes, allowing the mechanical resonance frequencies to be detected. When there is a uniformly distributed thin film deposited on the crystal surface, the added mass of the thin film results in changes in TSM resonant frequency, which can be expressed by the Sauerbrey Equation [123]:

$$\Delta f = -\frac{2 f_0^2 \Delta m}{A\sqrt{\mu_q \rho_q}} \qquad (2\text{-}3)$$

where Δf is the frequency shift, f_0 is the fundamental mode of the crystal, Δm is the mass change per unit area (g/cm^2), A is the active area on the surface, ρ_q is the density of quartz and μ_q is the shear modulus of quartz. Mass sensitivity can be derived from the above equation:

$$S_m = -\frac{f_0}{(t\rho)_{quartz}} \qquad (2\text{-}4)$$

where t and ρ is the thickness and density of the thin film layer on the crystal. A TSM resonator can be operated in a liquid in order to determine its properties (i.e. viscosity, density [124, 125]) by measuring the mass loading on the crystal surface from the liquid

environment. TSM resonators have also successfully been used for microbial contamination detection (i.e. *S. typhimurium*, *B. anthracis* spores) by immobilizing biological active elements on the surface (i.e. antibody, phage) [69, 126-128].

2.3.2.2. SAW devices

SAW devices are usually comprised of ST-cut piezoelectric crystals with two patterned gold/titanium-interdigitated transducers (IDTs) (emitter & receiver) deposited on the same side of crystal surface. This surface acoustic wave, also known as a Rayleigh wave [118], is utilized for sensor applications because the propagation of waves is confined to the surface, making the acoustic waves extremely sensitive to surface perturbations and allowing them to be detected by lithographically patterned interdigital surface electrodes [129]. SAW sensors exhibit the highest sensitivity of the acoustic sensors reviewed [128], because the acoustic wave confines all the acoustic energy to the zone within one wavelength of the surface. When applying an alternating voltage on one of the electrodes, an acoustic wave will be produced that propagates along the surface until it reaches the other electrode [113]. However, when the SAW sensor is placed in a liquid medium, the waves will be strongly damped since they are surface-normal waves, making SAW sensors unsuitable for liquid sensing. One of the most common applications for SAW sensors is to detect the interaction, in terms of the fundamental resonance frequency change, that results from changes in the areal/mass density on the sensor surface.

2.3.2.3. FPW devices

In an FPW device, the acoustic wave is excited in a membrane that is relatively thin compared to the acoustic wavelength. An FPW sensor is usually fabricated by a micromachining process and uses silicon nitride, silicon dioxide, oxy-nitride, aluminum nitride, or diamond as the membrane layer. This membrane is deposited onto a silicon substrate for ease of handling, and then the substrate is etched away. After depositing a conducting layer, a layer of piezoelectric zinc oxide will be sputtered on, followed by sputtering of a second conducting layer. Two interdigitated conducting electrodes are formed in the conducting layer, one of which is used as a wave generator (output) and the other as the wave receiver (input). The piezoelectric film is deformed and excited by the interdigitated conducting electrodes in order to generate and detect acoustic waves. When a wave propagates, the membrane moves both perpendicularly and parallel to its surface, such that the shape of the entire membrane is like a flag waving in the wind [113, 130]. FPW has very high sensitivity compared to other acoustic wave devices. Since the operating frequencies are of the order of few MHz or even lower, this makes it relatively easy to design the electronics for the operation. Also, the wave propagates at low speeds in the plate, so it is possible to use FPW sensors in liquid. However, the fabrication of FPW devices is difficult as it is hard to make a low stress membrane layer with a thickness of few microns, and the resulting membrane is fragile. Because of this, FPW sensors have not made much progress in terms of miniaturization.

2.3.2.4. Microcantilevers

Micromachined cantilevers were first used as force probes in atomic force microscopy (AFM). Due to their extremely high sensitivity to a variety of environmental factors, including acoustic noise, temperature, ambient pressure, and humidity [131], researchers at Oak Ridge National Laboratory and IBM Zurich investigated converting them into a new sensor platform [132, 133] and found that this standard cantilever provided a substantial improvement (i.e. sensitivity) over more traditional approaches (i.e. QCM, SAW). A microcantilever (MC) also acts as a mass sensitive device, producing a frequency shift when there is a mass loading on the device [134-136]. In the last decade, with the development of microelectromechanical systems (MEMS) that integrate electronics and micromechanical structure on chips, microcantilevers have become one of the simplest MEMS-based devices. A large number of papers have reported on the potential of MCs for physical, chemical, and biological sensing [137-141], as well as for applications in the medical field, for example screening for diseases such as cancer [142], glucose monitoring [143], and the discrimination of single-nucleotide (SNP) mismatches in DNA [144]. Moreover, nano-cantilevers have been successfully fabricated in the last few years, significantly increasing the sensitivity for sensing applications and allowing the detection of even smaller masses, ranging from several molecules to a single bacteria cell (i.e. *E. coli* [145]) or spore [146, 147]. Recently, it was reported that a mass sensitivity of as low as a few femtograms can be achieved using nano-cantilevers [148]. Sensors using cantilevers as

a platform have a high sensitivity and a good safety record, as well as being cheap, simple, fast, low power, and having a low analyte requirement for testing. These advantages make them very promising for the next generation of miniaturized and highly sensitive sensors [149].

A fundamental cantilever is constructed from a long and thin micro-beam with one end fixed by a support. The readout schemes for a cantilever can broadly be classified into two types: optical and electrical. Depending upon the parameters measured (i.e. cantilever tip position, spatial orientation, intrinsic stress, or radius of curvature [150]), cantilever operation can also be divided into static and dynamic modes. The static bending mode is used to detect cantilever deflection, which can be caused either by external forces added to the cantilever (i.e. adsorption of molecules) or intrinsic stresses produced in the cantilever (i.e. thermal expansion, physicochemical changes). In the dynamic mode, the MC operates as a mechanical oscillator whose resonance frequency changes due to three main mechanisms: 1) the mass loaded on the beam; 2) the viscosity of the medium; and 3) the environmentally induced elasticity changes in the MC material [150, 151]. When the target binds to the cantilever beam, the frequency shifts from f_0 to f_1 due to the additional suspended mass (Δm), and the relationship can be expressed as [150]:

$$\frac{1}{f_1^2} - \frac{1}{f_0^2} = \frac{\Delta m}{\left(4\pi^2 \mathrm{K}\right)} \qquad (2\text{-}5)$$

Here, K is the spring constant of the cantilever. Hence, in order to obtain an appreciable mass sensitivity, high frequencies are required.

Dynamic MCs can also be divided into three types: single beam MCs (i.e. silicon-based MCs), composite-beam MCs (i.e. piezoelectric/piezoresistance MCs), and magnetoelastic MCs.

Silicon-based MCs are driven by mechanical force and the deflection is detected by optical methods, which includes optical beam deflection [152] and optical interferometry [153, 154]. A typical optical method applies a position sensitive photodetector (PSD) and a laser beam of very low power. The laser beam falls on the cantilever beam surface and the reflected beam is then captured by the PSD. If an additional mass loaded on the beam has caused the deflection of cantilever, the reflected beam falls on a different part of the PSD and the magnitude of this deflection can be calculated by appropriate electronics. Optical methods offer significant advantages of miniaturization, batch fabrication, and integration of signal-processing circuitry with a relatively high mechanical quality factor (Q), which greatly increases the sensitivity of the device. However, a high Q value is likely to adversely affect the stability of device by acting to promote mechanical coupling, resulting in a change in the vibration mode. The system is also complex, expensive and bulky, and requires a sophisticated data acquisition system and extra driving equipment to make it vibrate. Of particular importance for many applications, because of the dispersion of the laser beam in a liquid, optical sensing methods are limited for in-liquid applications [152].

Compared with silicon-based cantilevers, piezoelectric cantilevers are optimized by using electrical means, which overcomes the need for complex optical detection equipment. It can be used electrically for both actuation and sensing, and is able to integrate the driving and characterizing circuits in the chip with MCs. By applying an AC voltage to the driving electrode, the cantilever vibrates due to the converse piezoelectric effect. At resonance, these vibrations produce piezoelectric voltages that can be detected by the direct piezoelectric effect at the sensing electrode. An impedance analyzer can also be used to measure the resonance frequencies and characterize the sensor using the impedance spectrum (impedance *vs.* frequency). Since only one electrode is needed, the measurements can all be obtained conveniently using an impedance analyzer.

The two types of platforms employed by piezoelectric-based MCs are unimorph and bimorph. Unimorph MCs are composed of one piezoelectric layer bound to a substrate layer (stiff metal). There are two types of bimorph connections, parallel and series, and these consist of two piezoelectric layers with different pole directions bonded together. When mass is added to the cantilever, the oscillation of the cantilever is damped. Thus, a piezoelectric actuator can be used as a viscosity-meter or as a microbalance to detect mass change. No external detection devices or tedious alignment are required and they are also capable of enclosing an integrated electromechanical system. Piezoelectric cantilevers not only act as mass detectors, but also function well in liquids by monitoring peak broadening and the resonance frequency shift. Since MCs

are highly mass sensitive, its length, width, and resonance mode all have an effect on an individual cantilever. Mutharasan and his coworkers at Drexel University successfully utilized piezoelectric-excited, millimeter-sized, cantilever (PEMC) sensors that consisted of a piezoelectric and a borosilicate glass layer immobilized with different biorecognition elements to develop a sensitive, reliable and near real-time method for the detection of cryptosporidium parvum oocyst [155], airborne *B. anthracis* spores in conjunction with a commercial air sampler (at 5 spores/L) [156], *Staphylococcus aureus* enterotoxin B (SEB, at 12.5-50 pg/mL) [157], and *E. coli* O157:H7 in ground beef samples (50–100 cells/mL) [158].

2.3.2.5. Magnetoelastic sensors

Magnetoelastic (ME) materials are generally amorphous, soft-ferromagnetic materials. Nickel, laminated metallic glass alloys, and rare-earth iron compounds are common ME materials. This class of materials is a subset of magnetostrictive materials, which undergo a change in dimensions when exposed to a magnetic field. Magnetoelastic materials can be made to resonate in a time varying ("AC") magnetic field at a specific frequency that is dependent on their geometry and mass. For rectangular sheet sensor platforms, varying the magnetic field can be used to cause oscillations mainly along the length direction. ME materials have been used to remotely sense temperature [159, 160], pressure [161-163], pH [164, 165], liquid viscosity/density [166, 167], magnetic fields, and thin film elasticity [168]. They have also been used in

chemical and gas sensing for glucose [169], NH_3 [170] and CO_2 [171], and are widely used as position sensors [172], identification markers [173] and anti-theft tags [174], in addition to their more recent use as biosensing platforms [168, 175-178]. A more detailed treatment of magnetoelastic sensors will be given in Chapter 3.

3. Comparison of biosensor types

All the biosensor types discussed above have been applied in food-borne pathogens detection. Electrochemical biosensors are especially widely used for clinical diagnosis, as well as biochemical and environmental analysis. Optical biosensors are important because they can detect bacteria very quickly. Acoustic sensors are attractive for many applications due to their real-time detection as well as their simplicity of use. Currently, several popular devices, including PCR, QCM, SPR, Love Wave, ELISA and ME biosensors, are used for bacterial detection. Table 2-2 below discusses the advantages and disadvantages of each type of biosensor. The acoustic wave devices are compared in Table 2-3, clearly showing their overall excellent performance, simplicity of use, good Q factor, high sensitivity and suitability for working in a liquid medium.

Table 2- 2. Comparison of Bacterial Detection Techniques.

Techniques	Advantages	Disadvantages
ELISA	1. Versatile, sensitive, highly specific, and relatively economical 2. Decrease detection analysis time from two weeks to two to three days	1. Require pure cultures or high cell numbers 2. Procedures are complex and require trained personnel to accomplish. 3. Each incubation step lasts more than one hour.
PCR	1. Very robust, capable of amplifying small quantities of genetic material to determine the presence of bacteria 2. Good sensitivity, simplicity, low detection limit.	1. Complex sample preparation and detection process: reactive components of limited shelf life, precise temperature, sophisticated hardware and trained personnel
SPR	1. Able to detect tiny changes in the refractive index when cells bind to receptors immobilized on the transducer surface 2. Provide rapid, remote sensing	1. Suffer from interference due to ambient light 2. Require high-energy sensors (UV light or laser) 3. Detection is limited to a narrow concentration range
QCM	1. Use for both liquid and gas measurements 2. For liquid systems with label free detection with molecules 3. High sensitivity 4. Easy to use	1. Two electrodes required to excite the oscillation 2. Sensitive material has to be brought onto one of these electrodes externally 3. Need a external voltage source to generate the signal
Love Wave	1. Offer higher sensitivity compared to other acoustic devices because of the higher operating frequencies 2. Use other piezoelectric materials like lithium niobate and lithium antalite. Due to the higher coupling coefficients of these materials,	1. Not yet fully developed and lot of work remains to be done for commercial use of these sensors. 2. Design of electronics is difficult when compared to TSM resonators due to higher frequency operations.

	sensitivity can be higher. 3. Packaging of these sensors is easy	
ME Biosensor	1. Fast measurement time, reliable, simple to use, detect without physical wire connection, very cheap 2. Accurate measurements in liquid media with good sensitivity and specificity	1. Corrosion issue will affect testing results 2. Q value and amplitude need to be increased when exposed to liquid system

Table 2- 3. Comparison of acoustic wave devices.

Device	S_m	Immersible	Fabrication	Sensing method
TSM	Low	Yes	Complicated	Electrical system
SAW	Med	No	Complicated	Electrical system
APM	Low-Med	Yes	Complicated	Electrical system
FPW	High	Yes	Complicated	Electrical system
Silicon-based cantilever	High	Difficult	Complicated	Mechanical system
Piezo-based cantilever	Med	Difficult	Complicated	Electrical system
Magnetoelastic-based cantilever	Very High	Yes	Simple	Magnetic field (Wireless)
Magnetoelastic biosensor	Very High	Yes	Very simple	Magnetic field (Wireless)

4. References

[1] R. M. Lequin, "Enzyme Immunoassay (EIA)/Enzyme-Linked Immunosorbent Assay (ELISA)," *Clin. Chem.,* vol. 51, pp. 2415-2418, 2005.

[2] MedLinePlus. "HIV ELISA/western blot." U.S. National Library of Medicine. Last accessed April 16, "http://www.nlm.nih.gov/medlineplus/ency/article/003538.htm."

[3] R. A. Hall, A. K. Broom, A. C. Hartnett, M. J. Howard, and J. S. Mackenzie, "Immunodominant epitopes on the NS1 protein of MVE and KUN viruses serve as targets for a blocking ELISA to detect virus-specific antibodies in sentinel animal serum," *Journal of Virological Methods,* vol. 51, pp. 201-210, 1995.

[4] O. S. Frankfurt and A. Krishan, "Apoptosis-based drug screening and detection of selective toxicity to cancer cells," *Anti-Cancer Drugs,* vol. 14, pp. 555-561 2003.

[5] S. L. Bahna, "Diagnostic tests for food allergy," *Clin. Rev. Allergy,* vol. 6, pp. 259-284, 1988.

[6] A. H. Peruski and L. F. Peruski, Jr., "Immunological Methods for Detection and Identification of Infectious Disease and Biological Warfare Agents," *Clin. Diagn. Lab. Immunol.,* vol. 10, pp. 506-513, July 1, 2003 2003.

[7] J. Ehlers, M. Alt, D. Trepnau, and J. Lehmann, "Use of new immunoglobulin isotype specific ELISA—systems to detect *Salmonella* infections in pigs (German)," *Berliner und Münchener Tierärztliche Wochenschrift* vol. 119, pp. 461-466, 2006.

[8] J. Lehmann, T. Lindner, M. Naumann, T. Kramer, G. Steinbach, T. Blaha, J. Ehlers, H.-J. Selbitz, J. Gabert, and U. Roesler, "Application of a novel pig immunoglobulin-isotype-specific enzyme-linked immunoadsorbent assay for detection of *Salmonella enterica* serovar *typhimurium* antibodies in serum and meat juice," *Proceedings of the 18th International Pig Veterinary Society World Congress, Hamburg,* vol. 1, p. 383, 2004.

[9] J. Mousing, P. T. Jensen, C. Halgaard, F. Bager, N. Feld, B. Nielsen, J. P. Nielsen, and S. Bech-Nielsen, "Nation-wide *Salmonella enterica* surveillance and control in Danish slaughter swine herds," *Preventive Veterinary Medicine,* vol. 29, pp. 247-261, 1997.

[10] B. Nielsen, D. Baggesen, F. Bager, J. Haugegaard, and P. Lind, "The serological response to *Salmonella* serovars typhimurium and infantis in experimentally infected pigs. The time course followed with an indirect anti-LPS ELISA and bacteriological examinations," *Veterinary Microbiology,* vol. 47, pp. 205-218, 1995.

[11] S. L. Welkos, C. K. Cote, K. M. Rea, and P. H. Gibbs, "A microtiter fluorometric assay to detect the germination of Bacillus anthracis spores and the germination inhibitory effects of antibodies," *Journal of Microbiological Methods,* vol. 56, pp. 253-265, 2004.

[12] A. P. Phillips, K. L. Martin, N. L. Cross, and R. G. Drake, "Evaluation of immunoradiometric and ELISA Versions of a microtitre plate assay for Bacillus

anthracis spores," *Journal of Immunological Methods,* vol. 70, pp. 75-81, 1984.

[13] P. Rabinow, *Making PCR: A Story of Biotechnology*. Chicago: University of Chicago Press, 1996.

[14] K. Mullis, "The unusual origin of the polymerase chain reaction," *Scientific American* vol. 262, pp. 56-61, 64-65, 1990.

[15] J. Sambrook and D. W. Russel, *Molecular Cloning: A Laboratory Manual, 3rd ed.* Cold Spring Harbor, N.Y.: Cold Spring Harbor Laboratory Press, 2001.

[16] http://www.horizonpress.com/pcr/.

[17] A. Pavlov, N. Pavlova, S. Kozyavkin, A. Slesarev, "Thermostable DNA Polymerases for a Wide Spectrum of Applications: Comparison of a Robust Hybrid TopoTaq to other enzymes," in *DNA sequencing II : optimizing preparation and cleanup*, J. Kieleczawa, Ed. Sudbury, Mass.: Jones and Bartlett Publishers, 2006, pp. 241-257.

[18] J. A. Higgins, S. Nasarabadi, J. S. Karns, D. R. Shelton, M. Cooper, A. Gbakima, and R. P. Koopman, "A handheld real time thermal cycler for bacterial pathogen detection," *Biosensors and Bioelectronics,* vol. 18, pp. 1115-1123, 2003.

[19] M. Lund, S. Nordentoft, K. Pedersen, and M. Madsen, "Detection of Campylobacter spp. in chicken fecal samples by real-time PCR," *Journal of Clinical Microbiology,* vol. 42, pp. 5125-5132, 2004.

[20] Z. Fu, S. Rogelj, and T. L. Kieft, "Detection of Escherichia coli 0157:H7 by immuno-magnetic separation and real-time PCR," *International Journal of Food*

Microbiology, vol. 99, pp. 47-57, 2005.

[21] E. R. Castanha, R. R. Swiger, B. Senior, A. Fox, L. N. Waller, and K. F. Fox, "Strain discrimination among B. anthracis and related organisms by characterization of bclA polymorphisms using PCR coupled with agarose gel or microchannel fluidics electrophoresis," *Journal of Microbiological Methods,* vol. 64, pp. 27-45, 2006.

[22] G. B. Jensen, N. Fisker, T. Sparso, and L. Andrup, "The possibility of discriminating within the Bacillus cereus group using gyrB sequencing and PCR-RFLP," *International Journal of Food Microbiology,* vol. 104, pp. 113-120, 2005.

[23] R. W. Reiman, D. H. Atchley, and K. J. Voorhees, "Indirect detection of Bacillus anthracis using real-time PCR to detect amplified gamma phage DNA," *Journal of Microbiological Methods,* vol. 68, pp. 651-653, 2007.

[24] A. Cavalcanti, B. Shirinzadeh, M. Zhang, and L. C. Kretly, "Nanorobot Hardware Architecture for Medical Defense," *Sensors,* vol. 8, pp. 2932-2958, 2008.

[25] P. Leonard, S. Hearty, J. Brenan, L. Dunne, J. Quinn, T. Chakraborty, and R. O'Kennedy, "Advances in biosensors for detection of pathogens in food and water," *Enzyme and Microbial Technology,* vol. 32, pp. 3-13, 2003.

[26] G. W. Litman, J. P. Rast, M. J. Shamblott, R. N. Haire, M. Hulst, W. Roess, R. T. Litman, K. R. Hinds- Frey, A. Zilch, and C. T. Amemiya, "Phylogenetic diversification of immunoglobulin genes and the antibody repertoire," *Mol Biol*

Evol, vol. 10, pp. 60-72, January 1, 1993 1993.

[27] J. M. Woof and D. R. Burton, "Human antibody-Fc receptor interactions illuminated by crystal structures," *Nat Rev Immunol,* vol. 4, pp. 89-99, 2004.

[28] E. Market and F. N. Papavasiliou, "V(D)J Recombination and the Evolution of the Adaptive Immune System," *PLoS Biology,* vol. 1, p. e16, October 01, 2003 2003.

[29] C. Janeway, *Immunobiology : the immune system in health and disease*. New York: Garland Pub., 2001.

[30] P. FW, L. YS, and L. TL, "Primary structure of a human IgA1 immunoglobulin. IV. Streptococcal IgA1 protease, digestion, Fab and Fc fragments, and the complete amino acid sequence of the alpha 1 heavy chain," *J. Biol. Chem. ,* vol. 254, pp. 2865-2874, 1979.

[31] S. Kabir, "Immunoglobulin purification by affinity chromatography using protein A mimetic ligands prepared by combinatorial chemical synthesis," *Immunological Investigations,* vol. 31, pp. 263-278, 2002.

[32] P. D. Skottrup, M. Nicolaisen, and A. F. Justesen, "Towards on-site pathogen detection using antibody-based sensors," *Biosensors and Bioelectronics,* vol. In Press, Corrected Proof.

[33] "Animated depictions of how antibodies are used in ELISPOT assays," Cellular Technology Ltd.—Europe, 2007-05-08.

[34] P. GL and F. DP, "Rituximab: a review of its use in non-Hodgkin's lymphoma and chronic lymphocytic leukaemia," *Drugs,* vol. 63, pp. 803-843, 2003.

[35] R. Rhoades, *Human physiology*. Pacific Grove, Calif.: Brooks/Cole, 2003.

[36] M. Feldmann and R. N. Maini, "Anti-TNF alpha therapy of rheumatoid arthritis: what have we learned?," *Annual Review of Immunology,* vol. 19, pp. 163-196, 2001.

[37] S. Doggrell, "Is natalizumab a breakthrough in the treatment of multiple sclerosis," *Expert Opin Pharmacother,* vol. 4, pp. 999-1001, 2003.

[38] G. G. Krueger, R. G. Langley, C. Leonardi, N. Yeilding, C. Guzzo, Y. Wang, L. T. Dooley, M. Lebwohl, and C. P. S. G. the, "A Human Interleukin-12/23 Monoclonal Antibody for the Treatment of Psoriasis," *N Engl J Med,* vol. 356, pp. 580-592, February 8, 2007 2007.

[39] C. L. Vogel, M. A. Cobleigh, D. Tripathy, J. C. Gutheil, L. N. Harris, L. Fehrenbacher, D. J. Slamon, M. Murphy, W. F. Novotny, M. Burchmore, S. Shak, and S. J. Stewart, "First-Line Herceptin? Monotherapy in Metastatic Breast Cancer," *Oncology,* vol. 61, pp. 37-42, 2001.

[40] B. F. Brehm-Stecher and E. A. Johnson, "Single-Cell Microbiology: Tools, Technologies, and Applications," *Microbiol. Mol. Biol. Rev.,* vol. 68, pp. 538-559, September 1, 2004 2004.

[41] N. E. Williams, J. A. David, and D. F. James, "Chapter 23 Immunoprecipitation Procedures," in *Methods in Cell Biology*. vol. Volume 62: Academic Press, 1999,

pp. 449-453.

[42] B. T. Kurien and R. H. Scofield, "Western blotting," *Methods,* vol. 38, pp. 283-293, 2006.

[43] E. Scanziani, "Immunohistochemical staining of fixed tissues," *Methods Mol. Biol. ,* vol. 104, pp. 133-140, 1998.

[44] D. Reen, "Enzyme-linked immunosorbent assay (ELISA)," *Methods Mol. Biol. ,* vol. 32, pp. 461-466, 1994.

[45] A. Kalyuzhny, "Chemistry and biology of the ELISPOT assay," *Methods Mol. Biol. ,* vol. 302, pp. 15-31, 2005.

[46] C. B. Bird, R. L. Miller, and B. M. Miller, "Reveal for *salmonella* test system," *Journal of AOAC int.,* vol. 82, pp. 625-633, 1999.

[47] E. Soini and H. Kojola, "Time-resolved fluorometer for lanthanide chelates-a new generation of nonisotopic immuoassays," *Clin. Chem.,* vol. 29, pp. 65-68, 1983.

[48] H. Yang, J. K. Leland, D. Yost, and R. J. Massey, "Electrochemiluminescence: A New Diagnostic and Research Tool," *Nat. Biotech,* vol. 12, pp. 193-194, 1994.

[49] H. Yu, "Comparative studies of magnetic particle-based solid phase fluorogenic and electrochemiluminescent immunoassay," *Journal of Immunological Methods,* vol. 218, pp. 1-8, 1998.

[50] P. M. Fratamico, T. P. Strobaugh, M. B. Medina, and A. G. Gehring, "Detection of Escherichia coli 0157:H7 using a surface plasmon resonance biosensor," *Biotechnology Techniques* vol. 12, pp. 571-576, 1998.

[51] P. Leonard, S. Hearty, J. Quinn, and R. O'Kennedy, "A generic approach for the detection of whole Listeria monocytogenes cells in contaminated samples using surface plasmon resonance," *Biosensors & Bioelectronics,* vol. 19, pp. 1331-1335, 2004.

[52] A. A. Bergwerff and F. Van Knapen, "Surface plasmon resonance biosensors for detection of pathogenic microorganisms: Strategies to secure food and environmental safety," *Journal of AOAC International* vol. 89, pp. 826-831, 2006.

[53] S. H. Lee, D. D. Stubbs, J. Cairney, and W.D. Hunt, "Rapid detection of bacterial spores using a quartz crystal microbalance (QCM) immunoassay," *IEEE Sensors Journal* vol. 5, pp. 737-743, 2005.

[54] R. D. Vaughan, R. M. Carter, C. K. O'Sullivan, and G. G. Guilbault, "A Quartz Crystal Microbalance (QCM) Sensor for the Detection of Bacillus cereus," *Analytical Letters* vol. 36, pp. 731-747, 2003.

[55] L. Prescptt, *Microbiology*: Wm. C. Brown Publishers, 1993.

[56] E. Kutter and A. Sulankvelidze, *Bacteriophages: Biology and Application*: CRC Press, 2004.

[57] S. M. Grath and D. v. Sinderen, *Bacteriophage: Genetics and Molecular Biology*, 1st ed.: Caister Academic Press, 2007.

[58] H.-W. Ackermann, "Tailed bacteriophages. The order Caudoviurales," *Adv. Virus Res. ,* vol. 51, pp. 135-201, 1999.

[59] H.-W. Ackermann, "Frequency of morphological phage descriptions in the year 2000," *Arch. Virol.,* vol. 146, pp. 843-857, 2001.

[60] C. Martin, "The Application of Bacteriophage Tracer Techniques in South West Water," *Water and Environment Journal* vol. 2, pp. 638-642, 1988.

[61] "U.S. FDA/CFSAN: Agency Response Letter: GRAS Notice No. GRN 000198."

[62] L. Goodridge, J. Chen, and M. Griffiths, "The use of a fluorescent bacteriophage assay for detection of Escherichia coli O157:H7 in inoculated ground beef and raw milk," *International Journal of Food Microbiology,* vol. 47, pp. 43-50, 1999.

[63] P. A. Mosier-Boss, S. H. Lieherman, J. M. Andrews, F. L. Rohwer, L. E. Wegley, and M. Breitbart, "Use of Fluorescently Labeled Phage in the Detection and Identification of Bacterial Species," *Applied Spectroscopy,* vol. 57, pp. 1138-1144, 2003.

[64] J. McCafferty, A. D. Griggiths, G. Winter, and D. J. Chiswell, "Phage antibodies: filamentous phage displaying antibody variable domains," *Nature,* vol. 348, pp. 552-554, 1990.

[65] C. F. Barbas, A. S. Kang, R. A. Lerner, and S. J. Benkovic, "Assembly of combinatorial antibody libraries on phage surfaces: the gene III site," *Proceedings of the National Academy of Sciences of the United States of America,* vol. 88, pp. 7978-7982, 1991.

[66] P. A. Emanuel, J. Dang, J. S. Gebhardt, J. Aldrich, E. A. Garber, H. Hulaga, P. Stopa, J. J. Valdes, and A. Dion-Schultz, "Recombinant antibodies: a new reagent

for biological agent detection," *Biosensors & Bioelectronics,* vol. 14, pp. 751-759, 2000.

[67] V. A. Petrenko and G. P.Smith, "Phages from landscape libraries as substitute antibodies," *Protein Engineering,* vol. 13, pp. 589-592, 2000.

[68] V. A. Petrenko, G. P. Smith, X. Gong, and T. Quinn, "A library of organic landscapes on filamentous phage," *Protein Engineering,* vol. 9, pp. 797-801, 1996.

[69] E. V. Olsen, I. B. Sorokulova, V. A. Petrenko, I. H. Chen, J. M. Barbaree, and V. J. Vodyanoy, "Affinity-selected filamentous bacteriophage as a probe for acoustic wave biodetectors of Salmonella typhimurium," *Biosensors and Bioelectronics,* vol. 21, pp. 1434-1442, 2006.

[70] J. Wan, M. L. Johnson, R. Guntupalli, V. A. Petrenko, and B. A. Chin, "Detection of Bacillus anthracis spores in liquid using phage-based magnetoelastic micro-resonators," *Sensors and Actuators B: Chemical,* vol. 127, pp. 559-566, 2007.

[71] R. S. Lakshmanan, R. Guntupalli, J. Hu, D.-J. Kim, V. A. Petrenko, J. M. Barbaree, and B. A. Chin, "Phage immobilized magnetoelastic sensor for the detection of Salmonella typhimurium," *Journal of Microbiological Methods,* vol. 71, pp. 55-60, 2007.

[72] R. S. Lakshmanan, R. Guntupalli, J. Hu, V. A. Petrenko, J. M. Barbaree, and B. A. Chin, "Detection of Salmonella typhimurium in fat free milk using a phage

immobilized magnetoelastic sensor," *Sensors and Actuators B: Chemical,* vol. 126, pp. 544-550, 2007.

[73] A. M. Samoylov, T. I. Samoylova, S. T. Pathirana, L. P. Globa, and V. J. Vodyanoy, "Peptide biosensor for recognition of cross species cell surface markers," *Jounral of Molecular Recognition,* vol. 15, pp. 1-7, 2002.

[74] S. E. Hufton, P. T. Moerkerk, E. V. Meulemans, A. de Bruïe, J.-W. Arends, and H. R. Hoogenboom, "Phage display of cDNA repertoires: the pVI display system and its applications for the selection of immunogenic ligands," *Journal of Immunological Methods,* vol. 231, pp. 39-51, 1999.

[75] W. M. Gommans, H. J. Haisma, and M. G. Rots, "Engineering Zinc Finger Protein Transcription Factors: The Therapeutic Relevance of Switching Endogenous Gene Expression On or Off at Command," *Journal of Molecular Biology,* vol. 354, pp. 507-519, 2005.

[76] T. Bratkovic, M. Lunder, T. Popovic, S. Kreft, B. Turk, B. Strukelj, and U. Urleb, "Affinity selection to papain yields potent peptide inhibitors of cathepsins L, B, H, and K," *Biochemical and Biophysical Research Communications,* vol. 332, pp. 897-903, 2005.

[77] M. Lunder, T. Bratkovic, S. Kreft, and B. Strukelj, "Peptide inhibitor of pancreatic lipase selected by phage display using different elution strategies," *J. Lipid Res.,* vol. 46, pp. 1512-1516, July 1, 2005 2005.

[78] M. Lunder, T. Bratkovič, B. Doljak, S. Kreft, U. Urleb, B. Štrukelj, and N. Plazar, "Comparison of bacterial and phage display peptide libraries in search of target-binding motif," *Applied Biochemistry and Biotechnology,* vol. 127, pp. 125-131, 2005.

[79] K. C. Gough, Y. Li, T. J. Vaughan, A. J. Williams, W. Cockburn, and G. C. Whitelam, "Selection of phage antibodies to surface epitopes of Phytophthora infestans," *J. of Immunological Methods,* vol. 228, pp. 97-108, 1999.

[80] U. Schmitz, A. Versmold, P. Kaufmann, and H. G. Frank, "Phage Display: A Molecular Tool for the Generation of Antibodies: A Review," *Placenta,* vol. 21, pp. S106-S112, 2000.

[81] D. L. Siegel, "Research and clinical applications of antibody phage display in transfusion medicine " *Transfusion Medicine Reviews,* vol. 15, pp. 35-52, 2001.

[82] V. A. Petrenko and G. P. Smith, "Vectors and Modes of Display," in *Phage Display in Biotechnology and Drug Discovery*, S. S. Sidhu, Ed. Bo Raton, FL, USA: CRC Press, Taylor & Francis Group, 2005, p. 714.

[83] G. P. Smith and V. A. Petrenko, "Phage Display," *Chem. Rev.,* vol. 97, pp. 391-410, 1997.

[84] J. W. Kehoe and B. K. Kay, "Filamentous Phage Display in the New Millennium," *Chem. Rev.,* vol. 105, pp. 4056-4072, 2005.

[85] D. A. Marvin, L. C. Welsh, M. F. Symmons, W. R. Scott, and S. K. Straus, "Molecular structure of fd (f1, M13) filamentous bacteriophage refined with

respect to X-ray fibre diffraction and solid-state NMR data supports specific models of phage assembly at the bacterial membrane," *J. Mil. Biol. ,* vol. 355, pp. 294-309, 2006.

[86] D. V. Marvin, "Filamentous phage structure infection assembly " *Curr. Opin. Struct. Biol.,* vol. 8, pp. 150-158, 1998.

[87] V. A. Petrenko, "Landscape phage as a molecular recognition interface for detection devices " *Microelectronics Journal,* vol. 39, pp. 202-207, 2008.

[88] A. J. Cunningham, *Introduction to bioanalytical sensors*. New York: Wiley, 1998.

[89] V. A. Petrenko and V. J. Vodyanoy, "Phage display for detection of biological threat agents," *Journal of Microbiological Methods,* vol. 53, pp. 253-262, 2003.

[90] L. Olofsson, J. Ankarloo, P. O. Andersson, and I. A. Nicholls, "Filamentous bacteriophage stability in non-aqueous media," *Chemistry & Biology,* vol. 8, pp. 661-671, 2001.

[91] E. W. Jasmin Shah, "Electrochemical Biosensors for Detection of Biological Warfare Agents," *Electroanalysis,* vol. 15, pp. 157-167, 2003.

[92] L. D. Mello and L. T. Kubota, "Review of the use of biosensors as analytical tools in food and drink industries," *Food Chemistry,* vol. 77, pp. 237-256, 2002.

[93] S. Sukeerthi and A. Q. Contractor, "Applications of Conducting Polymers as Sensors," *Ind. J. Chem. ,* vol. 33A, pp. 565-571, 1994.

[94] M. Gerard, A. Chaubey, and B. D. Malhotra, "Application of conducting polymers to biosensors," *Biosens. Bioelectron. ,* vol. 17, pp. 345-359, 2002.

[95] M. S. DeSilva, Y. Zhang, P. J. Hesketh, G. J. Maclay, S. M. Gendel, and J. R. Stetter, "Impedance based sensing of the specific binding reaction between Staphylococcus enterotoxin B and its antibody on an ultra-thin platinum film," *Biosensors and Bioelectronics,* vol. 10, pp. 675-682, 1995.

[96] D. Ivnitski, I. Abdel-Hamid, P. Atanasov, and E. Wilkins, "Biosensors for detection of pathogenic bacteria," *Biosensors & Bioelectronics,* vol. 14, pp. 599-625, 1999.

[97] B. Mirhabibollahi, J. L. Brooks, and R. G. Kroll, "A semi-homogeneous amperometric immunosensor for protein A-bearing Staphylococcus aureus in foods " *Applied Microbiology and Biotechnology,* vol. 34, pp. 242-247, 1990.

[98] J. L. Brooks, B. Mirhabibollahi, and R. G. Kroll, "Sensitive enzyme-amplified electrical immunoassay for protein A-bearing Staphylococcus aureus in foods," *Appl. Envir. Microbiol.,* vol. 56, pp. 3278-3284, 1990.

[99] J. D. Brewster, A. G. Gehring, R. S. Mazenko, L. J. Van Houten, and C. J. Crawford, "Immunoelectrochemical Assays for Bacteria: Use of Epifluorescence Microscopy and Rapid-Scan Electrochemical Techniques in Development of an Assay for Salmonella," *Anal. Chem.,* vol. 68, pp. 4153-4159, 1996.

[100] N. Nakamura, A. Shigematsu, and T. Matsunaga, "Electrochemical detection of viable bacteria in urine and antibiotic selection," *Biosensors and Bioelectronics,* vol. 6, pp. 575-580, 1991.

[101] I. Abdel-Hamid, D. Ivnitski, P. Atanasov, and E. Wilkins, "Flow-through immunofiltration assay system for rapid detection of E. coli O157:H7," *Biosensors and Bioelectronics,* vol. 14, pp. 309-316, 1999.

[102] A. L. Ghindilis, P. Atanasov, M. Wilkins, and E. Wilkins, "Immunosensors: electrochemical sensing and other engineering approaches," *Biosensors and Bioelectronics,* vol. 13, pp. 113-131, 1998.

[103] A. P. F. Turner, I. Karube, and G. S. Wilson, *Biosensors: Fundamentals and Applications*. Moscow: Mir Publishers, 1992.

[104] A. Mulchandani and K. R. Rogers, *Enzyme and Microbial Biosensors: Techniques and Protocols.* Totowa, NJ: Humana Press, 1998.

[105] M. C. Tran, *Biosensors*. Paris: Chapman and Hall and Masson, 1993.

[106] S. R. Mikkelsen and E. Cortón, *Bioanalytical Chemistry*. New Jersey John Wiley and Sons, 2004.

[107] L. J. Blum and P. R. Coulet, *Biosensor Principles and Applications*. New York: Marcel Dekker, 1991.

[108] P. Leonard, S. Hearty, J. Brennan, L. Dunne, J. Quinn, T. Chakraborty, and R. O'Kenndy, "Advances in biosensors for detection of pathogens in food and water," *Enzyme and Microbial Technology,* vol. 32, pp. 3-13, 2003.

[109] R. S. Sethi, "Transducer Aspects of Biosensors," *Biosensors & Bioelectronics,* vol. 9, pp. 243-264, 1994.

[110] Z. Xu, A. Mulchandani, and W. Chen, "Detection of Benzene, Toluene, Ethyl Benzene, and Xylenes (BTEX) Using Toluene Dioxygenase-Peroxidase Coupling Reactions," *Biotechnol. Prog. ,* vol. 19, pp. 1812-1815, 2003.

[111] A. N. Naimushin, C. B. Spinelli, S. D. Soelberg, T. Mann, R. C. Stevens, T. Chinowsky, P. Kauffman, S. Yee, and C. E. Furlong, "Airborne analyte detection with an aircraft-adapted surface plasmon resonance sensor system," *Sensors and Actuators B: Chemical,* vol. 104, pp. 237-248, 2005.

[112] J. Homola, S. S. Yee, and G. Gauglitz, "Surface plasmon resonance sensors: review," *Sens. Actuat. B: Chemical,* vol. 54, pp. 3-15, 1999.

[113] D. S. Ballantine, R. M. White, S. J. Martin, A. J. Ricco, G. C. Frye, E. T. Zellers, and H. Wohltjen, *Acoustic wave sensors: theory, design and physico-chemical applications*: Academic Press, 1997.

[114] R. E. Hummel, *Electronic Properties of Materials*, 3rd. ed.: Springer-Verlag New York, Inc., 2001.

[115] E. Benes, M. Gröschl, W. Burger, and M. Schmid, "Sensors based on piezoelectric resonators," *Sensors and Actuators A: Physical,* vol. 48, pp. 1-21, 1995.

[116] J. W. Grate, S. J. Martin, and R. M. White, "Acoustic-Wave Microsensors. 1," *analytical Chemistry,* vol. 65, pp. A940-A948, 1993.

[117] J. W. Grate, S. J. Martin, and R. M. White, "Acoustic-Wave Microsensors. 2," *Analytical Chemistry,* vol. 65, pp. A987-A996, 1993.

[118] L. Rayleigh, "On Waves Propagated along the Plane Surface of an Elastic Solid" *Proc. London Math. Soc. ,* vol. 17, pp. 4-11, 1885.

[119] M. D. Ward and D. A. Buttry, "In situ Interfacial Mass Detection with Piezoelectric Transducers," *Science,* vol. 249, pp. 1000-1007, 1990.

[120] B. A. Auld, *Acoustic Fields and Waves in Solids*. New York: Wiley, 1973.

[121] N. V. Lavrik, M. J. Sepaniak, and P. G. Datskos, "Cantilever transducers as a platform for chemical and biological sensors," *Review of Scientific Instruments,* vol. 75, pp. 2229-2253, 2004.

[122] T. Thundat, P. I. Oden, and R. J. Warmack, "Microcantilever sensors," *Microscale Thermophysical Engineering,* vol. 1, pp. 185-199, 1997.

[123] G. Z. Sauerbrey, "The use of quartz oscillators for weighing thin layers and for microweighing," *Phys. ,* vol. 155, pp. 206-222, 1959.

[124] A. L. Kipling and M. Thompson, "Network Analysis Method Applied to Liquid-Phase Acoustic Wave Sensors," *Analytical Chemistry,* vol. 62, pp. 1514-1519, 1990.

[125] L. V. Rajakovic, B. A. Cavic-Vlasak, V. Ghaemmaghami, K. M. R. Kallury, A. L. Kipling, and M. Thompson, "Mediation of acoustic energy transmission from acoustic wave sensors to the liquid phase by interfacial viscosity," *Anal. Chem.,* vol. 63, pp. 615-621, 1991.

[126] S. T. Pathirana, J. Barbaree, B. A. Chin, M. G. Hartell, W. C. Neely, and V. Vodyanoy, "Rapid and sensitive biosensor for Salmonella," *Biosensors and*

Bioelectronics, vol. 15, pp. 135-141, 2000.

[127] X. Su, S. Low, J. Kwang, V. H. T. Chew, and S. F. Y. Li, "Piezoelectric quartz crystal based veterinary diagnosis for Salmonella enteritidis infection in chicken and egg," *Sensors and Actuators B: Chemical,* vol. 75, pp. 29-35, 2001.

[128] B. Drafts, "Acoustic wave technology sensors," *IEEE Transactions on Microwave Theory and Techniques,* vol. 49, pp. 795-802, 2001.

[129] R. M. White, "Surface elastic waves," *Proceedings of the IEEE,* vol. 58, pp. 1238-1276, 1970.

[130] A. Hierlemann and H. Baltes, "CMOS-based chemical microsensors," *Analyst,* vol. 128, pp. 15-28, 2003.

[131] G. Binnig, C. F. Quate, and C. Gerber, "Atomic Force Microscope," *Physical Review Letters,* vol. 56, p. 930, 1986.

[132] T. Thundat and R. J. Warmack, "Thermal and ambient-induced deflections of scanning force microscope cantilevers," *Applied Physics Letters,* vol. 64, p. 2894, 1994.

[133] J. R. Barnes, R. J. Stephenson, M. E. Welland, C. Gerber, and J. K. Gimzewski, "Photothermal spectroscopy with femtojoule sensitivity using a micromechanical device," *Nature,* vol. 372, pp. 79-81, 1994.

[134] T. Thundat, E. A. Wachter, S. L. Sharp, and R. J. Warmack, "Detection of Mercury Vapor Using Resonating Microcantilevers. ," *Applied Physics Letters* vol. 66, pp. 1695-1697, 1995.

[135] T. Thundat, G. Y. Chen, R. J. Warmack, D. P. Allison, and E. A. Wachter, "Vapor detection using resonating microcantilevers. ," *Anal. Chem. ,* vol. 67, pp. 519-521 1995.

[136] E. A. Wachter and T. Thundat, "Micromechanical sensors for chemical and physical measurements," *Rev. Sci. Instrum. ,* vol. 66, pp. 3662-3671, 1995.

[137] P. G. Datskos and I. Sauers, "Detection of mercaptoethanol using gold-coated micromachined cantilevers, ," *Sens. Actuators B, Chem. ,* vol. 61, pp. 75-82, 1999.

[138] A. Boisen, J. Thaysen, H. Jensenius, and O. Hansen, "Environmental sensors based on micromachined cantilevers with integrated read-out," *Ultramicroscopy,* vol. 82, pp. 11-16, 2000.

[139] K. M. Hansen, H.-F. Ji, G. Wu, R. Datar, R. Cote, A. Majumdar, and T. Thundat, "Cantilever-based optical deflection assay for discrimination of DNA single-nucleotide mismatches," vol. 73, pp. 1567-1571, 2001.

[140] J.-P. McGovern, W. Y. Shih, and W.-H. Shiha, "In situ detection of Bacillus anthracis spores using fully submersible, self-exciting, self-sensing PMN-PT/Sn piezoelectric microcantilevers," *The Analyst,* vol. 132, pp. 777-783, 2007.

[141] Q. Zhu, W. Y. Shih, and W.-H. Shih, "In-Situ, In-Water Detection of Salmonella typhimurium Using Lead Titanate Zirconate/Gold-Coated Glass Cantilevers at any Dipping Depth," *Biosensors and Bioelectronics,* vol. 22, p. 3132, 2007.

[142] G. H. Wu, R. H. Datar, K. M. Hansen, T. Thundat, R. J. Cote, and A. Majumdar, "Bioassay of prostate-specific antigen (PSA) using microcantilever," *Nat.*

Biotechnol., vol. 19, pp. 856-860, 2001.

[143] A. Subramanian, P. I. Oden, S. J. Kennel, K. B. Jacobson, R. J. Warmack, T. Thundat, and M. J. Doktycz, "Glucose biosensing using an enzyme-coated microcantilever," *Appl. Phys. Lett.,* vol. 81, pp. 385-387, 2002.

[144] Z. Jiri, *Piezoelectric Resonators and their Applications,*, 1st ed.: Elsevier Science Publishers, 1986.

[145] B. Ilic, D. Czaplewski, H. G. Craighead, P. Neuzil, C. Campagnolo, and C. Batt, "Mechanical resonant immunospecific biological detector," *Applied Physics Letters,* vol. 77, pp. 450-452, 2000.

[146] V. L. Nickolay, J. S. Michael, and G. D. Panos, "Cantilever transducers as a platform for chemical and biological sensors," *Review of Scientific Instruments,* vol. 75, pp. 2229-2253, 2004.

[147] J. Mertz, O. Marti, and J. Mlynek, "Regulation of a microcantilever response by force feedback," *Applied Physics Letters,* vol. 62, pp. 2344-2346, 1993.

[148] N. V. Lavrik and P. G. Datskos, "Femtogram mass detection using photothermally actuated nanomechanical resonators," *Applied Physics Letters,* vol. 82, p. 2697, 2003.

[149] S. K. Vashist, "A Review of Microcantilevers for Sensing Applications," *Journal of Nanotechnology,* vol. 3, pp. 1-15, 2007.

[150] N. V. Lavrik, M. J. Sepaniak, and P. G. Datskos, "Cantilever transducers as a platform for chemical and biological sensors," *Review of Scientific Instruments,*

vol. 75, pp. 2229-2253, 2004.

[151] M. Sepaniak, P. Datskos, N. Lavrik, and C. Tipple, "Microcantilever Transducers: A New Approach in Sensor Technology," *Anal. Chem.,* vol. 74, pp. 568A-575A, 2002.

[152] C. Ziegler, "Cantilever-based biosensors," *Analytical and Bioanalytical Chemistry,* vol. 379, pp. 946-959, 2004.

[153] D. Rugar, H. J. Mamin, and P. Guethner, "Improved fiber-optic interferometer for atomic force microscopy," *Applied Physics Letters,* vol. 55, p. 2588, 1989.

[154] B. Ilic, D. Czaplewski, M. Zalalutdinov, H. G. Craighead, P. Neuzil, C. Campagnolo, and C. Batt, "Single cell detection with micromechanical oscillators," *Journal of Vacuum Science & Technology B,* vol. 19, pp. 2825-2828, 2001.

[155] G. A. Campbell and R. Mutharasan, "Near real-time detection of Cryptosporidium parvum oocyst by IgM-functionalized piezoelectric-excited millimeter-sized cantilever biosensor," *Biosensors and Bioelectronics,* vol. 23, pp. 1039-1045, 2008.

[156] G. A. Campbell, D. deLesdernier, and R. Mutharasan, "Detection of airborne Bacillus anthracis spores by an integrated system of an air sampler and a cantilever immunosensor," *Sensors and Actuators B: Chemical,* vol. 127, pp. 376-382, 2007.

[157] G. A. Campbell, M. B. Medina, and R. Mutharasan, "Detection of Staphylococcus enterotoxin B at picogram levels using piezoelectric-excited millimeter-sized cantilever sensors," *Sensors and Actuators B: Chemical,* vol. 126, pp. 354-360, 2007.

[158] G. A. Campbell, J. Uknalis, S.-I. Tu, and R. Mutharasan, "Detect of Escherichia coli O157:H7 in ground beef samples using piezoelectric excited millimeter-sized cantilever (PEMC) sensors," *Biosensors and Bioelectronics,* vol. 22, pp. 1296-1302, 2007.

[159] M. K. Jain, S. Schmidt, K. G. Ong, C. Mungle, and C. A. Grimes, "Magnetoacoustic remote query temperature and humidity sensors," *Smart Mater. Struct. ,* vol. 9, pp. 502-510, 2000.

[160] M. K. Jain, Q. Y. Cai, and C. A. Grimes, "A wireless micro-sensor for simultaneous measurement of pH, temperature, and pressure," *Smart Mater. Struct. ,* vol. 10, pp. 347-353, 2001.

[161] D. Kouzoudis and C. A. Grimes, "The frequency response of magnetoelastic sensors to stress and atmospheric pressure," *Smart Mater. Struct. ,* vol. 8, pp. 885-889, 2000.

[162] C. A. Grimes, P. G. Stoyanov, D. Kouzoudis, and K. G. Ong, "Remote query pressure measurement using magnetoelastic sensors," *Rev. Sci. Instrum. ,* vol. 70, pp. 4711-4714, 1999.

[163] C. A. Grimes and D. Kouzoudis, "Remote query measurement of pressure, fluid-flow velocity, and humidity using magnetoelastic thick-film sensors," *Sens. Actuators* vol. 84, pp. 205-212, 2000.

[164] Q. Y. Cai and C. A. Grimes, "A remote query magnetoelastic pH sensor," *Sens. Actuators B,* vol. 71, p. 112, 2000.

[165] Q. Y. Cai and C. A. Grimes, "A salt independent pH sensor," *Sens. Actuat. B,* vol. 79, pp. 144-149, 2001.

[166] C. A. Grimes, D. Kouzoudis, and C. Mungle, "Simultaneous measurement of liquid density and viscosity using remote query magnetoelastic sensors " *Rev. Sci. Instrum.,* vol. 71, pp. 3822-3824, 2000.

[167] P. G. Stoyanov and C. A. Grimes, "A remote query magnetostrictive viscosity sensor," *Sens. Actuators,* vol. 80, pp. 8-14, 2000.

[168] K. G. Ong, M. K. Jain, C. Mungle, S. Schmidt, and C. A. Grimes, "A. Magnetism-based sensors (Invited paper)," *Proceedings of SPIE,* vol. 4467, pp. 158-172, 2001.

[169] J. M. Barandiaran and J. Gutierrez, "Magnetoelastic sensors based on soft amorphous magnetic alloys," *Sensors and Actuators A: Physical,* vol. 59, pp. 38-42, 1997.

[170] Q. Y. Cai, M. K. Jain, and C. A. Grimes, "A wireless, remote query ammonia sensor," *Sensors and Actuators B: Chemical,* vol. 77, pp. 614-619, 2001.

[171] Q. Y. Cai, A. Cammers-Goodwin, and C. A. Grimes, "A wireless remote query magnetoelastic CO_2 sensor," *J Environ. Monit. ,* vol. 2, pp. 556-560, 2000.

[172] C. Ruan, K. Zeng, O. K. Varghese, and C. A. Grimes, "Magnetoelastic Immunosensors: Amplified Mass Immunosorbent Assay for Detection of Escherichia coli O157:H7," *Anal. Chem.,* vol. 75, pp. 6494-6498, 2003.

[173] J. Gutiérrez and J. M. Barandiarán, "High magnetostriction metallic glasses used as magnetoelastic labels," *IEEE Trans. Magn. ,* vol. 31, pp. 3146-3148, 1995.

[174] "http://www.electronicmaterials.com/businesses/sem/amorph."

[175] K. G. Ong, L. G. Puckett, B. V. Sharma, M. Loiselle, C. A. Grimes, and L. G. Bachas, "Wireless passive resonant-circuit sensors for monitoring food quality," *Proc. of SPIE-The Int. Soc. for Opt. Eng. ,* vol. 4575, p. 150, 2001.

[176] K. G. Ong, K. Zeng, X. Yang, K. Shankar, C. Ruan, and C. A. Grimes, "Quantification of multiple bioagents with wireless, remote-query magnetoelastic micro-sensors," *IEEE Sensors J.,* vol. 6, pp. 514-523, 2006.

[177] C. Ruan, K. Zeng, O. K. Varghese, and C. A. Grimes, "A staphylococcal enterotoxin B magnetoelastic immunosensor," *Biosens. Bioelectron. ,* vol. 20, pp. 585-591, 2004.

[178] L. G. Puckett, G. Barrett, D. Kouzoudis, C. Grimes, and L. G. Bachas, "Monitoring blood coagulation with magnetoelastic sensors," *Biosensors and Bioelectronics,* vol. 18, pp. 675-681, 2003.

CHAPTER 3

FUNDAMENTAL BACKGROUNDS

1. Magnetoelastic sensor

1.1. Magnetostriction

Magnetoelastic (ME) materials have an interesting and potentially very useful property in that the material's physical dimensions change in response to variations in its magnetic environment: this is the direct magnetoelastic effect, known as magnetostriction. This phenomenon is also called Joule magnetostriction after the person who discovered it, James P. Joule, who saw it when observing a sample of nickel in 1842. Conversely, the magnetic properties of a ME material change when mechanical stress and strain is applied: this is the inverse magnetoelastic effect. Most ferromagnetic materials are now known to exhibit these phenomenons [1, 2]. When magnetic saturation is achieved, the strain λ reaches its saturation magnetostriction λ_s. When the material expands along the external field, λ_s is positive, while if the strain contracts the material, λ_s is negative. Figure 3-1 [1] illustrates the phenomenon of magnetostriction.

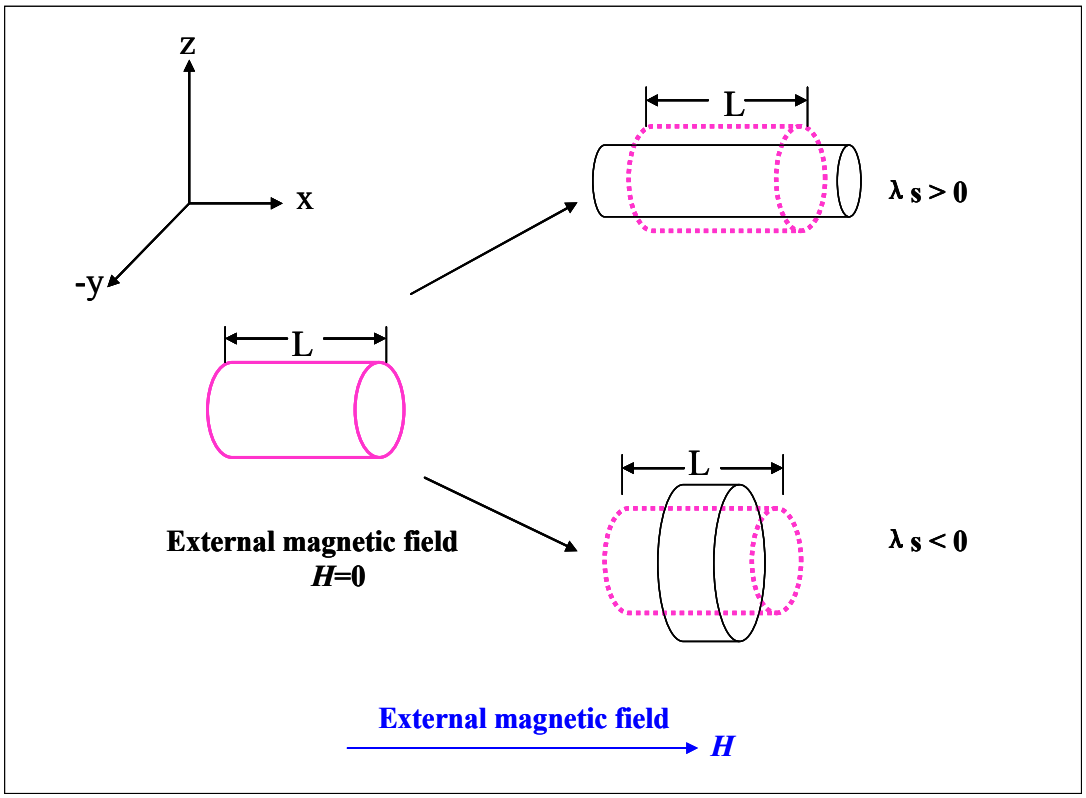

Figure 3- 1. Scheme of Joule magnetostriction.

In this research, Metglas 2826 MB ($Fe_{40}Ni_{38}Mo_4B_{18}$) ribbon, acquired from Honeywell International, was selected as the ME biosensor platform due to its excellent magnetoelastic properties. Metglas ribbons are iron-rich alloys which have a high mechanical tensile strength (~1000-1700 MPa), with magnetostriction on the order of 10^{-5}, and a high magnetoelastic coupling coefficient (0.98). These unique properties allow them to convert magnetic energy to elastic energy and vice versa very effectively [3-5]. In addition, such ME materials have a low material cost, thus allowing them to be used on a disposable basis [6]. Unlike piezoelectric materials, which need external

electrical connections, ME materials can be monitored wirelessly since they are activated remotely by a magnetic field. When a time-varying AC external magnetic field is used to resonate the ME platform, the resulting magnetostriction causes the ME platform to exhibit a pronounced magnetoelastic resonance and hence change the magnetic flux which can be remotely detected using a pickup coil. Since no physical connection is needed between the ME platform and the device, a biosensor based on this ME platform can conveniently be used in difficult environments such as sealed containers and packages.

1.2. Theoretical Model

Like other acoustic resonance sensors, the environmental parameter of interest for an ME material based sensor is measured by tracking its resonant frequency.

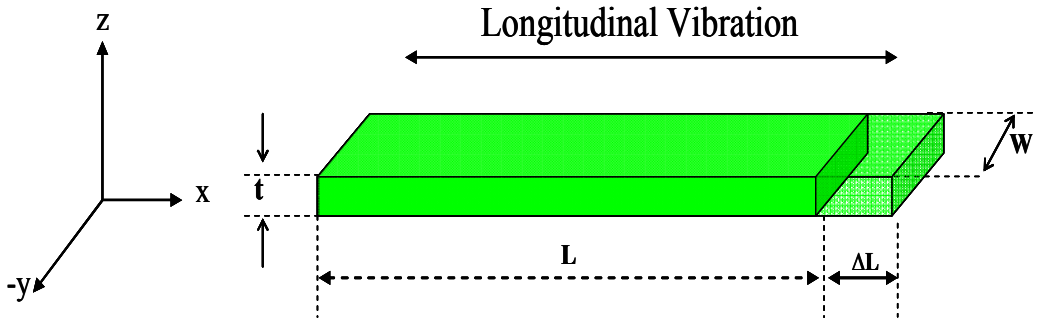

Figure 3- 2. A thin, ribbon-shaped sensor exhibiting a longitudinal vibration.

The precise mechanical resonance frequency of an ME sensor is based on its physical characteristics, and it can be made to vibrate at this frequency by applying an oscillating magnetic field to cause an elastic length change. For a thin, ribbon-shaped sensor of length L (length parallel to x-axis) excited by an x-directed ac magnetic field, as shown in Figure 3-2, and vibrating in its basal plane, the motion can be described as [7]:

$$\frac{\partial^2 u_x}{\partial t^2} = \frac{E_s}{\rho(1-\sigma^2)} \frac{\partial^2 u_x}{\partial x^2} \quad (3\text{-}1)$$

where E is Young's modulus of elasticity, σ is the Poisson ratio, ρ is the density of the sensor material, and u_x is the local displacement along the x-axis, which is taken to be the long dimension of the ribbon-shaped sensor. The fundamental resonance frequency of the longitudinal vibrations is given by:

$$f_n = \frac{n}{2L}\sqrt{\frac{E}{\rho(1-\sigma^2)}} \qquad n=1,2,3, \quad (3\text{-}2)$$

where L is the long dimension of the sensor. In most applications, only the fundamental resonance frequency f_0 (n = 1) is considered because of the higher signal amplitude and lower frequency. Consequently, the frequency can be determined by equation (3-3):

$$f = \sqrt{\frac{E}{\rho(1-\sigma^2)}}\frac{1}{2L} \qquad (3\text{-}3)$$

Due to the shape demagnetizing factors of the ribbon-like sensor, the magnetic permeability is greatest along its length; hence an incident magnetic field will generate longitudinal vibrations in the sensor from almost any orientation except normal to the basal plane of the sensor.

Liang [8, 9] recently demonstrated that plane-stress conditions dominate for thin, slender ribbons resonating mainly in the longitudinal direction. Thus the ME platform will vibrate mainly along the longitudinal direction, and its fundamental resonance frequency is given by equation (3-4):

$$f = \sqrt{\frac{E}{\rho(1-\upsilon)}}\frac{1}{2L} \qquad (3\text{-}4)$$

where υ *is* the Poisson's ratio of the sensor material. In this dissertation, the frequency is determined by this equation (3-4), from which we can tell that the resonance frequency is dependent on the material properties as well as geometry of the sensor.

1.3. Mass sensitivity of ME sensors

If the mass increase (Δm) is small compared to the mass of the sensor (M), and it is uniformly applied on the sensor surface with the area of A, thickness of d, according to Eq. (3-4), the frequency after mass loading can be expressed as below:

$$f_{load} = \sqrt{\frac{E}{\rho_{load}(1-\upsilon)}}\frac{1}{2L} = \sqrt{\frac{E}{\frac{(\Delta m + M)}{Ad}(1-\upsilon)}}\frac{1}{2L} = \frac{1}{2L}\sqrt{\frac{E}{\frac{(\Delta m + M)M(1-\upsilon)}{MAd}}}$$

$$= \frac{1}{2L}\sqrt{\frac{E}{\frac{(\Delta m + M)}{M}\rho(1-\upsilon)}} = \frac{1}{2L}\sqrt{\frac{E}{\rho(1-\upsilon)}}\sqrt{\frac{1}{1+\frac{\Delta m}{M}}} = f_0\sqrt{\frac{1}{1+\frac{\Delta m}{M}}} \qquad (3\text{-}5)$$

Since the loading mass (Δm) is small relative to the mass of sensor (M), based on Eq. (3-5), the shift in resonant frequency (Δf) is given by:

$$\Delta f = f_{load} - f_0 = f_0 \left(\sqrt{\frac{1}{1+\frac{\Delta m}{M}}} - 1 \right)$$

$$= f_0 \left(\left(1 - \frac{1}{2}\frac{\Delta m}{M} \right) - 1 \right) = -\frac{f_0}{2}\frac{\Delta m}{M} \qquad (3\text{-}6)$$

where f_0 is the initial resonance frequency. Eq. (3-6) shows that the resonant frequency shifts linearly and decreases with increasing mass on the sensor surface. Hence, with the binding of the target organism to the sensor surface, the mass increases, and the mechanical oscillation will change, producing a shift in the resonant frequency to a lower value.

Combined with Eq. 3-5, the mass sensitivity of the ME sensor can be expressed as:

$$S_m = \frac{\Delta f}{\Delta m} = -\frac{f_0}{2M} = -\frac{1}{2M}\frac{1}{2L}\sqrt{\frac{E}{\rho(1-\upsilon)}} = -\frac{1}{4l^2 wt\rho}\sqrt{\frac{E}{\rho(1-\upsilon)}} \qquad (3\text{-}7)$$

where S_m is the mass sensitivity of ME sensor, w and t are the width and thickness of sensor respectively. From this equation, it is clear that when a small mass is loaded on the sensor, the mass sensitivity depends primarily on the length of the sensor and is inversely proportional to l^2.

1.4. Operating principles of ME biosensors

In order to detect the presence of selective and specific pathogens (which may be spores, bacteria, or viruses), bio-molecular recognition elements (phages, antibodies or, enzymes) will be coated onto the surface of the ME platform to form a ME biosensor. This research uses a filamentous phage as the bio-molecular recognition element, after Petrenko et al. [10-12]. The working principles of an ME biosensor (after immobilization of the bacteriophage on the ME platform) are the same as for an ME platform. A time-varying (AC) magnetic field, supplied by a network analyzer is used to resonate the ME biosensors. Before loading the spores/bacteria cells, the frequency of the ME biosensor is recorded as $f_{0.}$ Upon coming into contact with the biosensor, the target spores/cells are captured by the specific phage immobilized onto the biosensor's surface, resulting in an increase in the mass on the ME biosensor. This added mass will cause a corresponding decrease in the biosensor's resonance frequency (f_{mass}). These measurements are performed remotely and wirelessly.

Figure 3-3 illustrates the wireless nature of the individual ME biosensor and the basic principle for detecting bound mass (spores/cells). The frequency spectrum of the biosensor can be obtained by sweeping an AC magnetic interrogation field over a pre-determined frequency range while monitoring the response of the biosensor using a pickup coil. At the resonance frequency of the biosensor, the conversion of the magnetic energy into elastic energy is maximal and the biosensor undergoes a maximal oscillation.

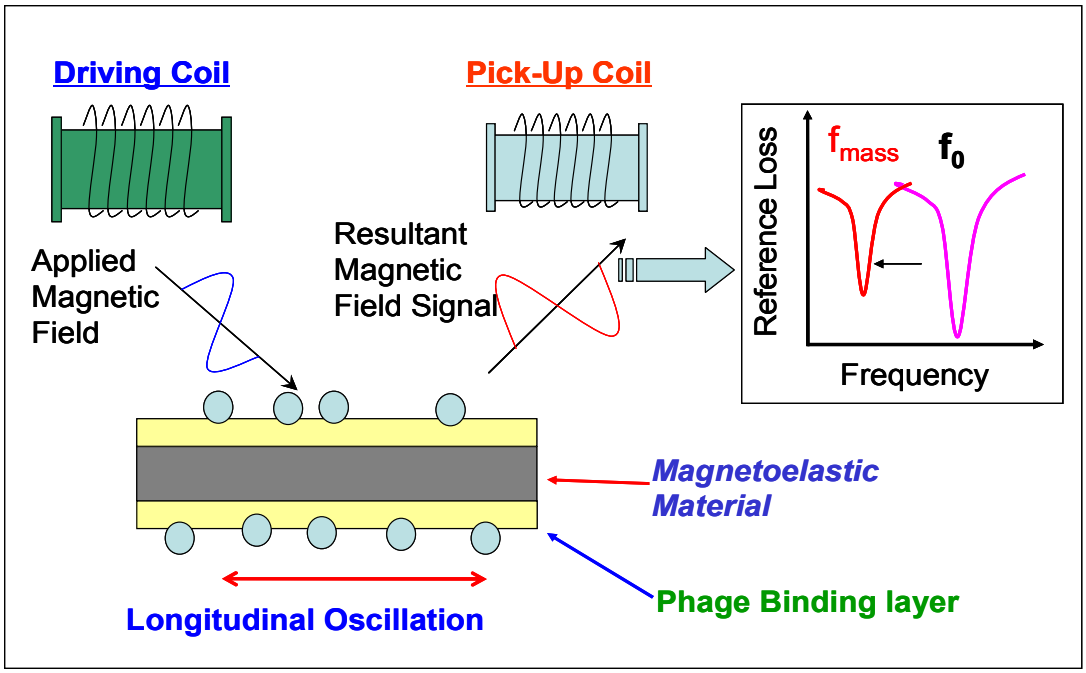

Figure 3- 3. Wireless ME biosensor operation and the basic principle for detecting bacterial cells and spores. The fundamental resonant frequency of the biosensor f_0 without target binding decreases to f_{Mass} due to target binding.

1.5. Signal Amplification with Variable DC bias

Changing the DC bias (H_n) will vary the amplification of the output signal of the ME biosensor. This can be clearly shown from Figure 3-4 [13], where H_2 provides the maximum amplification. For an ME biosensor, the optimum frequency signal can be obtained by adjusting the DC bias field until the amplitude of the signal reaches a peak. This research uses a DC biasing magnetic field provided by a bar magnet to amplify the resonance signal. The distance between the magnet and the coil can be adjusted to maximize the amplitude of the resonance signal.

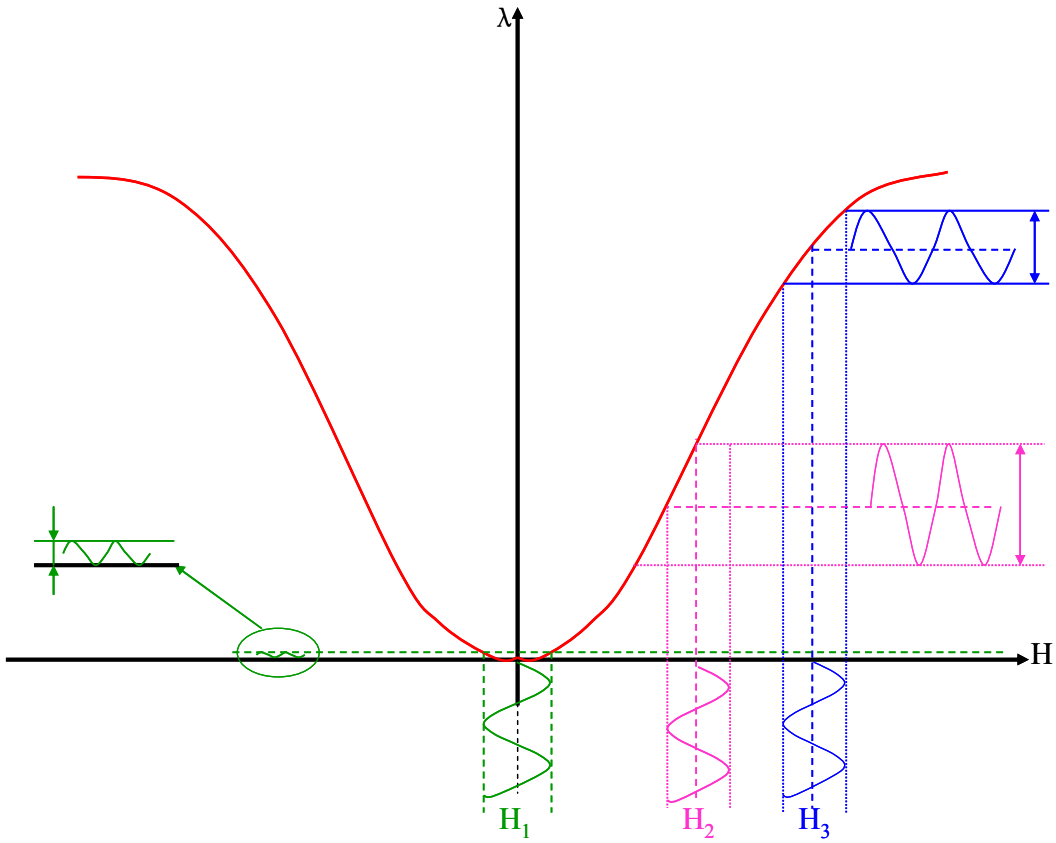

Figure 3- 4. Magnetoelastic biosensor for a range of DC bias conditions.

2. Use of a bacteriophage as a biorecognition element

2.1. JRB7/E2 phage

The general selection procedure for spore/salmonella–binding phage clones (JRB7/E2 phage clone) involves three-steps [11, 14]: 1) Construction of an f8/8 landscape phage library by replacing amino acids on every copy of pVIII protein coat with eight amino acids; 2) Affinity selection of phage specific to *B. anthracis* spores/*S. typhimurium* from the new landscape library; and 3) ELISA with *B. anthracis* spores/*S.*

typhimurium. The second step is a typical biopanning procedure used to obtain a specific phage ligand by using target spores/bacteria as a selector, and involves two to four rounds of selection [14-16]. The procedure for each biopanning selection proceeds as follows: a) coat spores/bacteria suspension onto an empty Petri dish and dry overnight; b) block the well with 0.1% BSA in TBS and wash 3 times with TBS/0.1% tween; c) add landscape phage library f8/8 to the dish and incubate 1hr; d) wash the dish 6 times with TBS/0.1% tween to remove the unbound phage particles; e) add the elution buffer to contract the selected phage, transfer the selected phage suspension to a microcentrifuge tube, centrifuge, and neutralize using Tris (pH 9.1), followed by another wash with TBS. These concentrated phage clones will be propagated and purified for use in the next round of selection; and, finally, f) add the phage clones selected from the first round to the spore-coated well and repeat the selection process described above. After two to four rounds of selection, individual specific phage clones will be amplified and sequenced to determine the amino acid sequences of the displayed peptides [17]. A schematic drawing to depict the selection procedure for specific phage is shown in Figure 3-5 below.

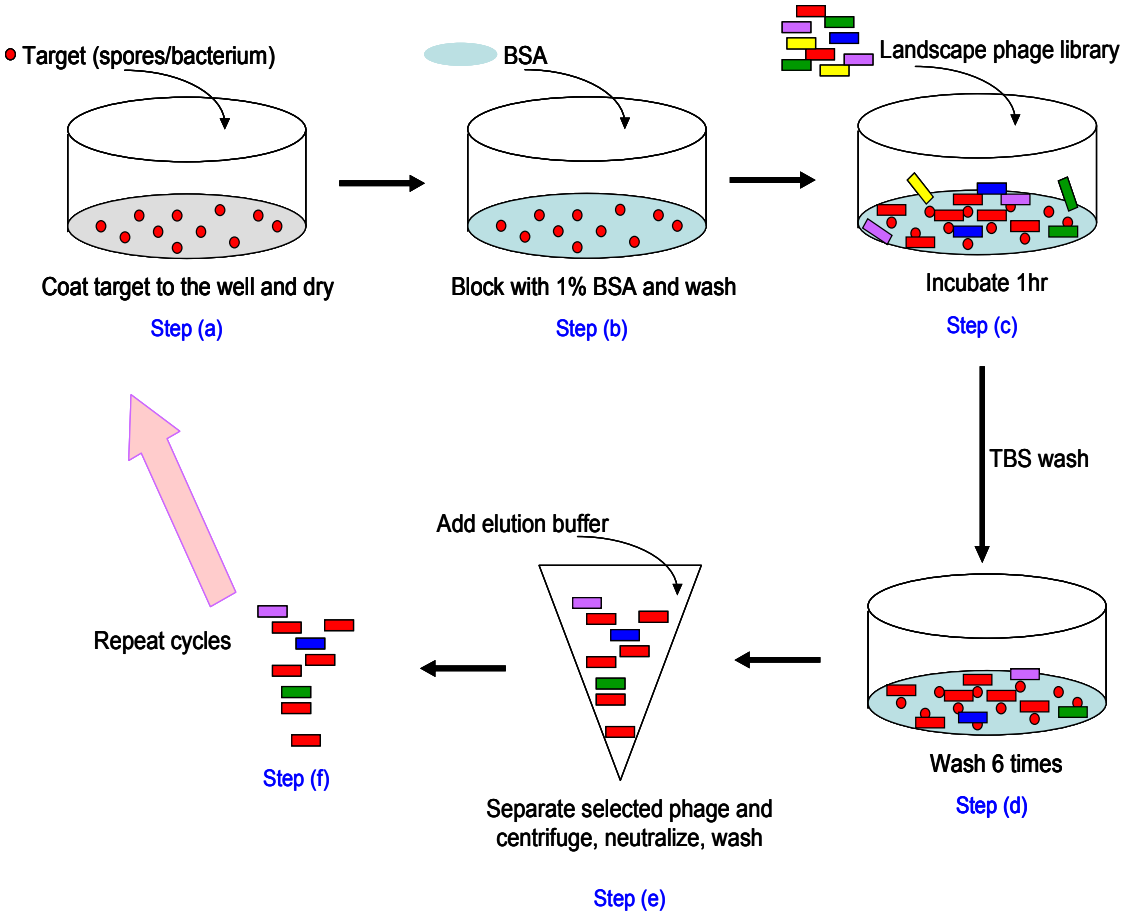

Figure 3- 5. The selection procedure for phages.

2.2. Effect of salt concentration on phages

According to the well-known Poisson-Boltzman theory [18], in an aqueous medium, two parallel like-charge biopolymers would always be expected to repel each other [19]. However, a variety of experiments on rod-like polyelectrolytes (i.e. DNA, F-actinic, filamentous viruses and microtubules) have shown the opposite phenomenon, where the attractive interaction holds these like-charged biopolymers together [20-26]. For the densely packed molecules that occur in DNA solutions, this phenomenon is

known as DNA condensation [27], while, for F-actin and filamentous viruses, it is known as bundling or lateral aggregation [25].

Over the last few decades, a great deal of attention has been devoted to exploring the cause of this self-assembly interaction in solutions and the presence of multivalent counterions is known to be a major contributing factor [25]. This was first noted by Kirkwood and Schumaker (1952), and several possible theories have since been put forth to explain the mechanism. The concept of Manning condensation was proposed to explain the observed behavior when the distance between ions becomes smaller. This theory posits that there will be a strong spatial correlation between ions when they condense on the surface of a polyelectrolyte [25] that creates an attractive force that induces like-charge interactions. Alternatively, the Wigner crystal (WCR) model [28, 29] suggested a similar concept that was related to the correlation between counterions. According to the WCR model, counterions will form a WCR structure on a background of parallel polyelectrolytes. The counterions neutralize the charge of these polyelectrolytes and enable them to approach each other more closely. Attractive interactions will be induced because of the cohesive energy of these counterions. In an alternative approach, the Oosawa model predicts that temperature will have an opposite effect to that suggested by the WCR model, and that higher temperatures will make it easier to destroy the crystal structure, resulting in weaker ion correlations [29-32].

In order to evaluate the theoretical analyses above, experimental studies are required to demonstrate how this electrostatic attraction functions in real systems.

Monte Carlo simulation [33] is one of the most widely used methods to determine the molecular interactions of hexagonally packed rod-like polyelectrolytes within a bulk salt solution. Different experimental conditions can be simulated by varying the distances between two phages, their diameters and the concentrations of the divalent salt concentrations. Monte Carlo simulation thus provides a quantitative way to predict the threshold concentration of divalent salt for the attractive force to come into play, as well as explain how the osmotic pressure varies with distance between the two phages.

Filamentous bacteriophages have been widely used as a test system to determine the effect of counterions on the aggregation of like-charge polyelectrolytes. Phages fd (infecting *E. Coli*), M13, Pf1 (infecting *P. aeruginosa*, strain K), Pf3 (infecting *P. aeruginosa*, strain PAO), and PH75 (infecting *T. thermophilus*) are all well-characterized filamentous phages [34]. They are usually cylindrical particles with rough surfaces and are known to survive in high temperature and high salinity environments. These properties make them ideal for any analysis of attractive interactions. Among these phages, phage fd and M13 have been of particular interest as both are long and stiff, allowing them to be considered as straight rods.

In most experiments, di- or polyvalent salts have been introduced as the counterions [35]. Several groups [24, 25] have already performed a large number of experiments to show the effect of radius and concentrations of Mg^{2+}, Ca^{2+} on phage bundling. In addition to experiments with multivalent ions, monovalent ions have also been used to determine the effect of counterions. Overman's group [34] has used

Raman Spectroscopy to determine the isotropic and anisotropic status of phage suspensions containing different amounts of NaCl, and their results show that there is indeed a balance between salt concentration and phage concentration. They reported observing phage bundling in a low-virus (<10mg/ml) suspension containing a high amount of salt (>200mM).

The phage-based wireless magnetoelastic (ME) biosensors used in this project consist of a magnetoelastic resonator interfaced with an engineered filamentous phage that serves as a bio-recognition element. Biosensor performance can be affected by a tertiary structure of immobilized filamentous phage, which has a tendency to form bundles due to polarization-based, attractive interactions. The bundling of the phage can lead to a reduction in the specific binding surface of the biosensor and hence decreased sensitivity of the biosensor towards the target analyte. Consequently, unlike the approaches described above, which depend on the biophysical application of filamentous phages and divalent ions as the counterions, this research will utilize an engineering approach to analyze the bundling of phage. This dissertation therefore focuses on the effect of monovalent salt concentration on the lateral aggregation status of phages in solution, as well as their distribution on ME biosensor platforms for the detection of bacterial cells and spores.

3. Target analytes to be detected

B. anthracis spore and *S. typhimurium* are the two primary pathogenic targets of this research, and they are discussed in more detail below.

3.1. *S. typhimurium*

S. typhimurium is one of the most common intestinal infections and the second most common foodborne illness in the U.S., with cases being especially common during the warmer months of the year. The reported incidence of Salmonellosis is about 17 cases per 100,000 persons in the U.S. [36]. Every year, there are approximately 500 to 1,000 fatalities [37] related to S*almonella* infections, and these account for 31% of all food-related deaths [38, 39].

Daniel E. Salmon, a veterinary scientist, identified the first *Salmonella* strain, *S. Choleraesuis*, in the intestine of a pig in 1885 [38] and there are now approximately 2,000 different known serotypes of *Salmonella* bacteria. Among those, *S. typhimurium* is an emerging pathogen and a particularly virulent strain that usually causes typhoid fever, and is becoming a leading cause of gastrointestinal foodborne illness (Preliminary foodnet data, 2003). This organism is now the second most prevalent strain of *Salmonella* after *S. serotype Enteritidis* [39]. *S. typhimurium* is also a potential weapon for bioterrorism.

The conventional methods for detecting S. *typhimurium* are slow, labor-intensive and cost-inefficient. Current research mainly utilizes antibodies as bioreceptors to form

biosensors to capture the cells. Although these are sensitive and selective, this approach has many disadvantages, including high cost, low availability, high fragility, lack of reusability, and the need for laborious immobilization. In our research, a filamentous phage, selected from a landscape library, will act as a substitute for the antibody. Phages are more reliable, cheaper, simpler, and faster to use than traditional antibodies.

3.2. *B. anthracis* spores

B. anthracis is a spore-forming bacterium that causes anthrax, an acute infectious disease. These spores can survive harsh environments, such as exposure to ultraviolet and ionizing radiation, heat, and treatment with various chemicals [40, 41]. Usually, *B. anthracis* is a rod-shaped, gram positive, aerobic, nonmotile, facultative anaerobic and spore-forming bacterium [40]. It may occur in a chain, and its spore has an oval structure.

Anthracis spores may survive in the soil, in water, and on surfaces for many years. Anthrax typically occurs in wild and domestic lower vertebrates. It can also be transmitted to humans upon exposure to infected animal products (e.g. the handling of contaminated samples through the skin or the inhalation of airborne spores) or tissues from infected animals (e.g. ingesting undercooked meat contaminated with anthrax organisms). It is found globally, mainly in developing countries or countries without sufficient veterinary/public health programs. Certain regions in the western hemisphere (i.e. South and Central America) are reported to have more cases of anthrax in animals

than others. Spores of *B. anthracis* can be produced and stored in a dry form and remain viable for decades in storage or after release. The possibility of creating aerosols containing anthrax spores has made *B. anthracis* a prime candidate as a weapon of bioterrorism. As an agent of biological warfare, *B. anthracis* spores could be used to infect individuals through inhalation. In the United States, such an incident caused a respiratory infection that sickened and killed several individuals in the fall of 2001.

Cutaneous, gastrointestinal and inhalational infections are the three pathways of human infections of anthrax. Each form progresses within a few days without showing obvious symptoms. The cutaneous form, which is the most common, is easiest to diagnose due to the presence of a painless black scar on the skin. In the other two forms, the illness will be accompanied by a mild fever or flu-like symptoms. Because the illness is insidious and develops into a systemic form abruptly, which is rapidly fatal, it is difficult to achieve early diagnosis, resulting in medical failure [42].

Since *B. anthracis*, *B. cereus*, *B. thuringiensis* all belong to the *B. cereus* group, it is difficult to distinguish between them. In the past decade, scientists have tried to find a rapid and reliable way to identify *B. anthracis* when the spores are used as a biological weapon. Recently, several methods have been developed for the identification of *B. anthracis*, including QCM, real-time PCR, love-wave biosensors, ELISA, and fluorescence-activated cell sorting. However, most of these are expensive, complicated, and time-consuming, requiring spore germination and outgrowth of vegetative cells. Daffonchio et al. reported a method of using a randomly amplified polymorphic DNA

marker, but it is uninformative about the plasmid content and consequently the strain virulence [43]. PCR-RFLP, ribotyping, and ERIC-PCR techniques are also used for typing *B. anthracis* and *B. cereus* strains, but Shangkuai et al. report that none have been developed into a perfect tool [44]. Patra et al. [45] isolated specific chromosomal DNA of *B. anthracis* for diagnosis, while Ramisse et al. [46] combined the *B. anthracis*–chromosomal DNA with analysis of PCR. However, *B. anthracis* strains can't as yet be unambiguously distinguished from other strains of the *B. cereus* group due to their chromosomal markers [45].

Hence, a simple, cheap, real-time method with high selectivity and accurate sensitivity is urgently needed to detect the presence of *B. anthracis* spores. In response to this, the Auburn University Detection & Food Safety (AUDFS) Center is focusing its efforts on developing improved detection techniques capable of providing good specificity, sensitivity, reliable identification, and short detection time of these spores. This research will not only help protect the public by providing early warning of terrorist attacks, but also protect our society against foodborne illness. Additionally, this method is also capable of detecting the spores in a liquid environment.

It is important to note that, for our experiments, the Sterne strain of *Bacillus anthracis* spores will be used. This is the nonpathogenic, veterinary vaccine strain of anthrax which lacks the internal plasmid that carries the genes required for capsule reproduction in vegetative cells. However the Sterne strain spore has on its exterior all the antigenic markers common with pathogenic *Bacillus anthracis* strains, so the binding

efficiency of phage to *Bacillus anthracis* Sterne strain spores should be identical to that of pathogenic *Bacillus anthracis* spores.

4. References

[1] E. T. Lacheisserie, D. Gignoux, and M. Schlenker, *Magnetism - Materials and Applications*: Springer, 2005.

[2] R. E. Hummel, *Electronic Properties of Materials*, 3rd. ed.: Springer-Verlag New York, Inc., 2001.

[3] A. Hernando, M. Vazquez, and M. Barandiaran, "Metallic glasses and sensing applications," *J. Phys. E: Sci. Instrum. ,* vol. 21, pp. 1129-1139, 1988.

[4] C. Modzelewski, H. T. Savage, L. T. Kabacoff, and A. E. Clark, "Magnetomechanical coupling and permeability in transversely annealed Metglas 2605 alloys," *IEEE Trans. Magn. ,* vol. MAG-17(6), pp. 2837-2839, 1981.

[5] R. C. O'Handley, *Modern Magnetic Materials: Principles and Applications*. New York,: John Wiley & Sons Inc., 2000.

[6] C. A. Grimes, C. S. Mungle, K. Zeng, M. K. Jain, W. R. Dreschel, M. Paulose, and K. G. Ong, "Wireless Magnetoelastic Resonance Sensors: A Critical Review," *Sensors* vol. 2, pp. 294-313, 2002.

[7] C. A. Grimes, Q. Cai, K. G. Ong, and K. Loiselle, "Environmental monitoring using magnetoelastic sensors," *Proc. SPIE* vol. 4097, pp. 123-133, 2000.

[8] C. Liang, S. Morshed, and B. C. Prorok, "Correction for longitudinal mode

vibration in thin slender beams," *Applied Physics letter. ,* vol. 90, p. 221912, 2007.

[9] C. Liang and B. Prorok, "Measuring the thin film elastic modulus with a magnetostrictive sensor," *J. Micromech. Microeng. ,* vol. 17, pp. 709-716, 2007.

[10] V. A. Petrenko and G. P.Smith, "Phages from landscape libraries as substitute antibodies," *Protein Engineering,* vol. 13, pp. 589-592, 2000.

[11] V. A. Petrenko, G. P. Smith, X. Gong, and T. Quinn, "A library of organic landscapes on filamentous phage," *Protein Engineering,* vol. 9, pp. 797-801, 1996.

[12] V. A. Petrenko and V. J. Vodyanoy, "Phage display for detection of biological threat agents," *Journal of Microbiological Methods,* vol. 53, pp. 253-262, 2003.

[13] S. Li, "Development of Novel Acoustic Wave Biosensor Platforms Based on Magnetostriction and Fabrication of Magnetostrictive Nanowires," in *Materials Engineering*. vol. Ph.D. Auburn: Auburn University, 2007, p. 25.

[14] J. Brigati, D. D. Williams, I. B. Sorokulova, V. Nanduri, I. H. Chen, C. L. Turnbough, and V. A. Petrenko, "Diagnostic probes for Bacillus anthracis spores selected from a landscape phage library," *Clinical Chemistry,* vol. 50, pp. 1899-1906, Oct 2004.

[15] V. A. Petrenko and I. B. Sorokulova, "Detection of biological threats. A Challenge for directed molecular evolution," *Journal of Microbiological Methods,* vol. 58, pp. 147-168, 2004.

[16] I. B. Sorokulova, E. V. Olsen, I. Chen, B. Fiebor, J. M. Barbarree, V. J. Vodyanoy, B. A. Chin, and V. A. Petrenko, "Landscape phage probes for Salmonella typhimurium," *Journal of Microbiological Methods,* vol. 63, pp. 55-72, 2005.

[17] S. J. Haas and G. P. Smith, "Rapid sequencing of viral DNA from filamentous bacteriophage," *Biotechniques,* vol. 15, pp. 422-424, 1993.

[18] J. Israelachvili, *Intermolecular and Surface Forces* London: Academic Press, 1985.

[19] F. Oosawa, "PB theory of infinitely thin rods, and discussion of fluctuation-induced attraction," *Biopolymers,* vol. 6, p. 134, 1960.

[20] P. G.. Arscott, C. Ma, J. R. Wenner, and B. A. Bloomfield, "DNA condensation by cobalt hexaammine(III) in alcohol-water mixtures: Dielectric constant and other solvent effects," *Biopolymers,* vol. 36, pp. 345-364, 1995.

[21] J. X. Tang and P. A. Janmey, "The Polyelectrolyte Nature of F-actin and the Mechanism of Actin Bundle Formation," *J. Biol. Chem.,* vol. 271, pp. 8556-8563, April 12, 1996 1996.

[22] T. E. Angelini, H. Liang, W. Wriggers, and G. C. L. Wong, "Like-charge attraction between polyelectrolytes induced by counterion charge density waves," *Proceedings of the National Academy of Sciences of the United States of America,* vol. 100, pp. 8634-8637, July 22, 2003 2003.

[23] J. C. Butler, T. Angelini, J. X. Tang, and G. C. L. Wong, "Ion Multivalence and Like-Charge Polyelectrolyte Attraction," *Physical Review Letters,* vol. 91, p.

028301, 2003.

[24] A. P. Lyubartsev, J. X. Tang, P. A. Janmey, and L. Nordenskiöld, "Electrostatically Induced Polyelectrolyte Association of Rodlike Virus Particles," *Physical Review Letters,* vol. 81, p. 5465, 1998.

[25] J. X. Tang, P. A. Janmey, A. Lyubartsev, and L. Nordenskiold, "Metal Ion-Induced Lateral Aggregation of Filamentous Viruses fd and M13," *Biophysical Journal,* vol. 83, pp. 566-581, July 1, 2002.

[26] E. Raspaud, M. O. de la Cruz, J. L. Sikorav, and F. Livolant, "Precipitation of DNA by polyamines: A polyelectrolyte behavior," *Biophysical Journal,* vol. 74, pp. 381-393, Jan 1998.

[27] J. Ray and G. S. Manning, "An attractive force between two rodlike polyions mediated by the sharing of condensed counterions," *Langmuir,* vol. 10, pp. 2450-2461, 1994.

[28] B. I. Shklovskii, "Wigner Crystal Model of Counterion Induced Bundle Formation of Rodlike Polyelectrolytes," *Physical Review Letters,* vol. 82, p. 3268, 1999.

[29] I. Rouzina and V. A. Bloomfield, "Macroion Attraction Due to Electrostatic Correlation between Screening Counterions. 1. Mobile Surface-Adsorbed Ions and Diffuse Ion Cloud," *J. Phys. Chem.,* vol. 100, pp. 9977-9989, 1996.

[30] N. Grønbech-Jensen, R. J. Mashl, R. F. Bruinsma, and W. M. Gelbart, "Counterion-Induced Attraction between Rigid Polyelectrolytes," *Physical Review Letters,* vol. 78, p. 2477, 1997.

[31] J. J. Arenzon, J. F. Stilck, and Y. Levin, "Simple model for attraction between like-charged polyions " *The European Physical Journal B - Condensed Matter and Complex Systems,* vol. 12, pp. 79-82, 1999.

[32] B. I. Shklovskii, "Screening of a macroion by multivalent ions: Correlation-induced inversion of charge," *Physical Review E,* vol. 60, p. 5802, 1999.

[33] L. A. Day, C. J. Marzec, S. A. Reisberg, and A. Casadevall, "DNA packing in filamentous bacteriophages," *Ann. Rev. Biophys. Biophys. Chem. ,* vol. 17, pp. 509-539, 1988.

[34] S. A. Overman, D. M. Kristensen, P. Bondre, B. Hewitt, and G. J. T. Jr., "Effects of virion and salt concentrations on the Raman signatures of filamentous phages fd, Pf1, Pf3, and PH75," *Biochemistry,* vol. 43, pp. 13129-13136, 2004.

[35] M. T. Record, W. Zhang, and C. F. Anderson, "Analysis of effects of salts and uncharged solutes on protein and nucleic acid equilibria and processes : A practical guide to recognizing and interpreting polyelectrolyte effects, Hofmeister effects, and osmotic effects of salts," *Adv. Protein Chem. ,* vol. 51, pp. 281-353, 1998.

[36] CDC, "Preliminary FoodNet Data on the Incidence of Foodborne Illnesses - Selected Sites, United States, 1999," *MMWR Weekly,* vol. 49, pp. 210-205, 2000.

[37] "http://www.cdc.gov/health/diseases.htm."

[38] "http://www.about-salmonella.com/."

[39] "http://www.cfsan.fda.gov/~dms/a2z-s.html."

[40] M. Mock and A. Fouet, "ANTHRAX," *Annual Review of Microbiology,* vol. 55, pp. 647-671, 2001.

41] A. Sjöstedt, U. Eriksson, V. Ramisse, and H. Garrigue, "Detection of *Bacillus anthracis* spores in soil by PCR," *FEMS Microbiology Ecology,* vol. 23, pp. 159-168, 1997.

[42] P. Turnbull, "Anthrax vaccines: past, present and future," *Vaccine,* vol. 9, pp. 533-539, 1991.

[43] D. Daffonchio, S. Borin, G. Frova, R. Gallo, and E. Mori, "A randomly amplified polymorphic DNA marker specific for the Bacillus cereus group is diagnostic for *Bacillus anthracis*," *Appl. Environ. Microbiol. ,* vol. 65, pp. 1298-303, 1999.

[44] Y. H. Shangkuan, J. F. Yang, H. C. Lin, and M. F. Shaio, "Comparison of PCR-RFLP, ribotyping and ERIC-PCR for typing *Bacillus anthracis* and *Bacillus cereus* strains," *J. Appl. Microbiol. ,* vol. 89, pp. 452-462, 2000.

[45] G. Patra, J. Vaissaire, M. Weber-Levy, C. L. Doujet, and M. Mock, "Molecular characterization of Bacillus strains involved in outbreaks of anthrax in France in 1997," *J. Clin. Microbiol. ,* vol. 36, pp. 3412-3414, 1998.

[46] V. Ramisse, G. Patra, H. Garrigue, J.-L. Guesdon, and M. Mock, "Identification and characterization of *Bacillus anthracis* by multiplex PCR analysis of sequences on plasmids pXO1 and pXO2 and chromosomal DNA," *FEMS Microbiol. Lett.,* vol. 145, pp. 9-16, 1996.

CHAPTER 4

MATERIALS AND METHODS

1. Magnetoelastic sensor platform fabrication

1.1. Sensor platform

In this research, commercially available ME material (2826MB Metglas™ film, $Fe_{40}Ni_{38}Mo_4B_{18}$, Honeywell) was selected as the sensor platform. Metglas™ 2826MB was received in the form of rolls of ribbon with a width of 12.5 mm and a thickness of 30 μm. This material has a Curie temperature of 353 °C and a crystallization temperature of 410 °C, with a magnetostriction (λ_s) of 12ppm. Table 4-1 shows the detailed parameters for Metglas™ 2826MB [1]. In order to fabricate the ME sensor platform, it was cut off the roll and hand polished to 15 μm using grit paper 1000-2000 micron. This polishing provided a smoother surface for bio-recognition element immobilization and also a thinner platform, decreasing the initial mass of sensor in order to increase its sensitivity (discussed in more detail in Chapter **3,** Section **1.3.**).

Table 4- 1. Properties of METGLAS™ 2826MB.

Property	Value
Poisson ratio	0.5
Tensile Strength (GPa)	1-2
Elastic Modulus (GPa)	100-110
Density (g/cm^3)	7.9
Thermal Expansion (ppm/°C)	11.7
Continuous Service Temp. (°C)	125
Saturation Magnetostriction (ppm)	12
Saturation Induction (Tesla)	0.88
Maximum D.C. Permeability (μ): Annealed	800,00
Maximum D.C. Permeability (μ): As Cast	>50,000

After polishing, the ME alloy was sandwiched between 2 sheets of polymer film and cut by a micro-dicing saw to obtain sensor platforms with final dimensions of 1.9 × 0.4 × 0.015 mm and 2.0 × 0.4 × 0.015 mm. All the platforms used for these experiments were fabricated with a length (L) to width (w) ratio of 5:1. In order to remove any residual film after dicing, these ME sensor platforms were ultrasonically cleaned in acetone with micro-90 solution for 1 h, in ethanol for 0.5 h, and then dried in air. After dicing, the cleaned ME sensor platforms were annealed to relieve residual

internal stress and correct defects due to the mechanical polishing and dicing operations. Annealing was carried out at 220 °C for 2 hr in a vacuum oven (Fisher Isotemp Model 281A, Vacuum Oven), under a vacuum of at least 10^{-3} Torr. Afterwards, the sensor platforms were cooled to room temperature in the oven while still under vacuum. Then, thin films of chromium followed by gold were deposited onto both sides of the ME platforms using a Denton™ Vacuum Discovery-18 sputtering system (Moorestown, NJ) with two cathodes (RF and DC). All deposition of metals was conducted in a vacuum chamber evacuated to a background pressure of no more than 5×10^{-6} Torr. Argon was used as the sputtering gas to bring the deposition pressure up to between 5 and 6 mTorr. On each side of the ME platforms, Cr was deposited first after which the Au layer is deposited without breaking the vacuum. The fabricated platforms were then stored in a desiccator until use. Prior to immobilization of the bio-recognition element, the sensor platforms were washed with hexane and air dried.

1.2. Measurement setup

Figure 4-1 shows the schematic of the system for the detection of the resonance frequency of the ME sensor platform in air. The resonance frequency of the sensor platform was detected using a network analyzer with an S-parameter adapter operating in the S11 reflection mode. A coil of wire (pickup coil) was used to sense the change in flux through the sensor. The inductance of this coil of wire changes with flux density through the coil. Since an increase in inductance results in a higher resistance

(impedance) to a current change in the coil, a device that senses current change is a convenient way of determining the resonant frequency of the ME sensor platform.

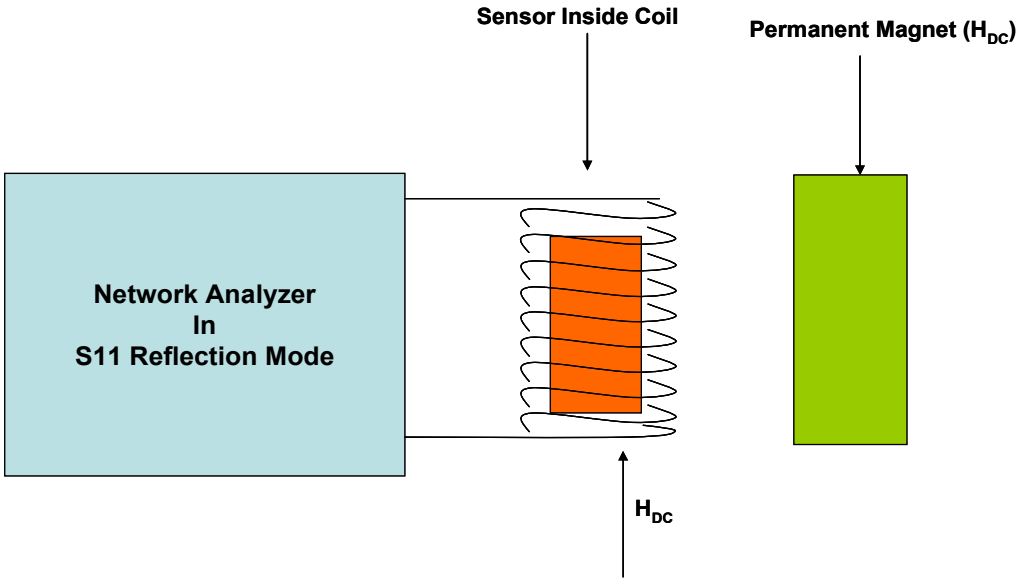

Figure 4- 1. Schematic of the Detection System.

During testing, the sensor platform was placed inside the pickup coil, which was connected to the port of the network analyzer. The analyzer then applied a time varying (AC) current through this coil to produce an AC magnetic field, creating mechanical oscillations in the sensor platform. Since the sensor platform has a magnetic hysteresis loop characteristic (details explained in Chapter **3** Section **1.5.**), a certain DC magnetic field intensity exists which results in the greatest physical length change for an incremental change in applied field intensity. For this experiment, a permanent magnet is placed in the proximity of the pickup coil (with its magnetic field lines parallel to the

pickup coil axis). The position of this magnet with respect to the coil was then adjusted until the amplitude of the resonance peak reached a maximum. This DC magnetic bias field then remained fixed during the testing of each sensor. The network analyzer sweeps the frequency from a low starting value to a higher ending value and determined the resonant frequency by identifying the minimum in the amplitude versus frequency curve. Figure 4-2 shows the measured fundamental resonance of the ME platform in air at room temperature, where the resonant frequency is at the minimum of the curve at 1.142 kHz. Following the procedure described above, this ME platform was fabricated by dicing the Metglas material to a size of 1.9 × 0.4 × 0.015 mm, followed by depositing thin film layers of first Cr (92.3 nm), and then gold (154.4 nm).

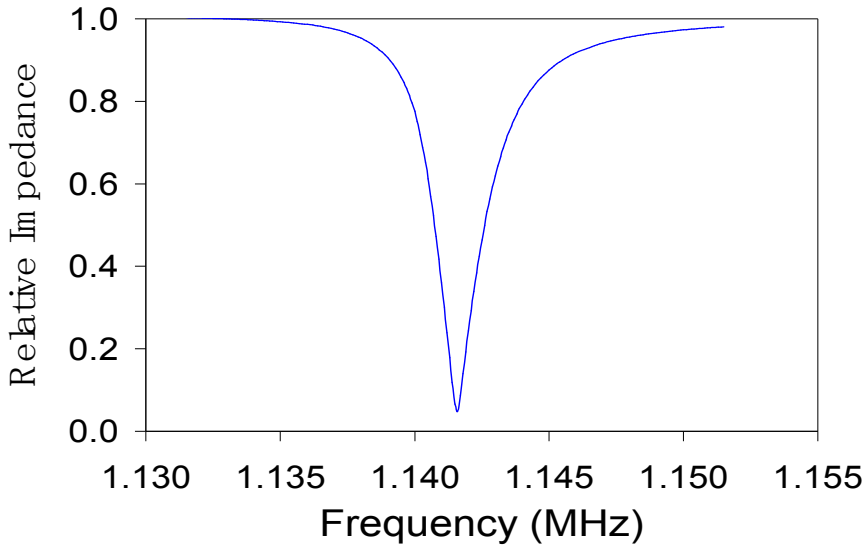

Figure 4- 2. Relative impedance of the ME sensor platform measured in air at room temperature.

In this dissertation, a phage-based ME biosensor was formed by immobilizing the bacteriophage on the ME sensor platform. The resonance frequency measurements for the ME biosensors were the same as for the ME sensor platform described above.

2. Cultures and phage suspensions

2.1. Filamentous phages

The affinity selected filamentous phage clones E2 and JRB7 used for this work, with a concentration of 1.06×10^{13} vir/mL, were provided by Dr. Barbaree of the Department of Biological Sciences at Auburn University. Dr. Petrenko and his coworkers [2-5] have shown that the E2 phage clone and JRB7 phage clone are highly specific to *S. typhimurium* and *B. anthracis* spores, respectively. The detailed preparation procedures for both phages are described in Chapter **3** Section **2.1.**. The phage clones were derived from the landscape f8/8 phage library and all phage suspensions were diluted in 1xTBS (25 mM Tris, 3 mM KCl, and 140 mM NaCl at a pH of 7.5) before use.

2.2. Bacterial and spore suspensions

Spores of the nonpathogenic Sterne strain of *B. anthracis*, *B. cereus* and *S. typhimurium* (ATCC13311) and *E. coli* suspensions ($5x10^8$ spores/ml) were provided by Dr. Barbaree's lab at the Department of Biological Sciences at Auburn University. Concentration were measured using a spectrophotometer OD600 followed by plate culture confirmation. *B. anthracis* Sterne strain is a nonpathogenic vaccine strain of *B.*

anthracis that lacks one plasmid on the interior of the spore. The suspensions were serially diluted with sterile distilled water to prepare bacterial suspensions ranging from 5 $\times 10^1$ to 5 $\times 10^8$ cfu/mL. Prior to each dilution, the solutions were mixed using a vortex mixer for 1 min to ensure homogeneity. This is especially important for spore-containing suspensions because spores cluster more easily than bacteria cells. All biological test solutions used for this study were prepared and tested on the same day. Test solutions were stored at 4°C and equilibrated to room temperature prior to testing.

3. Experimental procedures

3.1. Improving the performance of the ME platform

3.1.1. Annealing effects

In order to choose the optimum temperature for annealing, thirty ME sensor platforms with the dimensions 2.0 × 0.4 × 0.015 mm were chosen after dicing. After testing and recording the resonance frequency for each platform, these samples were annealed at 150 °C, 200 °C, 250 °C or 300 °C, with 6 samples tested for each temperature, for 2 h in a vacuum oven, under a vacuum of 10^{-3} Torr and then cooled to room temperature. The resonance frequency of each sample was again tested and recorded while keeping all other testing conditions the same. The amplitude of the frequency signal and spectrum quality Q-factor before and after annealing were compared. Also in order to determine the surface microstructure of the ME platform before and after annealing, samples were annealed at 75°C, 150 °C, 200 °C, 250 °C or 300 °C and

observed using scanning electronic microscopy (SEM).

3.1.2. Sputtering effects

After annealing, thin films of Cr and Au were deposited, in order to allow the immobilization of phage on the platform surface and to further protect the ME material from degradation in the saline solutions. Cr was chosen specifically because it not only provided extra electrochemical resistance from corrosion for the sensor platform, but also improved the adhesion between the substrate and the Au layer. The purpose of the Au layer was twofold: it protected the ME material from corrosion in aqueous environments, and provided a bioactive surface upon which bacteriophages could be easily adsorbed.

In order to determine the optimum sputtering condition, Cr / Au film was deposited onto different glass slides at a sputtering power of either 50, 100, 150, 200, or 250 w for 600 s. One part of each slide was covered by Kapton tape that was then removed before measuring the film thickness using a profilometer. The film thickness was measured in several different places on each slide in order to obtain an average value. Also the optimum sputtering power for deposition of Cr/Au layer can be determined by the uniformity of the Cr/Au film. Figure 4-3 shows the relationship between deposition rates and different power levels for Au and Cr.

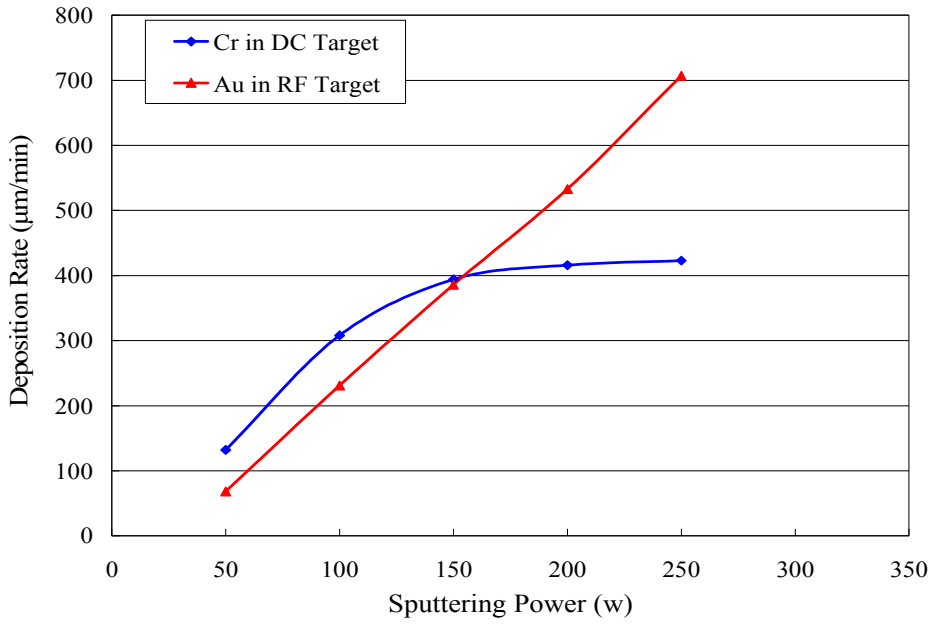

Figure 4- 3. Deposition rates for different sputtering powers.

3.1.3. Corrosion resistance / Effect of gold layer thickness

The performance of an ME biosensor will inevitably be affected by the properties of its ME platform and this is made of an iron rich material which is easily corroded. Also, the biosensor must work in analyte solutions, which are often based upon buffered salt solutions that preserve the living pathogenic organisms. The most commonly used salt solutions used for this type of experiment are described in Table 4-2, after Petrenko and Sorokulova [4]. These solutions can induce accelerated corrosion of the iron-containing ME materials and lead to rapid delamination of the gold layer. Thus, enhancing the corrosion resistance is a key parameter for improving ME biosensors. Although corrosion resistance is related to different thicknesses of the Au layer of ME

sensor platforms, there is an optimum thickness of the Au layer that not only protects the biosensor from corrosion but is also thin enough to avoid excess non-magnetoelastic mass, which reduces sensitivity. In Section **3.1.2.**, the optimum sputtering powers for deposition of Cr and Au layers were determined, and these sputtering powers were used in this section. In order to determine this optimum value, after coating with a fixed thickness of Cr (92.3 nm), various Au sputtering times of 200 s, 400 s, 600 s and 800 s were used to obtain different thicknesses of Au layers (77–309 nm). Based on the optimum annealing condition from above (220 °C, 2 hr), all the samples were annealed in vacuum using that condition. The resulting ME sensor platforms were then immersed in 1xTBS (PH 7.5, 0.14 M NaCl) solution for three hours followed by rinsing in distilled water, drying, and optical microscope observation. The minimum thickness of gold required for the ME sensor platform was thus determined for future experimentation. Table 4-3 summarizes the optimum sputtering conditions for sensor preparation.

Table 4- 2. Salt solutions, compositions and media.

Solution	Composition
PBS	0.15 M NaCl, 5 mM NaH2PO4, PH 7.0 adjusted with NaOH
1xTBS	50 mM Tris–HCl (PH 7.5), 0.14 M NaCl
Binding buffer	1% BSA, 0.5% Tween in TBS

Table 4- 3. Sputtering conditions for ME sensor pre-coating.

	DC	**RF**
	Cr	Au
Pre-sputter Power (w)	100	150
Pre-sputter Time (s)	300	300
Sputter Power (w)	100	100
Sputter Time (s)	300	400
Sputtering rate (nm/s)	0.308	0.386
Pressure (mTorr)	5-6	
Sputter Gas	Ar	
Vacuum (Torr)	$5x10^{-6}$	

3.2. Biorecognition element modifications

This section describes how the optimum experimental conditions for fabricating a phage-based ME biosensor were chosen. These conditions included: 1) the optimum amount of salt contained in phage solution; 2) the optimum concentration of bovine serum albumin (BSA) used to block the non-specific binding. The details of choosing optimum phage conditions are explained below (Sections 3.2.1. & 3.2.2.).

3.2.1. Phage suspension with varying salt concentrations

JRB7 phage samples with an initial concentration of 1.06×10^{13} vir/mL, 20xTBS solution and dry NaCl were used in this experiment, in order to determine the effect of the amount of NaCl (contained in phage suspension) on the bundling of phage filaments. First, 20xTBS solution (USB Corporation Q4) was diluted with filtered water into 1xTBS. Dry NaCl was then added to 1xTBS solution separately to obtain five different salt concentrations: 140 mM, 280 mM, 420 mM, 560 mM, and 840 mM. Finally, JRB7 phage solution was diluted with 1xTBS to obtain phage concentrations of 5×10^{12} vir/mL, 5×10^{11} vir/mL, and 5×10^{10} vir/mL in five different concentrations of salt. Figure 4-4 displays the final conditions of these different phage suspensions. The phage filament distribution under this preparation condition was examined by transmission electron microscope (TEM) based on the detailed procedure described below in Section **5.2.**.

In order to examine the binding affinity of the biosensor after coating with phage solution containing different amounts of NaCl, ME platforms were exposed to the different JRB7 phage loading conditions (five sensors per condition) listed in Figure 4-4, and the resonance frequency (f_0) for each sensor was measured in air. Then the JRB7 phage biosensors were exposed to the same spore suspension (5×10^8 cfu/mL, suspended in water) using the "static loading" described in Section **3.2.3.** below. The incubation time was about 1 h, followed by a single rinse of distilled water. Finally, the biosensors were tested again under the same measurement condition for resonance frequency (f_{mass}) to determine the frequency shift (Δf) caused by the attached spores.

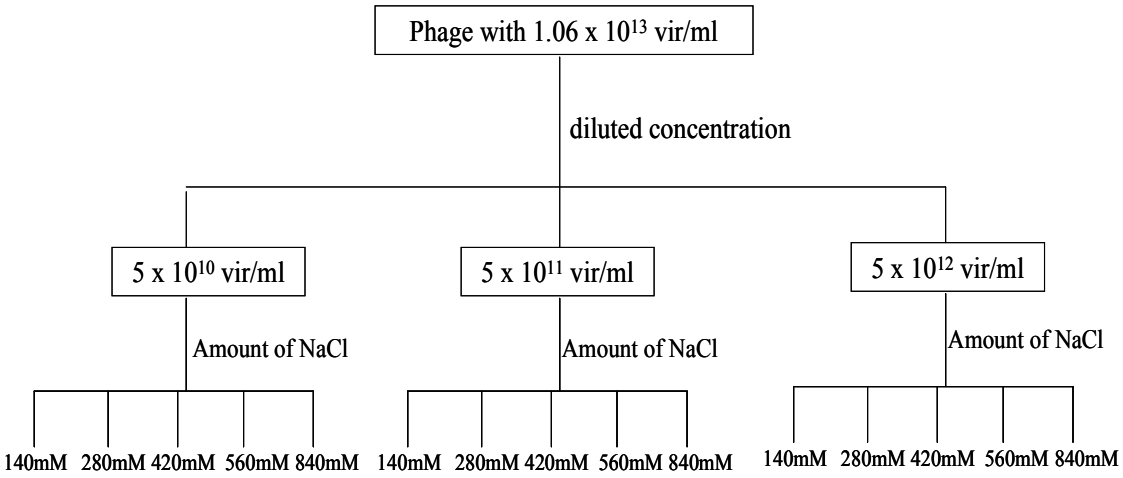

Figure 4- 4. Different conditions of phage suspensions.

The samples under each phage loading condition were prepared based on the protocol for taking SEM images (described in Section **5.1** below). Binding affinity was then determined by comparing the resonance frequency shift data and spore counts (based upon SEM images of the sensor surfaces) for each phage suspension. The salt concentrations affected the phage bundling, which in turn affected the distribution of the phage immobilized on the biosensor surface, changing the binding numbers of spores. Therefore, the amount of salt contained in the phage solution that promoted the highest binding numbers of spores on the biosensor surface was chosen as the optimum salt concentration.

3.2.2. Optimum concentration of BSA

The optimum concentration of BSA is the main variable for blocking non-specific binding. Proper blocking not only eliminates nonspecific binding, but also maintains the optimum binding affinity of the biosensors to bacteria cells or spores for which it is designed. In this experiment, the optimum phage solution chosen from Section **3.2.1** above was applied to immobilize E2 and JRB7 phage on ME platforms to form the phage-based biosensor. Three different concentrations (1 mg/ml, 5 mg/ml, and 10 mg/ml) of BSA solution were prepared, into which the phage-based ME biosensors were immersed for at least one hour, followed by tween-20 (rinse twice) and distilled water rinse (rinse once). This coating procedure is shown in Figure 4-5.

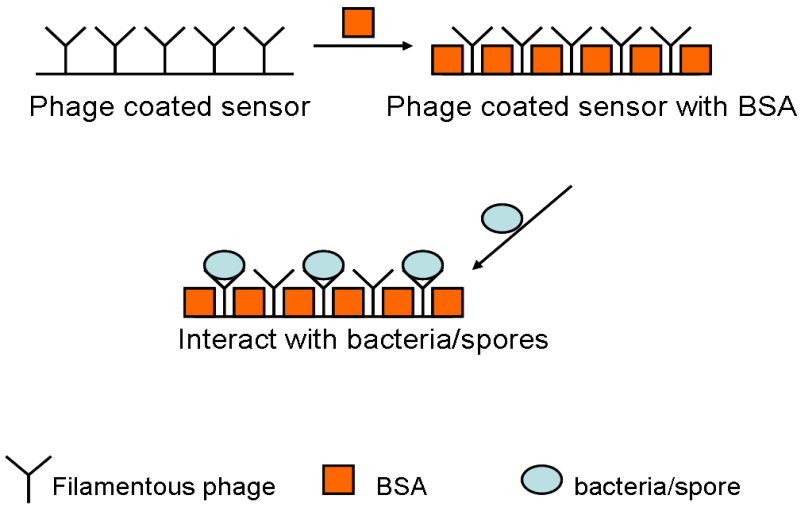

Figure 4- 5. Schematic representation the coating procedure of the detection of bacteria/spores using ME biosensor.

The SEM images of biosensor surface were taken after exposure to bacteria/spores suspension with the concentration of 5×10^8 cfu/mL. Based on the binding numbers of the bacteria/spores on the biosensor's surface, the optimum concentration of BSA solution was determined and used as the standard for subsequent sensor processing for both reference biosensor (no phage immobilization) and measurement biosensors (phage-based ME biosensor).

3.2.3. Static loading for phage-based ME biosensors

The phage-based ME biosensors were ready for testing after the immobilization under optimum conditions of the JRB7/E2 phage, and coating with the BSA. In order to determine the binding affinity of the phage-based ME biosensors, they were exposed to *B. anthracis* Sterne strain spores or *S. typhimurium* suspensions (5×10^8 cfu/mL) by "static loading." The procedure followed for static loading was: 1) incubate the phage-based biosensors in a tube containing the analyte (300 μl) and rotate using a mixer for another 1 h; 2) a single distilled water rinse. The biosensors were then prepared (based on the detailed procedure for preparing SEM samples described below in Section **5.1**) for analysis by scanning electron microcopy (SEM) in order to determine the phage distribution and the binding numbers of spores/bacterial cells on the surface of the ME biosensors.

3.2.4. Dynamic loading for biosensors fabricated under optimum conditions

In order to determine the sensitivity of the JRB7 phage biosensors produced using the optimized JRB7 phage loading conditions, "dynamic (flowing) loadings" were performed using solutions of varying spore concentrations ($5 \times 10^1 - 5 \times 10^8$ cfu/mL). Unlike with the static loading (described in Section **3.2.3** above), the dynamic loadings were conducted using a flowing system to pass the successive concentrations of *B. anthracis* spore solutions through a detection chamber, as shown in Figure 4-6.

The JRB7 phage biosensor (specific to *B. anthracis* spores), immobilized with JRB7 phage and BSA, was placed in the measurement chamber, which was filled with plain water. A peristaltic pump was used to achieve a flow rate of 100 µl/min, which was chosen to ensure laminar flow conditions over the biosensors. Water was passed through the chamber for 10 minutes in order to ensure a stable baseline signal, and then each concentration of spore solution was introduced, also for a duration of 10 minutes, moving from the lowest to the highest concentration. The resonance frequency of the biosensor was monitored in real-time by collecting data from the network analyzer with a personal computer.

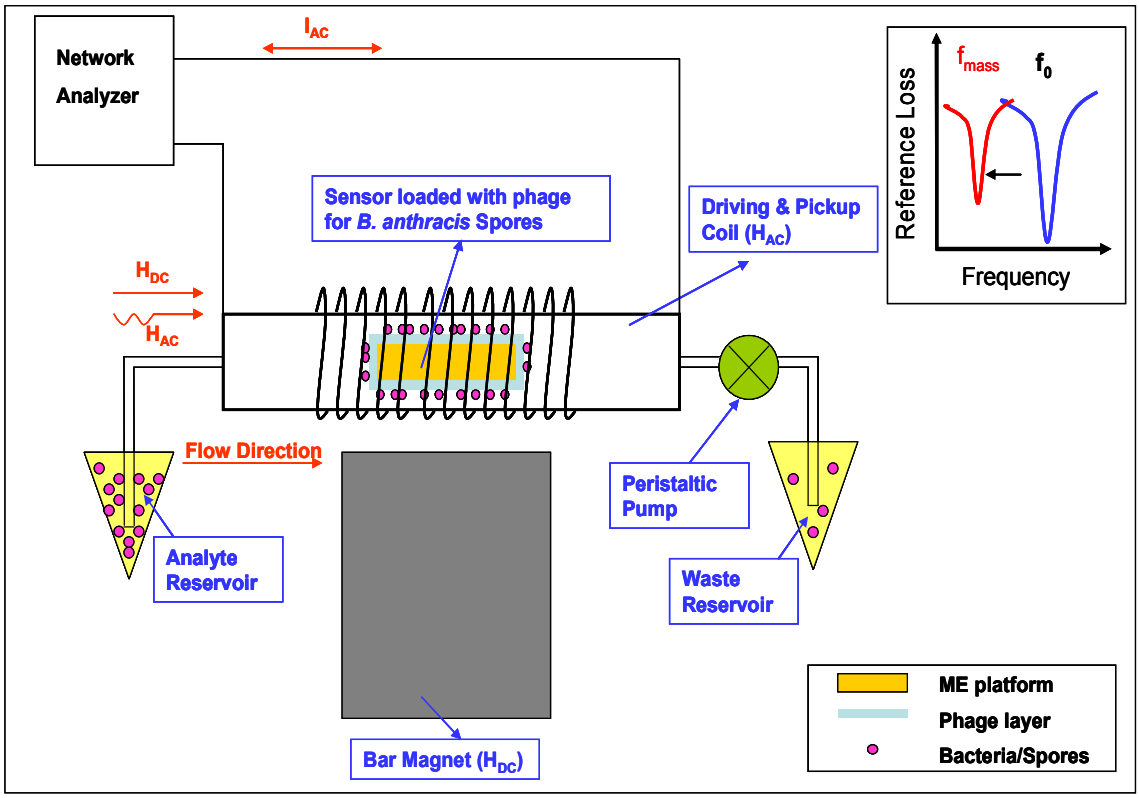

Figure 4- 6. Schematic drawing illustrating the ME biosensor system for detecting spores or cells using a flow system.

3.3. Simultaneous detection

In this section, three biosensors were tested simultaneously. Two of these were measurement biosensors, namely an E2 phage biosensor (coated with E2 phage, BSA blocking) and JRB7 phage biosensor (coated with JRB7 phage, BSA blocking), while the other was a reference sensor fabricated with only a coating of BSA. This option of deploying two sensors to simultaneously detect two different targets was implemented using "static loading" and the frequencies were measured in air.

3.3.1. Fabrication of phage-based measurement and reference biosensors

NaCl was added to 1xTBS (140 mM) until it reached a concentration 420 mM. Then initial phage solution (1.06×10^{13} vir/mL) was diluted with the 1xTBS (420 mM NaCl) to 5×10^{11} vir/mL. The E2/JRB7 phage was immobilized by incubating the ME platforms in the phage solutions (300 μl) for one hour. This immobilization was based on physical adsorption [6]. To form the measurement biosensor for the detection of *s. typhimurium*, an ME sensor platform was immersed into E2 phage solution (5×10^{11} vir/mL in 1xTBS), followed by rinsing with distilled water to remove any loosely-bound phage and residual salts.

To form the other measurement biosensor for the detection of *B. anthracis* spores, an ME platform was immobilized with JRB7 phage (5×10^{11} vir/mL in 1xTBS) using the same procedure as above. In order to prevent nonspecific binding of spores on the gold surface, the phage-immobilized biosensors were immersed into 1 mg/mL BSA for 1 h, followed by rinsing with tween-20 solution (0.05 %) twice and then rinsing once with distilled water. At this point, the ME biosensors were ready for bacteria/spore detection. In this research, a reference sensor (blocked with BSA only, with no phage immobilized on the surfaces) was also manufactured and used as a reference in order to eliminate any effects due to nonspecific binding with possible contaminants in the analyte, varying flow conditions, and variable temperature conditions.

3.3.2. Concept of simultaneous detection

A schematic of the simultaneous detection system is shown in Figure 4-7. The system was composed of a target analyte container, a peristaltic pump, two measurement chambers (connected by a capillary tube), a flush out container, three ME biosensors for detection, and a network analyzer system for data acquisition and control. Two measurement phage-based biosensors, an E2 phage biosensor (immobilized with E2 phage and specific to *S. typhimurium*) and a JRB7 phage biosensor, were placed together in measurement chamber (C). These two biosensors were fabricated with different lengths. The reason for using two different sizes of sensor platforms was to ensure that the detectors had different characteristic resonance frequencies and thus easily identify which pathogen had been detected. For instance, the larger biosensor (l=2.0mm) was used for the detection of *S. typhimurium* and the smaller biosensor (l=1.9mm) for *B. anthracis* spores. Therefore both detection of *B. anthracis* (by the JRB7 phage biosensor) and *S. typhimurium* (by the E2 phage biosensor) could be conducted simultaneously, as shown in Figure 4-8.

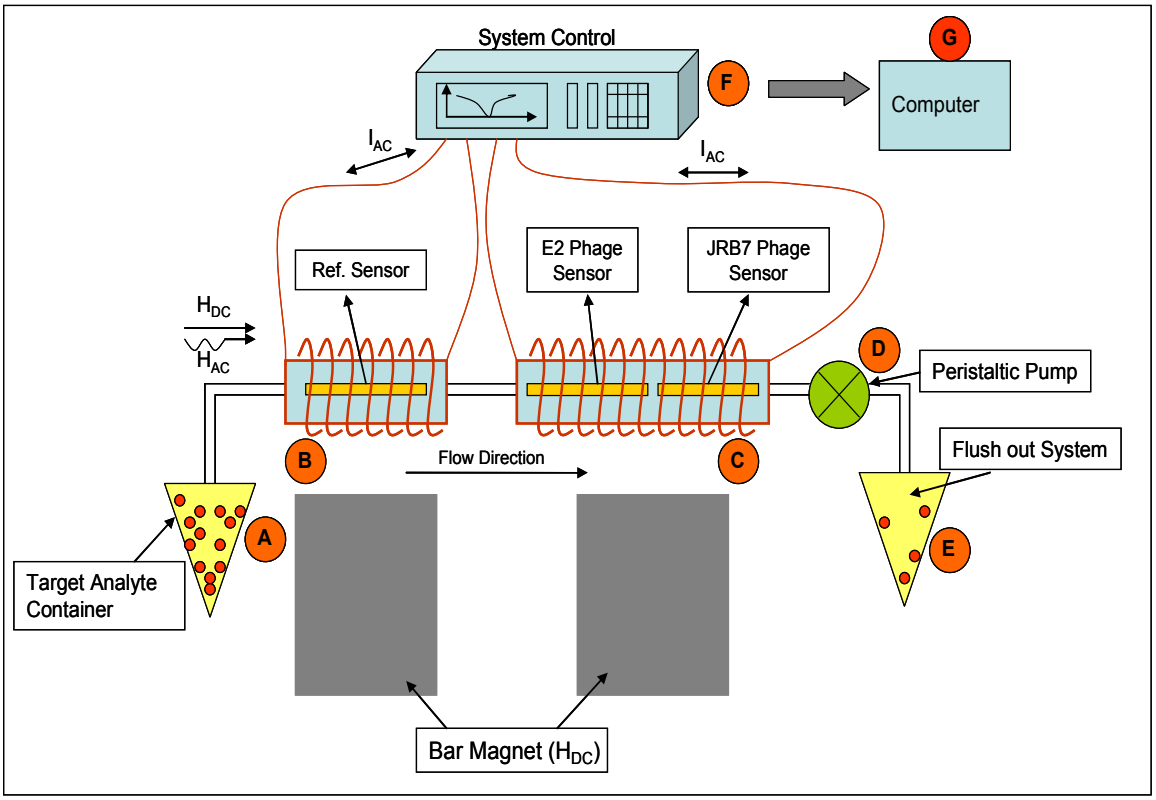

Figure 4- 7. Setup for measurements with multiple ME biosensors.

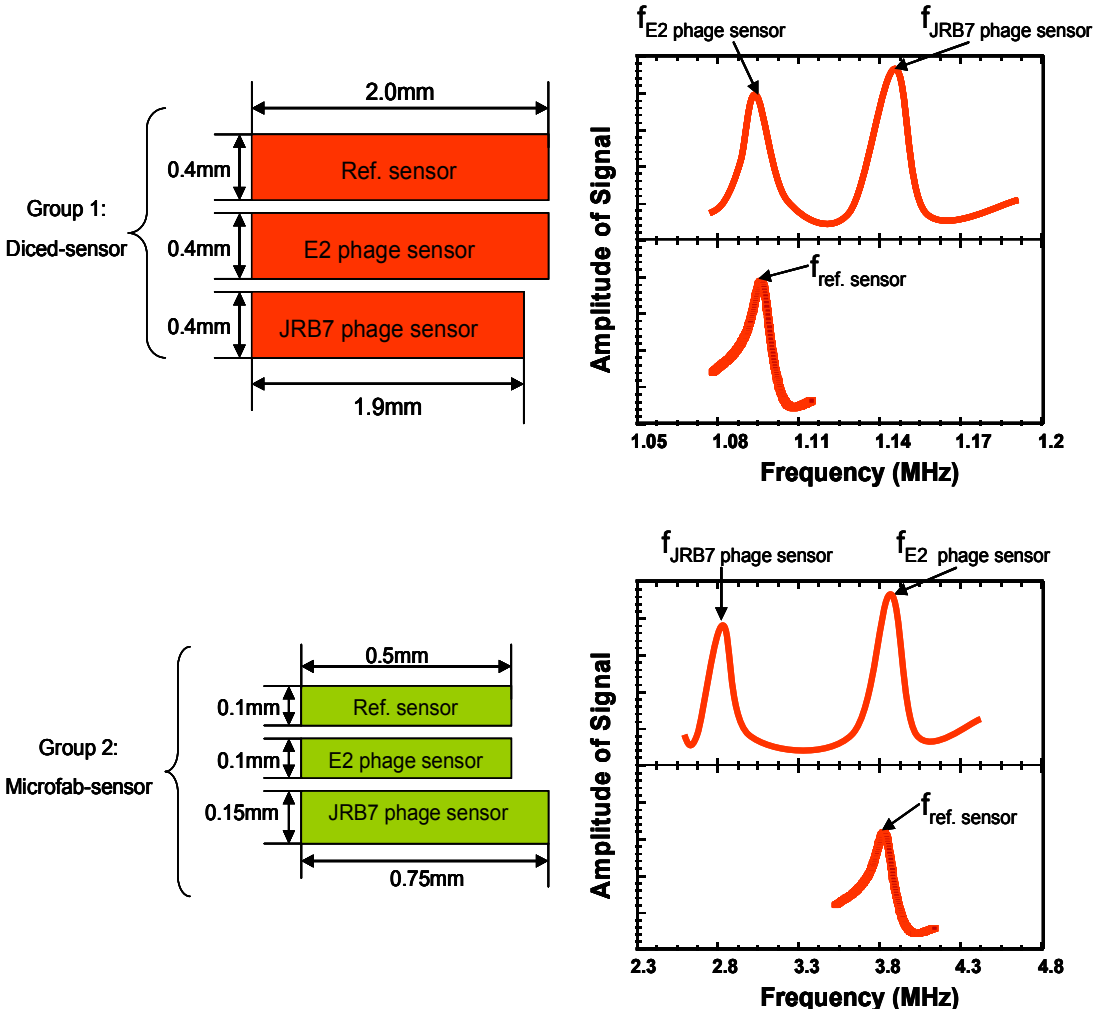

Figure 4- 8. Scheme for simultaneous detection analysis.

The reference biosensor was placed in the second measurement chamber (B). Each chamber was connected to the network analyzer (F) via its own, separate channel. The analyzer was able to measure and display the signals from both channels simultaneously (as shown in Figure 4-7), thus enabling the simultaneous measurement, display and recording of the three sensors' resonance frequencies in real time. For the

first set of biosensors (group 1), the length of the E2 phage and reference biosensors was 2mm, which produced a resonance frequency of about 1.8 MHz; while the JRB7-phage biosensor was constructed with a length of 1.9mm, giving a resonance frequency of about 1.14 MHz. For the second set of sensors (group 2), the length of the E2-phage and reference biosensors was about 500μm ($f_0 \approx 3.8$ MHz), and the JRB7-phage biosensor had a length of 750μm ($f_0 \approx 2.8$ MHz). These values are approximate since slight variations in size and shape of the sensor platforms, due to variances in the fabrication process, affect the exact resonance frequency of each individual biosensor. The experiment was conducted by using the Ismatec Reglo Digital peristaltic pump with 8 rollers and four channels (D) to drive an analyte containing only *S. typhimurium* or *B. anthracis* spores at a concentration of 5×10^8 cfu/mL from container (A) through the detection chambers. When the target bacterium/spores bound to the corresponding ME biosensor, a frequency shift was observed to confirm the interaction, while the frequencies of the other two biosensors remained relatively stable. A flow rate of 50 μl/min was used in order to ensure laminar flow over the ME biosensors. Resonance frequencies were continuously monitored and recorded by the analyzer (F) and computer system (G). Finally, the waste analyte was collected in the flush-out container (E) for disposal. Both *S. typhimurium* and *B. anthracis* Sterne suspensions were obtained in a concentration of 5×10^8 cfu/mL from the Department of Biological Sciences at Auburn University. All solutions were stored at 4°C and then equilibrated to room temperature prior to testing.

3.4. Simultaneous biosensor detection in air by static loading

A set of experiments was conducted to demonstrate that phage-based ME biosensors can be used to simultaneously detect the presence of multiple agents, in this case, *S. typhimurium* and *B. anthracis* spores.

As mentioned in Section **3.3.2**, simultaneous detection of different target agents can be accomplished by ME biosensors with discrete and different characteristic resonance peaks and different bio-recognition coatings. The characteristic resonance frequencies of ME biosensors can be controlled through composition, shape and size. In order to demonstrate the simultaneous detection approach, two ME biosensors with slightly different lengths were employed for detection after phage immobilization. One was a reference sensor with dimensions of $2 \times 0.4 \times 0.015$ mm, the other was the JRB7 phage biosensor with dimensions of $1.9 \times 0.4 \times 0.015$ mm. Both were placed in the same testing chamber and the distance of the bar magnet from the testing chamber was adjusted to obtain the maximum signal amplitude for the reference sensor. It is important to note that for different sensors the optimum DC bias field may be different. However,, since this only affects signal amplitude and not the frequency shifts due to mass loading, any error introduced by this compromise is negligible. Frequencies from both sensors were measured by an average of four frequency scans, after which both sensors were taken out and only the JRB7 phage biosensor exposed to specific *B. anthracis* spores with a concentration of 5×10^8 cfu/mL, again by static loading. After washing the loosely bounded spores with distilled water and drying in air, the frequencies

of both sensors were re-measured under the same conditions using a DC bias to amplify the reference sensor to the maximum amplitude. Only the JRB7 phage sensor, which was bound with spores, showed a shift of this peak to another frequency.

4. Characterization of multi-sensor detection system

As part of the development of the multi-sensor detection system, the performance of each sensor was characterized in terms of its sensitivity, stability, selectivity, specificity, dose response and detection limit.

4.1. Detection with bacteria/spores sequentially

The minimum detectable mass is dependent on the mass sensitivity of the device and the size of the active area of the biosensor. In order to measure the sensitivity of this multiple detection system, the sensors were therefore sequentially exposed to increasing concentrations of *S. typhimurium* (5×10^1 to 5×10^8 cfu/mL) and *B. anthracis* spores (5×10^1 to 5×10^8 cfu/mL) suspensions in water. The flow rate was 50 µl/min for each concentration, and a 1 ml suspension was used for detection.

4.2. Selectivity and specificity of multi-sensor detection system for a bacteria/spores cocktail

Selectivity is used to assess performance when there are *n* components of interest which can be determined simultaneously and independently from each other by the sensor. In contrast, specificity means that in a multi-component system only one individual component is measured by the sensor or detecting channel. Both the

selectivity and specificity are important in a multi-sensor and multi-component system. In order to demonstrate the selectivity and specificity of this multiple-sensor detection system, the sensors were exposed to increasing concentrations of *S. typhimurium* (5×10^1-5×10^8 cfu/mL) suspensions in water, which was co-spiked with a fixed concentration (5×10^7 cfu/mL) of other food borne pathogens (*E. coli* O157:H7). The flow rate was 50 μl/min and, for each concentration, a 1ml suspension was used for detection. This was repeated using an increasing concentration of *B. anthracis* spores (5×10^1-5×10^8 cfu/mL) in a mixture of a fixed concentration of *B. cereus* spores (5×10^7 cfu/mL). The reason *B. cereus* spores were chosen is because they are a nonpathogenic species that have very similar physical characteristics to *B. anthracis* spores, and so have the potential to mask specific detection of *B. anthracis* spores.

4.3. Multi-sensor detection system response to analytes in apple juice

In order to prepare a series of different concentrations mixtures of *S. typhimurium* with one additive bacteria (*E. coli*) in apple juice, the received *S. typhimurium* suspensions (5×10^8 cfu/mL) were first diluted with apple juice (Kroger® brand, purchased at a local grocery store) instead of water to form a series of concentrations (5×10^1 cfu/mL - 5×10^8 cfu/mL). For each condition there was a volume of 9 ml. One ml of *E. coli* suspension (5×10^8 cfu/mL) was added to each of the diluted concentrations of *S. typhimurium* in apple juice, separately. As a result, all the suspensions had 5×10^7 cfu/mL of *E. coli* species. The same method was used to prepare different

concentrations of *B. anthracis* spores spiked with 5×10^7 cfu/mL of *B. cereus* spores in apple juice for testing. The multi-sensor detection system was then exposed to each mixture (containing 5×10^1 cfu/mL - 5×10^8 cfu/mL of *S. typhimurium* / *B. anthracis* spores) using the exact same procedure described in Section **4.2**. Here, a high concentration of additive pathogen (*E. coli*) or similar strains from same group (*B. cereus*) was applied to mask the target analytes. The objective was to investigate the maximum masking effect of nonspecific bacteria/spores on the selectivity, specificity, and the performance of the sensor.

4.4. Dose response

In order to study the dose response for reference sensor and two measurement biosensors in the multiple systems, the frequency response of each sensor was monitored during exposure to different concentrations of *S. typhimurium* and *B. anthracis* spores sequentially. The different concentrations (5×10^1 cfu/mL-5×10^8 cfu/mL) were prepared by successive dilutions of the as-received *B. anthracis* spores / *S. typhimurium* suspensions (5×10^8 cfu/mL). Five groups of sensors (each group contained two measurement sensors and one reference sensor) were used to test the frequency change at each concentration of suspension using the multiple detection system shown in Figure 4-7. One concentration of *S. typhimurium* was introduced first to the system and allowed to flow for 20 minutes, during which time a total amount of 1mL passed over the sensors. The frequency at the end of 20 minutes was used to calculate the frequency shift caused

by that particular concentration. The same concentration of *B. anthracis* spores was then introduced under the same conditions and captured by the specific biosensor to create a frequency change. The dose response was used to determine the detection limit, sensitivity and specificity of each of the biosensors.

4.5. Sensitivity and detection limit

In this dissertation, the limit of detection (or Detection limit, LOD) refers to the lowest detectable pathogen concentration which can be detected by the output signal. Sensitivity is defined as the change in the sensor output signal obtained for an incremental change in the concentration of analyte [7]. Figure 4-9 gives an example of how to determine the parameters from the frequency shift-vs-analyte concentration curve. This curve is defined as dose-response curve. For the purposes of this research, the logarithm of the dose (in cfu/mL) was plotted on X axis and the frequency shift was plotted on the Y axis. In such case, the curve is typically sigmoid curve that have an "S" shape with the steepest portion in the middle. Sensitivity was defined as the slope of frequency shift-vs.-analyte concentration curve. This response curve has a linear dynamic range (LDR), where the analyte concentrations below the LOD cannot be detected. For higher values of output signal the response becomes nonlinear with sensitivity approaching zero. This is the saturation limit of the sensor.

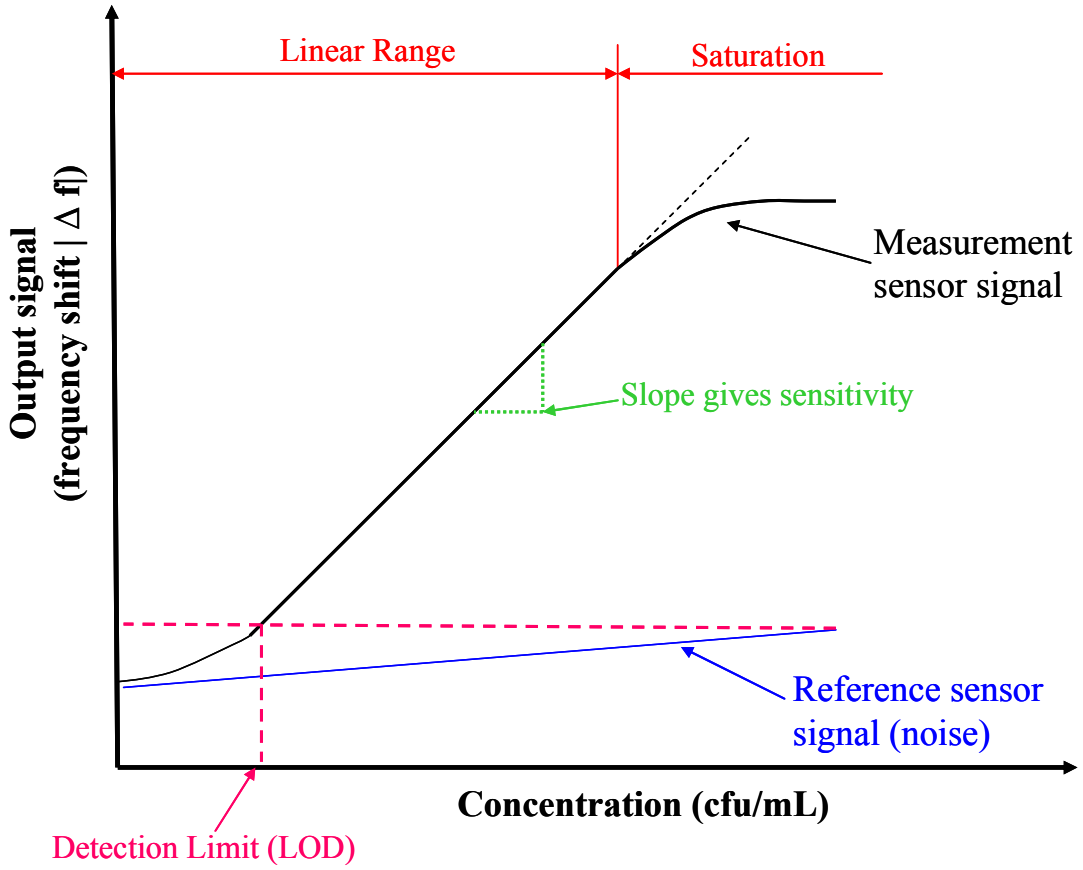

Figure 4- 9. Performance criteria of biosensor.

4.6. Hill plot-kinetics

The binding kinetics (binding strength and valency) of *Salmonella*-phage or *B. anthracis* spores-phage were analyzed using a Hill plot, which was constructed from the data obtained from the sensor's response [6, 8, 9]. The reaction between *S. typhimurium* (ST) / *B. anthracis* spores (BA) with the immobilized phage (P) on a sensor's surface can be expressed as a reversible reaction:

$$nST + P \leftrightarrow PST_n \quad (4\text{-}1)$$

$$nBA + P \leftrightarrow PBA_n \quad (4\text{-}2)$$

where *1/n* represents the binding valency and *N* is the number of binding sites of phage that interact with *ST* / BA on the sensor surface. The association reaction is caused by the binding of antigens to the immobilized phage, while the dissociation is dependant on the strength with which the antigens bind to the phage on the biosensor surface. The dissociation binding constant (K_d) for the above reversible reaction can be expressed as:

$$K_d = \frac{[ST]^n[P]}{[PST_n]} = \frac{1}{K_a} \quad (4\text{-}3)$$

$$K_d = \frac{[BA]^n[P]}{[PBA_n]} = \frac{1}{K_a} \quad (4\text{-}4)$$

where K_a is the association constant. It is therefore possible to study the kinetics of the reactions by constructing Hill plots, where the K_d value is the reciprocal of the ordinate intercept, and the *1/n* is the reciprocal of the slope. In a Hill plot, the reactant and the product concentrations are usually expressed using molar concentrations. However, in this dissertation, the concentration of *ST / BA* has the units of cfu/mL. So $k_{d(apparent)}$ is used here to take into account the scaling factor due to the use of different units for the concentrations of the analyte. The $k_{d(apparent)}$ is defined as the concentration at which half of the available binding sites are occupied. Hence, a lower value of K_d (apparent) indicates a stronger *Spore/Salmonella*-phage binding. The relationship between K_d (apparent) and K_d can be expressed as equation (4-5):

$$K_{d(apparent)} = (K_d)^{1/n} \quad (4\text{-}5)$$

The binding valency N ($1/n$) and the dissociation constant (K_d) can be estimated from a Hill plot [9], which can be determined from the equation below:

$$\log\left(\frac{Y}{1-Y}\right) = \log\left(\frac{1}{K_d}\right) + n\log[ST] \quad (4\text{-}6)$$

$$\log\left(\frac{Y}{1-Y}\right) = \log\left(\frac{1}{K_d}\right) + n\log[BA] \quad (4\text{-}7)$$

where Y is the fraction of the phage binding sites occupied by the antigen. A Hill plot is a plot of $\log\left(\frac{Y}{1-Y}\right)$-vs-log [*antigen*], where n can be estimated from the plot slope [8]. If the numbers of phages bound with nonspecific targets can be neglected, then the total number of phage binding sites (C_P) can be expressed as:

$$C_P = [P] + [PST_n] \quad (4\text{-}8)$$

$$\text{or} \quad C_P = [P] + [PBA_n] \quad (4\text{-}9)$$

$$Y = \frac{[PST_n]}{C_p} \quad \text{or} \quad Y = \frac{[PBA_n]}{C_p} \quad (4\text{-}10)$$

When phage particles are immobilized on the sensor surface, the concentration of phage-antigen complex [PST_n] or [PBA_n] is proportional to the mass loading (Δm) on the sensor due to the binding of target antigens to the phage immobilized on the sensor surface. So, [PST_n] or [PBA_n] is near Δm, while C_P is near Δm_{max}. Then, substituting this into Eqs. (4-10), the Hill plot can be constructed by plotting log X versus the log [*ST*] or log [*BA*], where X is given as:

$$\boldsymbol{X} = \frac{\boldsymbol{Y}}{(1-\boldsymbol{Y})} = \frac{\Delta \boldsymbol{m}}{\Delta \boldsymbol{m}_{\max}} = \frac{\Delta \boldsymbol{f}}{\Delta \boldsymbol{f}_{\max}} \quad (4\text{-}11)$$

where Δf is the real-time frequency shift obtained as a response to the binding of *S. typhimurium* or *B. anthracis* spores to the phage immobilized sensor, and Δf_{max} denotes the maximum frequency when the sensor reached saturation. Δf_{max} was calculated from the sigmoidal curve, which was fitted to the dose response curve.

Overall, lower values of K_d and K_d (apparent) indicate a stronger phage-antigen binding and thus a higher sensitivity of the sensor.

5. Microscopy analysis

5.1. Scanning electron microscope

A JEOL-7000F scanning electron microscope (SEM) was used to quantify the number of spores bound to the phage-immobilized ME biosensors, as well as obtain a visual verification of the phage distribution on sensor surface. In preparation for SEM observations, the tested biosensors were rinsed with distilled water once to remove loosely bound cells, salts, and debris left over from testing. The sensors were then mounted on the top of an aluminum stub using double sided carbon conductive tape (Ted Pella Inc.), followed by drying in a Petri dish for at least 15 minutes. A small amount (50 µl) of osmium tetroxide (OsO_4) was placed beside the aluminum stub in the Petri dish for exposure to OsO_4 vapor for 40 min. Osmium tetroxide is commonly used as a stain for biological samples in electron microscopy, and the diffusion of Os (a heavy metal) into the cell membrane improves the image contrast in an electron microscope. In order to clearly see the phage distribution on the sensor surface and how the sensors bind *S.*

typhimurium cells, the sensors mounted on aluminum stubs were directly observed by SEM. Other samples from the initial experiments were coated with 60 nm of Au using a sputter coater (PELCO SC-6, Ted Pella, Inc., Redding, CA) to provide a conductive surface for SEM imaging. The reason some samples were not coated with the extra Au layer is because the Au layer covers the individual phage filaments on the surface such that they cannot be viewed with the SEM. Also, the *S. typhimurium* cells without the additional Au coating usually appear in the SEM image as black cells, while *B. anthracis* spores appear white, making it easy to distinguish between the two. The images were taken at an accelerating voltage of 10 or 15 kV with a working distance of 10 mm, an aperture of 3, and a probe current of 54 μA. SEM images of the sensor surface at desired magnifications were recorded in the electronic format (jpeg files) using JEOL-Imaging software.

5.2. Transmission electron microscope

A PHILLIPS-301 transmission electron microscope (TEM) was used to verify the distribution of JRB7 phage under different salt and phage concentrations. The TEM samples were prepared on 400 mesh formvar/carbon coated nickel grids. The grid was floated on a drop (50 μl) of sample solution for one hour. Upon removal from the drop, excess fluid was drained from the grid by touching its edge to filter paper. The grid was then washed gently with one drop of stain solution (0.1% BSA / 2% KPTA), and floated on another drop of stain solution for 3 min to obtain a negative stain of the sample. The

phage coated grids were allowed to air dry for 15 minutes before examination and stored in grid holders in a desiccator.

5.3. Bacteria Cells / Spores Counting *vs.* Estimation of Bound numbers based on Δf of Sensor Response

To determine the number of bacteria cells or spores bound to the sensors, one side of each sensor was photographed in its entirety using the SEM. All bacteria or spores attached to the photographed surface were individually counted and the count multiplied by 2 to account for both sides of the sensor.

After each experiment, the frequency shift (Δf) of biosensor was recorded, and based on Eq. (3-5):

$$\Delta f = -\frac{f_0}{2}\frac{\Delta m}{M} \quad (4\text{-}12)$$

A small added mass (Δm) can be estimated from Eq. 4-13:

$$\Delta m = -\frac{2M\Delta f}{f_0} \quad (4\text{-}13)$$

For a sensor with the dimension of ($L \times w \times t$) and density of (ρ), the mass (M) of the sensor can be calculated by ($L \times w \times t \times \rho$) so Eq.(4-13) can be expressed as:

$$\Delta m = -\frac{2l \times w \times t \times \rho \times \Delta f}{f} \quad (4\text{-}14)$$

where Δf is in Hz and Δm is in picograms. Assuming the mass of each bacterium or spore is 2 pg, and, from Eq. (3-3), for a strip-like ME particle of length L, the fundamental resonance frequency or characteristic frequency f_0 is:

$$f_0 = \frac{1}{2L}\sqrt{\frac{E}{\rho(1-\sigma^2)}} \qquad (3\text{-}3)$$

Hence, the estimation of the number of bacteria / spore ($n_{calculated}$) attached to the sensors is:

$$n_{calculated} = \frac{\Delta m}{2} = \frac{l \times w \times t \times \rho \times \Delta f}{f_0} = \frac{2l^2 wt\rho}{\sqrt{\frac{E}{\rho(1-\sigma^2)}}}\Delta f \quad (4\text{-}15)$$

Young's modulus (E), density (ρ), and Poisson ratio (σ) of the material are 110 GPa, 7.9×10^3 kg/m^3, and 0.5, respectively.

So the number of bound bacterium/spores can be estimated by substituting required parameters into Eq. (4-15), as shown in Table 4-4 (all the sensors were fabricated with length (l) and width (w) ratio of 5:1 and thickness of 15μm). Δf is in Hz and, after the target pathogens bind, the resonance frequency will shift to a lower value, so Δf will be a negative value.

Table 4- 4. Predicted binding numbers of different sizes of ME sensors.

L (mm)	w (mm)	t (mm)	V (μm^3) $\times 10^9$	f (MHz)	Mass (pg) $\times 10^6$	$n_{calculated}$
5	0.1	0.015	7.5	0.4308	59.25	$-137.51\Delta f$
2	0.4	0.015	12	1.07719	94.80	$-88.01\Delta f$
1	0.2	0.015	3	2.1544	23.70	$-11.00\Delta f$
0.75	0.15	0.015	1.69	2.8725	13.33	$-4.64\Delta f$
0.5	0.1	0.015	0.75	4.3088	5.93	$-0.71\Delta f$
0.2	0.04	0.015	0.12	10.7719	0.95	$-0.09\Delta f$
0.1	0.02	0.015	0.03	21.5438	0.24	$-0.01\Delta f$

6. References

[1] "www.metglas.com."

[2] V. A. Petrenko, G. P. Smith, X. Gong, and T. Quinn, "A library of organic landscapes on filamentous phage," *Protein Engineering,* vol. 9, pp. 797-801, 1996.

[3] J. Wan, H. Shu, S. Huang, I.-H. Chen, V. A. Petrenko, and B. A. Chin, "Phage-based magnetoelastic wireless biosensors for detecting Bacillus anthracis spores," *IEEE Sens. J. ,* vol. 7, pp. 470-477, 2007.

[4] I. B. Sorokulova, E. V. Olsen, I. Chen, B. Fiebor, J. M. Barbarree, V. J. Vodyanoy,

B. A. Chin, and V. A. Petrenko, "Landscape phage probes for Salmonella typhimurium," *Journal of Microbiological Methods,* vol. 63, pp. 55-72, 2005.

[5] E. V. Olsen, I. B. Sorokulova, V. A. Petrenko, I. H. Chen, J. M. Barbaree, and V. J. Vodyanoy, "Affinity-selected filamentous bacteriophage as a probe for acoustic wave biodetectors of Salmonella typhimurium," *Biosensors and Bioelectronics,* vol. 21, pp. 1434-1442, 2006.

[6] V. Nanduri, I. B. Sorokulova, A. M. Samoylov, A. L. Simonian, V. A. Petrenko, and V. Vodyanoy, "Phage as a molecular recognition element in biosensors immobilized by physical adsorption," *Biosens. Bioelectron. ,* vol. 22, pp. 986-992, 2007.

[7] D. S. Ballantine, R. M. White, S. J. Martin, A. J. Ricco, G. C. Frye, E. T. Zellers, and H. Wohltjen, *Acoustic wave sensors: theory, design and physico-chemical applications*: Academic Press, 1997.

[8] V. A. Petrenko and V. J. Vodyanoy, "Phage display for detection of biological threat agents," *Journal of Microbiological Methods,* vol. 53, pp. 253-262, 2003.

[9] I. H. Segel, *Biochemical Calculations*. New York: John Wiley and Sons, 1976.

CHAPTER 5

OPTIMIZATION OF PHAGE-BASED MAGNETOELASTIC BIOSENSOR PERFORMANCE

1. Design and fabrication

1.1. Frequency response signal vs. annealing temperature

After dicing, several of the ME platforms showed a slight bending and bowing upon observation with an SEM. These deformations were hypothesized to be due to internal residual stress generated during the original material manufacture and/or from the polishing/dicing operations, so annealing treatments were utilized in an attempt to reduce this residual stress. In order to test the effect of annealing, five groups of sensor platforms (with six sensors in each group) were annealed under four different temperatures, with the resonance frequency of each sensor being measured and compared before and after annealing. The spectrum quality (Q) factor and the amplitude of frequency signal are the main elements used to represent the performance of the sensor platforms. As discussed in chapter 2, the Q factor is given by Eq. (2-2); Figure 5-1 shows a graph depicting the Q factor parameters:

$$Q = \frac{f_0}{\Delta w} \qquad (2\text{-}2)$$

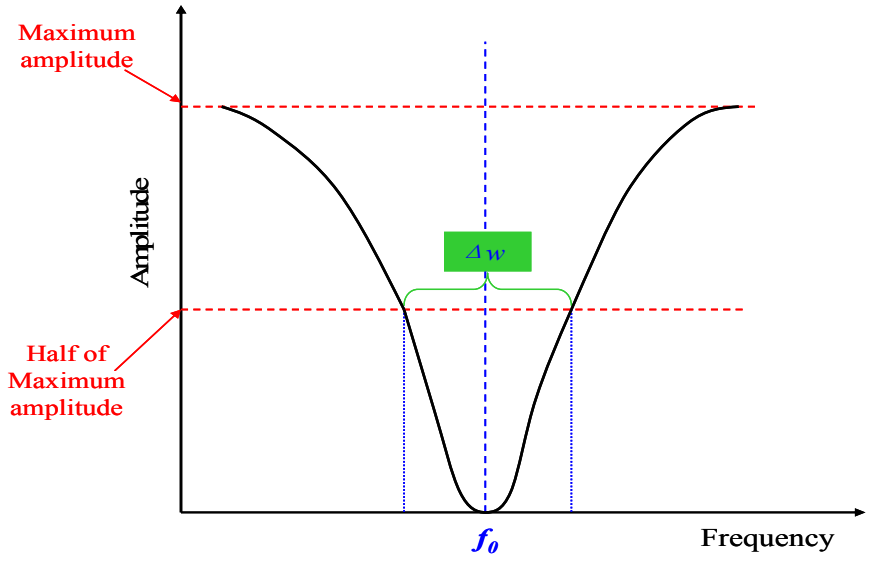

Figure 5- 1. The Q-factor parameters.

The typical spectrum and resonance frequency shift for the platforms with dimensions of 2 × 0.4 × 0.015 mm before and after annealing at different temperatures for 2 hrs is shown in Figure 5-2. The original frequency difference is due to slight dimensional variations of the samples as a result of the fabrication processes. Thus, this analysis focuses on the changes between un-annealed and annealed data for each sample. Signal response is not measured as an absolute value, but rather relative impedance with respect to the signal baseline. The resonance frequency of the platform before and after annealing at 150 ºC is shown in Figure 5-1(a). The resonance frequency increased by about 3 kHz after annealing, with the *Q* value remaining almost constant. For platforms annealed at 200 ºC (Figure 5-1 (b)) and 250 ºC (Figure 5-1 (c)), the *Q* values increased by about 30% after annealing. Additionally, the resonance frequency shift of the platform

annealed at 250 ºC was larger than that of the platform annealed at 200 ºC. When the annealing temperature was increased to 300 ºC (Figure 5-1 (d)), there was an even larger frequency increase of 20 kHz.

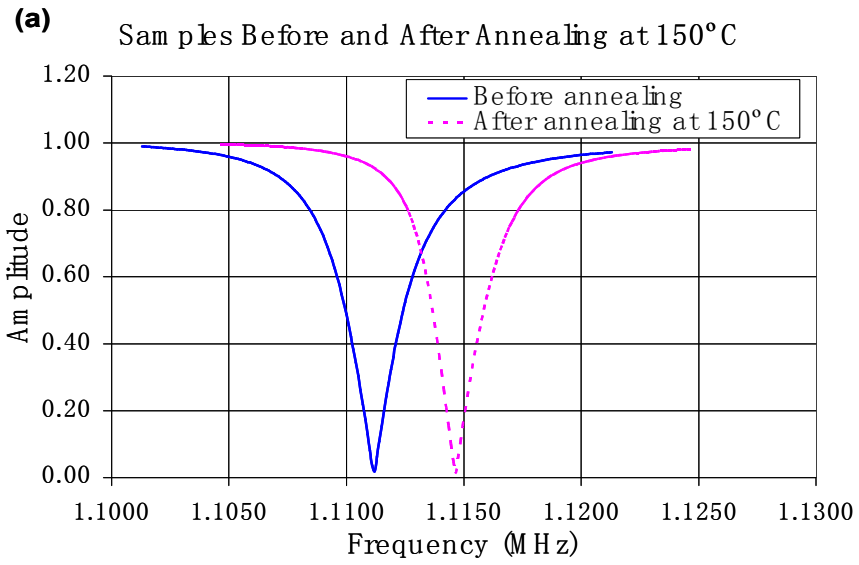

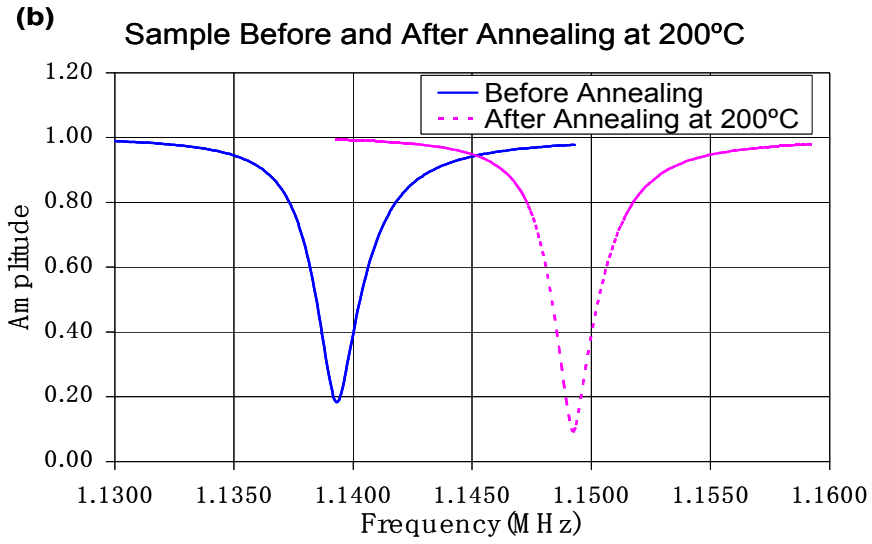

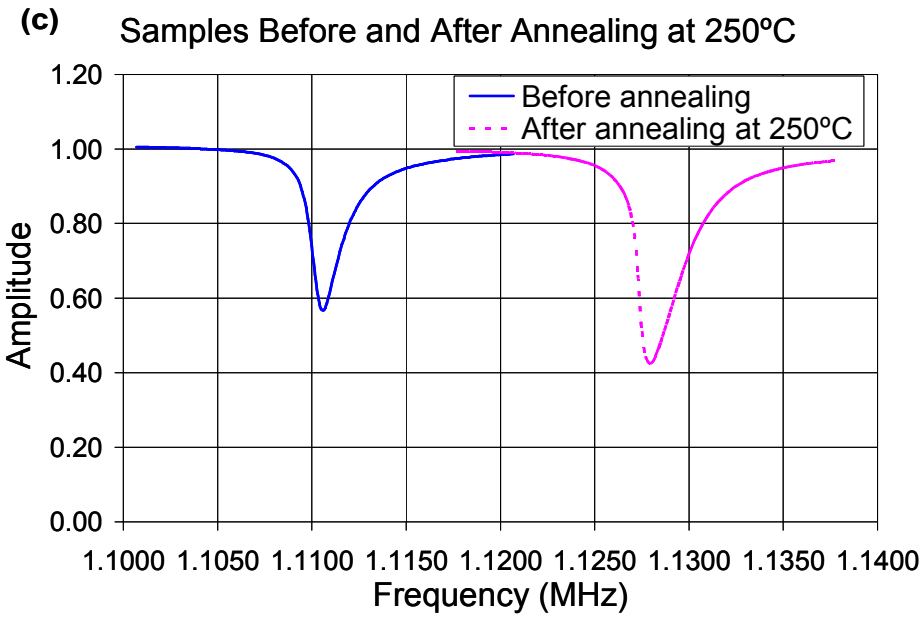

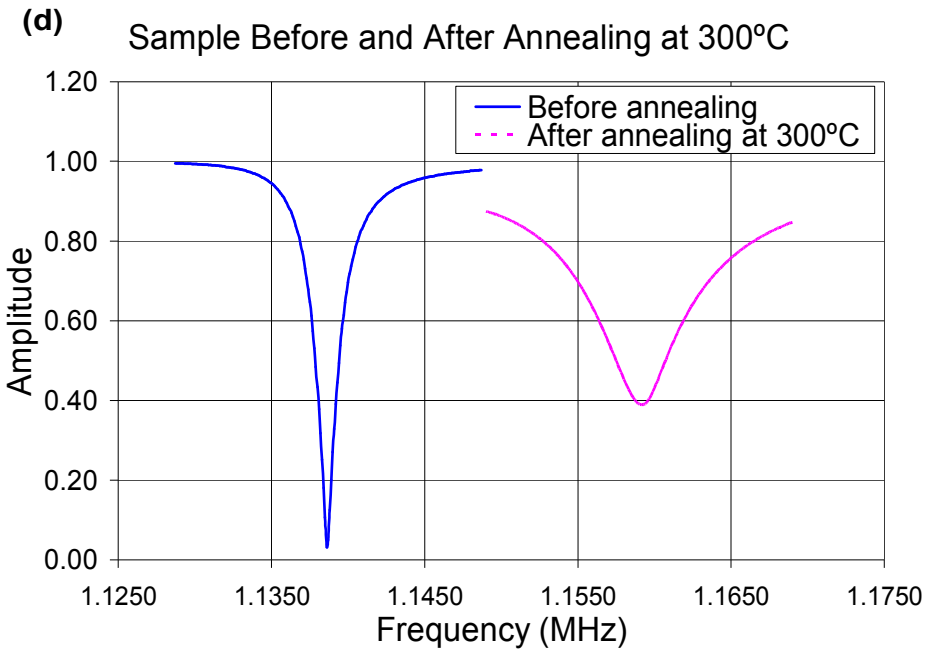

Figure 5- 2. Spectrum of 2.0 × 0.4 × 0.015 mm sensor platforms before and after annealing for 2 hours at different temperatures: (a) 150 ºC; (b) 200 ºC; (c) 250 ºC; and (d) 300 ºC.

Figure 5-3 shows the measured of *Q*-factor and amplitude change after annealing at different temperatures for the four groups of sensor platforms. The Q-factor was calculated using Eq. 2-2. As shown in Fig. 5-3, as the temperature increased the *Q*-factor of the sensors increased until a maximum was achieved between 200 ºC and 250 ºC. As temperature increased further to 300 ºC, the *Q*-factor decreased by about 60 %. A similar trend was shown for amplitude, which reached a maximum after annealing at 200 ºC. Since a higher *Q*-value enable a more accurate determination of the resonance frequency, the optimum annealing temperature was thus determined to be in the range of 200 ºC-250 ºC.

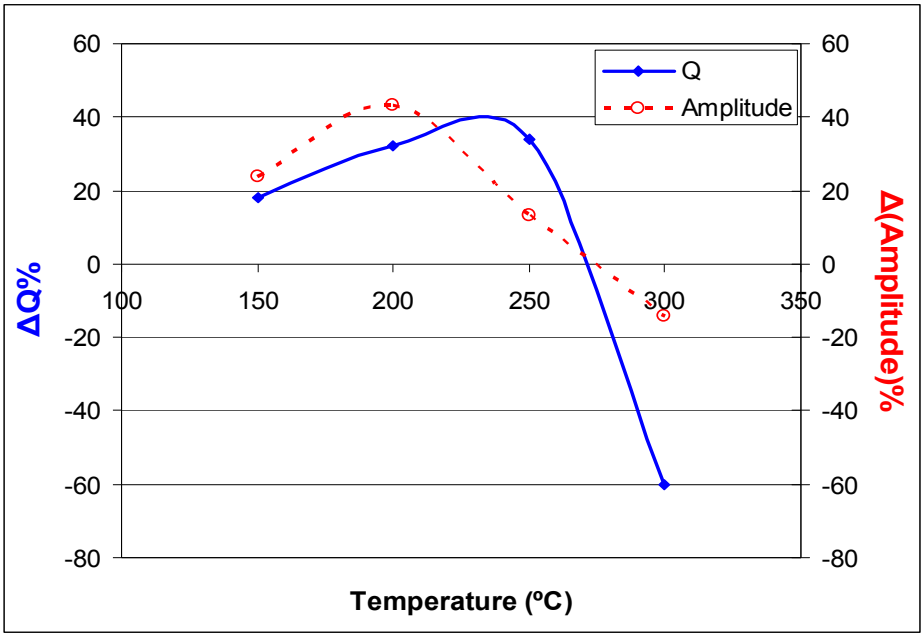

Figure 5- 3. Effect of annealing temperature on Q factor and amplitude of the resonance frequency after annealing at different temperatures (150 ºC-300 ºC).

Figure 5-4 describes the average frequency shift at different annealing temperatures. As the annealing temperature increased, larger frequency shifts were obtained; the largest frequency shift (20 kHz) was obtained when the annealing temperature was 300 ºC.

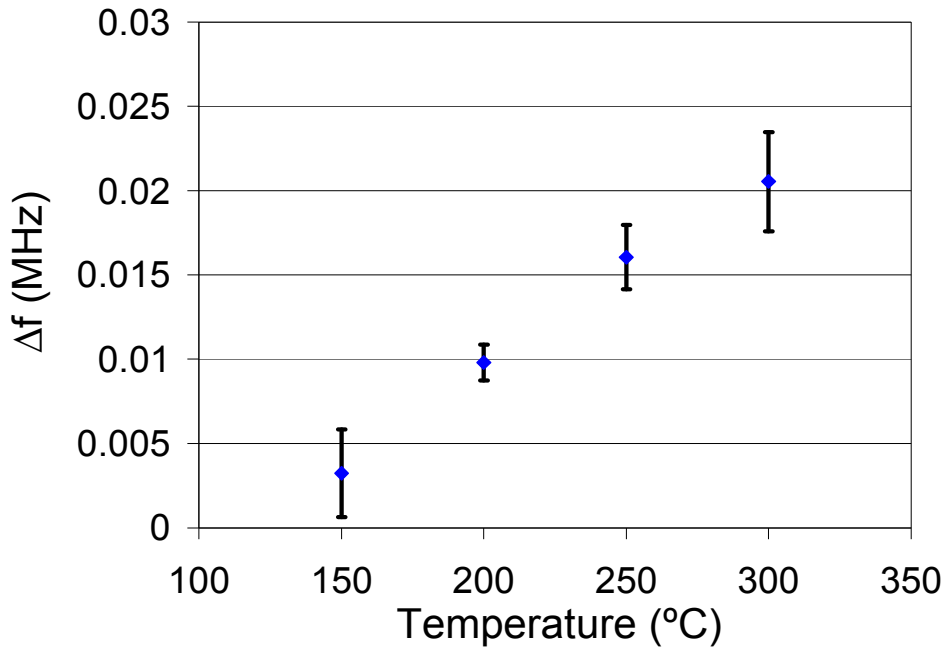

Figure 5- 4. Average frequency shift after annealing at different temperatures for 2 hours for the sensor platforms with the size of 2 × 0.4 × 0.015 mm.

1.2. Surface microstructure of sensor platform

SEM pictures (at an original magnification of 30,000 ×) were taken to determine the effect of annealing on the surface micro-structure of the ME platforms. To show the effect of annealing on the gold surface micro-structure, the platforms were sputtered with a thin layer of Cr (~ 92.3nm) and Au (~ 154 nm), and then were annealed at 75 ºC, 150 ºC, 200 ºC, 250 ºC and 300 ºC for 2 hrs, respectively. The SEM images in Figure 5-5

show that the platform surface was full of micro-cracks within the gold coating layer in its unannealed state.

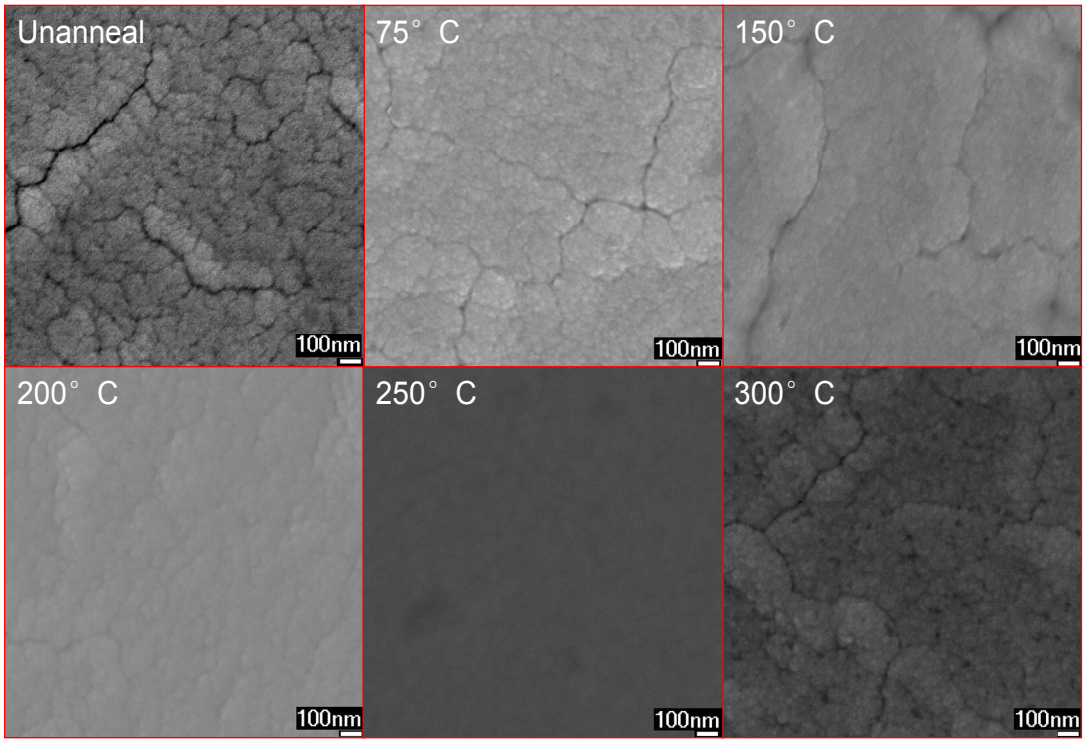

Figure 5- 5. Surface microstructure of sensor platform before and after annealing at different temperatures.

For an annealing temperature of 75 ºC, the surface condition had very little change. For an annealing temperature of 150 ºC, compared with the original unannealed state, there were still some cracks on the surface, although the small cracks had started to heal. When annealed at 200 °C, the surface became much smoother, and the cracks disappeared altogether once the temperature reached 250 °C. Finally, when

the annealing temperature was increased to 300 °C, the surface became cracked again, similar to the platform without annealing. Some crystallization of the ME material was also found at this temperature from X-Ray diffraction tests. Based on these results, the optimal annealing temperature range is 200-250 ºC, where the residual stresses are removed and the structural defects are also corrected. This conclusion is consistent with the results obtained from the measurements of Q-factor and resonance frequency amplitude changes after annealing.

1.3. Corrosion resistance vs. annealing temperature

Based on the results above, the sputtered platforms used for the following experiments were all annealed at 200 ºC–250 ºC. A vacuum oven setpoint of 220 ºC was used; the time for annealing was 2 hours and the vacuum was 10^{-3} Torr.

Adhesion testing of the Au thin film was conducted by immersing the sputtered ME sensor platforms in 1xTBS (PH 7.5, 140 mM NaCl) solution, which contains the same amount of chloride ions as the phage solution. Samples were soaked in the TBS solution for three hours followed by rinsing in distilled water, drying, and SEM observation. As Table 5-1 shows, the annealed samples possessed much better adhesion than the unannealed samples. After soaking in the TBS solution for 3 hrs, very little of the gold film peeled off. However, gold started to peel off at around 30 minutes for most unannealed samples, as can been clearly seen from the pictures in Table 5-1. For the unannealed samples, the sample sputtered with Au for 800 s was the first to show corrosion

and peeling of the Au coating. This may be because the gold layer was too thick and defects were produced in the coating that led to corrosion initiation and delamination of the surface layer. With a sputtering time of 200 s, the sample shows non-uniform surface coverage after soaking. This is probably due to the short sputtering time resulting in formation of a non-continuous film. With sputtering times of 400 s and 600 s, the gold started to peel off after 40 minutes, but the peel off area did not show further delamination after 2 hrs.

Annealed samples, for 400-800 s sputtering times, showed excellent adhesion. All the samples were still in good condition after more than 3 hours. Even after 6 hours, the films sputtered for 400 s, 600 s and 800 s showed no sign of corrosion or peeling.

On the basis of these results, it was concluded that the thickness of the gold film is not a critical factor as long as a certain minimum thickness is reached. The experiment shows that the film sputtered for 400 s provided a good quality film. It is also important to control the interlayer between the substrate and the Au layer. During the whole experiment, no Cr layer peeling was found. In this research, the Cr layer thickness was about 92 nm while the Au layer was about 154 nm.

Table 5- 1. The effect of annealing and Au sputtering time on Au film adhesion.

Au Sputter time(s)	Calculated Thickness (nm)	Anneal	Peeling Time	Peeling condition (after 3hrs)
200	77	No	<30mins	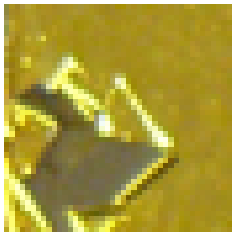
		Yes	>3hr	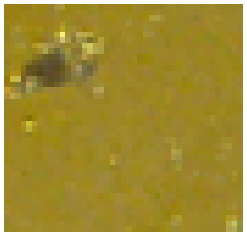
400	154	No	<40mins	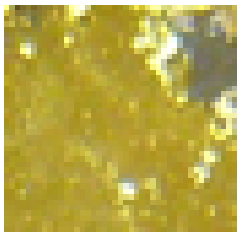
		Yes	>6hr	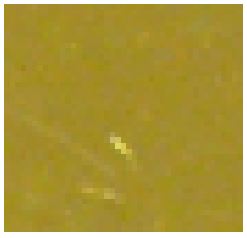

Au Sputter time(s)	Calculated Thickness (nm)	Anneal	Peeling Time	Peeling condition (after 3hrs)
600	232	No	<40mins	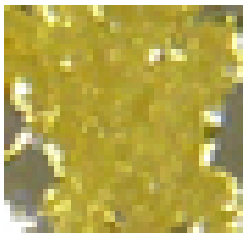
		Yes	>6hr	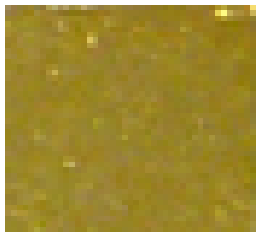
800	308	No	<30mins	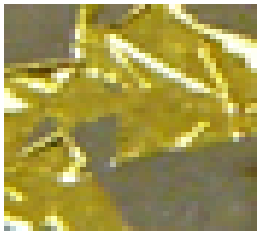
		Yes	>6hr	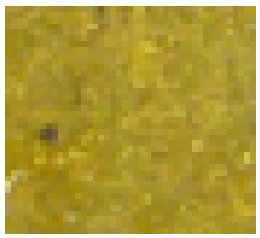

2. Immobilization process

The immobilization of the phage on the ME platform will be discussed in two parts: with the first part covering the investigation of the effect of salt and phage concentrations on the binding affinity of the ME biosensors, while the second part describes the investigation of the optimum concentration of blocking agent needed to

eliminate the non-specific binding and at the same time preserve the binding sensitivity of the ME biosensors. These results were obtained using biosensors which were fabricated by immobilizing JRB7 filamentous phage on the ME platform surface for the detection of *B. anthracis* spores.

The first part, where the effect of the chemistry of the phage solution on the phage bundling characteristics and, hence, its effect on both the sensitivity and detection limit of the ME biosensor, is presented in four sections. In the first section, the performance of the ME biosensors was examined by immobilizing with different phage concentrations that contained the same amount of NaCl. In the second section, the performance of ME biosensors immobilized with a phage concentration of 5×10^{11} vir/mL but with different concentrations of NaCl was measured and compared with SEM images. In the third section, TEM was used to determine the bundling characteristics of the phage as both the phage and NaCl concentrations were varied. Also the spore counting results obtained from the SEM images under different phage immobilization conditions are summarized in this section. In the last section, the dynamic response of a sensor immobilized with a phage concentration of 5×10^{11} vir/mL (420 mM NaCl) to increasing concentrations (5×10^{1} to 5×10^{8} cfu/mL) of spores in water in a flowing system is discussed.

The second part describes the process involved in selecting the optimum concentration of BSA as the blocking agent condition for further experiments. Three different concentrations were used for comparison: 1 mg/ml, 5 mg/ml and 10 mg/ml. Based on the static loading procedure described in detail in Chapter **4** Section **3.2.2**, the

non-specific binding blocking results, as well as the specific binding blocking results are considered together to determine the optimum concentration.

2.1. Phage chemistry modification

Phage filaments bundle in solution when counterions are present. Although we expected that such "bundles" would present a concentrated number of available sites for the antigen to attach and provide stronger bindings, it proved difficult to obtain a uniform distribution of phage bundles on the biosensor surface. Because the bundles were immobilized only at certain regions on the sensor surface, this resulted in less binding of targets. Alternatively, when the phage concentration was too high, the numbers of available phage filaments were so high that it became too easy to form phage bundles. Consequently, in this experiment it was preferable to use individual filaments of phage that saturate the entire sensor surface with randomly oriented phages to obtain a relatively uniform binding of cells/spores.

After phage coating, the exposure of the phage-based ME biosensor to the target analyte was carried out using two methods, namely static and dynamic loading. For static loading, each phage-based ME biosensor was simply incubated in a tube containing the target analyte (300 μl), and rotated by a laboratory mixer at room temperature at a speed of 8 rpm for 1 hour, followed by one distilled water washing. Dynamic loading was processed by placing each phage-based ME biosensor in a testing chamber in a flowing system (as shown in Figure 4-4 in Chapter 4), into which the target analyte was

introduced using an Ismatec Reglo Digital peristaltic pump with 8 rollers and four channels. A low flow rate (50 μL/min) was maintained to ensure laminar flow over the sensor.

2.1.1. Different phage concentrations in140mM NaCl solution

Recent studies [3-7] have used phages suspended in 1xTBS solution (containing 140 mM NaCl) in order to ensure stability of the phage over time. Another study [8] has shown that salt concentrations lower than 100 mM will promote intervirion association and alignment of the filaments, resulting in bundles. Therefore, we chose 140mM NaCl as the lowest salt concentration investigated.

Figure 5-6 shows electron microscopy pictures of the ME biosensors, immobilized with different phage concentrations (5×10^{10} vir/mL-5×10^{13} vir/mL) but containing the same concentration of salt (140 mM NaCl), after exposure to a concentrated spore solution (5×10^{8} spores/ml) by the static loading method. In Figure 5-6, a distinct difference between the attachment of spores to the JRB7 phage biosensors immobilized with different phage concentrations can be observed from the SEM images of the sensor surfaces. The biosensor immobilized with a phage concentration of 10^{13}vir/mL (Figure 5-6 (a)) showed very little binding. The biosensor immobilized with a phage concentration of 5×10^{11} vir/mL (Figure 5-6 (c)) shows the best binding. The biosensors with phage concentrations of 5×10^{12} vir/mL and 5×10^{10} vir/mL (Figures 5-6 (b) and (d), respectively) showed similar numbers of spores bound to the biosensors.

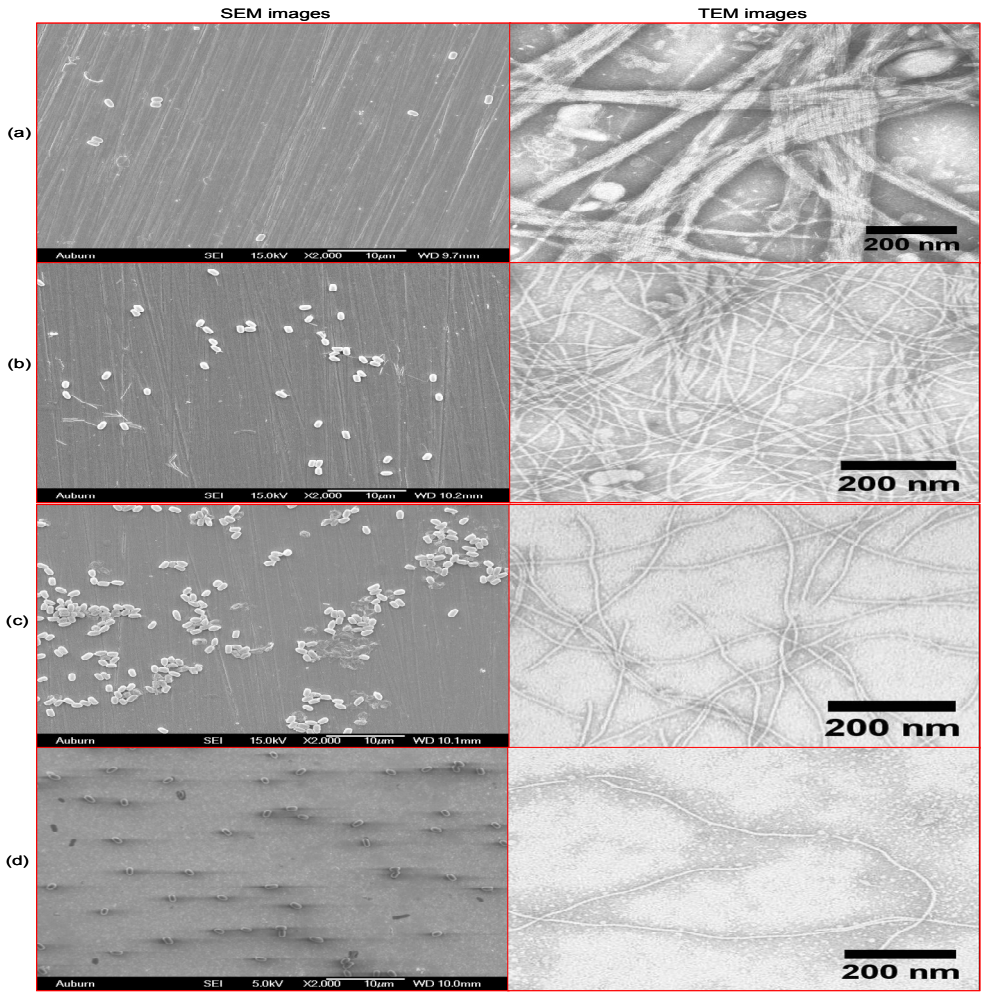

Figure 5- 6. SEM images of sensor surfaces exposed to spores after loading different concentrations of phage in solutions containing 140 mM NaCl; and TEM images of phage at concentrations of (a) 5×10^{13} vir/mL, (c) 5×10^{12} vir/mL, (e) 5×10^{11} vir/mL, and (g) 5×10^{10} vir/mL.

On the basis of the SEM microscopic analysis, we hypothesize that there are two reasons for the observed spore binding affinity: 1) *Concentration of phage solution*. The greater the number of phage filaments present in the solution, the larger the number

of potential binding sites there will be for spores. However, if the concentration of phage is too high, the individual filaments will form bundles or clusters, causing a reduction in the number of available binding sites. 2) *Adsorption of phage onto the ME biosensor*. There is an optimum phage concentration that leads to a uniform distribution of individual phage filaments on the surface of the biosensor. Too high a concentration once again leads to bundling and a corresponding decrease in available binding sites. From the above SEM results, a phage concentration of 5×10^{11} vir/mL appears to be the optimum condition for uniform immobilization.

A further examination was conducted using TEM images to verify the distribution of phage for different phage concentrations at a fixed salt concentration of 140 mM. For high phage concentrations of 5×10^{13} vir/mL and 5×10^{12} vir/mL (Figure 5-6 (a) and (b)), the phage filaments in solution tend to cluster together, affording fewer binding sites when immobilized onto the sensor surface. For a phage concentration of 10^{10} vir/mL (Figure 5-6 (d)), the phage exists as individual filaments in solution. However the density of phage filaments in solution is less than that needed to fully cover the sensor surface. This results in a less than optimal number of available binding sites and, hence, a lower number of captured spores. The TEM picture for a phage concentration of 5×10^{11} vir/mL (Figure 5-6 (c)) shows the evenly distributed phages with a minimal number of bundles, provides the optimal condition for the capture of spores.

Therefore, we recommend 5×10^{11} vir/mL as the optimum phage concentration that can be adsorbed onto the ME biosensors in such a manner as to result in the

maximum availability of binding sites for spores. As a result, this concentration was chosen for the experiments involving changes in salt concentration. Similar results were obtained after repeating these conditions for several batches of ME biosensors.

2.1.2. Phage distribution under different salt concentrations

Figure 5-7 shows the average frequency shift of each group of JRB7 phage biosensors immobilized using phage at a concentration of 5×10^{11} vir/mL, with varying concentrations of salt and exposed to the same spore suspension. Each data point represents the average of 5 individual biosensors. As the salt concentration increased from 140 mM to 840 mM, the frequency shift of the biosensors increased until a maximum was achieved at a salt concentration of 420 mM. As the salt concentration increased further, the shift in resonance frequency of the sensors decreased. At the maximum studied concentration of 840 mM, the frequency shift of the sensors was similar to that of the lowest salt concentration. Since a higher frequency shift corresponds to a higher mass load on the sensor (as per Eq.3-5), and since this mass load is due to spore binding, it is evident that the 420 mM salt concentration represents the optimum binding condition for 5×10^{11} vir/mL phage suspension.

$$\Delta f = -\frac{f_0}{2}\frac{\Delta m}{M} \qquad (3\text{-}5)$$

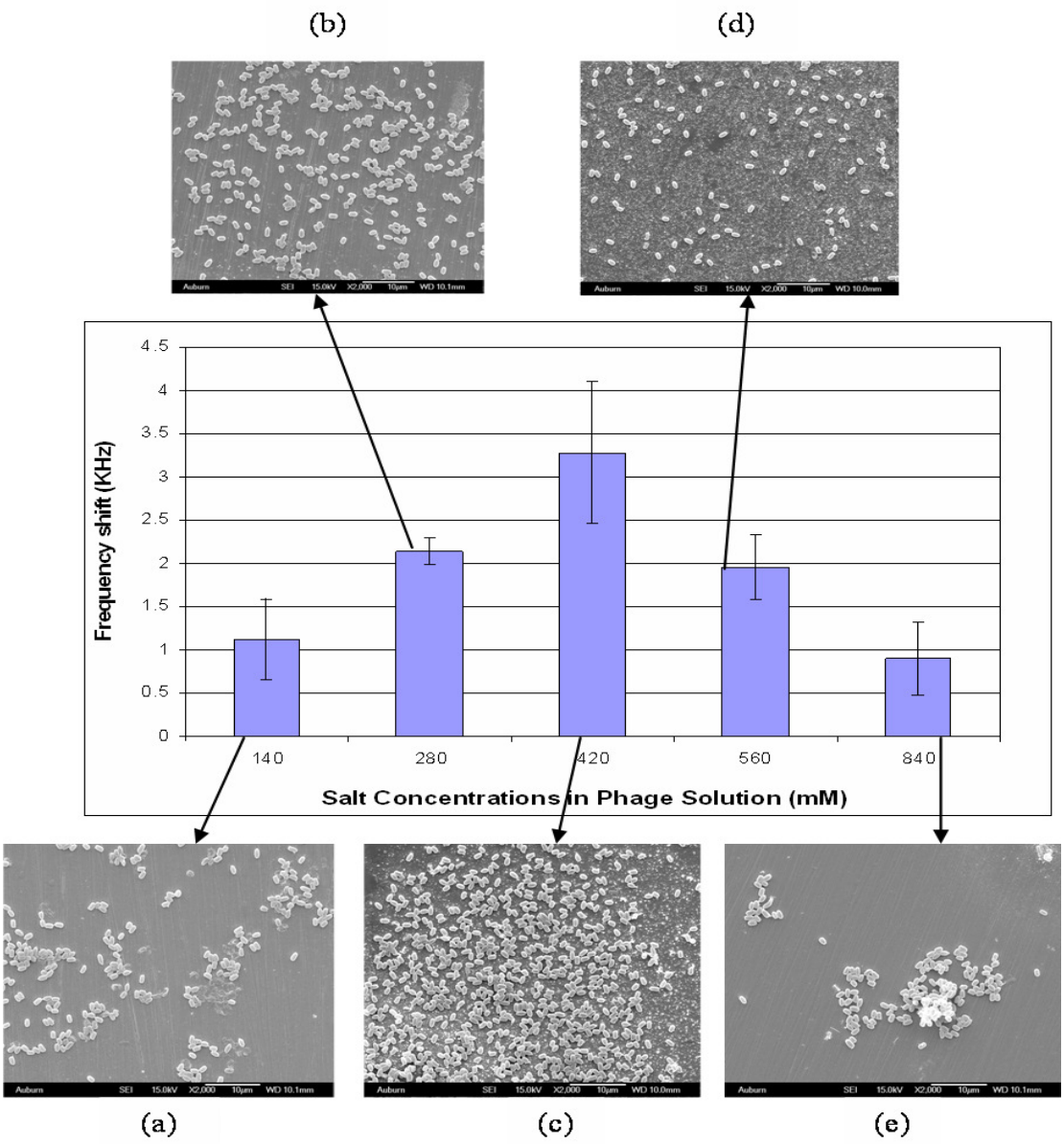

Figure 5- 7. Frequency shift of sensors vs. salt concentrations in 5×10^{11}vir/mL phage solution and SEM photographs of sensors immobilized with 5×10^{11}vir/mL phage in solutions with NaCl concentrations of: (a) 140mM, (b) 280mM, (c) 420mM, (d) 560mM (e) 840mM.

SEM images were used to verify the biosensor response. Figure 5-8 (a-e) depicts the results under five (140 mM-840 mM) salt concentrations. As can be seen, the results are consistent with the biosensor response curve, which shows that the maximum number of spores bound to the sensor occurred when JRB7 phage was immobilized in a solution containing 420 mM NaCl. Moreover, the uniformity of the spore distribution under each condition may clearly be seen. For the lowest salt concentration (Figure 5-8 (a)), the spores tended to cluster, which is similar to the case of the highest salt concentration (Figure 5-8 (e))

2.1.3. Effect of salt concentration on phage bundles

Earlier works reported by Tang and coworkers show that lateral aggregation phenomena (i.e. bundle formation or clustering) may occur with filamentous phage fd depending upon the properties of the solution in which the phage is suspended [9, 10].

TEM was used to investigate the effect of salt concentration on phage distribution. Under some solution conditions, the phage tends to aggregate into bundles, thereby reducing the number of protein sites available for binding. The TEM images in Figure 5-8 show the distribution of phage for different phage concentrations (5×10^{10}, 10^{11}, and 10^{12} vir/mL) at different salt concentrations (140 mM, 420 mM and 840 mM). The phage filaments in solution clustered together when the phage concentration was high (5×10^{12} vir/mL). Upon increasing the amount of salt to 420 mM, the phage filaments tended to disaggregate, but a further increase in the salt content again resulted

in the formation of bundles. A similar trend was also found for the phage concentration of 5×10^{11} vir/mL. For a phage concentration of 10^{10} vir/mL, the distribution of the phage filaments was very low, and there was no bundle formation regardless of salt concentration.

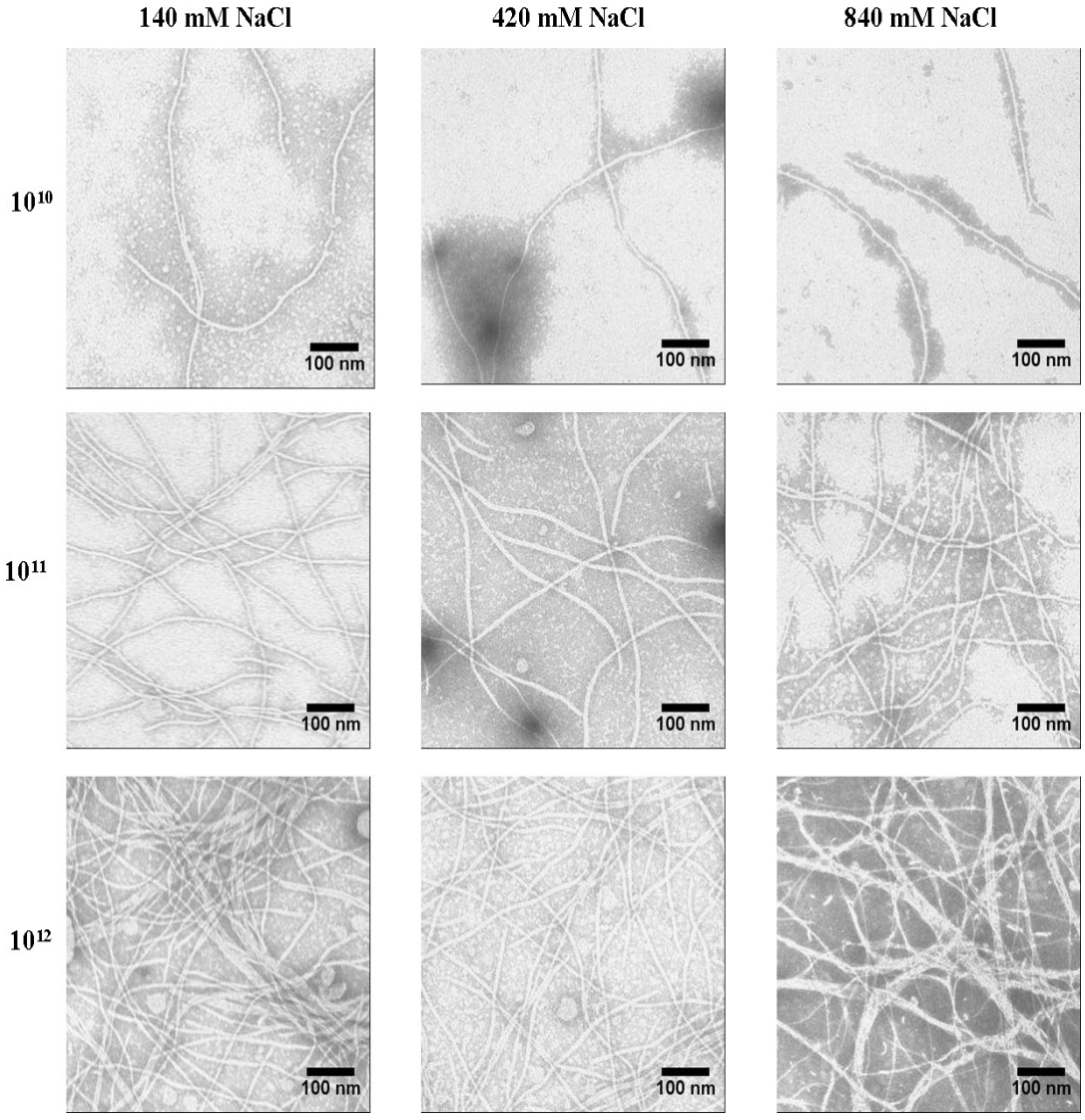

Figure 5- 8. TEM images of different concentrations of phage in selected NaCl concentrations.

Similar results were obtained after repeating these conditions for several batches of ME biosensors. An optimum balance of phage/salt concentration is critical to the binding affinity of the ME biosensor. Salt induced aggregation of filamentous phage has previously been studied and documented by other researchers [10-13]. In most of these reports, the effect of the presence of divalent counterions in wild type fd phage suspensions was studied. Evidence from these earlier studies [8, 14] indicates that decreasing the salt concentration in the phage suspension decreases the axial charge density of the filaments, promoting aggregation or "clustering". Likewise, as salt concentration is increased, axial charge density of the phage filaments increases, leading to less aggregation up to some optimum level and, hence, more even distribution of filaments in solution. As yet, the understanding of the exact molecular mechanism for this phenomenon remains unclear and needs to be studied further.

2.1.4. Effect of salt concentration on spore binding

To evaluate the effect of NaCl concentration on the phage immobilization and, thus, the biosensors' performance, the numbers of spores bound to the biosensor's surface were counted using the SEM. The entire surface of one side of the biosensor was photographed and spores were counted individually. This number was then multiplied by 2 to account for both sides of the sensor. Table 5-2 and Figure 5-9 show a comparison of the number of spores bound on each ME sensor immobilized for different phage concentrations (5×10^{10}-10^{12} vir/mL) and under different salt concentrations (140

mM - 840 mM).

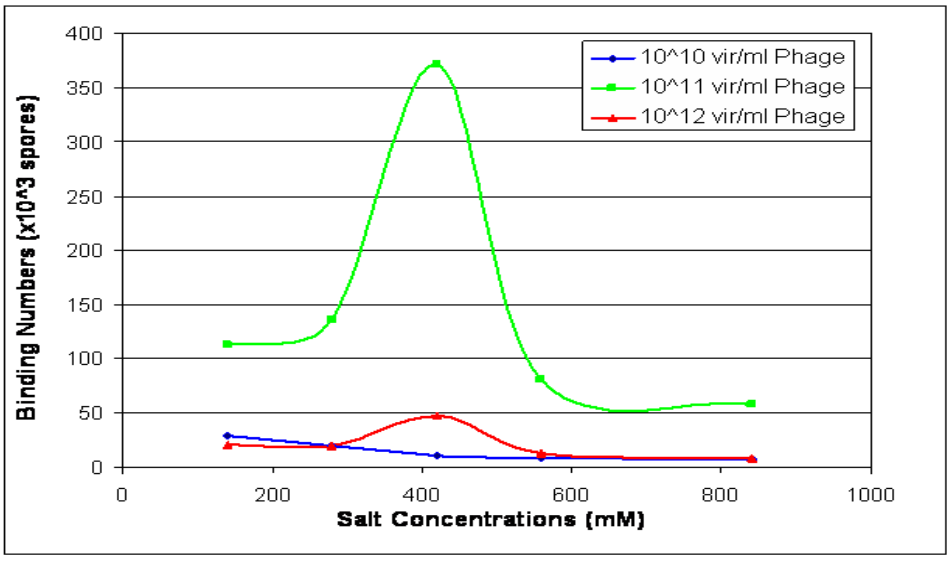

Figure 5-9. The binding numbers of spores as a function of different NaCl concentrations.

Table 5- 2. Binding numbers of spores under different conditions.

Phage [C] (vir/mL)	Salt [C] (mM)				
	140	280	420	560	840
5×10^{10}	28,801	19,258	10,735	8,211	7,152
5×10^{11}	112,173	136,212	370,856	80,000	57,856
5×10^{12}	20,502	19,012	47,664	12,168	8,596

Figure 5-9 reveals a noticeable difference in the attachment of spores to the biosensors under each condition. The SEM results were observed to be consistent with the results obtained from the TEM observations. The biosensor immobilized with a phage at a concentration of 5×10^{11} vir/mL showed the most binding. With an increase in the salt concentration from 140 mM to 420 mM, an increase in number of spores bound to the sensor was observed, with a maximum at the salt concentration of 420 mM. However, a further increase in salt concentration resulted in a decrease in the number of spores bound. A similar trend was found with a phage concentration of 5×10^{12} vir/mL, although the number of spores bound was significantly lower than that for the phage at a concentration of 5×10^{11} vir/mL. For the phage at a concentration of 10^{10} vir/mL, an increase in salt concentration resulted in a decrease in attached spores. The binding of spores to the sensor with concentrations 5×10^{10} vir/mL and 5×10^{12} vir/mL was significantly lower than that for 5×10^{11} vir/mL. The lower number of bound spores observed at 5×10^{12} vir/mL was mainly due to the large number of phage filaments forming bundles. In the case of 5×10^{10} vir/mL, the low binding is the result of the small number of phage filaments present in the solution. As a result, the phage at a concentration of 5×10^{11} vir/mL with 420 mM NaCl in 1xTBS was selected as the optimum condition likely to result in the most favorable environment for the binding of spores.

2.1.5. Phage distribution on ME biosensor

The objective of this experiment was to show the distribution of phage filaments on the biosensor surface. The SEM studies (Fig. 5-10) show three stages of the sensor surface and clearly demonstrate the ability of the biosensors to capture *Salmonella typhimurium* or *B. anthracis* spores using phage immobilized onto the ME sensor surface. The first stage (Figure 5-10(a)) shows the surface before any experimentation was done and is just the plain gold surface. The second stage (Figure 5-11(b)) shows the surface after coating with a 5×10^{11} vir/mL phage suspension containing 420 mM NaCl. This step was carried out by incubating the ME sensor platforms in a tube containing phage solution on a rotor for at least 1 hour. Many phage filaments are distributed uniformly on the biosensor surface, as can be clearly seen in the figures. The third stage (Figure 5-10 (c) and (d)) shows the surface after exposure to 5×10^{8} cfu/mL of *S. typhimurium* or *B. anthracis* spores by static loading. The figure shows the capture of the target pathogen by the phage on the sensor surface. This process was also carried out by incubating the sensor in the target analytes for another 1 hour, after which the assayed sensors were mounted on aluminum stubs using double-sided carbon tape and exposed to OsO_4 vapor for 45 minutes. The figure shows a clear surface with the phage capturing the bacteria cells / spores. In order to take clear SEM images with phage filaments, the biosensors were observed directly under microscopy without a final gold coating layer. Previously, a very thin layer of gold (≈15 nm) was sputtered on the top of assayed biosensors to provide a conductive surface after OsO_4 exposure, but this made it

impossible to resolve the phage filaments because they were covered by the gold film. Later it was determined that the initial Au layer on the ME platforms was enough to provide a conductive layer for clear SEM pictures, making it possible to eliminate the final step of an additional thin gold layer deposition. During SEM analysis, a low probe current is also crucial for obtaining higher resolution pictures. Moreover, with the presence of Os in the bacteria cells / spores, the low probe current minimized the charging of the samples in the SEM chamber.

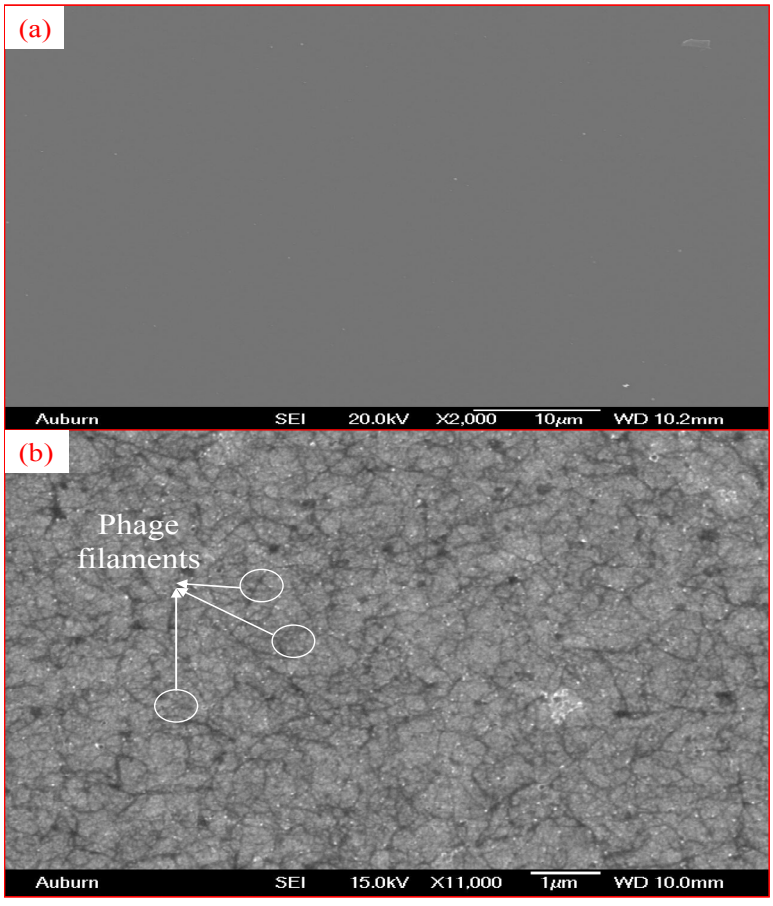

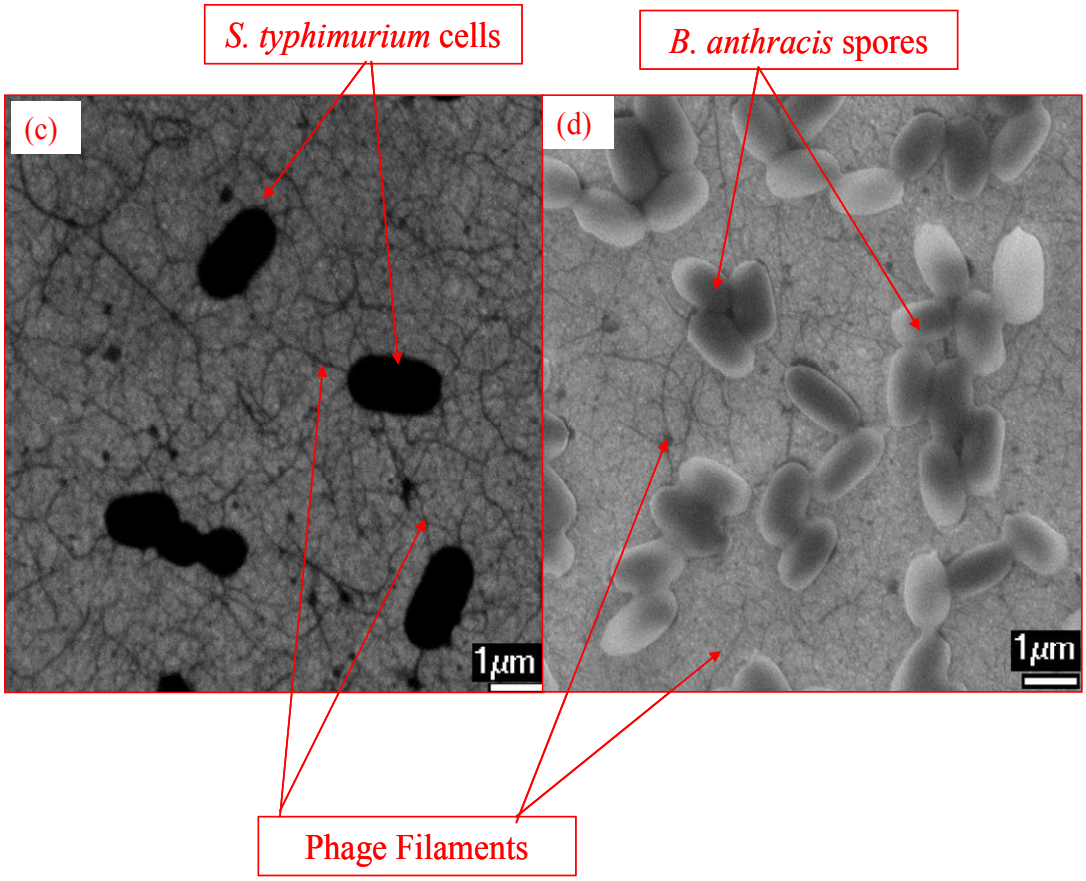

Figure 5- 10. SEM photographs of phage distribution on ME sensor surface (a) before phage immobilization (bare gold coating); (b) after immobilization of phage with the concentration of 5×10^{11} vir/mL; (c) after exposure with *S. typhimurium* suspension (phage and salmonella cells interaction); (d) after exposure with *B. anthracis* spores (phage and spores interaction).

In order to determine the number of bacterium / spores bound to the phage-based biosensors, the same counting method described in detail in Chapter **4** Section **5.3** was applied. A comparison of this number obtained by SEM observations with the theoretical number of bound spores calculated from the resonance frequency shifts is shown in Table 5-3. The numbers are in reasonable agreement. The difference between the calculated number and the counted number is mainly due to two reasons: 1) Some spores/cells were only loosely bound and were washed away by the filter water when rinsed prior to SEM analysis; 2) Errors in counting could have occurred, particularly around the edges of the sensors where spores and cells tend to pile up or cluster.

Table 5- 3. Comparison of the No. of bound cells/spores calculated and observed.

Sensor exposure to analytes	Frequency shift (Hz)	Original frequency (MHz)	Calculated No. of binding	Counted No. from SEM
S. typhimurium	1125	1.082409	98,530	91,500 (93 %)
B. anthracis spores	1020	1.076652	89,811	76,300 (85 %)

2.1.6. Dynamic response in different concentrations of *B. anthracis* spores

Figure 5-11 shows the dynamic response of a biosensor immobilized with JRB7 phage using the optimum conditions (5×10^{11} vir/mL and 420 mM NaCl) to increasing concentrations of *B. anthracis* spores ($5 \times 10^{1} - 5 \times 10^{8}$ cfu/mL). As the concentration of the spore solution was increased, the resonance frequency experienced the expected decrease. The initial frequency remained stable until the solution with a spore concentration of 5×10^{3} cfu/mL was introduced, where the first detectable drop of frequency can be seen. At the end of the test, after introduction of the highest spore concentration, the total resonance frequency shift for this biosensor was 1420 Hz.

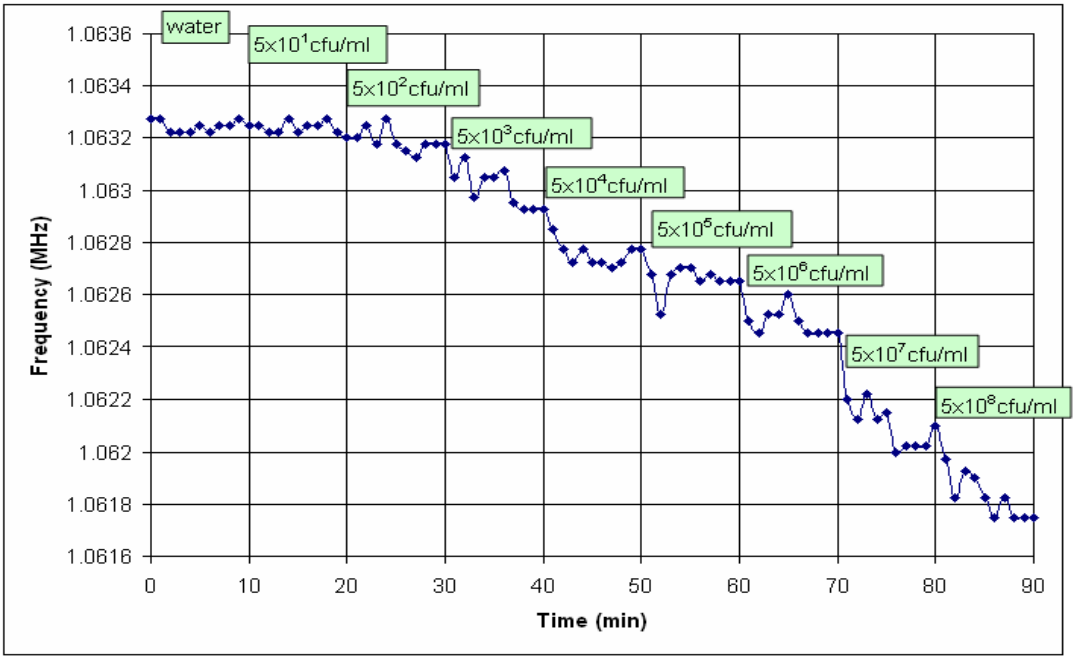

Figure 5- 11. Response of a ME biosensor exposed to different concentrations of *B. anthracis* spores (5×10^{1}-5×10^{8} cfu/mL).

SEM images (Figure 5-12) show the interaction of spores with JRB7 phage on the biosensor surface where the spores were uniformly distributed on the surface. Figure 5-13 shows the dose response curve of the ME biosensor dynamic response and represents the sigmoidal fit of the data.

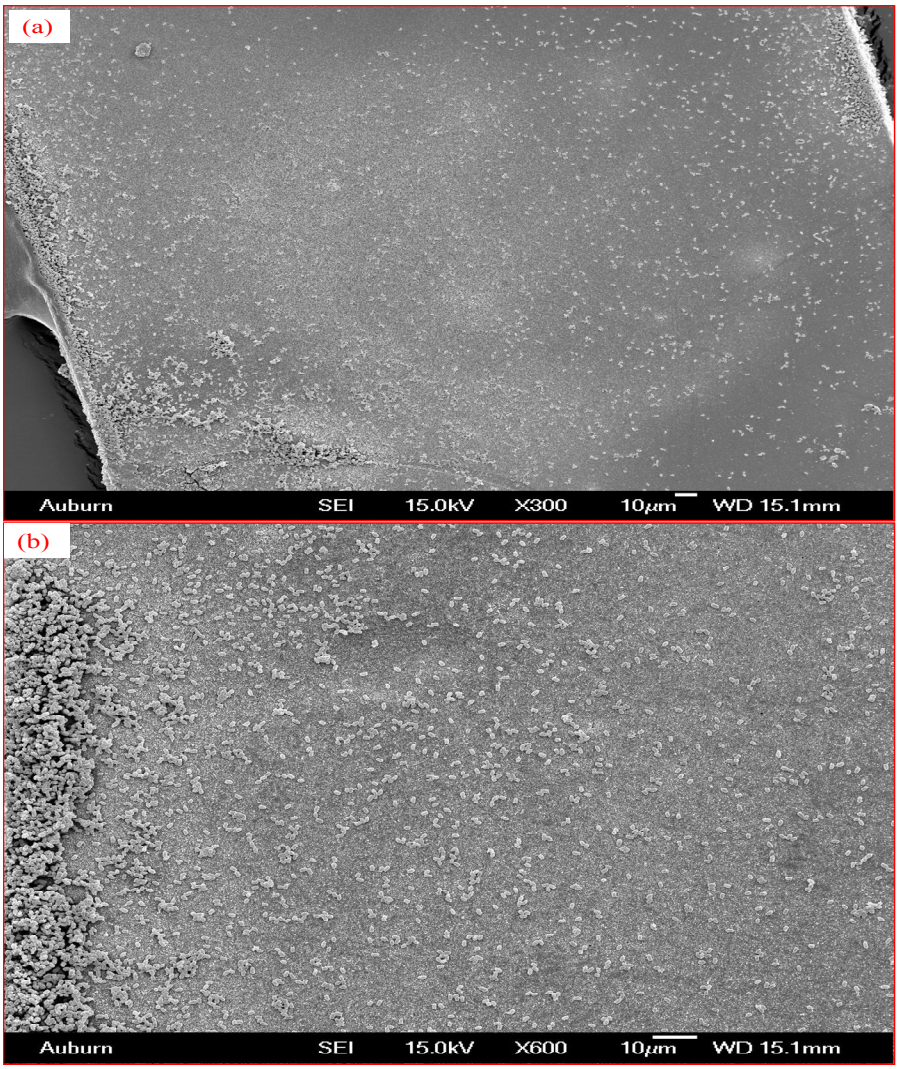

Figure 5- 12. SEM photographs of ME sensor surface after exposure to different concentrations of *B. anthracis* spores (5×10^{1}-5×10^{8} cfu/mL) dynamically.

In the Hill plot (Figure 5-14), the biosensors show a sensitivity of 226.3 Hz/decade in the linear range (5×10^3 to 5×10^8 cfu/mL). The detailed performance is summarized in Table 5-4.

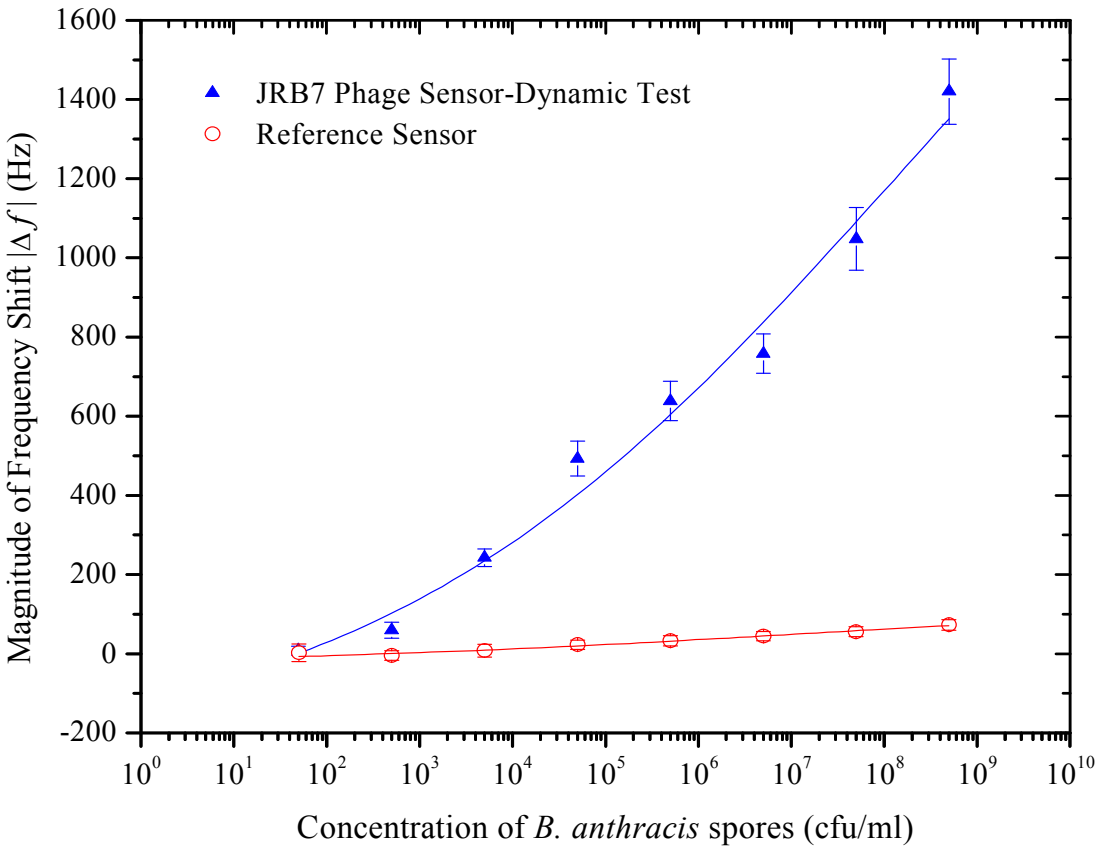

Figure 5- 13. Dose response curve of ME biosensor ($2 \times 0.4 \times 0.015$ mm) coated with 5×10^{11} cfu/mL phage suspension (contain 420 mM NaCl) and then exposed to increasing concentrations (5×10^1-5×10^8 cfu/mL) of *B. anthracis* spores suspensions in water ((▲) (R^2=0.984)). Reference sensor (o) represents the uncoated (devoid of phage) sensor's response. The curve represents the sigmoidal fit of signals obtained.

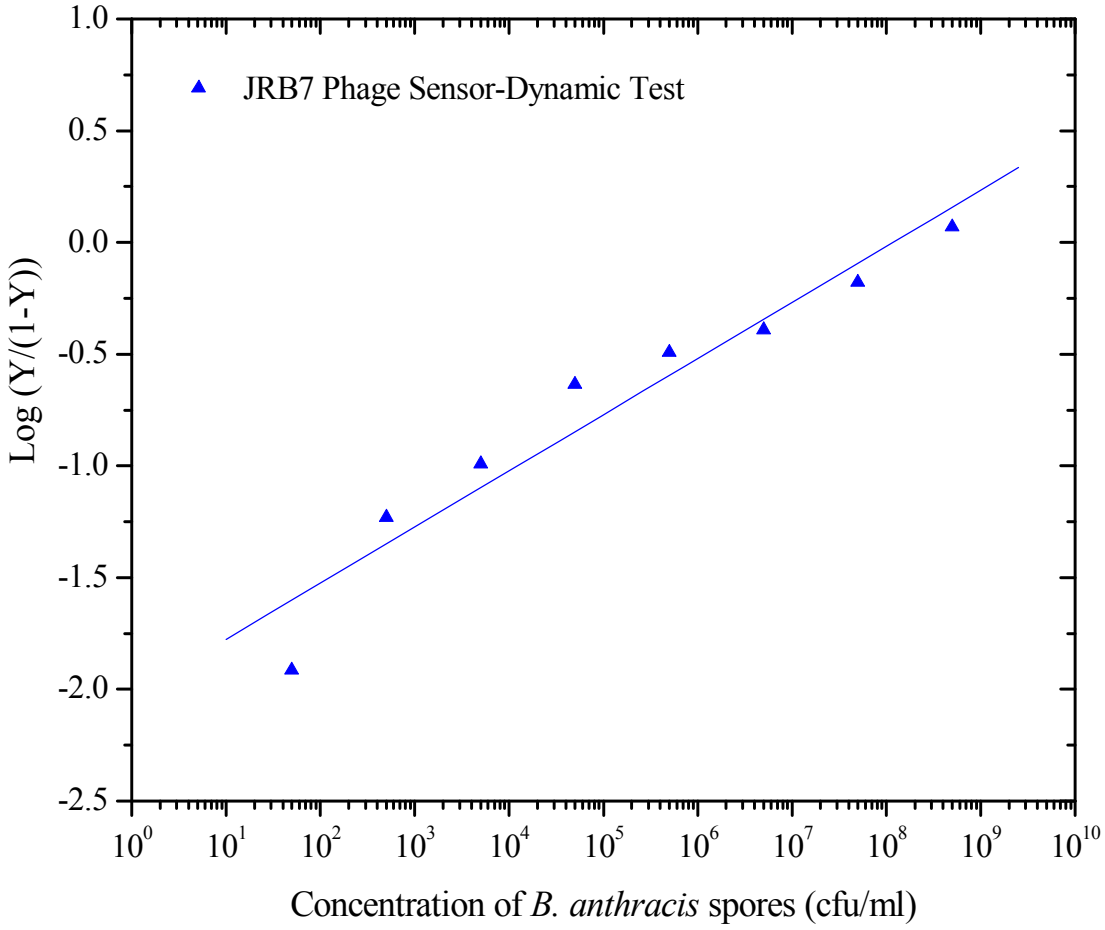

Figure 5- 14. The Hill plot of binding isotherms for ME biosensor (2 × 0.4 × 0.015 mm) showing the ratio of occupied and free phage sites as a function of *B. anthracis* spores concentrations. The straight line is the linear least squares fit to the data points ((▲) slope = 0.25124 ± 0.02, R = 0.965).

Table 5- 4. The sensitivity, dissociation constant and binding valency of ME biosensor coated with phage concentration of 5×10^{11} vir/mL (containing 140mM NaCl) and exposure to different concentration of spore suspensions.

Analyte	Sensitivity (Hz/Decade)	Binding valency (*1/n*)	K_d (cfu/mL)	$K_{d(apparent)}=(K_d)^{1/n}$ (cfu/mL)
B.anthracis spores	226.3	2.98	104.7	1.04×10^6

2.1.7. E2 phage biosensor exposure to *S. typhimurium* by static loading

From the above discussion, the optimum concentration of NaCl contained in the JRB7 phage suspension (5×10^{11} vir/mL) specific to *B. anthracis* spores was 420mM. In this section, we want to ensure that this concentration of NaCl can also produce a uniform distribution of E2 phage (specific to *S. typhimurium*) on the biosensor surface. Experiments were carried out by coating ME platforms with E2 phage (concentration of 5×10^{11} vir/mL), but containing different amounts of NaCl (140 - 840 mM) and then exposing the sensor to *S. typhimurium* suspensions (5×10^8 cfu/mL) by static loading (described in Chapter **4** Section **3.2.3.**), followed by OsO_4 treatment as described in Chapter **4** Section **5.1**. The SEM photographs after static loading are shown below in Figure 5-15. The E2 phage biosensor coated with E2 phage solution containing 420mM NaCl showed the best binding (Figure 5-15 (a)) with the entire surface covered uniformly

by *Salmonella* cells. The distribution for a larger area of the sensor under this condition can be seen in Figure 5-15 (b) at a lower magnification.

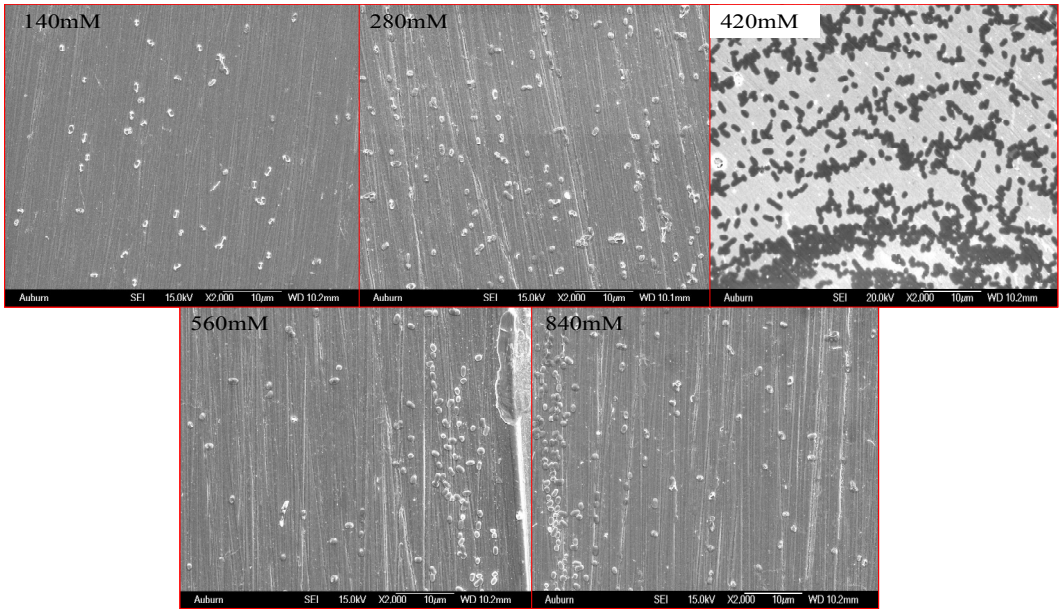

(a)

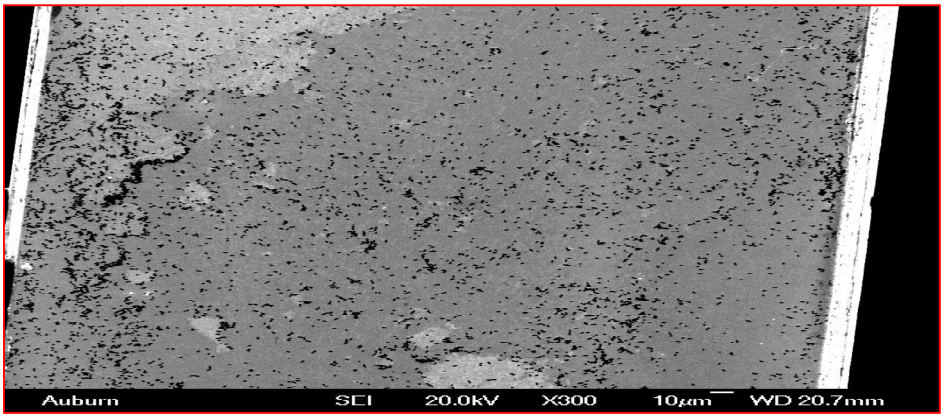

(b)

Figure 5- 15. SEM of phage (5×10^{11} vir/mL, 140 – 840 mM NaCl)-based ME biosensor surface after exposure to high concentrations of *S. typhimurium* (5×10^{8} cfu/mL) by static loading (a); low magnification of phage (420 mM NaCl) based sensor surface (b).

2.2. Proper concentration of BSA to block non-specific binding

Scanning electron microscopy was used to determine the most favorable BSA concentration by comparing the binding affinity of the sensors coated with different concentrations of BSA solution. Figures 5-16 - 5-18 show the results of a series of cell binding experiments that were obtained after exposure to the highest concentration (5×10^8 cfu/mL) of analytes. Clear differences in the attached numbers of bacteria/spores to sensors were observed depending on the concentration of the BSA coating solution. In the case of the sensors coated with either 5 or 10 mg/ml BSA, only a few cells bound to the surface of the sensors, as shown in Figure 5-18. It is inferred from this result that the concentration of BSA was too great, covering not only the bare gold areas unoccupied by filamentous phage, but also the phage layer itself, resulting in very few available binding sites on the sensor surfaces. When the reference and JRB7 phage-coated (*B. anthracis*) sensors without BSA coating were exposed to the *S. typhimurium* suspension, there was a small degree of nonspecific binding, as can be seen in Figure 5-16. However, after treatment with 1 mg/ml BSA, the amount of this nonspecific binding was greatly reduced, while the E2 phage-coated (*S. typhimurium*) sensor still showed similar binding characteristics to the sensor without BSA coating. Similarly, with exposure to *B. anthracis* spores, as shown in Figure 5-17, while the JRB7 phage-coated (*B. anthracis*) sensor was relatively unchanged. A BSA solution at a concentration of 1 mg/ml was therefore chosen for use in preparation of the blocking agent for subsequent experiments.

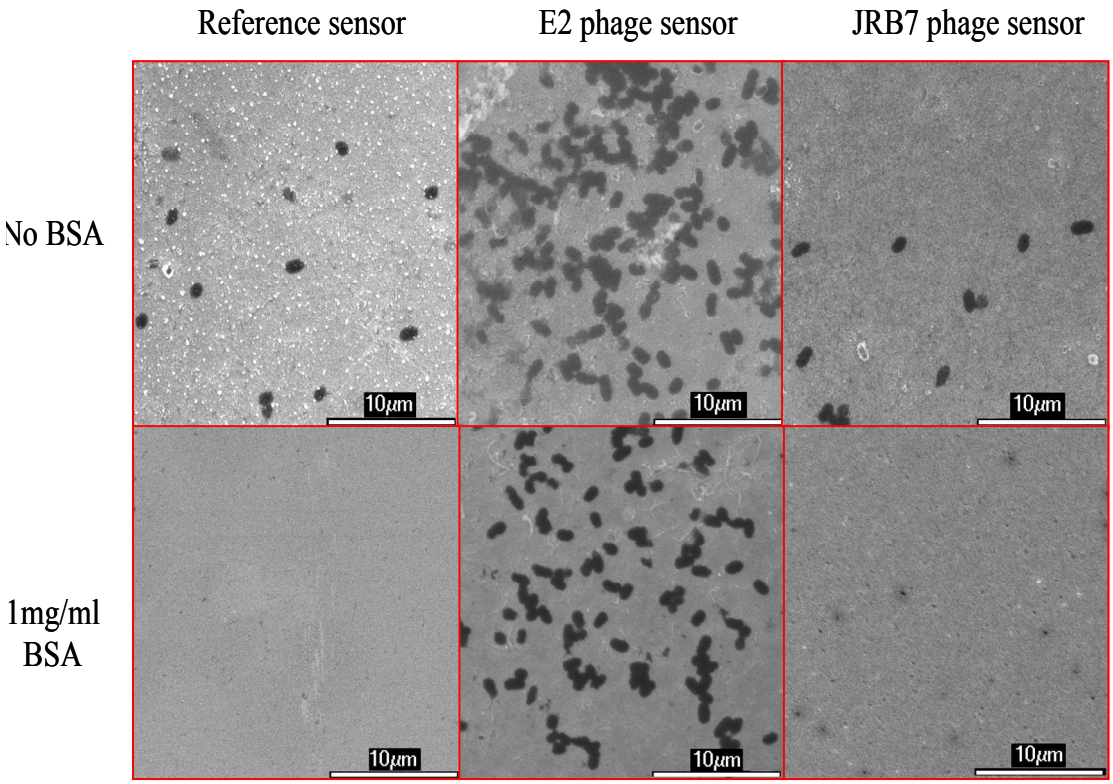

Figure 5-16. SEM binding images of the sensors with and without 1 mg/ml BSA after exposure to *S. typhimurium* suspension (5×10^8 cfu/mL).

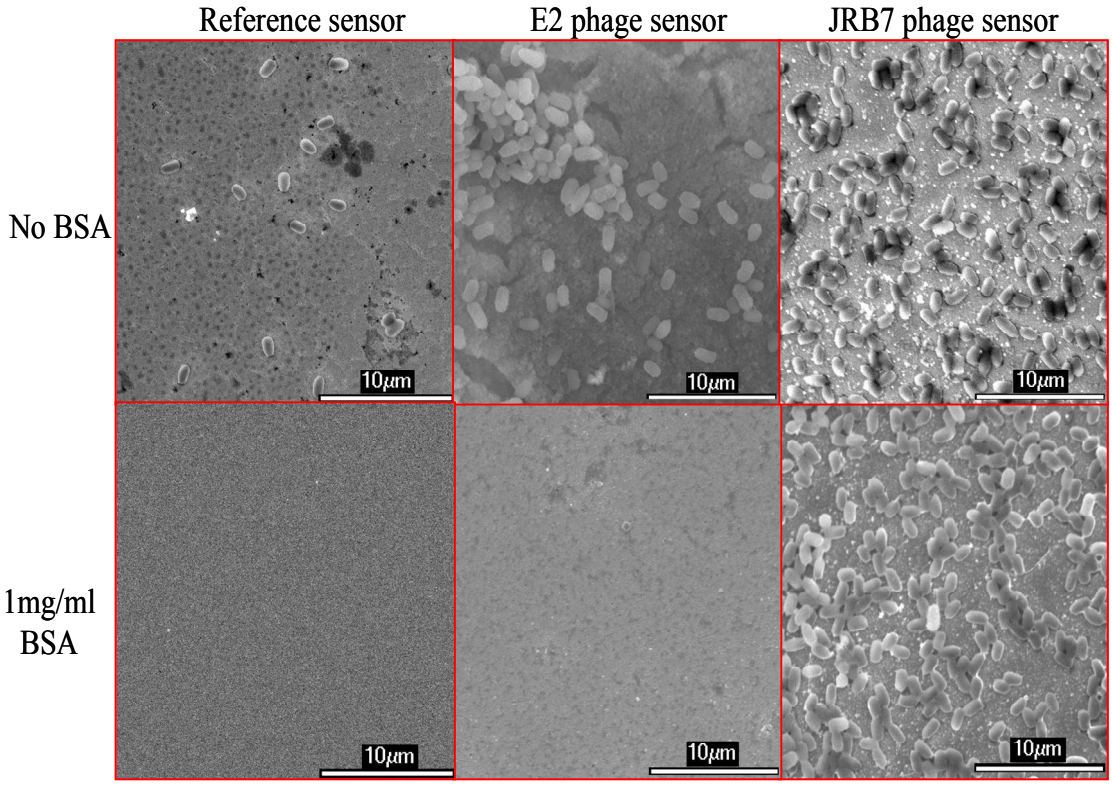

Figure 5- 17. SEM binding images of the sensors with and without 1 mg/ml BSA after exposure to *B. anthracis* spores suspension at a concentration of 5×10^8 cfu/mL.

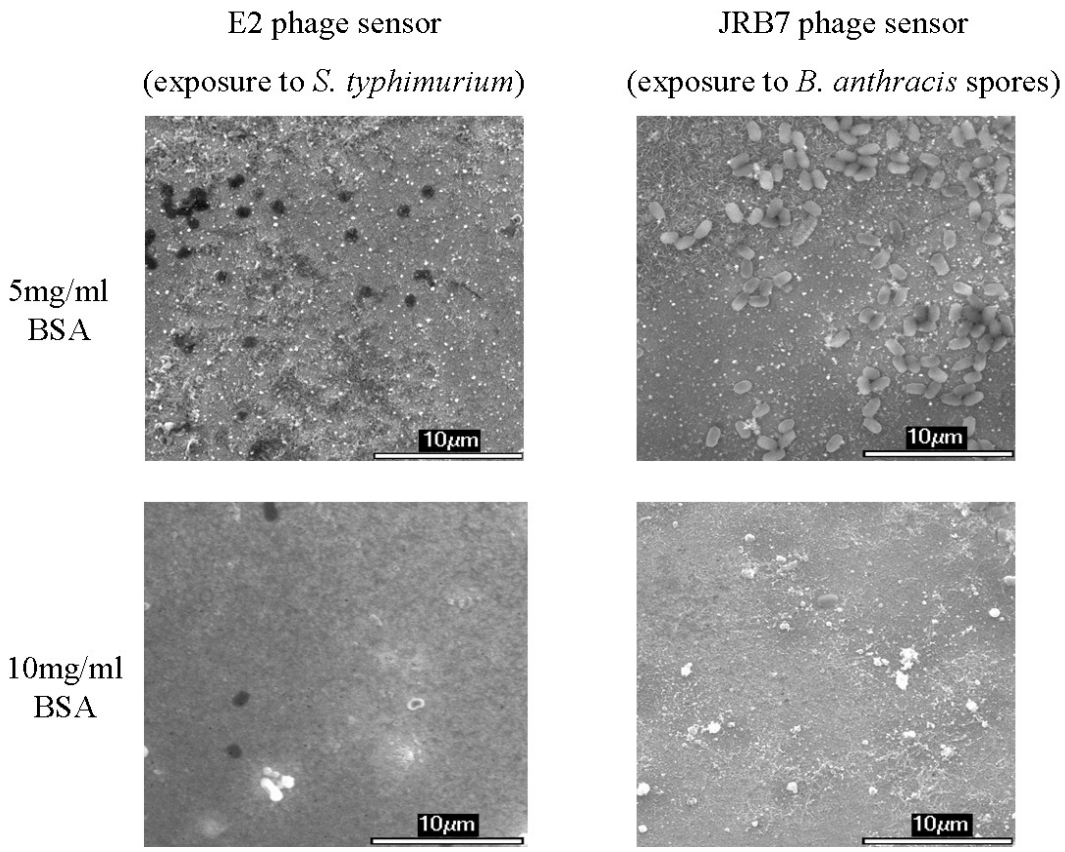

Figure 5- 18. SEM binding images of the sensors coated with 5 mg/ml and 10 mg/ml BSA after exposure to *S. typhimurium / B. anthracis* spores suspension at a concentration of 5×10^8 cfu/mL.

3. Conclusions

The work detailed in this chapter focused on improving the mass sensitivity of a phage-based, magnetoelastic biosensor by changing the phage suspension chemistry. The results of this study indicate that the optimum binding condition for gold-coated, magnetoelastic biosensors occurs when the phage is immobilized at a concentration of 5

$\times 10^{11}$ vir/mL. Furthermore, the concentration of salt in the phage suspension will affect the binding affinity of the biosensor. The higher the number of spores bound to the sensor's surface, the better the mass sensitivity of the sensor. For a solution of phage at a concentration of 5×10^{11} vir/mL in 1xTBS, a salt concentration of 420 mM will promote an optimum number of binding sites for spores due to even distribution of the phage filaments. In contrast, a low-salt concentration will lead to the formation of phage bundles, resulting in a smaller amount of spore binding. Conversely, a salt concentration that is too high will also cause clustering of the phage filaments. Both SEM images of spore binding on the sensor surfaces and TEM images of phage distribution in solution are consistent with our findings. Additionally, non-specific binding was effectively eliminated by 1mg/ml BSA blocking.

4. References

[1] K. E. Haq, K. H. Behrndt, and I. Kobin, "Adhesion Mechanism of Gold-Underlayer Film Combinations to Oxide Substrates," *Journal of Vacuum Science and Technology,* vol. 6, pp. 148-152, 1969.

[2] D. M. Mattox, "Thin film metallization of oxides in microelectronics," *Thin Solid Films,* vol. 18, pp. 173-186, 1973.

[3] J. Wan, M. L. Johnson, R. Guntupalli, V. A. Petrenko, and B. A. Chin, "Detection of *Bacillus anthracis* spores in liquid using phage-based magnetoelastic micro-resonators," *Sensors and Actuators B: Chemical,* vol. 127, pp. 559-566,

2007.

[4] J. Wan, H. Shu, S. Huang, I.-H. Chen, V. A. Petrenko, and B. A. Chin, "Phage-based magnetoelastic wireless biosensors for detecting *Bacillus anthracis* spores," *IEEE Sens. J. ,* vol. 7, pp. 470-477, 2007.

[5] R. S. Lakshmanan, R. Guntupalli, J. Hu, D.-J. Kim, V. A. Petrenko, J. M. Barbaree, and B. A. Chin, "Phage immobilized magnetoelastic sensor for the detection of *Salmonella typhimurium*," *Journal of Microbiological Methods,* vol. 71, pp. 55-60, 2007.

[6] R. S. Lakshmanan, R. Guntupalli, J. Hu, V. A. Petrenko, J. M. Barbaree, and B. A. Chin, "Detection of *Salmonella typhimurium* in fat free milk using a phage immobilized magnetoelastic sensor," *Sensors and Actuators B: Chemical,* vol. 126, pp. 544-550, 2007.

[7] S. Huang, H. Yang, R. S. Lakshmanan, M. L. Johnson, I. Chen, J. Wan, H. C. Wikle, V. A. Petrenko, J. M. Barbaree, Z. Y. Cheng, and B. A. Chin, "The Effect of Salt and Phage Concentrations on the Binding Sensitivity of Magnetoelastic Biosensors for *B. anthracis* Detection," *Biotechnology and Bioengineering,* vol. 101, pp. 1014-10221, 2008.

[8] S. A. Overman, D. M. Kristensen, P. Bondre, B. Hewitt, and G. J. T. Jr., "Effects of virion and salt concentrations on the Raman signatures of filamentous phages fd, Pf1, Pf3, and PH75," *Biochemistry,* vol. 43, pp. 13129-13136, 2004.

[9] J. X. Tang, P. A. Janmey, A. Lyubartsev, and L. Nordenskiold, "Metal Ion-Induced Lateral Aggregation of Filamentous Viruses fd and M13," *Biophysical Journal,* vol. 83, pp. 566-581, July 1, 2002 2002.

[10] J. X. Tang, T. Ito, T. Tao, P. Traub, and P. A. Janmey, "Opposite effects of electrostatics and steric exclusion on bundle formation by F-actin and other filamentous polyelectrolytes," *Biochemistry,* vol. 36, pp. 12600-12607, 1997.

[11] Q. Wen and J. X. Tang, "Temperature effects on threshold counterion concentration to induce aggregation of fd virus," *Phys. Rev. Lett.,* vol. 97, p. 48101, 2006.

[12] B.-Y. Ha and A. J. Liu, "Effect of non-pairwise-additive interactions on bundles of rodlike polyelectrolytes," *Phys. Rev. Lett. ,* vol. 81, pp. 1011-1014, 1998.

[13] T. T. Nguyen, I. Rouzina, and B. I. Shklovshii, "Reentrant condensation of DNA induced by multivalent counterions," *J. Chem. Phys. ,* vol. 112, pp. 2562-2568, 2000.

[14] M. T. Record, W. Zhang, and C. F. Anderson, "Analysis of effects of salts and uncharged solutes on protein and nucleic acid equilibria and processes : A practical guide to recognizing and interpreting polyelectrolyte effects, Hofmeister effects, and osmotic effects of salts," *Adv. Protein Chem. ,* vol. 51, pp. 281-353, 1998.

CHAPTER 6

CHARACTERIZATION OF MULTI-SENSOR DETECTION SYSTEM

1. Outline

In the work reported in this chapter, multiple phage-based ME biosensors were used to simultaneously monitor the detection of different biological pathogens that were sequentially introduced to the measurement system. Recently, Grimes and his coworkers have reported their multi-sensor detection system for simultaneous control of temperature and pressure [1], quantification of multiple bioagents [2], and the measurement of liquid density and viscosity [3]. Their system used a miniaturized array of sensors with different lengths which were adhered to a micro-machined PC board at their non-vibrating mid-points by a thin coating of polyurethane. Our study adopted a different approach, constructing a multi-sensor system composed of three sensors that were free standing during the test, being held in place by the magnetic field. Each of these ME measurement biosensors was formed by immobilizing the appropriate phage and 1 mg/ml BSA (blocking agent) onto the ME resonator's surface. The detection system included a reference sensor devoid of phage coating, an E2 phage-coated biosensor specific to *S. typhimurium*, and a JRB7 phage-coated biosensor specific to *B. anthracis* spores. Upon sequential exposure to single pathogenic solutions, only the

biosensor coated with the corresponding specific phage responded. As the cells/spores were captured by the specific phage-coated biosensor, the mass of the biosensor increased, resulting in a decrease in the biosensor's resonance frequency. Additionally, whether or not the non-specific binding was effectively eliminated by BSA blocking in this flowing detection system was verified by the reference sensor, which showed a negligible frequency shift. Scanning electron microscopy (SEM) was used to visually verify the interaction of each biosensor with its target analyte. Furthermore, this multi-sensor system was also tested with *S. typhimurium* (5×10^1-5×10^8 cfu/mL) in a mixture of *E. coli* O157:H7 (5×10^7 cfu/mL) and *B. anthracis* spores (5×10^1-5×10^8 cfu/mL) in a mixture of *B. cereus* (5×10^7 cfu/mL), separately. Again, only the specific phage-coated biosensor responded and captured the target antigens. These results demonstrate the selectivity and specificity of this system, confirming that this technique is an effective method for simultaneous detection. The characterization of this multi-sensor detection system, working in a liquid medium, includes measurements of its sensitivity, stability, selectivity, specificity and detection limit. Also, a Hill plot was used to analyze the dissociation constant (K_d) and K_d *(apparent)*, thus quantifying the binding strength between phage filaments and targets and making it possible to estimate how many phage filaments are required to bind with the target antigens. Finally, the performance of each sensor within the multi-sensor detection system was compared under different testing conditions, as mentioned above.

2. Multi-sensor system

2.1. Two biosensors in one test chamber

The measurement of multiple biosensors has been investigated in air. The first question was whether it was possible to measure the frequencies of two free standing sensors placed in the same test chamber simultaneously. In this experiment, two sensors, one with dimensions of 1.9 × 0.4 × 0.015 mm and one with dimensions of 2.0 × 0.4 × 0.015 mm, were coated with JRB7 phage and E2 phage, respectively. During testing both sensors were placed in the same coil. As Figure 6-1 clearly shows, it is indeed possible to measure the frequencies from two sensors in one test chamber simultaneously.

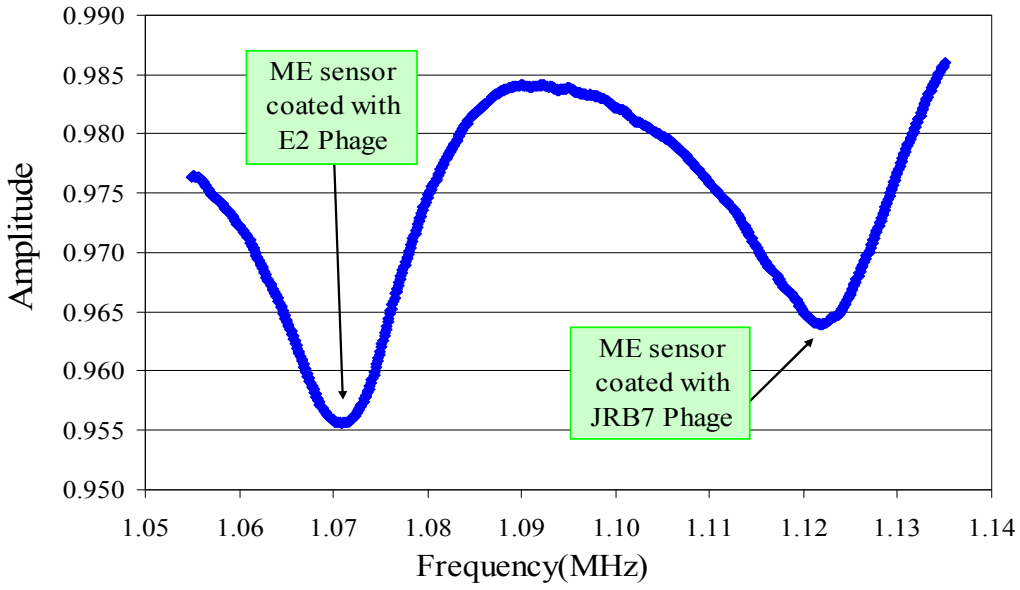

Figure 6- 1. Resonance frequencies of multiple sensors tested in air simultaneously.

2.2. Simultaneous sensors detection in air after static loading

The above section demonstrates that by employing two different sensors with two slightly different sizes, it is possible to measure two different characteristic resonance peaks simultaneously. It is then necessary to determine whether, after exposure to the target analyte on one sensor, the frequency shift from this sensor can be measured, while the other sensor is still in the same coil. In the experiment, the sensor with dimensions of 2 × 0.4 × 0.005 mm served as the reference sensor. A JRB7 phage-based biosensor (1.9 × 0.4 × 0.005 mm) coated with phage specific to *B. anthracis* spores was placed in the same testing chamber and measured in air. The frequencies were measured in a single scan and the results are shown in Figure 6-2, where once again two characteristic resonance peaks can be identified clearly. The black line shows the resonance frequency for each sensor before exposure to spores. The frequency for the reference sensor was about 1.0768 MHz, while for the JRB7 phage sensor it was about 1.0894 MHz. The JRB7 phage biosensor was exposed to *B. anthracis* spore suspension with concentration of 5×10^8 cfu/mL after measurement, followed by rinsing with distilled water once and drying in air. Again, both the reference sensor and JRB7 phage biosensor loaded with spores were placed back into the testing chamber and their resonance frequencies remeasured under the same conditions, as shown in Figure 6-2 (red line). Clearly, the frequency of the reference sensor is almost the same, while the JRB7 phage sensor experienced a large frequency shift of about 1700Hz. Also, a small amount of damping can be seen in the JRB7 phage biosensor signal after spore loading.

This was because the spores were captured by the JRB7 phage coated on the biosensor surface. As the mass loading on the sensor increased, the frequency of the biosensor decreased.

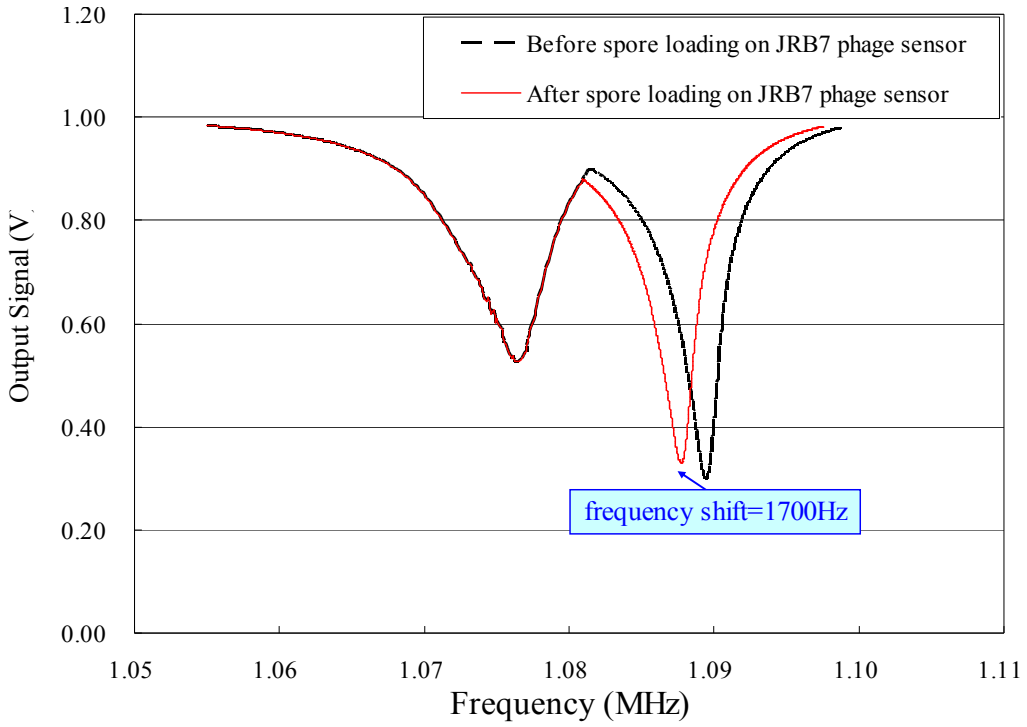

Figure 6- 2. The resonance frequency shift after exposure to spore suspension to demonstrate the simultaneous detection approach.

3. Characterization of multi-sensor detection system

In order to characterize the multi-sensor detection system, this particular investigation used two widely different classes of pathogens sequentially – *S. typhimurium* bacteria and *B. anthracis* spores – to prove the concept.

Later in this dissertation, work on more difficult scenarios such as species more commonly found together in nature (e.g. a mixture of the *S. typhimurium* and *E. coli*), similar targets from the same genus (e.g.. a mixture of *B. anthracis* and *B. cereus* spores), and even real food products (e.g. apple juice) will be discussed.

3.1. Multi-sensor system response with *S. typhimurium* / *B. anthracis* spores introduced sequentially

Figure 6-3 shows the simultaneous response of the multiple phage-based ME biosensors to water and different concentrations of *S. typhimurium* and *B. anthracis* spore suspensions. The data shown here is from one group of multi-sensor system for each concentration. For further analysis, the dose response for each measurement sensor (JRB7 phage biosensor / E2 phage biosensor) within a multi-sensor system is based on the average data from five groups for each concentration.

The experiment was controlled by pumping filtered water through the two chambers continuously at a flow rate of 50 μl/min until the frequencies for the three ME biosensors stabilized, which usually took about 10 min. Then, the concentrated *S. typhimurium* solution was introduced into the system and passed across the sensors for 20 min under the same flow conditions. At the end of 20 minutes, a concentrated *B. anthracis* spore solution was introduced continuously and allowed to flow for another 20 min. Figures 6-3 - 6-10 show the sensors' response to both solutions in a decreasing concentration from 5×10^8 to 5×10^1 cfu/mL, respectively. The reason that the detection was performed in two successive steps was because when both biosensors

responded to a mixture of two different pathogens, at the same time, it was hard to determine the specificity of the sensor to a certain pathogen and it would have been possible to incorrectly construe that non-specific binding caused the response. In order to avoid confusion, therefore, in this dissertation, we exposed the biosensors to two different pathogens in successive steps. Figures 6-3 – 6-10 show that the specific sensor normally responded within 1 minute, even when other non-specific sensors were present at the time of analyte introduction, which also means that it is possible for this method to detect two pathogens at the same time.

In Figure 6-3, the steady state response of all the sensors in water was observed during the first 10 minutes of the test. Then, within one minute after the introduction of *S. typhimurium*, the E2 phage biosensor showed a smooth decrease in resonance frequency due to the binding of these bacteria onto the biosensor surface. A steady state was achieved after about 15 minutes for the E2 phage biosensor due to the saturation of the *S. typhimurium*-phage conjugates on the sensor surface. During this time, the other two sensors showed a negligible frequency change, indicating that no appreciable binding had occurred to the reference or JRB7 phage biosensors. As soon as the 5×10^8 cfu/mL *B. anthracis* spore solution was introduced, a similar response was observed for the JRB7 phage biosensor in that a sudden drop of the resonance frequency was observed. In this case, however, no significant change in the resonance frequency of the reference sensor or the E2 phage biosensor was observed, which again indicated negligible non-specific binding to the reference and E2 phage biosensors. In both cases, the decrease in

frequency was only present when bacteria cells or spores bound to the specific phage on the sensor's surface. During the entire test, the frequency of the reference sensor exhibited no appreciable change regardless of the composition of analyte introduced. This showed that non-specific binding had been blocked during testing by the 1 mg/ml BSA pre-treatment. Also, the sensor showed good environmental stability in the flowing liquid system, because no corrosion was found during the test. Overall, the frequency shift was about 1280 Hz for the E2 phage sensor, and about 1123 Hz for the JRB7 phage sensor. This interaction was confirmed by the SEM photographs of the reference and measurement sensors, which provided visual evidence that the frequency shifts were indeed due to the spores/bacteria cells attached to the corresponding sensors.

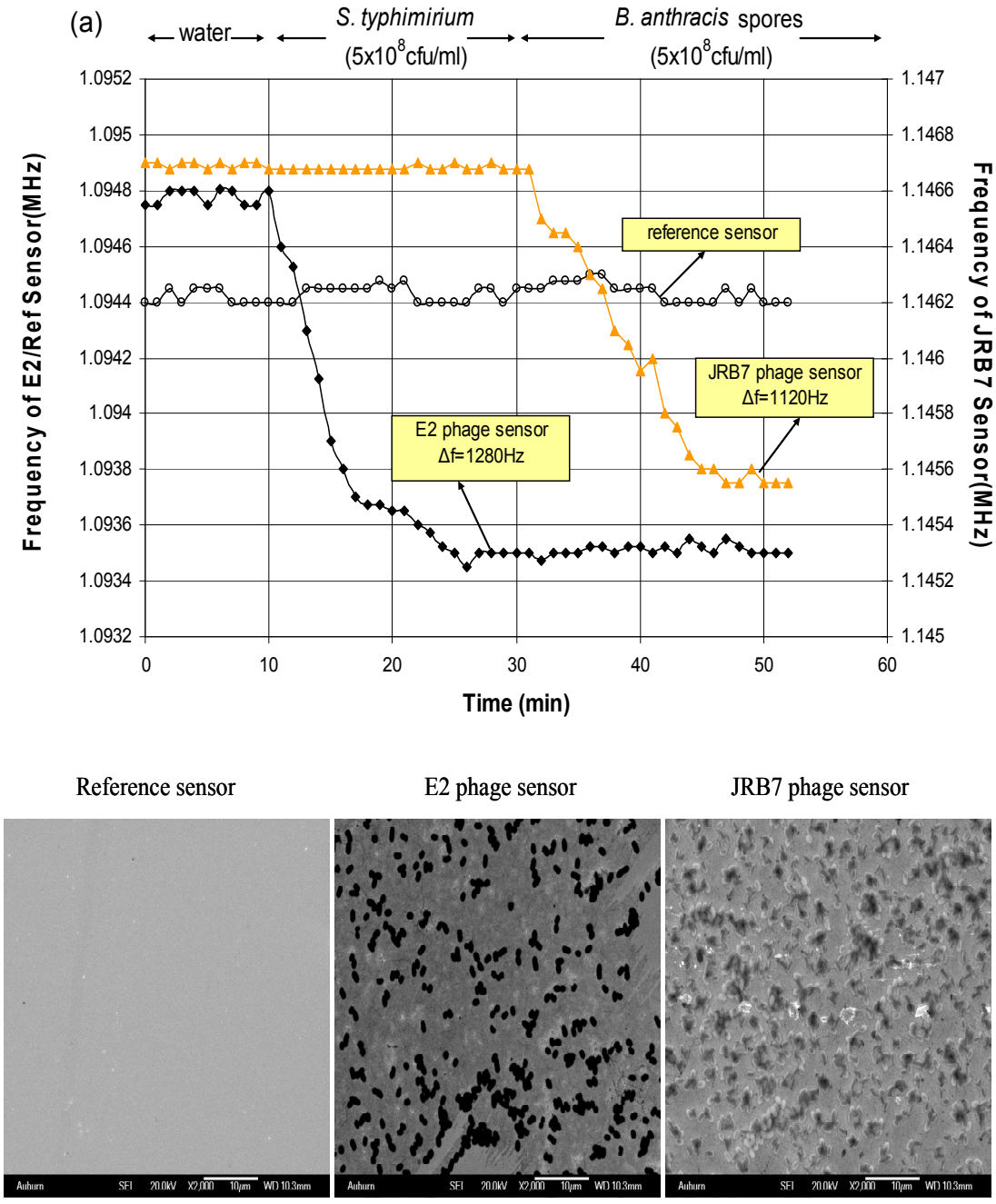

Figure 6- 3. Response curves and SEM pictures for three diced ME biosensors tested simultaneously when exposed to the *S. typhimurium* / *B. anthracis* spores suspension with a concentration of 5×10^{8}cfu/mL.

Similar trends in the frequency shifts were observed for Figures 6-4 – 6-10. At a concentration of 5×10^7 cfu/mL, the resonance frequency shifted by about 730 Hz for the JRB7 phage sensor, and about 770 Hz for E2 phage sensor, with good attachment and uniform distribution of spores/bacteria cells on the sensor surfaces. In Figure 6-5, where the sensors were exposed to a concentration of 5×10^6 cfu/mL, the frequency shifted by approximately 450 Hz and 410 Hz for the E2 and JRB7 phage sensors, respectively. Similar trends in the frequency shifts were observed for the remaining concentrations of 5×10^5 cfu/mL - 5×10^1 cfu/mL. As the concentration decreased, the binding numbers for both measurement sensors decreased significantly. Especially when the concentration was about 5×10^2 and 5×10^1 cfu/mL, there were only a few bacteria cells / spores bound on the specific sensor's surface. Since the attachment was quite uniform over the surface, only one SEM picture for each sensor under each testing concentration is shown in this dissertation. Since the measurement sensors were placed together in the same testing chamber, each of them still showed good performance comparable to the work previously reported by Lakshmanan et al. [4, 5] and Wan et al. [6, 7], whose efforts were focused towards the detection of a single target species (for example *B. anthracis* spores or *S. typhimurium*) using a single ME biosensor.

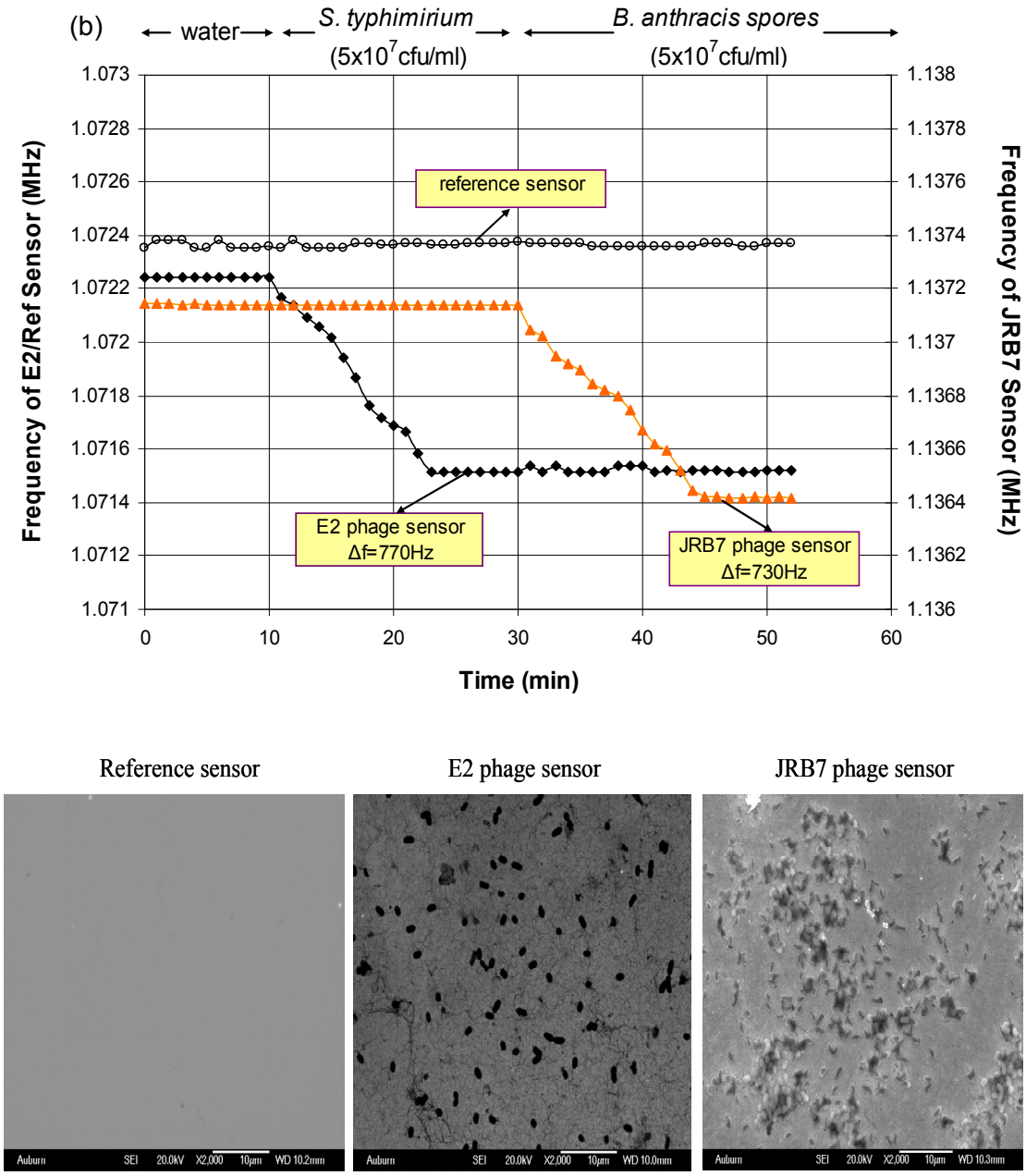

Figure 6- 4. Response curves and SEM pictures for three diced ME biosensors tested simultaneously when exposed to the *S. typhimurium* / *B. anthracis* spores suspension with a concentration of 5×10^7 cfu/mL.

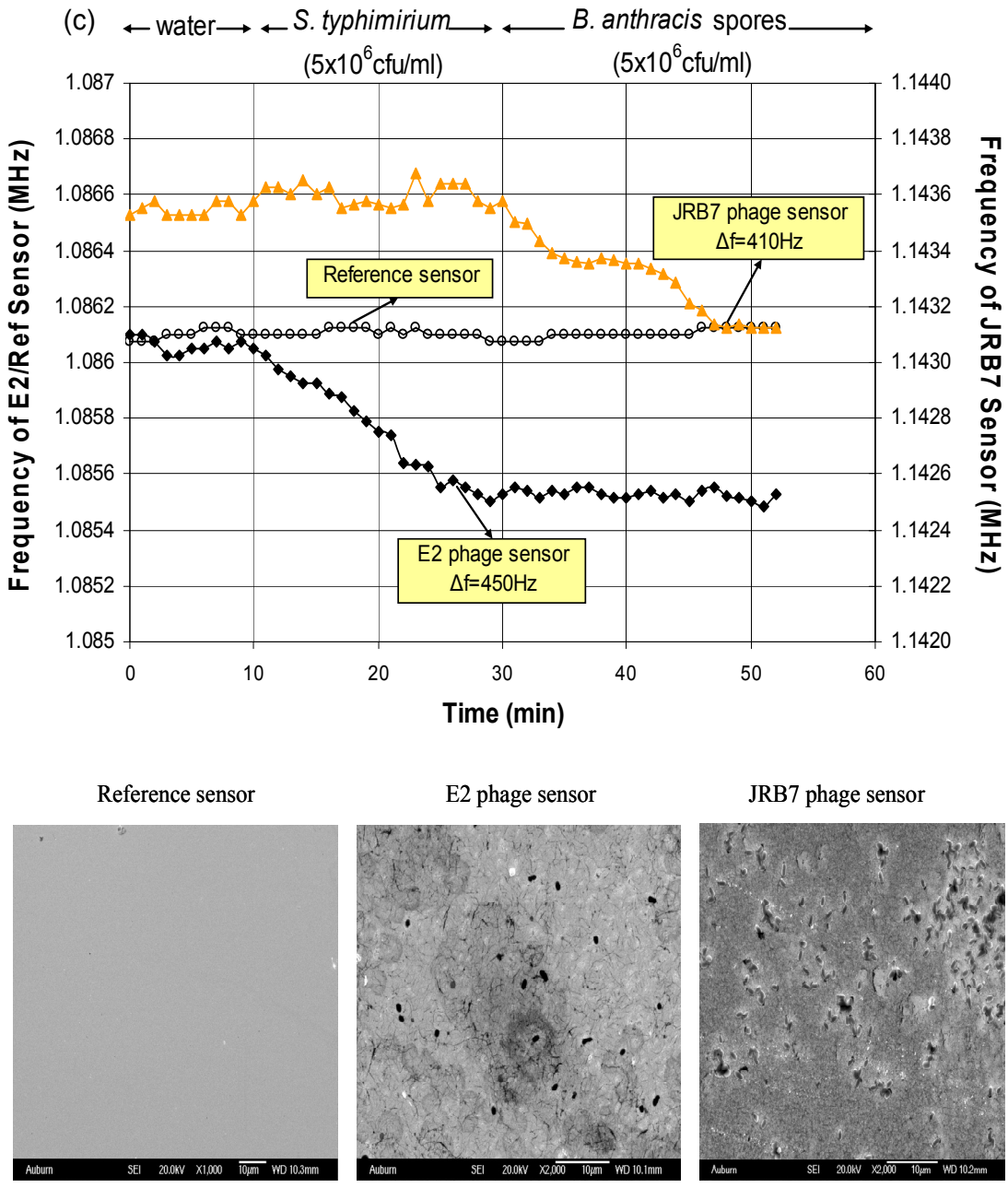

Figure 6- 5. Response curves and SEM pictures for three diced ME biosensors tested simultaneously when exposed to the *S. typhimurium* / *B. anthracis* spores suspension with a concentration of 5×10^6 cfu/mL.

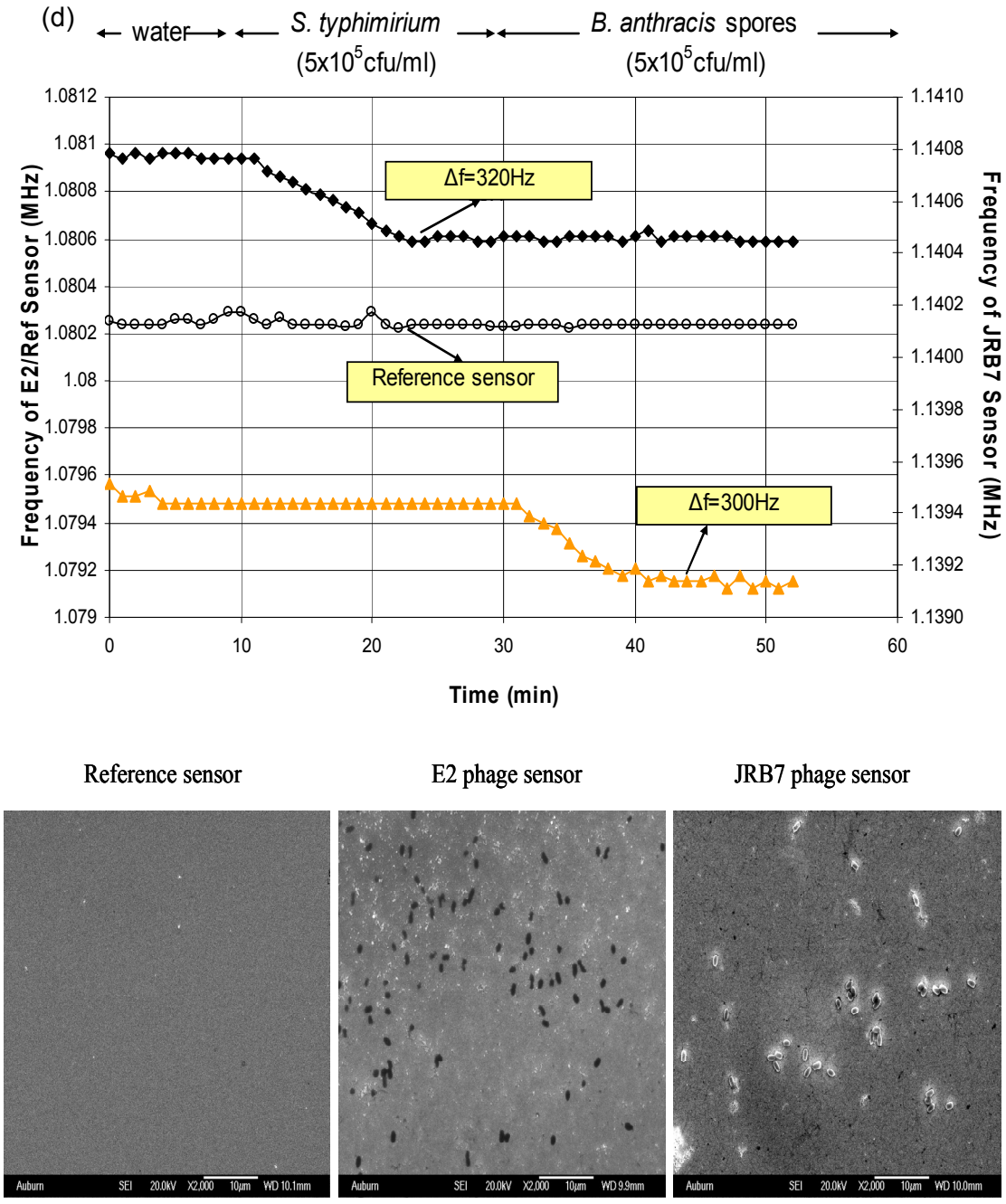

Figure 6- 6. Response curves and SEM pictures for three diced ME biosensors tested simultaneously when exposed to the *S. typhimurium* / *B. anthracis* spores suspension with a concentration of 5×10^5 cfu/mL.

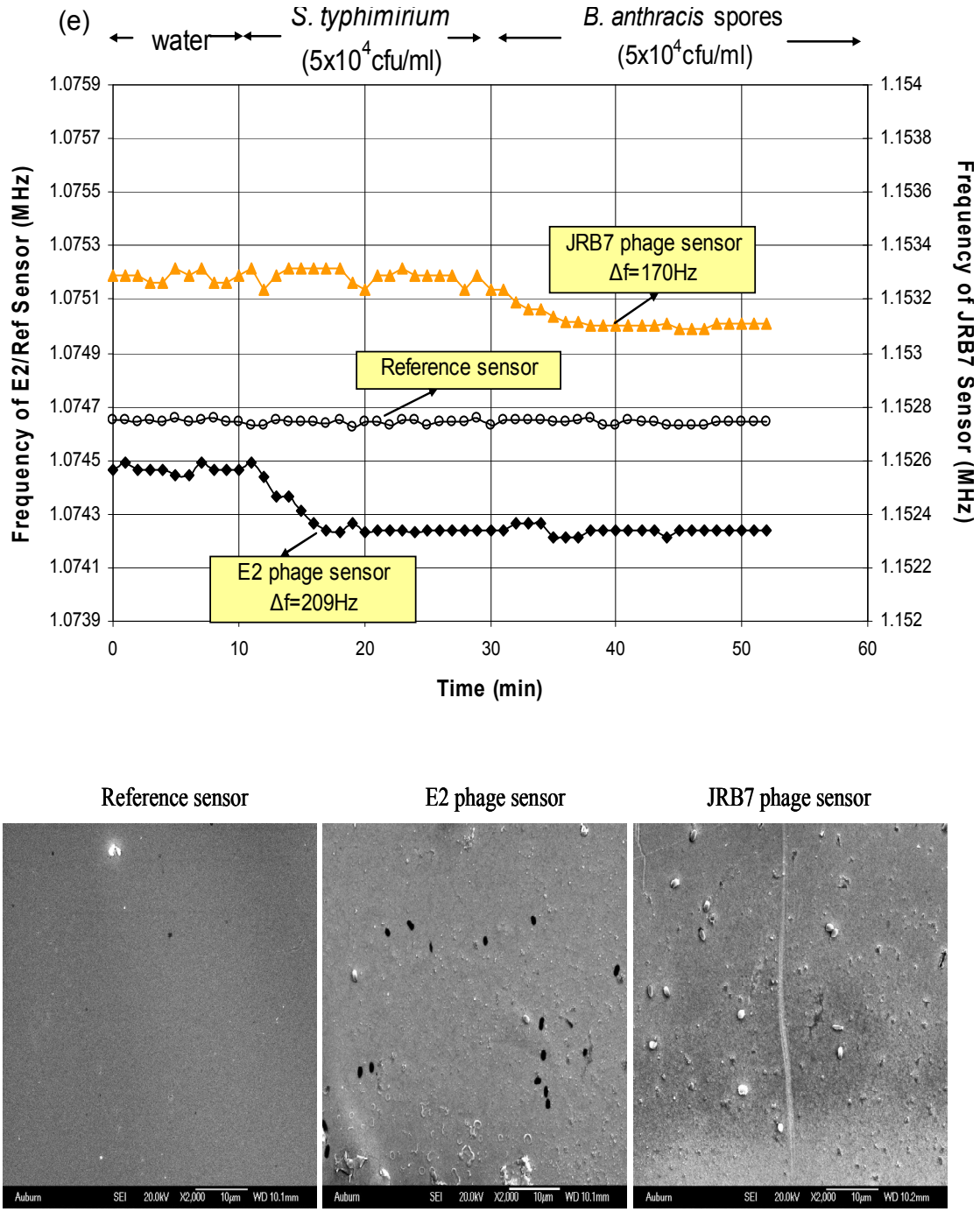

Figure 6- 7. Response curves and SEM pictures for three diced ME biosensors tested simultaneously when exposed to the *S. typhimurium* / *B. anthracis* spores suspension with a concentration of 5×10^4 cfu/mL.

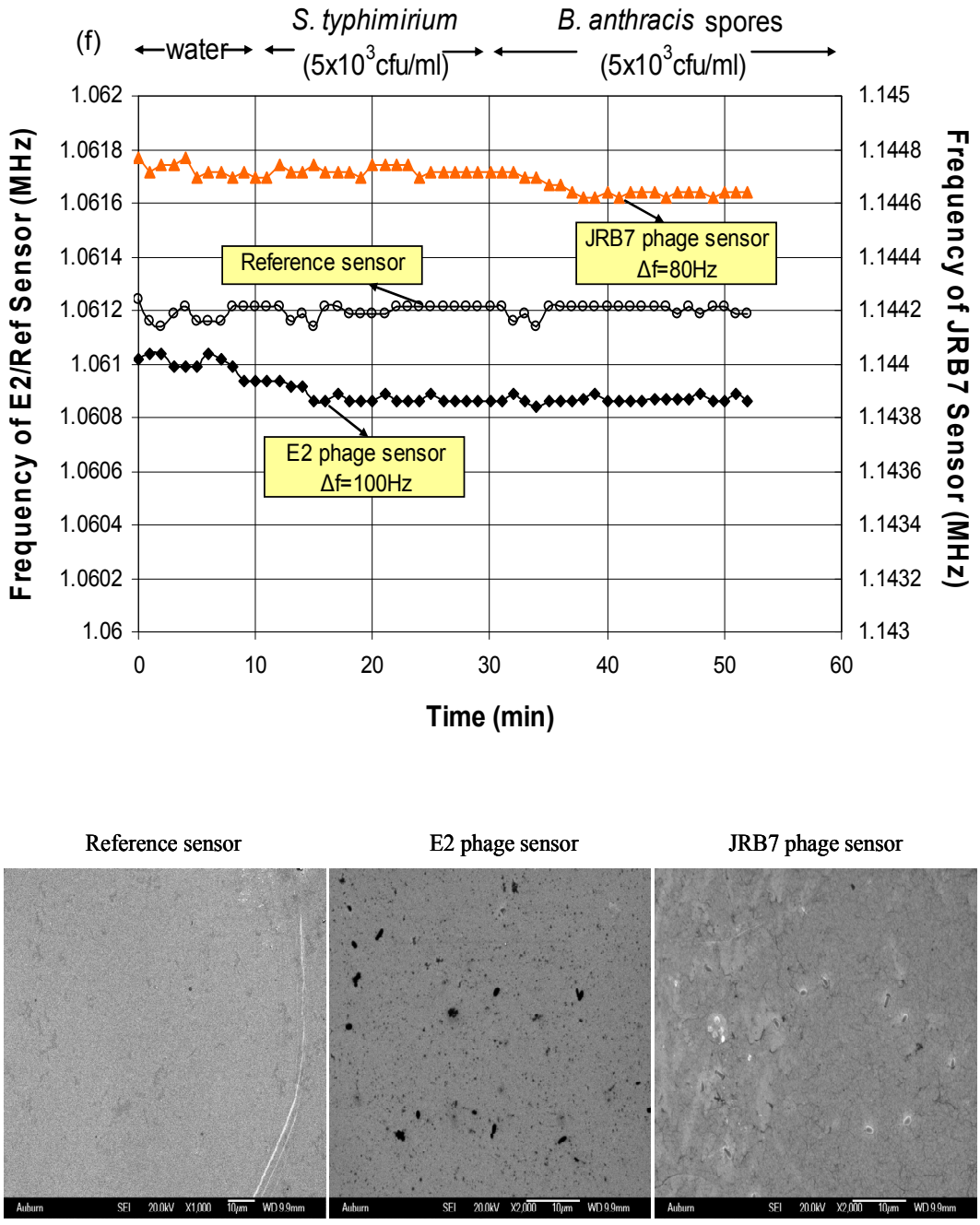

Figure 6- 8. Response curves and SEM pictures for three diced ME biosensors tested simultaneously when exposed to the *S. typhimurium* / *B. anthracis* spores suspension with a concentration of 5×10^3 cfu/mL.

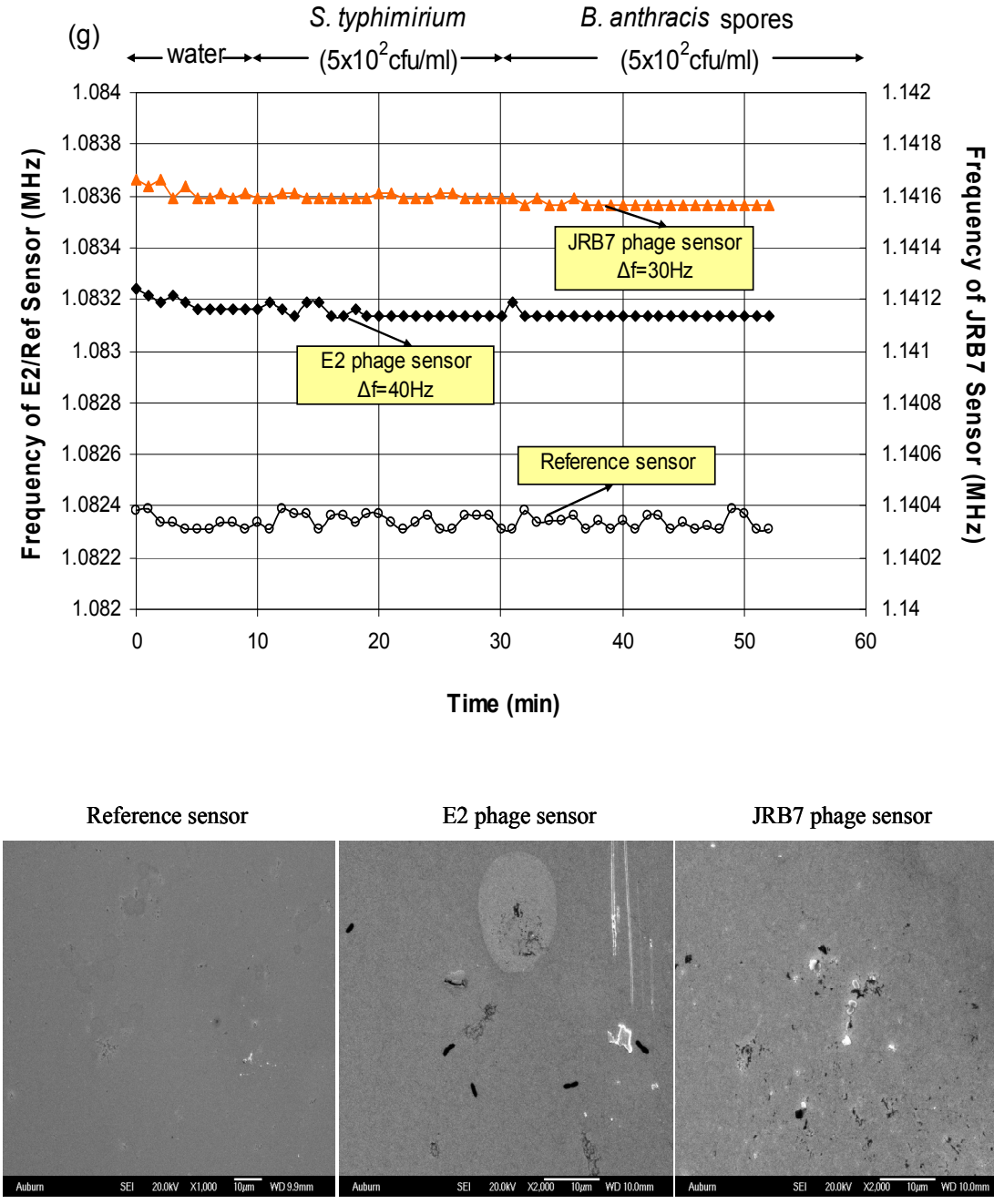

Figure 6- 9. Response curves and SEM pictures for three diced ME biosensors tested simultaneously when exposed to the *S. typhimurium* / *B. anthracis* spores suspension with a concentration of 5×10^2 cfu/mL.

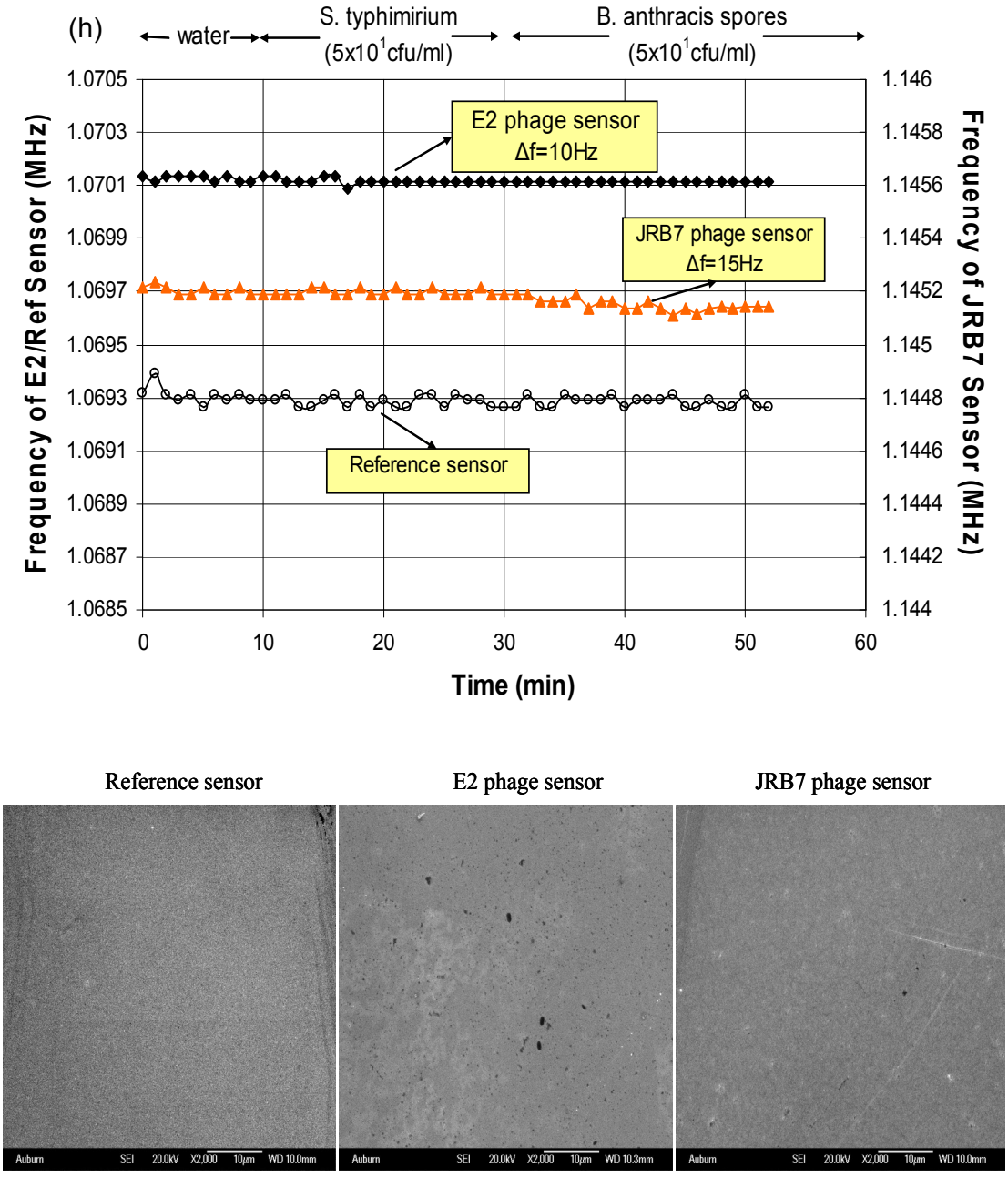

Figure 6- 10. Response curves and SEM pictures for three diced ME biosensors tested simultaneously when exposed to the *S. typhimurium* / *B. anthracis* spores suspension with a concentration of 5×10^{1} cfu/mL.

3.2. Dose response and kinetics of biosensors within a multi-sensor system

The dose response for each biosensor within this multi-sensor detection system, which was exposed to two different antigens sequentially, is summarized below. The smooth lines are the sigmoid fits of the experimental data and each data point is a mean value of the steady state frequency readings from five sensors within five multi-sensor systems.

3.2.1. E2 phage sensor (2 × 0.4 × 0.015mm)

The magnitude dose response of the three sensors simultaneously exposed first to *S. typhimurium* suspensions (followed by exposure to *B. anthracis* spore suspensions) in the range of 5×10^1 - 5×10^8 cfu/mL is shown in Figure 6-11. As the concentration increased, the frequency shifts for the E2 phage biosensor increased dramatically. This was because of the specific interaction between *S. typhimurium* cells with the E2 phage coated on the biosensor surface. The reference sensor showed a slight frequency shift with increasing analyte concentration, with a maximum shift of about 70 Hz at the largest concentration. There was a frequency shift of about 30 Hz for the JRB7 phage-coated biosensor due to exposure to the *S. typhimurium* suspension. This demonstrated that the non-specific binding had been blocked by the BSA coating. The average Δf_{max} for the E2 phage biosensor was 1185 Hz, and the detection limit for this biosensor was calculated to be 1.1×10^3 cfu/mL. Saturation of the E2 phage biosensor occurred at

greater than 5×10^8 cfu/mL. A linear response was found between the concentrations of 5×10^4 to 5×10^8 cfu/mL.

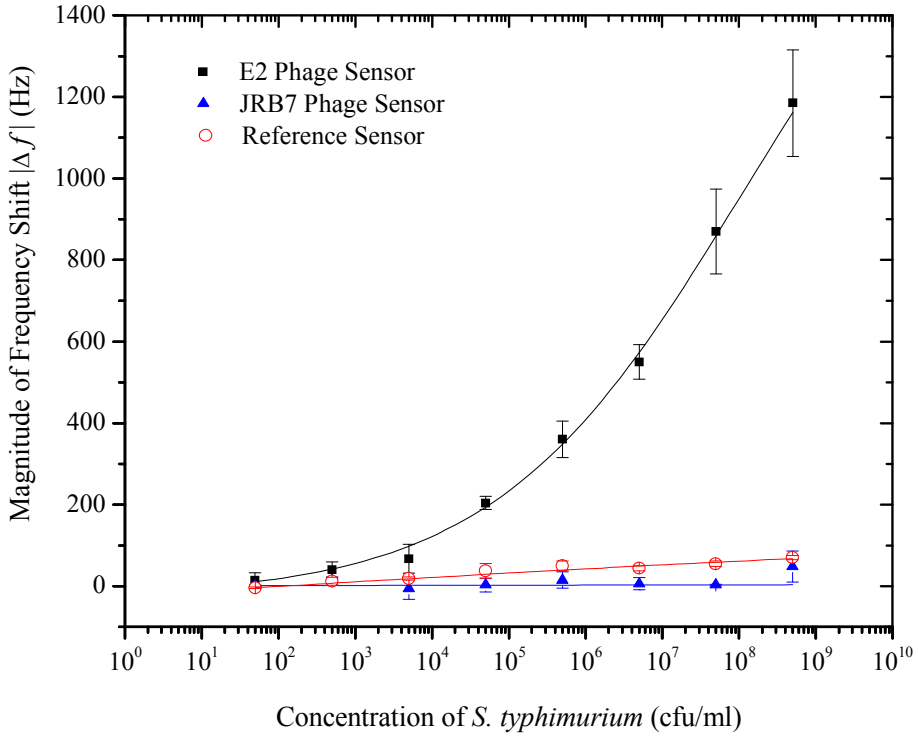

Figure 6- 11. Dose response curve of ME biosensors within a multi-sensor detection system exposed to increasing concentrations (5×10^1-5×10^8 cfu/mL) of *S. typhimurium* suspensions in water. The E2 phage sensor with dimensions of $2 \times 0.4 \times 0.015$ mm represents the specific response of ME biosensor coated with phage specific to *S. typhimurium* ((■) (R^2=0.987)). The reference sensor with dimensions of $2 \times 0.4 \times 0.015$ mm represents the uncoated (devoid of phage) sensor's response ((o) (R^2=0.99)). The JRB7 phage sensor with dimensions of $1.9 \times 0.4 \times 0.015$mm represents the non-specific response of the ME biosensor coated with phage specific to *B. anthracis* spores ((▲) (R^2=0.984)). The curve represents the sigmoidal fit of the signals obtained.

Based on this dose response curve, a Hill plot was constructed (Figure 6-12) to determine the binding kinetics (K_d) between E2 phage and *S. typhimurium* cells.

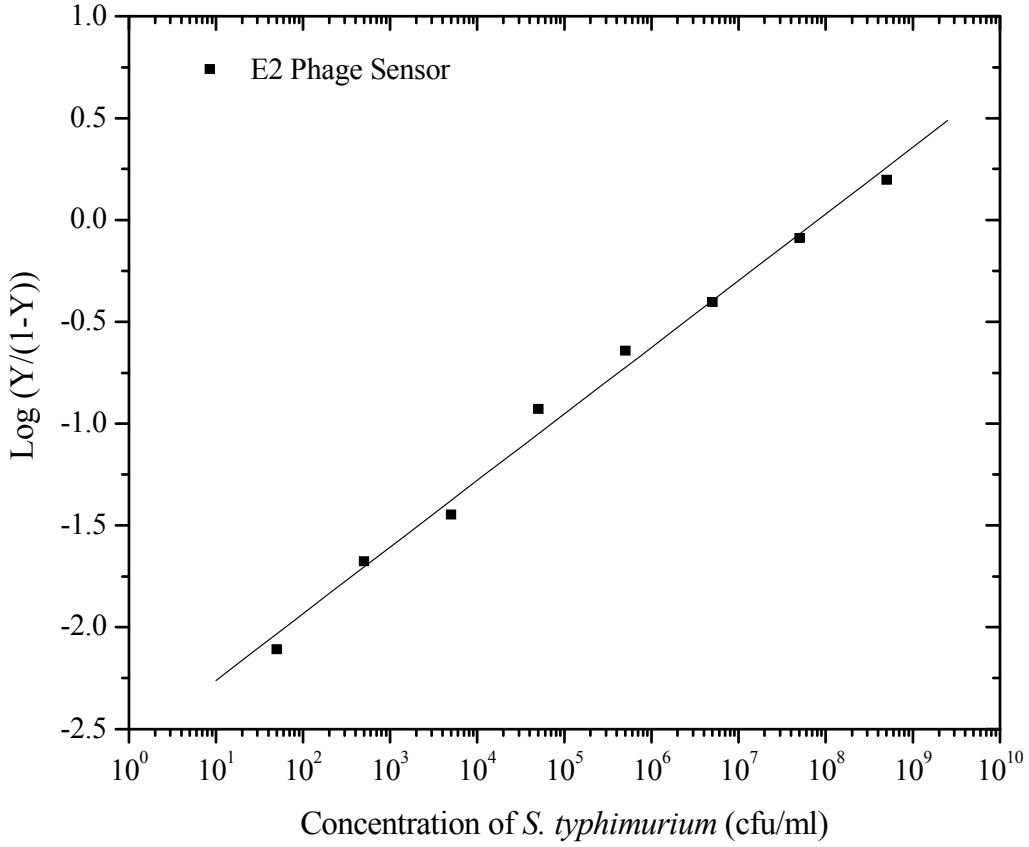

Figure 6- 12. The Hill plot of binding isotherms for E2 phage based ME biosensor (2 × 0.4 × 0.015mm) within a multi-sensor detection system, showing the ratio of occupied and free phage sites as a function of *S. typhimurium* concentrations. The straight line is the linear least squares fit to the data points ((■) slope = 0.25124±0.02, R = 0.965).

From the Hill plot, the binding valency number was calculated to be 3.05, which meant that about 3 phage filaments were required to bind with a single *S. typhimurium* cell. This value indicates that the binding of *S. typhimurium* cells to the immobilized phage on the biosensor surface was multivalent in nature. A summary of results from all the calculations for sensitivity, binding valency, and dissociation constant are presented in Table 6-1. The sensitivity was 238.5 Hz/decade, which was measured as the slope of the linear range on the dose response curve. The binding kinetic constant (K_d) was 387.2 cfu/mL, $K_{d(apparent)}$ was 7.8×10^7 cfu/mL.

Table 6- 1. The sensitivity, dissociation constant and binding valency of E2 phage based ME biosensor within a multi-sensor system and exposure to different concentration of *S. typhimurium* and *B. anthracis* spores suspensions sequentially.

Analyte	Detection Limit (cfu/mL)	Sensitivity (Hz/Decade)	Binding valency (1/n)	K_d (cfu/mL)	$K_{d(apparent)} = (K_d)^{1/n}$ (cfu/mL)
S.T. + B.A.	1.1×10^3	238.5	3.05	387.2	7.8×10^7

3.2.2. JRB7 phage sensor (1.9 × 0.4 × 0.015mm)

A similar trend was found for the simultaneous exposure of the three sensors to *B. anthracis* spores in the range of 5×10^1 to 5×10^8 cfu/mL immediately following the exposure to *S. typhimurium*, and is shown in Figure 6-13. The detection limit of 1.6×10^3 cfu/mL was calculated from the response curve. Again, the reference sensor exhibited a small frequency shift of about 70 Hz with increasing analyte concentration, while the sensor coated with E2 phage showed no appreciable response upon exposure to any concentration of the spore solution. The average Δf_{max} for JRB7 phage-based sensor was 1000 Hz. Saturation of the sensor occurred at greater than 5×10^8 cfu/mL. A linear response was found between the concentrations of 5×10^4 and 5×10^8 cfu/mL.

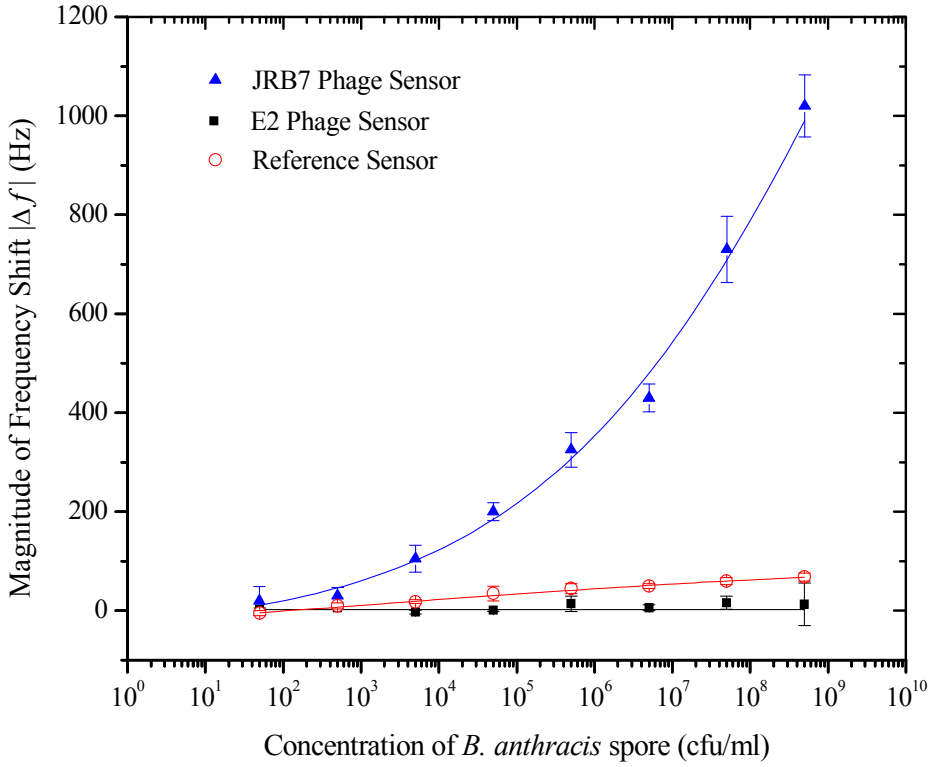

Figure 6- 13. Dose response curve of ME biosensors within a multi-sensor detection system exposed to increasing concentrations (5×10^1-5×10^8 cfu/mL) of *B. anthracis* spore suspensions in water. The JRB7 phage sensor with dimensions of 1.9 × 0.4 × 0.015mm represents the specific response of the ME biosensor coated with phage specific to *B. anthracis* spores ((▲) (R^2=0.988)). The reference sensor with dimensions of 2 × 0.4 × 0.015 mm represents the uncoated (devoid of phage) sensor's response ((o) (R^2=0.996)). The E2 phage sensor with dimensions of 2 × 0.4 × 0.015 mm represents the non-specific response of the ME biosensor coated with phage specific to *S. typhimurium* ((■) (R^2=0.997)). The curve represents the sigmoidal fit of the signals obtained.

A Hill plot was also constructed (Figure 6-14) and the summary of all the calculations from this plot for sensitivity, binding valency, and dissociation constant are presented in Table 6-2.

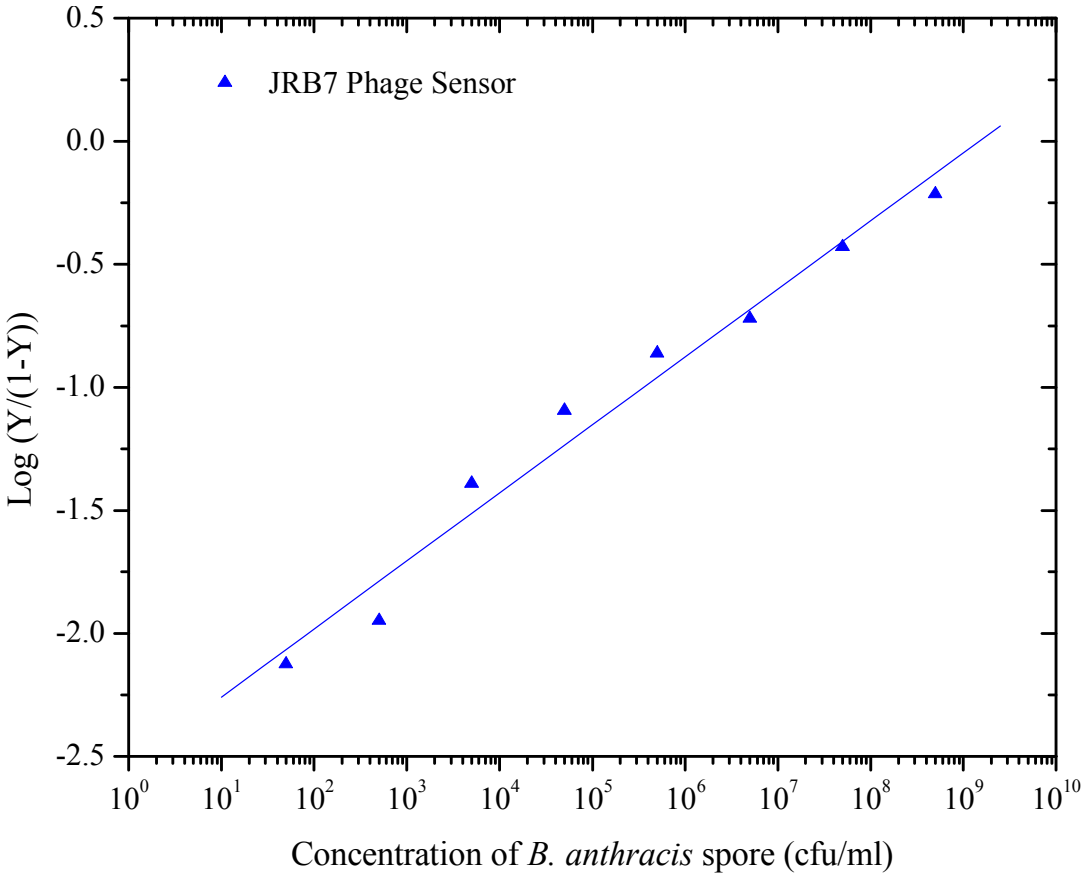

Figure 6- 14. The Hill plot of binding isotherms for JRB7 phage based ME biosensor (1.9 × 0.4 × 0.015mm) within a multi-sensor detection system, showing the ratio of occupied and free phage sites as a function of *B. anthracis* spores concentrations. The straight line is the linear least squares fit to the data points ((▲) slope = 0.25124±0.02, R = 0.965).

It was observed that about 3.62 phage filaments are required to bind with a single spore. The sensitivity for this JRB7 phage biosensor was 279.5 Hz/decade and the binding kinetics (K_d) was 342.8 cfu/mL, $K_{d(apparent)}$ was 1.5×10^9 cfu/mL.

Table 6- 2. The sensitivity, dissociation constant and binding valency of JRB7 phage based ME biosensor within a multi-sensor system and exposure to different concentrations of *B. anthracis* spore suspensions, which were sequentially introduced after *S. typhimurium* suspensions.

Analyte	Detection Limit (cfu/mL)	Sensitivity (Hz/Decade)	Binding valency (*1/n*)	K_d (cfu/mL)	$K_{d(apparent)} = (K_d)^{1/n}$ (cfu/mL)
S.T. + B.A.	1.6×10^3	279.5	3.62	342.8	1.5×10^9

3.3. Micro-fabricated sensor response

This experiment was carried out using the same procedures previously described. The highest concentrations of *S. typhimurium* and spore suspensions (5×10^8 cfu/mL) were used for this experiment. A similar trend to that seen with the diced sensors was observed for the micro-fabricated sensors, as shown in Figure 6-15. The frequency change due to the specific binding of the *S. typhimurium* onto the E2 phage sensor's surface was approximately 71 kHz, while the frequency shift for the JRB7 phage sensor

was 188 kHz upon exposure to *B. anthracis* spores. These results demonstrated that smaller micro-fabricated sensors can just as easily be used to perform simultaneous detection of multiple analytes.

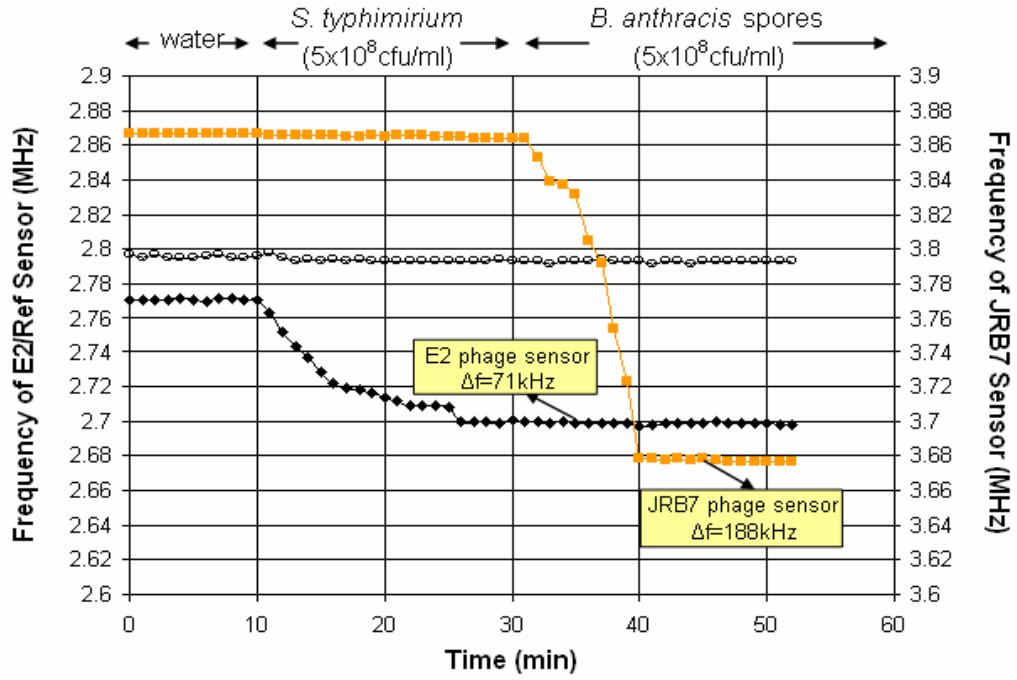

Figure 6- 15. Response curves for three micro-fabricated ME biosensors tested simultaneously. The biosensors were exposed to a *S. typhimurium* / *B. anthracis* spores suspension with a concentration of 5×10^8 cfu/mL.

4. Multi-sensor system response with a mixed microbial population

In order to determine the selectivity and specificity of this multi-sensor system, it was separately tested with a mixture of *S. typhimurium* (5×10^1-5×10^8 cfu/mL) in a fixed concentration of *E. coli* O157:H7 (5×10^7 cfu/mL) and a mixture of *B. anthracis* spores (5×10^1-5×10^8 cfu/mL) in a fixed concentration of *B. cereus* spores ($5x10^7$ cfu/mL).

4.1. Tested with a mixture of *S. typhimurium* in E. coli O157:H7

4.1.1. Performance of multi-sensor system

The functional performance of this multiple system was also evaluated against a mixture of more than one type of bacteria. Figure 6-16 shows the response from one group of a multi-sensor system (containing an E2 phage based sensor, a JRB7 phage based sensor, and a reference sensor) after exposure to a mixture of *E. coli* and *S. typhimurium* suspensions. The water and suspensions were passed over the sensors using an Ismatec Reglo Digital peristaltic pump with 8 rollers. After the frequencies of all three sensors stabilized in flowing water, the *E. coli* (1ml, 5×10^7 cfu/mL) suspension was pumped over the system for 20 min at a flow rate of 50 µl/min. A steady state response for all the sensors was achieved within this range (20 min), which meant there was no appreciable non-specific binding. Then, 1 ml of mixed bacterial suspension containing various concentrations of *S. typhimurium* suspension was pumped through the system. A similar steady state response (i.e. no detectable frequency shift) was observed

for concentrations of 5×10^1 cfu/mL - 5×10^2 cfu/mL. When the concentration reached 5×10^3 cfu/mL, the E2 phage biosensor responded within 1min, while the other two sensors still showed a negligible frequency change, indicating that no appreciable binding had occurred to the control or JRB7 phage biosensors. Upon increasing the concentration of *S. typhimurium*, the E2 phage biosensor showed progressively larger frequency shifts. This was because more *salmonella* cells were bound to the biosensor's surface. During the whole experiment, a small change in the frequency (about 70 Hz) for both reference and JRB7 phage sensor was observed at a *S. typhimurium* concentration of 5×10^6 cfu/mL co-spiked with *E. coli*. This small change was due to a small amount of non-specific cells bound onto the sensor. However, compared with specific binding, this shift was very small.

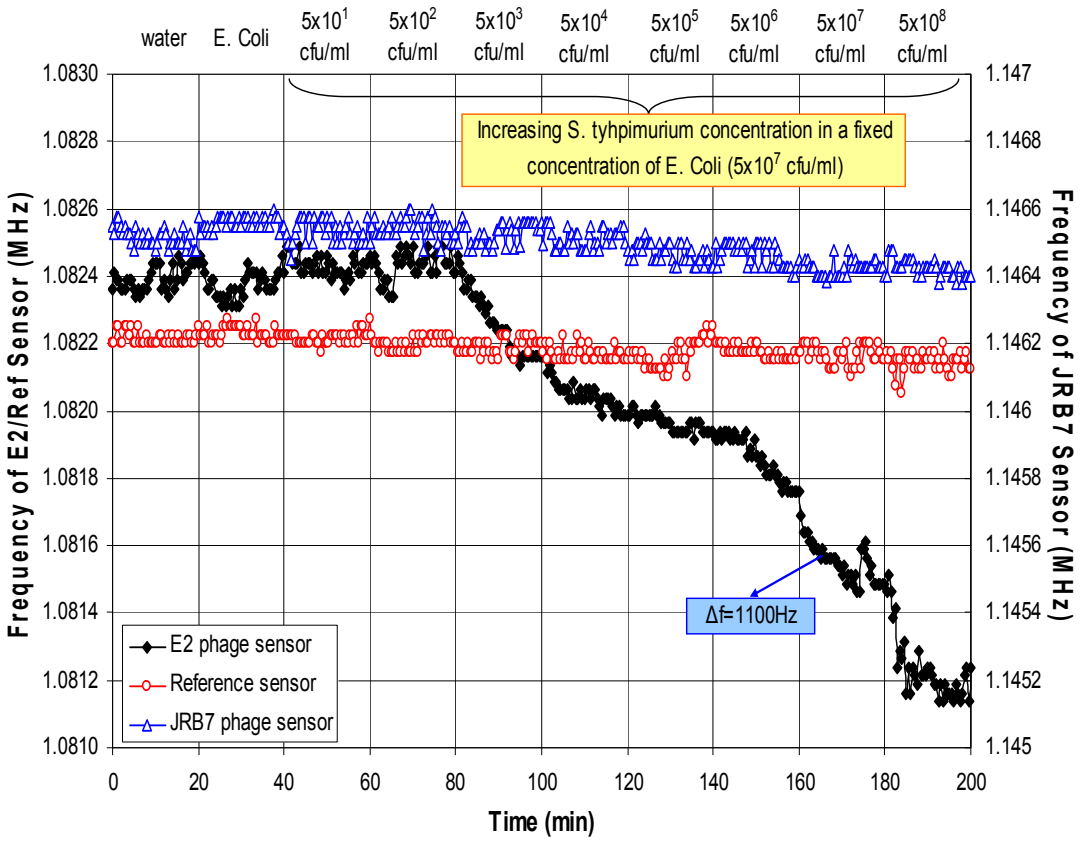
water
E. Coli
5x10^1 cfu/ml
5x10^2 cfu/ml
5x10^3 cfu/ml
5x10^4 cfu/ml
5x10^5 cfu/ml
5x10^6 cfu/ml
5x10^7 cfu/ml
5x10^8 cfu/ml
Increasing S. tyhpimurium concentration in a fixed concentration of E. Coli (5x10^7 cfu/ml)
Δf=1100Hz
E2 phage sensor
Reference sensor
JRB7 phage sensor
Frequency of E2/Ref Sensor (MHz)
Frequency of JRB7 Sensor (MHz)
Time (min)
1.0830
1.0828
1.0826
1.0824
1.0822
1.0820
1.0818
1.0816
1.0814
1.0812
1.0810
1.147
1.1468
1.1466
1.1464
1.1462
1.146
1.1458
1.1456
1.1454
1.1452
1.145
0
20
40
60
80
100
120
140
160
180
200

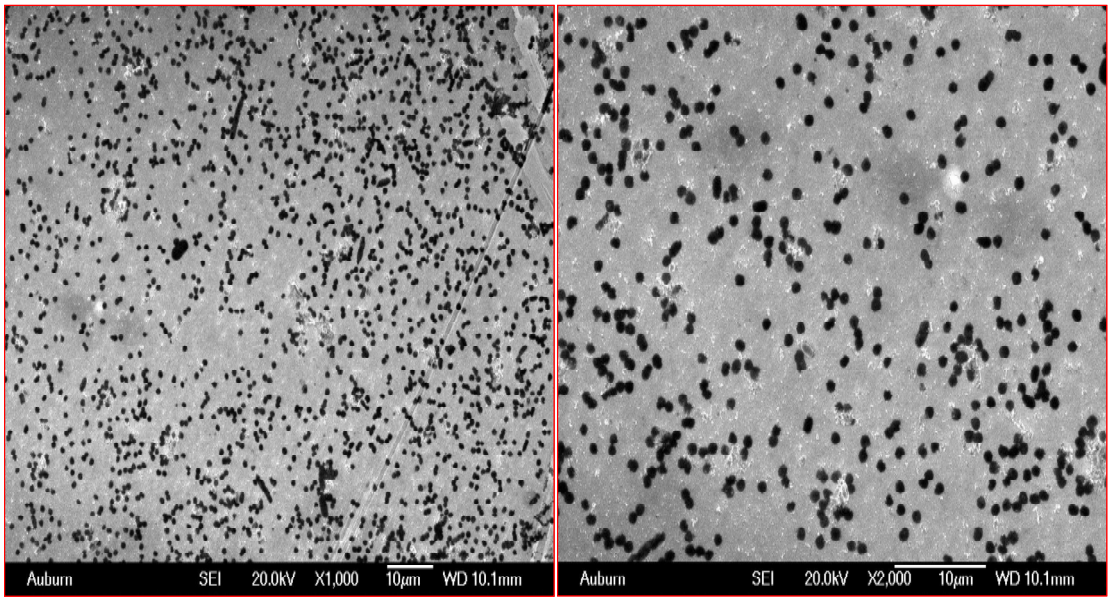
Auburn SEI 20.0kV X1,000 10μm WD 10.1mm
Auburn SEI 20.0kV X2,000 10μm WD 10.1mm

(a)

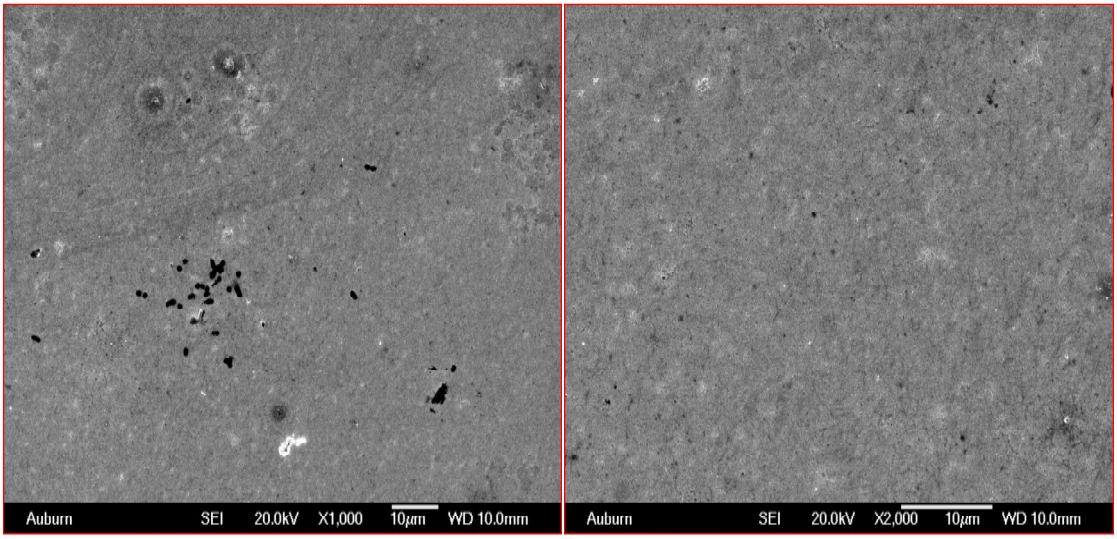

(b)

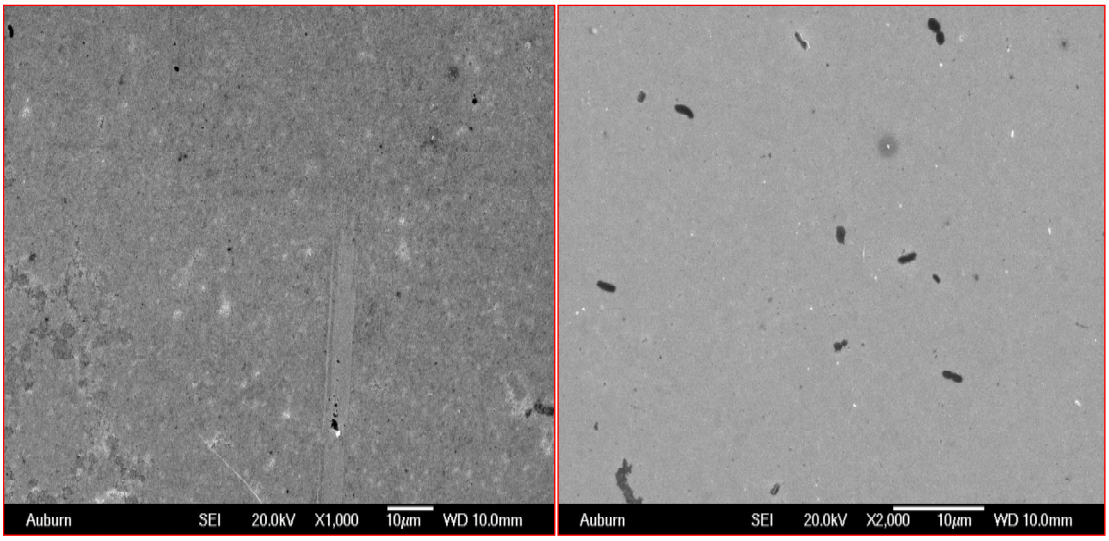

(c)

Figure 6- 16. Multiple detection system response when exposed to a mixture of various concentrations of *S. typhimurium* (5×10^1-5×10^8 cfu/mL) with a fixed concentration of *E. coli* O157:H7 (5×10^7 cfu/mL). Each concentration of bacterial suspension was run for 20 min at a flow rate of 50 µl/min. SEM images of sensor surface after experiment: (a) E2 phage biosensor with cells binding; (b) JRB7 phage biosensor; and (c) Reference sensor.

4.1.2. Dose Response

The performance of the E2 phage biosensor (within a multi-sensor system) when exposed to the analyte containing a mixture of *S. typhimurium* (5×10^1-5×10^8 cfu/mL) with masking bacteria *E. coli* O157:H7 (5×10^7 cfu/mL) is shown above in Figure 6-16. The objective of this experiment was to determine the performance of the E2 phage biosensor (within a multi-sensor system) when exposed to an analyte containing only *S. typhimurium* suspensions (5×10^1-5×10^8 cfu/mL). The binding affinity of the E2 phage biosensor was also compared between these two measurement conditions.

For an analyte containing only *S. typhimurium* suspensions, the measurement procedure was the same as in Chapter **6** Section **4.1.1** above. The accumulated resonant frequency shifts of the E2 phage biosensor in response with various concentrations of *S. typhimurium* ($5 \times 10^1 – 5 \times 10^8$ cfu/mL) under different conditions are plotted in Figure 6-17. The smooth lines are the sigmoid fits of the experimental data and each data point is a mean value of the steady state frequency readings from five sensors. In Figure 6-17, the response of E2 phage biosensor followed similar trends under both conditions. The E2 phage biosensor was highly specific and selective to *S. typhimurium* even within a multi-sensor system, as well as in the presence of high concentrations of masking bacteria (*E. coli* with concentration of 5×10^7 cfu/mL). This sensor was still capable of detecting when the analyte contained a lower concentration of *S. typhimurium* (5×10^3 cfu/mL) compared to high concentration of *E. coli* (5×10^7 cfu/mL). The dose responses for both conditions were linear over the range of 5×10^3 cfu/mL to 5×10^7

cfu/mL. The E2 phage biosensor became saturated, or achieved the largest frequency shift (Δf_{max}), between the concentrations of 5×10^7 and 5×10^8 cfu/mL, with the detection limit calculated to be 1.6×10^3 cfu/mL. However, lower frequency shifts were observed for the analytes containing only *S. typhimurium* suspension, which might be due to some cross-reaction binding between *E. coli* and the selected E2 phage. The reference sensor, which was devoid of immobilized bacteriophage, started to show a minimal response (≈ 70 Hz) at a concentration of 5×10^6 cfu/mL. This indicated non-specific binding but, compared to the specific response, it was negligible.

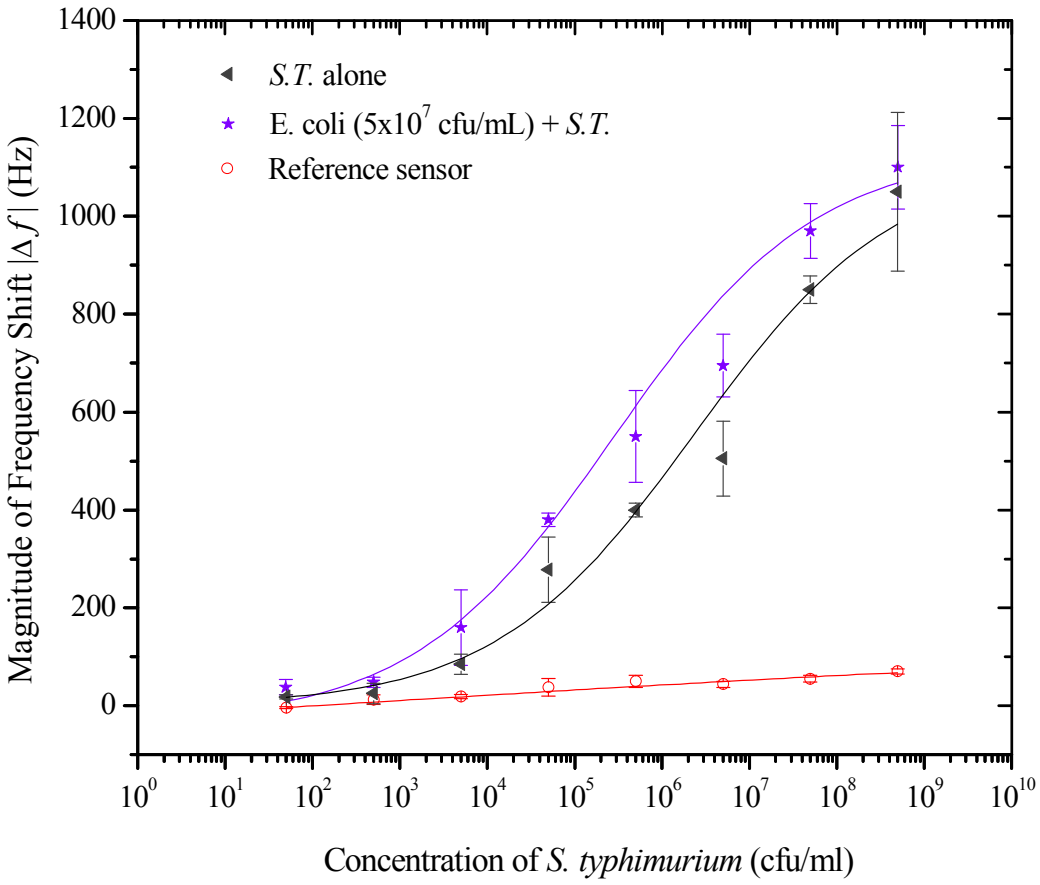

Figure 6- 17. The resonant frequency shifts of E2 phage-based sensor (2 × 0.4 × 0.015 mm) as a function of various concentrations of *S. typhimurium* (5×10^1-5×10^8 cfu/mL) with masking bacteria *E. coli* (5×10^7 cfu/mL). The smooth lines are the sigmoid fits of the experimental data and each data point is an average of the response from five sensors exposed to only *S. typhimurium* ((◀) R^2=0.997), *S. typhimurium* in mixture with *E. coli* ((★) R^2=0.987) and reference sensor to control non-specific binding ((o) R^2=0.99).

4.1.3. Hill Plot

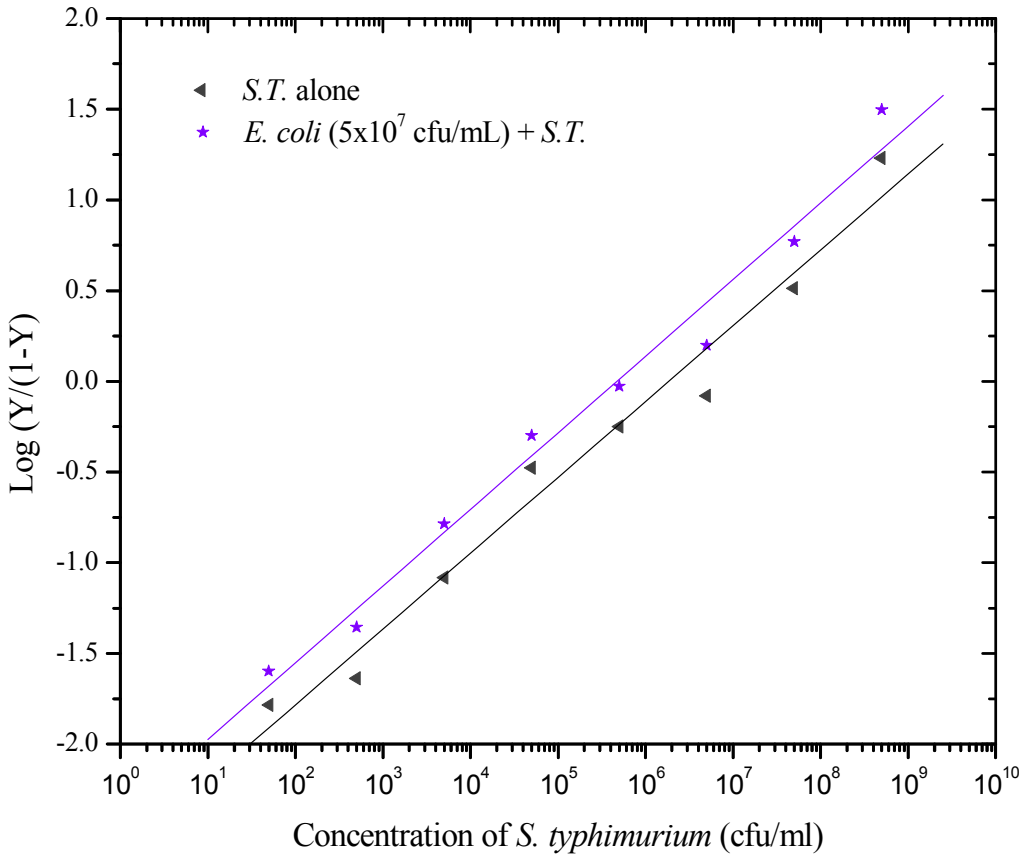

Figure 6- 18. Hill plot constructed from the dose response curves, showing the ratio of occupied (Y) and free phage sites (1-Y) as a function of bacterial concentrations in different conditions. The straight line is the linear least squares fit to the data (*S. typhimurium* (◀): slope=0.41767±0.027, R=0.987; *S. typhimurium* + *E. coli* (★): slope=0.42266±0.023, R=0.991.

The Hill plot was constructed using the dose response curves (Figure 6-18) to determine the binding kinetics (K_d), ($K_{d(apparent)}$) and binding valency ($1/n$). A summary of results from all the calculations for sensitivity, binding valency and dissociation constant are presented in Table 6-3. The sensitivity was measured as the slope of the linear range on the dose response curve. The E2 phage biosensor sensitivity was slightly different in the presence of masking bacteria, but, compared to the number of extraneous bacteria in mixture with *S. typhimurium*, the difference was not significant. In the absence of masking bacteria *E. coli*, the sensitivity was 175.5 Hz/decade, while in presence of one masking bacteria (*E. coli*), the sensitivity was 193.5 Hz/decade.

Table 6- 3. The sensitivity, dissociation constant and binding valency of magnetoelastic sensors in different bacterial mixtures.

Analyte	Detection Limit (cfu/mL)	Sensitivity (Hz/decade)	Binding valency ($1/n$)	K_d (cfu/mL)	$K_{d(apparent)} = (K_d)^{1/n}$ (cfu/mL)
Only *S.T.*	1.6×10^3	175.5	2.39	329	1.03×10^6
S.T. + *E. coli*	5×10^2	193.5	2.37	249	4.79×10^5

It was observed that the binding valency numbers were similar for the E2 phage biosensor (within a multi-sensor detection system) tested under both conditions, no matter whether the analytes contained more than one kind of bacteria or not. When the system was exposed to the mixture of non-specific pathogen (*E. coli*) together with the specific target (*S. typhimurium*), there may be a small amount of non-specific binding, although this binding will be relatively weak. The higher sensitivity obtained for E2 phage biosensors exposed to the mixture can be attributed to the presence of the other bacteria, which may have bound to the E2 phage biosensor as a cross-reaction.

4.2. Tested with a mixture of *B. anthracis* spores in *B. cereus* spores

Another experiment was conducted by exposing this multiple system to a mixture of *B. anthracis* spores (5×10^1-5×10^8 cfu/mL) with a fixed concentration of *B. cereus* spores (5×10^7 cfu/mL). The results from DNA-DNA hybridization experiments [8], multilocus enzyme electrophoresis, and multiple-locus sequence typing [9] have shown that *B. anthracis* and *B. cereus* are more closely related to each other than they are to other *B. cereus* strains. Consequently, in this experiment, we chose a suspension of *B. cereus* spores to co-spike with *B. anthracis* spores in order to demonstrate the specificity of the multi-sensor detection system.

4.2.1. Performance of multi-sensor detection system

The experiment started using plain water, which provided a steady baseline frequency response for the sensor, followed by the introduction of the *B. cereus* spore (5

$\times 10^7$ cfu mL^{-1}) suspension. Then, a mixture was introduced containing a fixed concentration of *B. cereus* spores (5×10^7 cfu mL^{-1}) with a low concentration of *B. anthracis* spores (5×10^1 cfu mL^{-1}) initially, followed by successively increasing *B. anthracis* concentrations (5×10^2 cfu mL^{-1} – 5×10^8 cfu mL^{-1}).

Figure 6-19 shows the response from one set of multi-sensors as a performance sample, plotted as a function of time and concentration versus the instant frequency value. A similar trend was seen to that observed in the multi-sensor system exposed to the mixture of bacteria (Figure 6-16). The total frequency change due to the specific binding of the *B. anthracis* spores onto the surface of JRB7 phage biosensor was approximately 950Hz. The reference sensor without phage coating and the E2 phage biosensor coated with phage specific to *S. typhimurium* showed about 70Hz and 90Hz in frequency shifts, respectively. When compared to a maximum shift (950 Hz) of the specific JRB7 phage biosensor, this indicated a negligible, non-specific binding of *B. cereus* spores to the gold surface. The JRB7 phage biosensor did not show an obvious frequency change when a high concentration of *B. cereus* spores (5×10^7 cfu/mL) was introduced after exposure to water, indicating that the cross-reaction with other *Bacillus* species was limited, and also that the multiple detection system had both good selectivity and binding ability. The JRB7 phage biosensor started to show an obvious frequency shift when the concentration of *B. anthracis* spore suspension reached 5×10^3 cfu/mL. Upon the initial introduction of each concentration, the frequency of the JRB7 phage biosensor suffered a sudden drop, and then became stable after 10-15 minutes due to

saturation. As the concentration increased, the saturation time became longer because higher concentrations provided more spores to bind with the specific phage on the sensor surface.

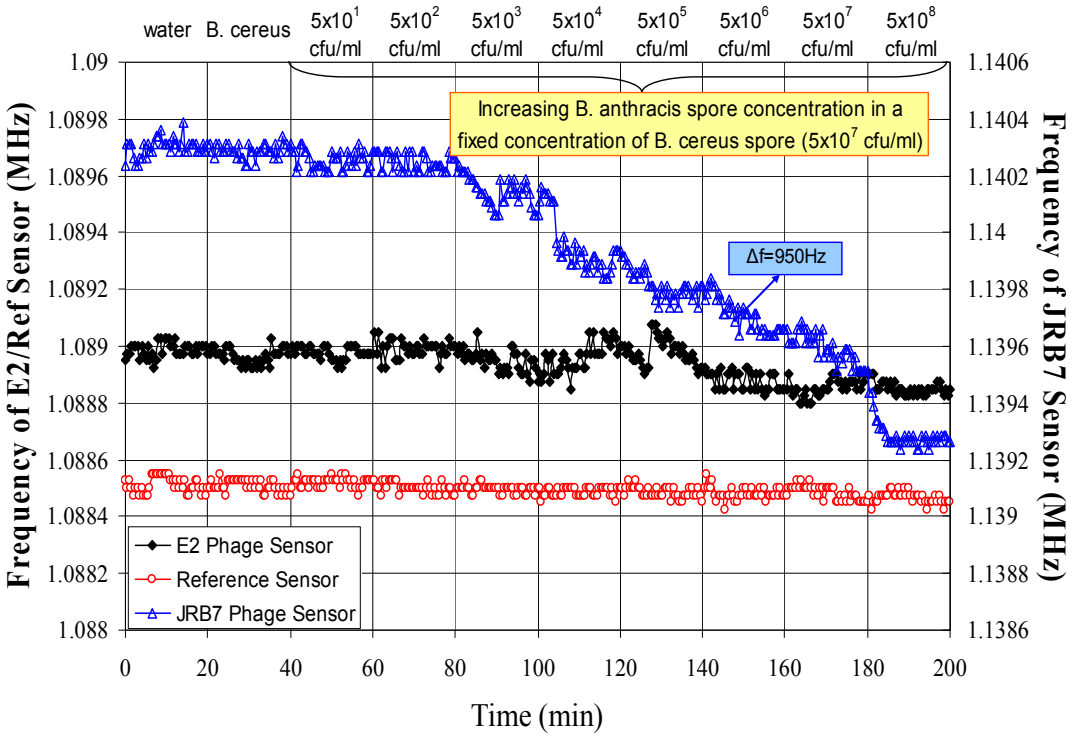

Figure 6- 19. Multiple detection system when exposed to a mixture of various concentrations of *B. anthracis* spores (5×10^1-5×10^8 cfu/mL) with a fixed concentration of *B. cereus* (5×10^7 cfu/mL). Each concentration of bacterial suspension was run for 20 min at a flow rate of 50 µl/min.

4.2.2. Dose Response

A similar dose response analysis was plotted in Figure 6-20 for the JRB7 phage biosensor in order to determine the effect of the presence of other *Bacillus* species in a mixture with *B. anthracis* spores. Five groups of the multi-sensor system were separately exposed to two conditions of prepared suspensions (*B. anthracis* and *B. anthracis* + *B. cereus*). The smooth lines are the sigmoid fits of the experimental data and each data point is a mean value of five biosensors. The response of the JRB7 phage biosensor followed similar trends for both condition. Similar frequency shifts were achieved when the concentration of *B. anthracis* spores reached 5×10^8 cfu/mL. The dose responses for both conditions were linear over the range of 5×10^4 cfu/mL to 5×10^8 cfu/mL. The detection limit of the JRB7 phage biosensor was calculated to be10^3 cfu/mL. The system did not reach the saturation range even though the concentration reached the highest level (5×10^8 cfu/mL). However, higher frequency shifts were observed for the mixture suspension test, which might be due to cross-reaction binding between *B. cereus* and the selected JRB7 phage, which was consistent with previous results reported by Wan et al. [6, 7].

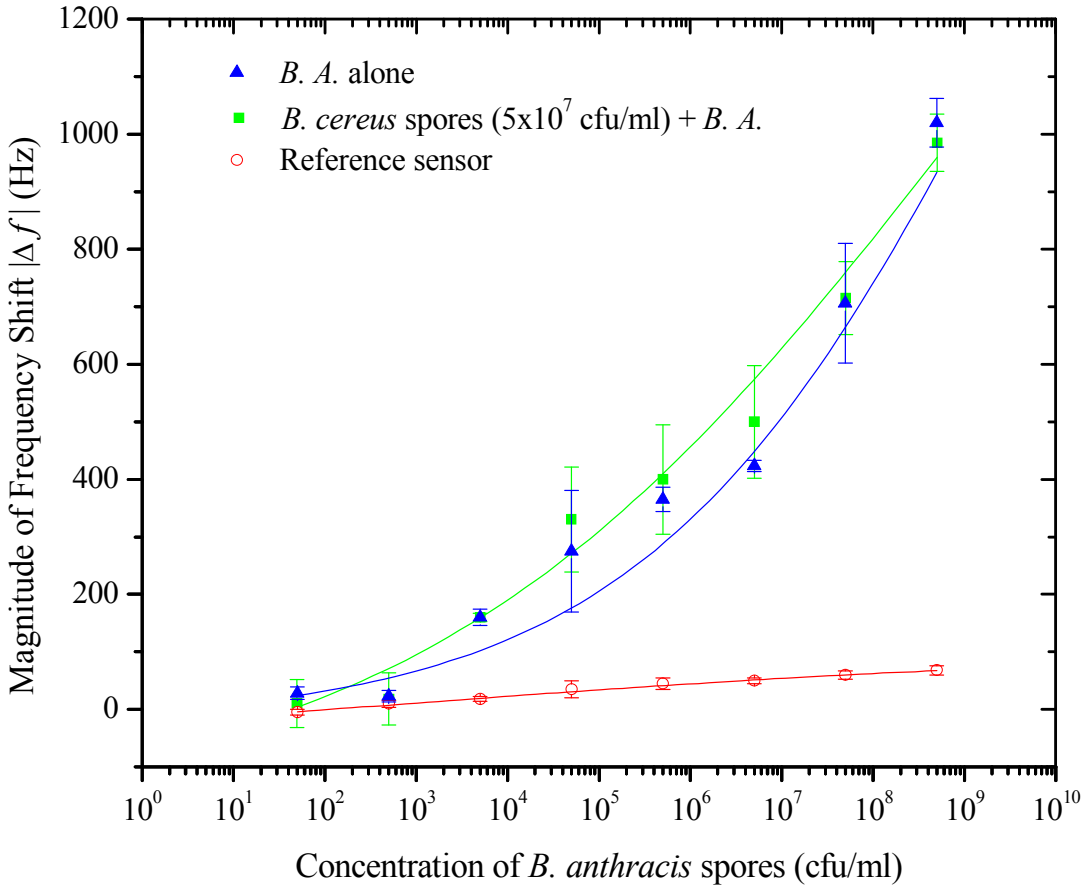

Figure 6- 20. The resonant frequency shifts of JRB7 phage based sensor (1.9 × 0.4 × 0.015 mm) as a function of a mixture of various concentrations of *B. anthracis* spores (5 × 10^1-5 × 10^8 cfu/mL) with masking *B. cereus* spores (5 × 10^7 cfu/mL). The smooth lines are the sigmoid fits of the experimental data and each data point is an average of the response from five sensors exposed to only *B. anthracis* spores ((▲) R^2=0.965), *B. anthracis* spores in mixture with *B. cereus* spores ((■) R^2=0.992) and reference sensor to control non-specific binding ((o) R^2=0.996).

4.2.3. Hill Plot

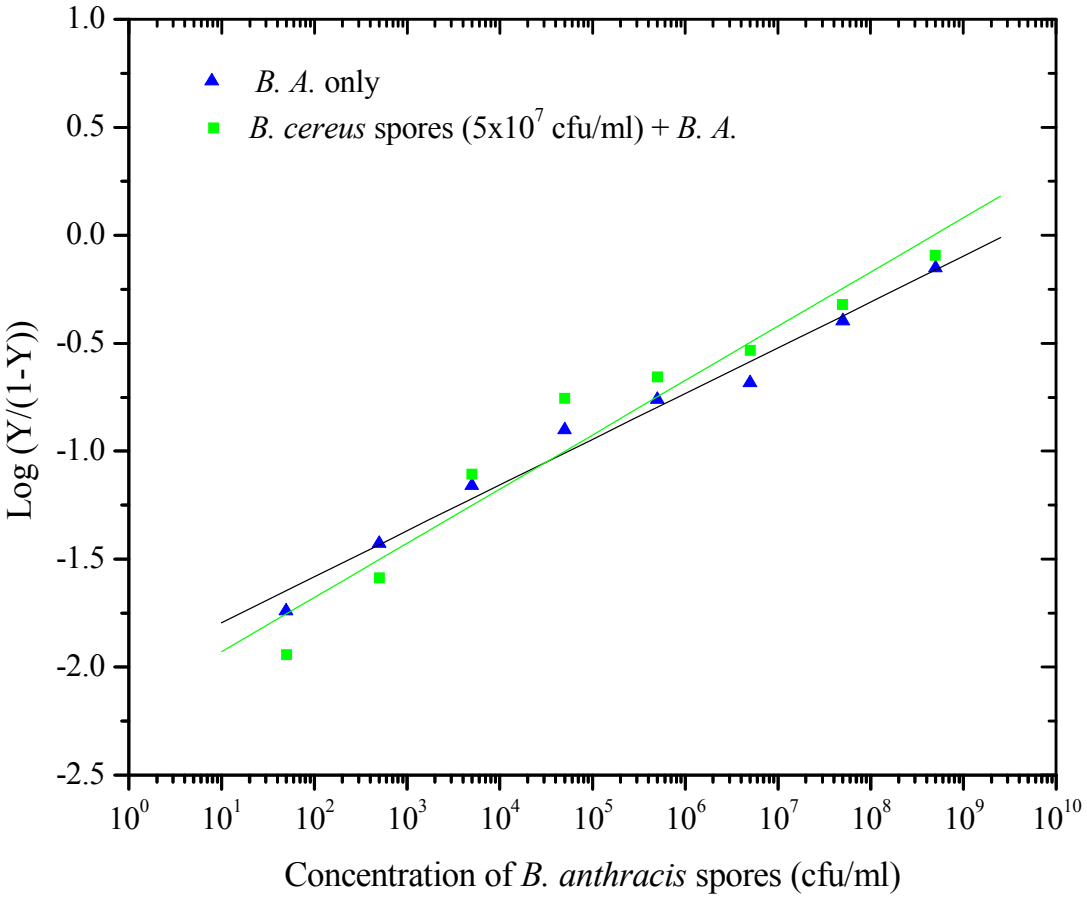

Figure 6- 21. Hill plot constructed from the dose response curves, showing the ratio of occupied (Y) and free phage sites (1-Y) as a function of spore concentrations in different conditions. The straight line is the linear least squares fit to the data (*B. anthracis* spores (▲): slope=0.21222±0.01, R=0.99; *B. anthracis* spores + *B. cereus* spores (■): slope=0.25099±0.02, R=0.973

A higher dissociation constant value was observed for the JRB7 phage biosensor exposed to more than one species of *Bacillus*. The higher the $K_{d(apparent)}$, the lower the binding strength that can be attributed to the presence of the other spores, as they compete to bind onto the JRB7 phage biosensor. A summary of results from all the calculations for sensitivity, binding valency and dissociation constant from the Hill plot is presented in Table 6-4. The sensor was highly sensitive even in the presence of high concentrations of masking agents, as well as in the presence of other sensors within a multi-sensor system. The sensitivity (measured as the slope of the linear range on the dose response curve) of the suspension in the absence of other masking agent was 224.8 Hz/decade. In the presence of *B. cereus* spores in the mixture, the sensitivity was 197 Hz/decade.

Table 6- 4. The sensitivity, dissociation constant and binding valency of magnetoelastic sensors in different bacterial mixtures.

Analyte	Detection Limit (cfu/mL)	Sensitivity (Hz/decade)	Binding valency (*1/n*)	K_d (cfu/mL)	$K_{d(apparent)} = (K_d)^{1/n}$ (cfu/mL)
B. A. only	10^3	224.8	3.71	101	2.72×10^7
B.A. + B.C.	3×10^2	197	3.98	151	4.7×10^8

5. Conclusions

These results demonstrated that multiple phage-based ME biosensors can be simultaneously monitored to detect and discriminate between different pathogens. Immobilized phage on the surface of ME sensor platform displayed a useful biomolecular recognition ability with good sensitivity and specificity, offering a simple method to detect multiple pathogens. For the currently reported ME biosensor dimensions, pre-enrichment in culture media for at least 2 or 3 hours may be necessary to achieve the minimum concentration to exceed the threshold detection limit of the biosensor.

The measurement sensors were compared within the multi-sensor detection system under three different conditions: 1) exposure to two widely different classes of pathogens – *S. typhimurium* bacteria and *B. anthracis* spore suspensions that were sequentially introduced into the system; 2) exposure to an analyte containing only *S. typhimurium* bacteria / *B. anthracis* spores; 3) exposure to an analyte containing additional bacteria / spore species.

A summary of the performance achieved by the E2 and JRB7 phage biosensors is provided in Tables 6-5 and 6-6, respectively. The JRB7 phage biosensor showed higher sensitivity than the E2 phage biosensor. Since the JRB7 phage biosensor (l=1.9mm) is slightly smaller than the E2 phage sensor (l=2mm), these results are consistent with the theory discussed in Chapter **4,** where smaller sensor dimensions are expected to impart higher sensitivity.

Table 6- 5. Summary of the performance of the E2 phage biosensor.

Analyte	Detection Limit (cfu/mL)	Sensitivity (Hz/Decade)	Binding valency (*1/n*)	K_d (cfu/mL)	$K_{d(apparent)} = (K_d)^{1/n}$ (cfu/mL)
S. T. + B. A.	1.1×10^3	238.5	3.05	387.2	7.8×10^7
S. T. only	1.6×10^3	175.5	2.39	329	1.03×10^6
S. T. + E. coli	5×10^2	193.5	2.37	249	4.79×10^5

Table 6- 6. Summary of the performance of the JRB7 phage biosensor.

Analyte	Detection Limit (cfu/mL)	Sensitivity (Hz/Decade)	Binding valency (*1/n*)	K_d (cfu/mL)	$K_{d(apparent)} = (K_d)^{1/n}$ (cfu/mL)
S. T. + B. A.	1.6×10^3	279.5	3.62	342.8	1.5×10^9
B. A. only	10^3	224.8	3.71	101	2.72×10^7
B. A. + B. C.	3×10^2	197	3.98	151	4.7×10^8

6. References

[1] M. K. Jain and C. A. Grimes, "A Wireless Magnetoelastic Micro-Sensor Array for Simultaneous Measurement of Temperature and Pressure," *IEEE TRANSACTIONS ON MAGNETICS,* vol. 37, 2001.

[2] K. G. Ong, K. Zeng, X. Yang, K. Shankar, C. Ruan, and C. A. Grimes, "Quantification of multiple bioagents with wireless, remote-query magnetoelastic micro-sensors," *IEEE Sensors J.,* vol. 6, pp. 514-523, 2006.

[3] C. A. Grimes, D. Kouzoudis, and C. Mungle, "Simultaneous measurement of liquid density and viscosity using remote query magnetoelastic sensors," *REVIEW OF SCIENTIFIC INSTRUMENTS,* vol. 71, pp. 3822-3824, 2000.

[4] R. S. Lakshmanan, R. Guntupalli, J. Hu, D.-J. Kim, V. A. Petrenko, J. M. Barbaree, and B. A. Chin, "Phage immobilized magnetoelastic sensor for the detection of *Salmonella typhimurium*," *Journal of Microbiological Methods,* vol. 71, pp. 55-60, 2007.

[5] R. S. Lakshmanan, R. Guntupalli, J. Hu, V. A. Petrenko, J. M. Barbaree, and B. A. Chin, "Detection of *Salmonella typhimurium* in fat free milk using a phage immobilized magnetoelastic sensor," *Sensors and Actuators B: Chemical,* vol. 126, pp. 544-550, 2007.

[6] J. Wan, M. L. Johnson, R. Guntupalli, V. A. Petrenko, and B. A. Chin, "Detection of *Bacillus anthracis* spores in liquid using phage-based magnetoelastic micro-resonators," *Sensors and Actuators B: Chemical,* vol. 127, pp. 559-566,

2007.

[7] J. Wan, H. Shu, S. Huang, I.-H. Chen, V. A. Petrenko, and B. A. Chin, "Phage-based magnetoelastic wireless biosensors for detecting *Bacillus anthracis* spores," *IEEE Sens. J. ,* vol. 7, pp. 470-477, 2007.

[8] T. Kaneko, R. Nozaki, and K. Aizawa, "Deoxyribonucleic acid relatedness between *Bacillus anthracis* and *Bacillus cereus* and *Bacillus thuringiensis*," *Microbiol. Immunol. ,* vol. 22, pp. 639-641, 1978.

[9] E. Helgason, O. A. Økstad, D. A. Caugant, H. A. Johansen, and A. Fouet, "*Bacillus anthracis*, *Bacillus cereus* and *Bacillus thuringiensis*-one species on the basis of genetic evidence," *Appl. Environ. Microbiol.,* vol. 66, pp. 2627-2630, 2000.

CHAPTER 7

CONCLUSIONS AND FUTURE WORK

1. Summary and conclusions

This dissertation has described and tested a new multi-sensor system capable of simultaneous real time monitoring of multiple biological pathogens introduced to the measurement system. The detection system developed for this study included a reference sensor as a control, an E2 phage biosensor specific to *S. typhimurium*, and a JRB7 phage biosensor specific to *B. anthracis* spores. The major findings of this research can be summarized in four main groupings:

1) *Optimization of sensor fabrication*. When sensors were annealed between 200-250 ºC in a vacuum oven before sputtering, the residual stresses created during dicing were largely relieved and many of the structural defects were removed. At the same time, the *Q*-factor of the resonance signal increased by about 30% and the amplitude increased by about 25%. Based on this and the other process optimization reported in this dissertation, it is now possible to construct a high quality sensor that exhibit good corrosion resistance, sensitivity, and binding properties.

2) Optimization of the interaction between the phage filaments and the gold surface of the sensor platform. By increasing the amount of NaCl in the 5×10^{11} vir/mL phage

solution to 420 mM, the tendency of the phage filaments to bundle will be minimized. Elimination of phage bundling will increase the available binding sites on the ME sensor's surface, allowing more target pathogens to be bound to the sensor surface and thus increasing the binding affinity of the ME biosensor

3) *Blocking the non-specific binding for the multi-sensor system*. Non-specific binding can be blocked using the standard blocking agent BSA with a concentration of 1mg/mL. This step is particularly important for the multi-sensor detection system, where several sensors are applied simultaneously in a flowing system. If the non-specific binding is not blocked, the specificity, sensitivity and selectivity of the sensor will be adversely affected.

4) *Construction of a new multi-sensor detection system that can simultaneously detect and discriminate between different pathogens or similar strains of the same group*. The sensitivity for the multi-sensor system is about 170-280 Hz/decade, with the average binding valency about 3, a dissociation constant K_d of about 250 cfu/mL and a $K_{d(apparent)}$ of about 10^5-10^8 cfu/mL and detection limit of 3×10^2-1.6×10^3 cfu/mL.

2. Future work

In the future, this ME biosensor based detection system could be extended to include hundreds to many individual ME biosensors. Using this approach, the statistical probability of a small number of target species interacting with one or more of a large number of ME biosensors will be greatly increased over that of interaction with a single

ME sensor. This technique may therefore offer significant advantages for monitoring large volumes of food products for a small number of biological pathogens or contaminants.

The results obtained in this dissertation also demonstrated that very small sensors (L < 500 μm) can be combined to form a multi-sensor detection system that is capable of detecting several different pathogens simultaneously. Since magnetoelastic sensors with smaller dimensions have a higher sensitivity, the performance of the multi-detection system consisting of small sensors will be an interesting topic for future research. The problem with working with ever-smaller sensors is their weaker frequency response signals and relatively smaller Q values, especially in flowing liquid media, which makes it harder to determine accurate frequency shifts. Alternatively, since these very small sensors can only be made by fabrication processes that utilize even thinner Cr and Au coatings in order to preserve the sensitivity of the sensor, the corrosion resistance of the sensor may not be as good as that of the diced sensors used for this dissertation.

A new methodology may be needed to obtain a better detection signal. For example, our group found that by adding a variable capacitor with the solenoid coil that can be adjusted to match the circuit resonance to the mechanical frequency of the sensor, a significant increase (at least 5 times) in both the amplitude and Q factor of the signal from the sensor can be obtained. The development of this method shows great promise for the development of a multi-sensor detection system with even higher sensitivity.

CHAPTER 8

SUPPLEMENTAL WORK-BACTERIUM & SPORES IN APPLE JUICE

1. The binding of *B. anthracis* spores (in apple juice) on the biosensor surface

We have demonstrated that ME biosensors can be used to simultaneously detect *S. typhimurium* and *B. anthracis* spores suspended in water. It is also essential to establish the field applicability of ME biosensors for applications in other media, so this work was extended to examine the viability of testing for bacterium/spores suspended in apple juice.

Since Lakshmanan et al [1] have already demonstrated that *S. typhimurium* can be detected in a mixed microbial population (milk or apple juice) by an E2 phage biosensor, this dissertation will focus on the application of a JRB7 phage biosensor in apple juice. Apple juice (Kroger® brand) was purchased from a local grocery store and was found to have a nominal pH of 4. Two methods, static (as described in Chapter **3** Section **3.2.3.**) and dynamic loading (as described in Chapter **3** Section **3.2.4.**), were then utilized to determine whether spores were able to bind onto the ME biosensor surface in this new liquid medium. For static loading, the apple juice was spiked with known concentrations of *B. anthracis* spores (5×10^8 cfu/mL). Ten JRB7 phage biosensors were then separately exposed to the solution by the static loading method. Figure 8-1. shows the SEM image of the JRB7 phage biosensor surface after static loading. The

images clearly show that very few of the spores bound onto the biosensor surface. The SEM images of the other JRB7 phage biosensors showed results consistent with those depicted in Figure 8-1.

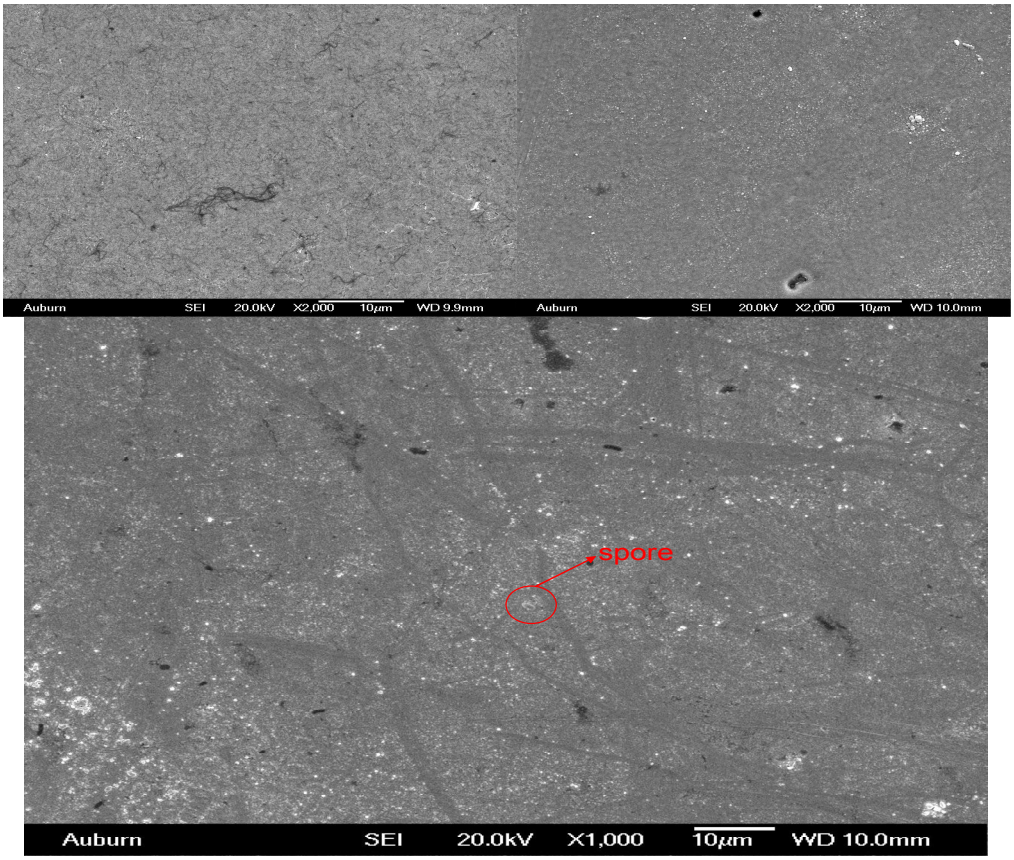

Figure 8- 1. SEM images of JRB7 phage biosensor surface after exposure to *B. anthracis* spores (5×10^8 cfu/mL) suspended in apple juice by static loading.

For the flowing measurement, apple juice was spiked with increasing concentrations of *B. anthracis* spores (5×10^1 through 5×10^8 cfu/mL). The JRB7 phage biosensor was then placed in the measurement chamber and exposed to the flowing

spiked sample continuously. The frequency of the JRB7 phage biosensor showed a dramatic decrease (7000 Hz) as shown in Figure 8-2. The average frequency decrease for ten JRB7 phage biosensors was about 5000 Hz. SEM image clearly show that very few of the spores bound onto the biosensor surface (Figure 8-3.) In order to determine the reason for such a dramatic frequency shift. A reference sensor (no phage coating) was exposed to the flowing apple juice continuously. The frequency of the reference sensor showed a dramatic decrease (7900 Hz) but there was no saturation trend as shown in Figure 8-4.. Based on these data, the dramatic frequency shift is not due to the binding of spores. Consequently, we hypothesized that this shift has the possible cause: the proteins in apple juice attach to the sensor surface.

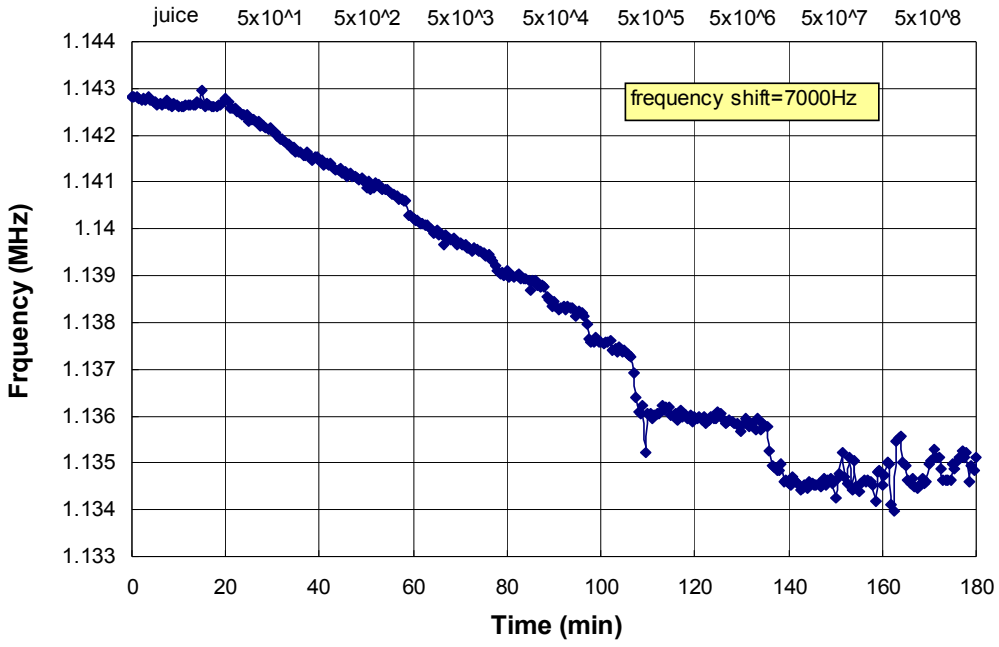

Figure 8- 2. JRB7 phage biosensor response when exposed to various concentrations of *B. anthracis* spores ($5 \times 10^1 - 5 \times 10^8$ cfu/mL) suspended in apple juice.

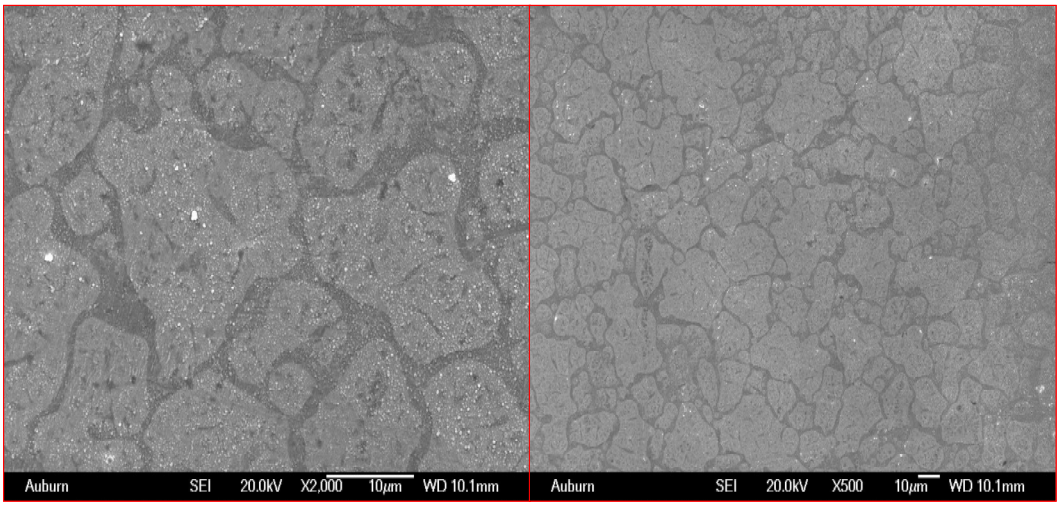

Figure 8- 3. SEM images of JRB7 phage biosensor surface after exposure to various concentrations of *B. anthracis* spores ($5 \times 10^1 - 5 \times 10^8$ cfu/mL) suspended in apple juice by dynamic loading.

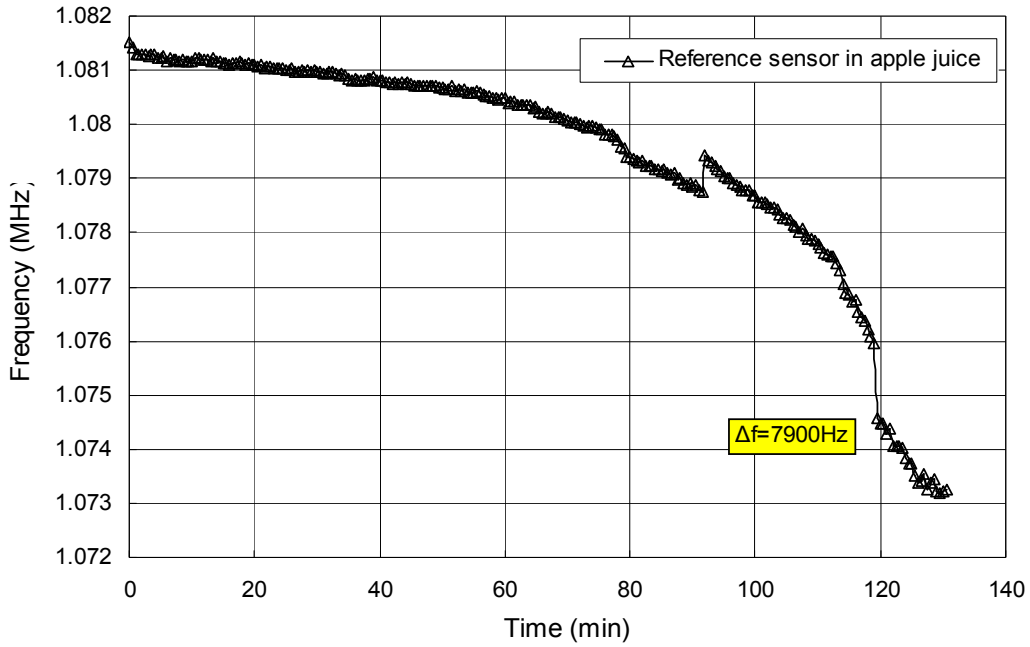

Figure 8- 4. Reference sensor response when exposed to apple juice.

2. Reasons for low binding numbers

In previous experiments, the phage was suspended in a buffer solution environment, while the spore was suspended in water with a pH of about 7. Consequently, we hypothesized that the poor binding seen above has three possible causes: 1.) the low pH of apple juice may affect the binding affinity between the spores and phages; 2.) the JRB7 phages could lose their binding affinity to spores when they are suspended in apple juice, or the components of the apple juice may block the binding sites of the sensor or phage peptides; or 3.) apple juice causes a change in the spore shell's properties, causing it to lose its binding affinity to the JRB7 phage.

2.1. Effect of apple juice pH

In order to determine the effect of pH, three sets of suspensions were applied: 1) *B. anthracis* spores (5×10^8 cfu/mL) suspended in water (pH= 7); 2) *B. anthracis* spores (5×10^8 cfu/mL) suspended in apple juice (pH= 4); 3) *B. anthracis* spores (5×10^8 cfu/mL) suspended in apple juice (KCl was added until pH= 7). After immobilization with JRB7 phage, the three biosensors were inserted into three suspensions separately for 1hr to allow spores to bind onto the biosensors. Figure 8-5 shows the binding results for these three biosensors after static loading. Figure 8-5 (a) represents the results of the JRB7 phage biosensor that was coated with spores in water. A large number of spores were distributed evenly on the sensor surface. The interaction between the JRB7 phage biosensor with spores in apple juice (pH= 4) is shown in Figure 8-5 (b), where very few

spores were bound onto the biosensor surface. A similar trend was found even when the pH of the apple juice was adjusted to 7. Based on these observations, adjusting the pH of the apple juice is likely to have no effect on the binding affinity between spores and JRB7 phage on the biosensor surface.

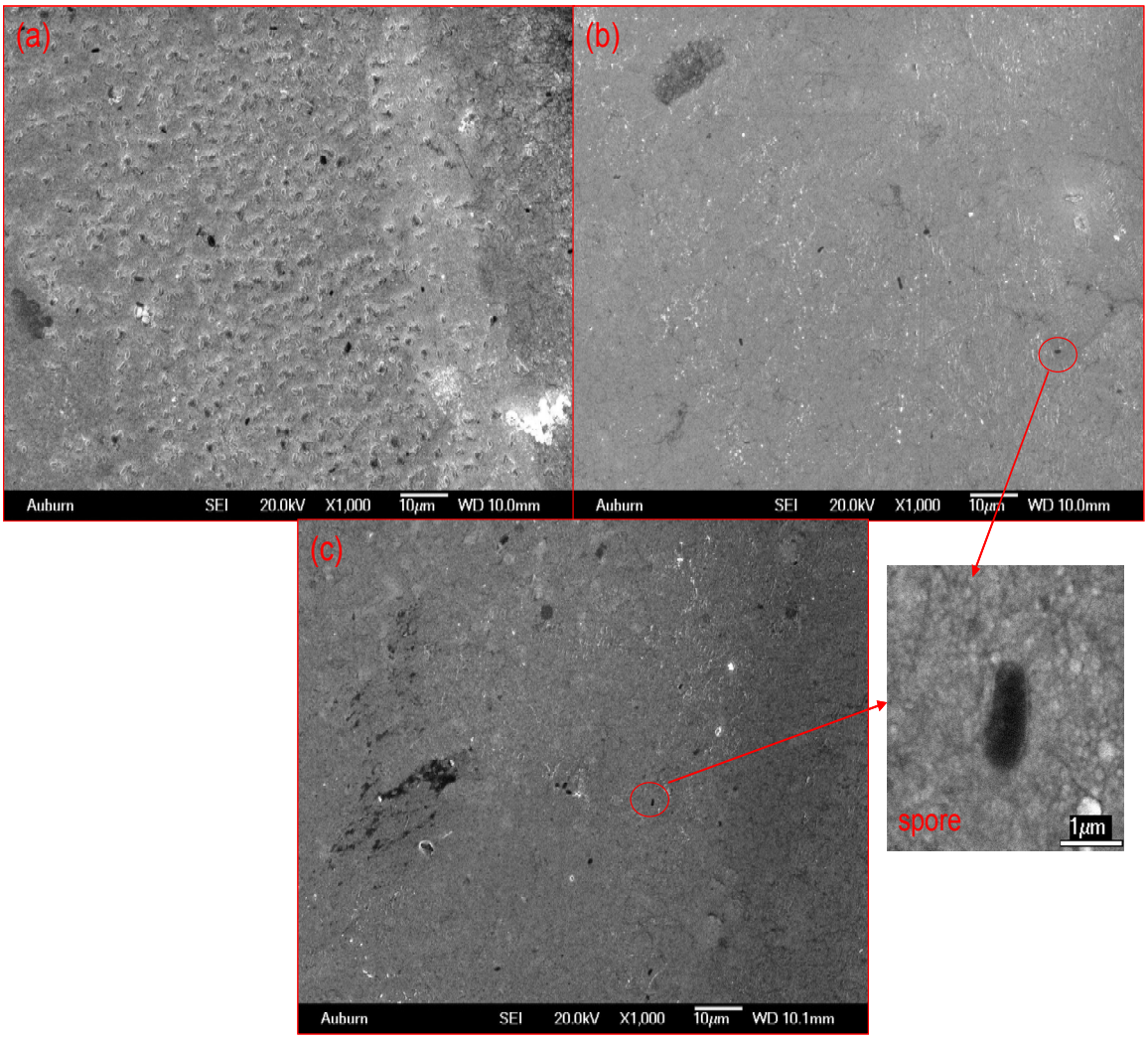

Figure 8- 5. SEM images of JRB7 phage biosensors after exposure to *B. anthracis* spores (5×10^8 cfu/mL) suspended in three different media: (a) water; (b) apple juice with pH= 4; and (c) apple juice with pH=7.

2.2. Effect of apple juice on phage filaments

In order to determine the effect of apple juice on the phage filaments, three types of fabrication conditions were utilized to fabricate three kinds of biosensors. The flow chart (Figure 8-4) below summarizes all three conditions. After fabrication, all three biosensors were exposed to the same suspension of *B. anthracis* spores (5×10^8 cfu/mL, suspended in water). Afterwards, SEM images were taken to show the binding numbers of spores on each biosensor surface under each condition.

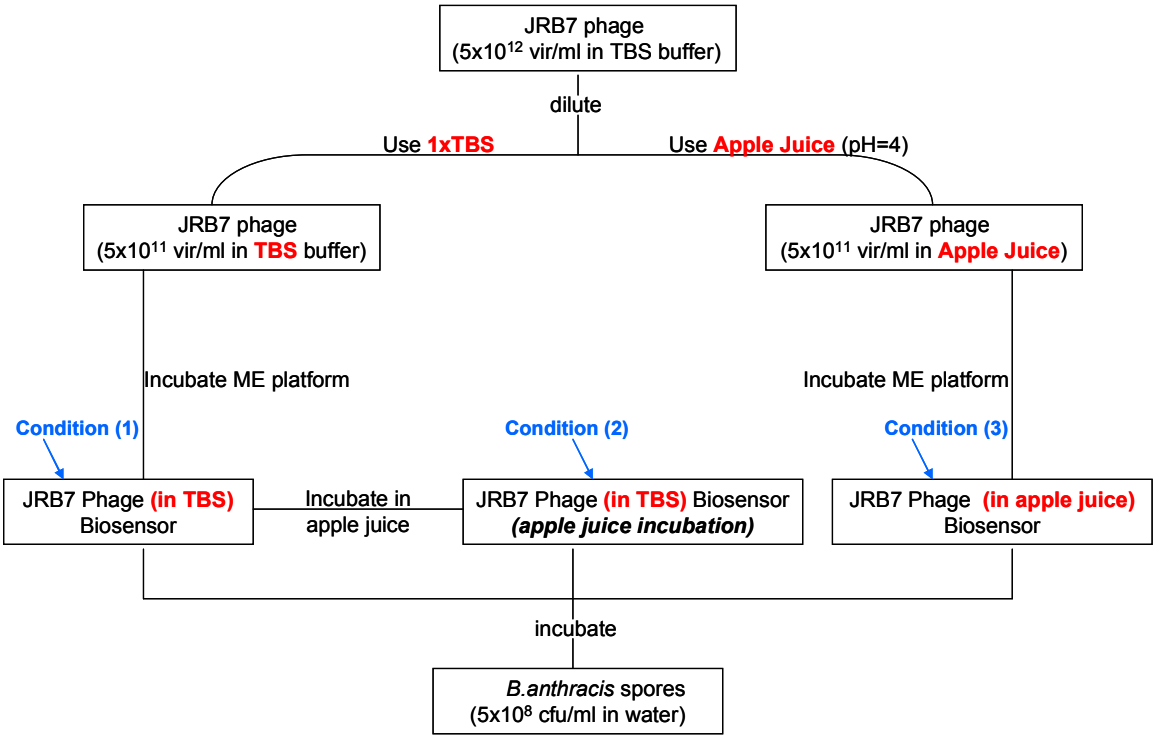

Figure 8- 6. Three fabrication conditions for ME biosensors.

Condition (1) represents a control condition where the ME platform was coated with JRB7 phage (5×10^{11} vir/mL, suspended in TBS buffer) to form a biosensor and then exposed to the suspension of *B. anthracis* spores. This biosensor was used as a reference to compare with the other two conditions. For condition (2), an ME platform was coated with JRB7 phage (5×10^{11} vir/mL, suspended in TBS buffer) for 1hr to form the biosensor, followed by incubating this biosensor in apple juice (Kroger Brand, pH= 4) for 1 hr, and then exposure to the *B. anthracis* spores. The objective of condition (2) was to check whether the ingredients of the apple juice blocked the binding sites of the biosensor or phage peptides. For condition (3), unlike the two conditions above, a high concentration (5×10^{12} vir/mL) of JRB7 phage was diluted to a lower concentration of 5×10^{11} vir/mL using apple juice (Kroger Brand, pH= 4) instead of 1xTBS. After immersing the ME platform in this phage suspension for 1hr, the resulting ME biosensor was exposed to the suspension of *B. anthracis* spores. The objective of condition (3)I was to determine whether the apple juice changed the binding affinity of the phage filaments. The SEM image of the biosensors fabricated under each condition and exposed to the same spore suspension is shown in Figure 8-7. Figures 8-7 (a)-(c) represent conditions (1)-(3), respectively. The three biosensors had similar numbers of spores bound on the surface, although in condition (3) ((Figure 8-7 (c)), where the JRB7 phage was diluted in apple juice, the phage filaments were much more clearly visible on the surface than in the other two conditions. Based on these observations, apple juice is likely to have a negligible affect on the binding affinity of phage filaments.

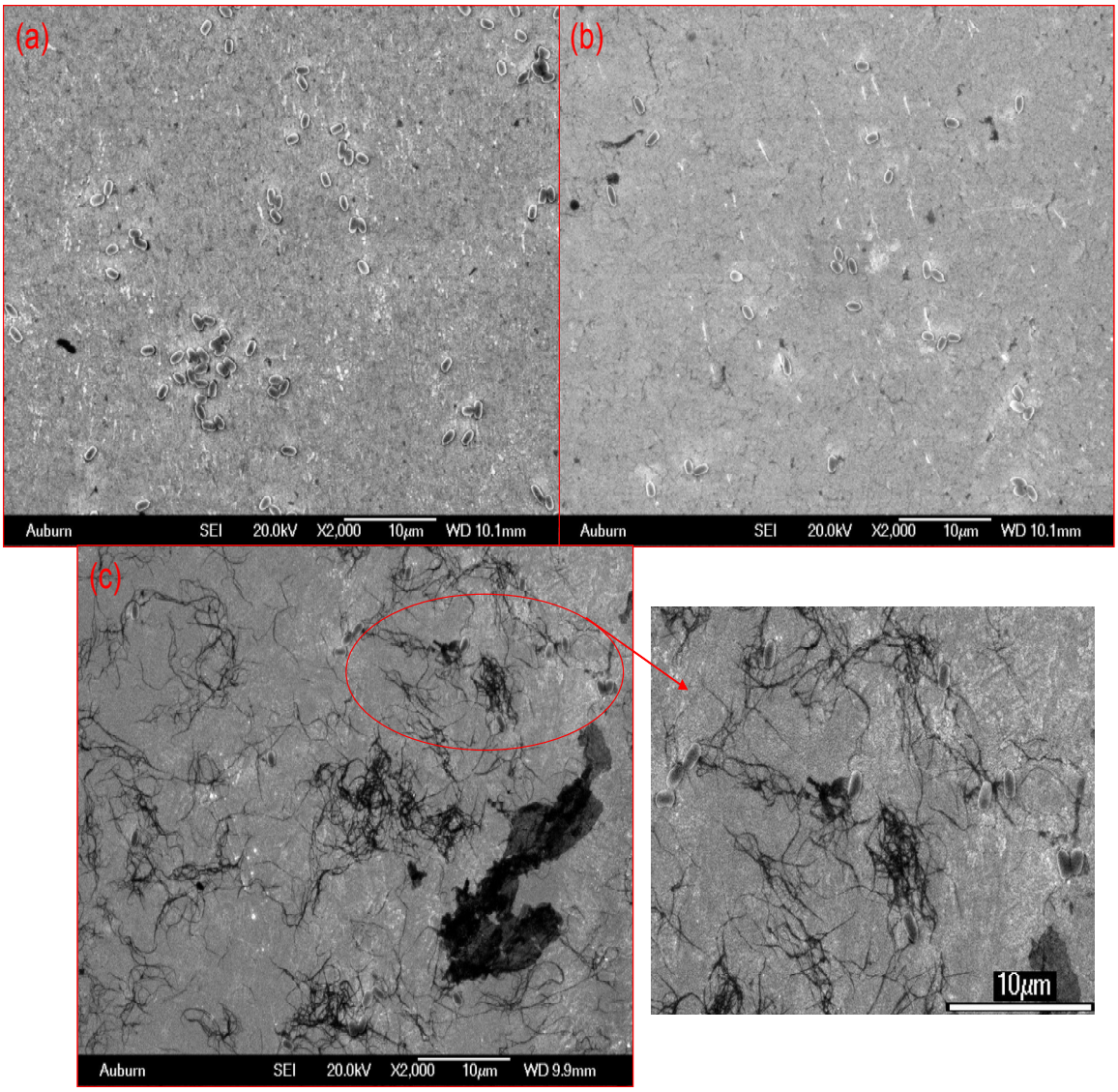

Figure 8- 7. SEM images of the three biosensors fabricated under different conditions and exposed to B. anthracis spores. (a) control biosensor fabricated under condition (1); (b) biosensor fabricated under condition (2); and (c) biosensor fabricated under condition (3).

2.3. Effect of apple juice on *B. anthracis* spore

In order to determine the effect of apple juice on the *B. anthracis* spores, 1 ml of the spore suspension (5×10^8 cfu/mL suspended in water) was centrifuged at a rate of 14.5 rpm/min for 10 min in order to form a spore pellet. The water was then pipetted off the spore pellet, and an equal volume of apple juice (pH= 4) added to the tube, followed by vortexing the spore pellet to mix with the apple juice. After a 1 hr incubation of the mixtures of spores in apple juice, the suspension was centrifuged using the same conditions, followed by pipetting the apple juice from the tube and replacing it with an equal volume (1 ml) of water. The objective of this step was to allow the apple juice to interact with the spores. ME platforms were coated with JRB7 phage (5×10^{11} vir/mL in water) to form JRB7 phage biosensors, and then exposed to the spore suspension prepared as described above. A control JRB7 phage biosensor exposed to an untreated spore suspension (5×10^8 cfu/mL suspended in water, no apple juice treatment) after phage immobilization was also used as a reference. The SEM images for the binding results on the biosensor surface are shown in Figure 8-8 below. There was a significant difference in the numbers of spores binding on the surfaces of both biosensors. Figure 8-8 (a) depicts the control biosensor, with many spores are distributed on the surface, while the other biosensor (treated by apple juice and then exposed to spores) has only a few spores on its surface. It is possible, therefore that apple juice does indeed affect the properties of spore shells, causing them to have a much lower binding affinity to the phage filaments, and thus leading to a low level of binding on the biosensor surface.

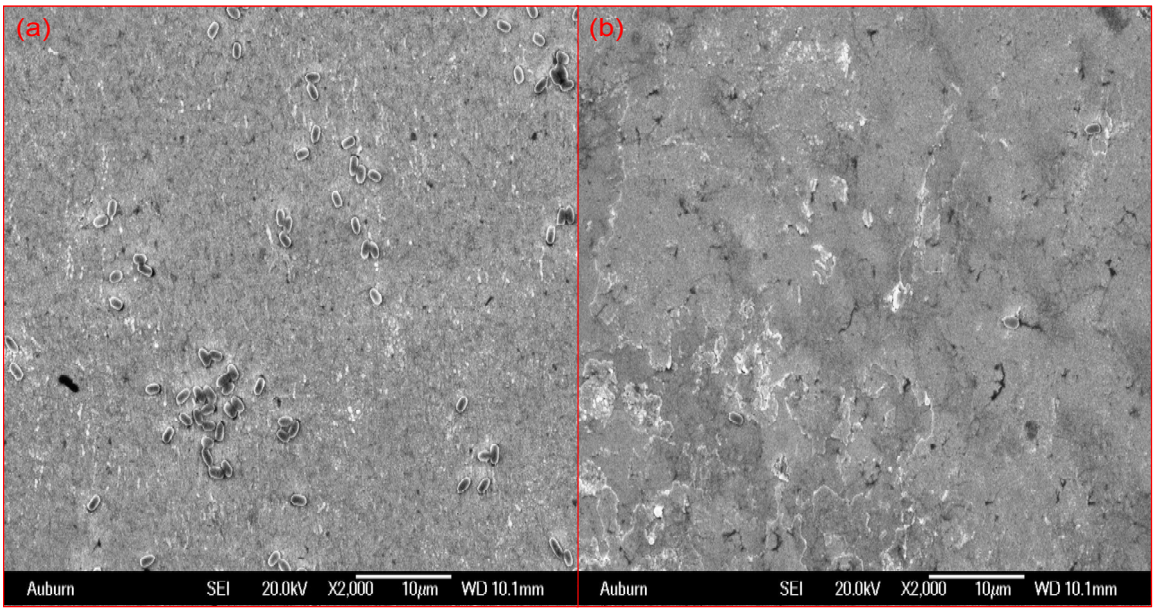

Figure 8- 8. SEM images of JRB7 phage biosensor surface (a) after exposure to *B. anthracis* spores (5×10^8 cfu/mL, suspended in water); (b) after exposure to *B. anthracis* spores (5×10^8 cfu/mL, incubated in apple juice for 1hr).

3. Fluorescence results

In addition to counting the binding numbers of spores on the biosensor surface by SEM, fluorescence spectroscopy provides valuable information regarding the interactions between the phage and its targets. In this section, several different experimental conditions were employed: 1) JRB7 phage and *B. anthracis* spores in apple juice (to determine the effect of apple juice on the spores); 2) JRB7 phage and *B. cereus* spores (to determine the cross-reactions, if any, of the JRB7 phage); 3) E2 phage and *S. typhimurium* in water (to determine the specificity of the E2 phage); 4) E2 phage and *E.*

coli in water (to determine the cross-reactions, if any, of the E2 phage); and 5) E2 phage and *S. typhimurium* in apple juice (to determine the effect of apple juice on bacteria).

In order to observe the interactions between spore species and JRB7 phage under a fluorescence microscope, various concentrations and volumes of solutions were tested and florescence images recorded to determine the optimum sample preparation conditions. Based on these results, the procedure used for preparing the samples was as follows: 1) bacteria/spore suspension (1×10^8 cfu/mL, 200 µl) was stored in a plastic tube (1.5 ml); 2) the bacteria/spore suspension was centrifuged to remove the water, followed by the addition of an equal amount of Kroger brand apple juice (pH= 4) and incubation for 1 hr; 3) 200 µl E2/JRB7 phage (5×10^{11} vir/mL) was added to the tube and allowed to incubate for another 1 hr; 4) the above mixed suspension was centrifuged to remove the liquid, leaving the pellet, which included both the individual bacteria/spores and bacteria/spores bound to E2/JRB7 phage, on the bottom of the tube; 5) this pellet was washed with PBST (PBS + 0.5% tween) three times, then 200 µl PBS was added to the tube to dissolve the pellet; 6) 2 µl of the first antibody α-fd was diluted in 200 µl PBS buffer at a ratio of 1:100, followed by the addition of this diluted antibody to the tube for an incubation period of one hour; 7) Fluorescein-isothiocyanate (FITC) coated secondary antibody was added to the tube and allowed to incubate for another one hour; and 8) the solution from step 7 was centrifuged and the pellet was washed 3 times using PBS and then observed using florescence spectroscopy.

Figure 8-7 shows the fluorescence images used to determine the effect of apple juice on the binding affinity between specific phage and target. Images were taken both with and without fluorescent light. Regardless of whether the spores/bacterium were bound with phage or not, they were observed under a standard microscope without fluorescence (white light). Under the fluorescent light, only those spores/bacterium bound with phage -antibody-secondary antibody-FITC were observed microscopically. So, by comparing the numbers of spores/bacterium observed with or without fluorescent light, it was possible to determine whether the apple juice affected the binding affinity of the spores/bacterium to the phages. From Figures 8-9 (a) and (c), where E2/JRB7 phage responded to *B. anthracis* spores/*S. typhimurium* in water, similar numbers of spores/cells were observed with and without fluorescent light. This indicates a good specificity of phage to targets. Figure 8-9 (b), where the *B. anthracis* spores were incubated in apple juice for 1hr, showed a significant difference in the numbers of spores when observed with and without fluorescent light. This phenomenon was consistent with the results in Section **2.3** above. Again, this demonstrated that apple juice affected the binding affinity of spores to the JRB7 phage. In Figure 8-9 (d), where the *S. typhimurium* was incubated in apple juice for 1hr, the numbers of cells observed were similar with and without fluorescent light. This result showed that *S. typhimurium* cells can exist within the apple juice without losing their binding affinity to the E2 phage. Also, *S. typhimurium* cells incubated in apple juice appeared much brighter and were more visible when compared with those cells suspended in water. This may be because the apple juice provided

enough sugar and nutrients to nourish the cells and encourage their growth.

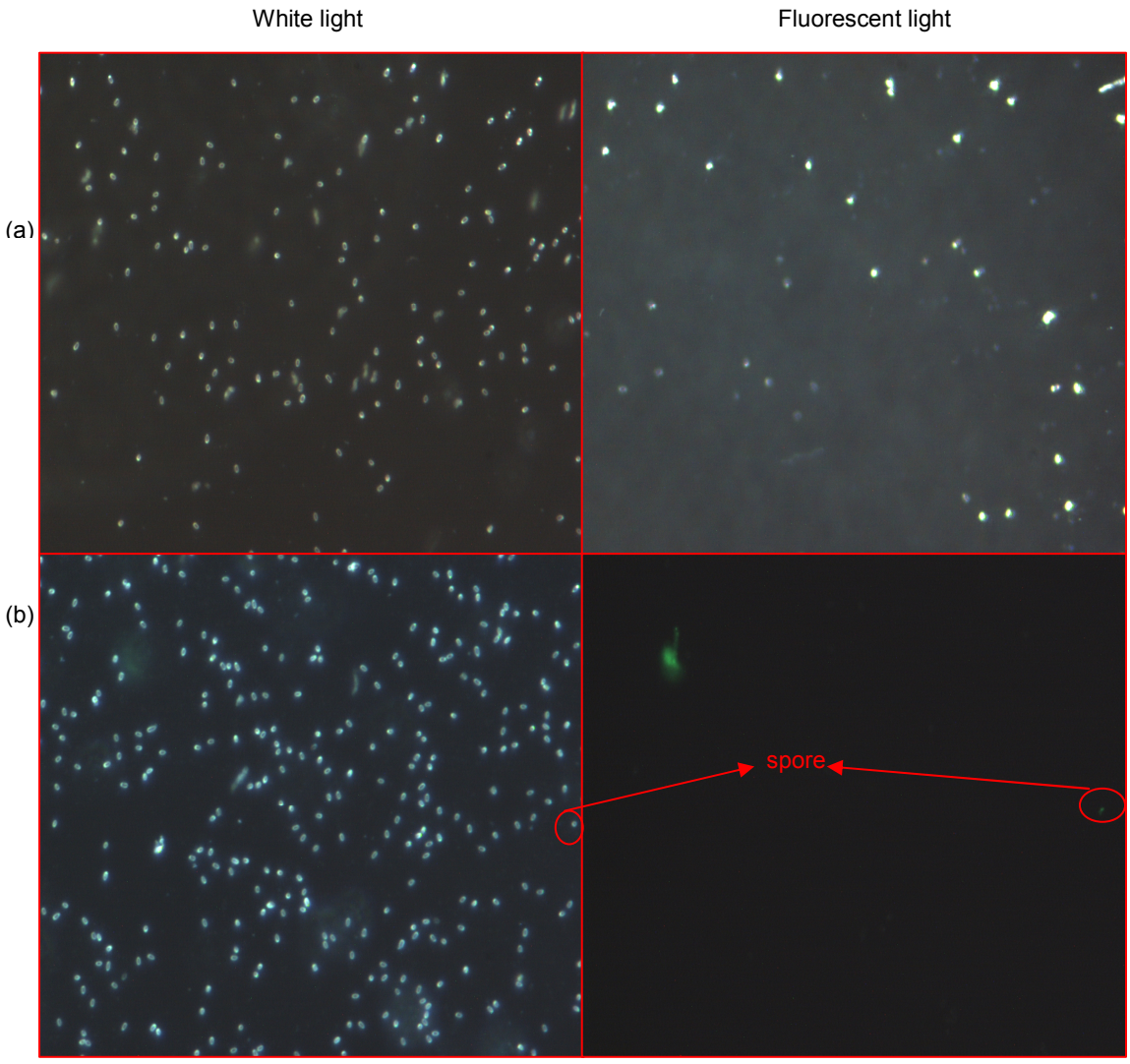

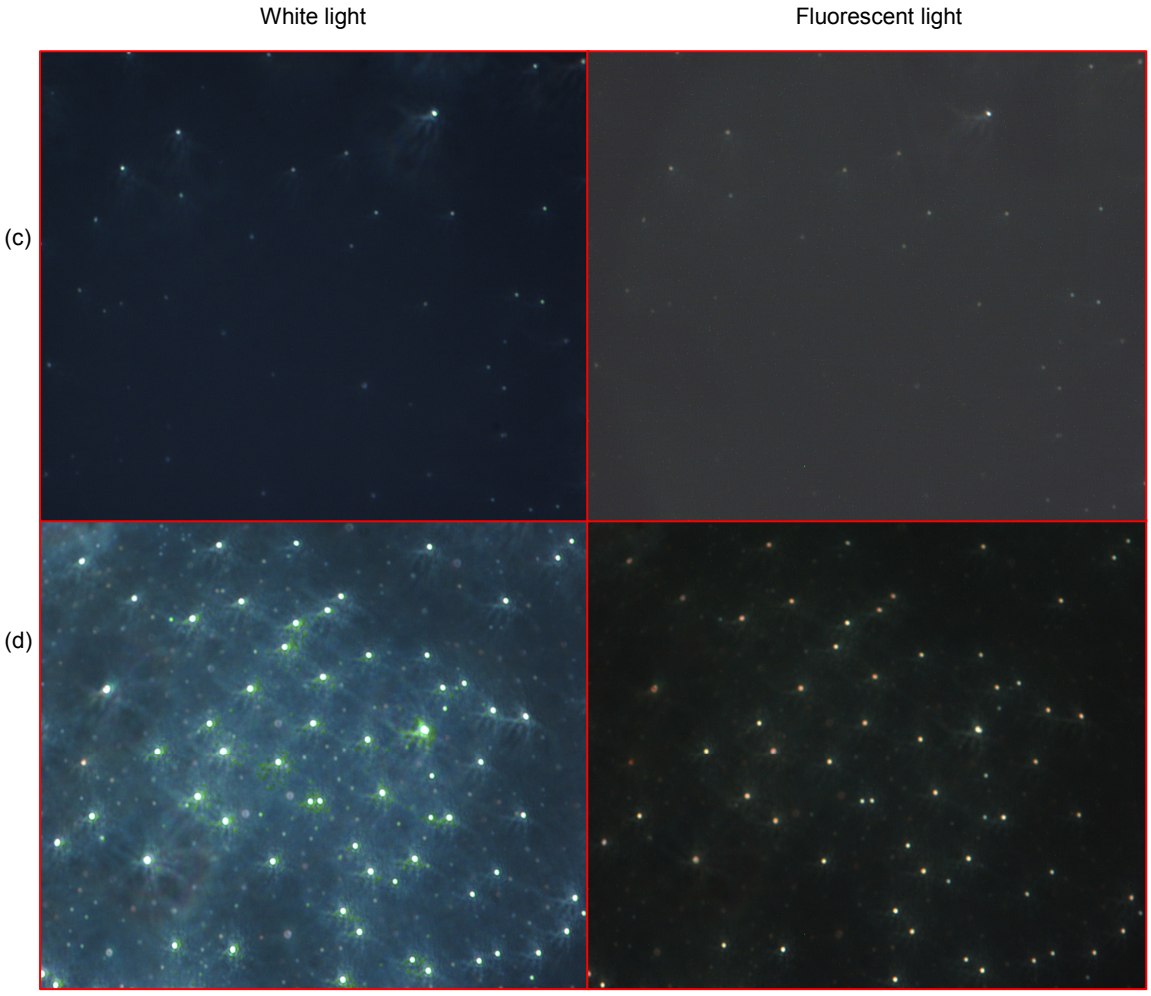

Figure 8- 9. Fluorescence images of different conditions: (a) JRB7 phage interacted with *B. anthracis* spores in water; (b) JRB7 phage interacted with *B. anthracis* spores incubated in apple juice; (c) E2 phage interacted with *S. typhimurium* in water; and (d) E2 phage interacted with *S. typhimurium* incubated in apple juice.

Fluorescence microscopy can also be used to demonstrate the specificity of phages. In the work reported in this section, *E. coli*/*B. cereus* spores suspended in water were used to interact with the E2/JRB7 phage. The procedures used for this experiment were the same as described above. The fluorescence images are shown in Figure 8-10. Figure 8-10 (a) and (b) represent the interaction between the JRB7 phage and *B. cereus* spores and the E2 phage and *E. coli*, respectively. Very few *B. cereus* spores/*E. coli* cells are visible under fluorescent light, which demonstrates that the specificity of the E2/JRB7 phages was good.

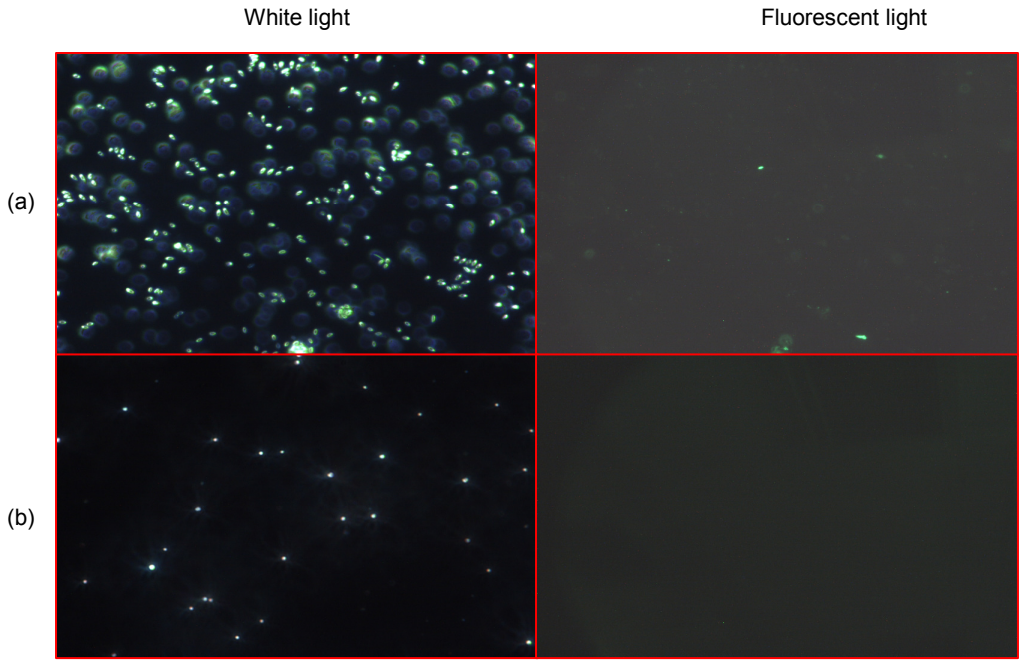

Figure 8- 10. Fluorescence images to demonstrate the specificity of phages: (a) JRB7 phage interacted with *B. cereus* spores suspended in water; (b) E2 phage interacted with *E. coli* suspended in water.

Table 8-1 below compares the numbers of cells/spores observed with and without fluorescent light, as counted individually from the images. Five samples were counted for each experimental condition and then the numbers were averaged. Both the JRB7 phage and E2 phage had good binding affinity/specificity to the *B. anthracis* spores and *S. typhimurium,* respectively, in water. The *S. typhimurium* cells present in apple juice did not lose their binding affinity to E2 phage, but *B. anthracis* spores experienced a change when exposed to apple juice that dramatically decreased their binding affinity to the phage.

Table 8- 1. Comparison of numbers of cells/spores under white and fluorescent light.

Media (Bacterial/spores suspended)	Experimental condition	White light	Fluorescent light	Percentage (%)
Water	B.A.+ JRB7	120	80	67%
	B.C. + JRB7	220	4	1.8%
	S.T. + E2	55	40	80%
	E. coli + E2	30	0	0
Apple Juice	B.A.+ JRB7	320	3	0.9%
	S.T. + E2	80	80	100%

4. References

[1] R. S. Lakshmanan, R. Guntupalli, J. Hu, V. A. Petrenko, J. M. Barbaree, and B. A. Chin, "Detection of *Salmonella typhimurium* in fat free milk using a phage immobilized magnetoelastic sensor," *Sensors and Actuators B: Chemical,* vol. 126, pp. 544-550, 2007.